UNIVERSITA' DEGLI STUDI DI PADOVA

SEDE AMMINISTRATIVA: UNIVERSITÀ DEGLI STUDI DI PADOVA

DIPARTIMENTO DI SCIENZE CHIMICHE

SCUOLA DI DOTTORATO DI RICERCA IN: SCIENZE MOLECOLARI

INDIRIZZO: SCIENZE CHIMICHE

CICLO XXI

Innovative catalytic processes for oxidation reactions

Coordinatore: Ch.mo Prof. Maurizio Casarin

Supervisore: Ch.mo Prof. Gianfranco Scorrano

Dottorando: Dr. Martino Gardan

31 gennaio 2009

A Bea

Alla mia Famiglia

Innovative catalytic processes for oxidation reactions.

Ph. D. Thesis by Martino Gardan, University of Padova, Italy.

The study and the development of innovative metal-catalysed systems for the oxygenation of organic molecules with sustainable oxidants, and especially molecular oxygen, O_2, or hydrogen peroxide, H_2O_2, is a very attractive perspective for the Chemical Industry.

In the Thesis project, different strategies have been addressed to implement benchmark oxidative transformations, including the autooxidation of benzylic derivatives, the hydroxylation of aromatic hydrocarbons and the epoxidation of olefins. In all cases, the research approach has been based on some key issues, namely the integrated use of: i) bulk oxidants with low environmental impact, such as O_2 and H_2O_2; ii) multi-metallic catalysts with thermal, hydrolytic and oxidative resistance, tailored functionality and solubility; iii) heterogeneous catalysis techniques with membrane-based hybrid organic-inorganic functional materials and solvent-free protocols; iv) microwave irradiation and/or photoirradiation as non-conventional activation techniques, v) multiple catalysis techniques, with sequential and/or parallel processes (Concurrent Tandem Catalysis).

The choice of the catalyst package has been established within the class of molecular polyanionic metals oxides clusters, known as polyoxometalates (POMs), with general formula $[X_xM_mO_y]^{q-}$, where M is the main metallic component (Mo, V, W) and X is an eventual heteroatom such as P or Si.

These complexes offer a unique opportunity because of their prevalent inorganic, robust nature, and high versatility in terms of structure, chemical composition, electron density and polyanionic charge. Moreover, a rewarding approach has been recently devised for the catalyst upgrade, by decorating the POM scaffold with organic domains, yielding hybrid organic-inorganic catalysts with superior performances. Since fluorinated phases are of particular interest for performing oxidative transformations, the research activity has been focused on the synthesis, characterization and catalytic activity of novel fluorous-tagged polyoxometalates. Two diverse synthetic approaches have been adopted, based on counterion metathesis and on the covalent functionalization of the POM inorganic surface. With the first strategy, the decatungstate polyanion $(W_{10}O_{32})^{4-}$ has been isolated in the presence of a fluorous-tagged tetraalkylammonium cation, yielding the fluorophilic salt $\{[CF_3(CF_2)_7(CH_2)_3]_3CH_3N\}_4W_{10}O_{32}$, ($RfN_4W_{10}$). Decatungstate is known to be an efficient initiator of autooxidation pathways under photoirradiation, in a oxygen atmosphere. Therefore, the photocatalyzed oxidation of benzylic hydrocarbons, including ethylbenzene and cumene, by RfN_4W_{10} and O_2, has been performed in 1,1,1,3,3,3-hexafluoroisopropanol (HFIP), both in homogeneous and heterogeneous conditions. The application of membrane technology for the heterogeneous catalysis, in particular, offers the combination of advanced molecular separation and selective transport properties, with the reactivity on a solid support. The photocatalyst heterogenisation has thus been obtained by incorporation of RfN_4W_{10} in perfluorinated polymeric films of HYFLON AD 60X, thus providing novel hybrid materials to be employed and recycled in multi-turnover processes, in solvent-free

conditions. Scanning electron microscopy (SEM) images of the film surface and cross-section highlight a highly dispersed, homogeneous distribution of the catalyst domains which appear as spherical particles with uniform size of approximately 2-3 μm in diameter. Furthermore, in particular conditions, a porous membrane has been obtained, allowing the use of a continuous flow reactor. In the conditions explored, the photooxygenation by $(R_fN)_4W_{10}O_{32}$ yields the benzylic hydroperoxide and the corresponding alcohol and ketone. Noteworthy, tetraline and indane photooxygenation proceeds with TON>6000 and remarkable alcohol selectivity, thus providing a convenient alternative to other radical-centered oxygenation systems.

Fluorous-tagged polyoxometalates have also been synthesised through a covalent functionalization approach. This alternative strategy employs vacant polyoxotungstates and the fluorinated organosilyl chloride $CF_3(CF_2)_7CH_2CH_2SiCl_3$ ($RfSiCl_3$) to afford hybrid derivatives through the covalent attachment of the organic groups on the POM surface. The resulting complexes, with general formula $Q_4[(RfSi)_xO_ySiW_wO_z]$, isolated as tetrabutylammonium (Q^+) salts, have been characterised and used as catalysts for the epoxidation of different olefins in the presence of H_2O_2. Kinetic and mechanistic studies have provided several insights on the synergistic effect between the catalysts and the fluorinated solvent used, the hexafluoro-*iso*propanol (HFIP). Noteworthy, under microwave irradiation, the epoxide is produced with quantitative yield and only after 20 minutes, even for terminal olefins. A further aspect concerns the self-assembly of the POM-based fluorous-tagged amphiphiles. Aggregation phenomena in HFIP solution have been studied by DLS and monitored in the solid state by electronic microscopy.

The upgrade to heterogeneous catalysis has also been achieved through the covalent functionalization approach. In this case, the vacant polyoxotungstate has been reacted with the organo silyl chloride $CH_2=CH(CH_2)_6SiCl_3$ ($RSiCl_3$), bearing a terminal alkene residues. The morphology and structure of the resulting hybrid materials have been tuned upon variation of comonomers and porogenic solvents ratio. Interestingly, the hybrid polymer swells in fluorinated alcohols, where the epoxidation of *cis*-cyclooctene, occurs with quantitative yield after 15 min.

Finally, POM-based catalysis has also been applied to the synthesis of phenol which is one of the most valuable intermediate and commodity chemical on the market. To this aim the research activity has been focussed on the implementing both the autoxidation pathway, and the direct mono-hydroxylation of benzene. (i) The application of Tandem Catalysis techniques, so to exploit the membrane-based photocatalytic production of the cumene hydroperoxide and foster its decomposition to phenol through a second step by a acid POM catalyst; (ii) the screening of several molybdovanadate catalyst to be used with H_2O_2 for benzene hydroxylation. In the first case, the POM mediated tandem catalysis yields 63% phenol with respect to the initial amount of cumyl-hydroperoxide.; in the second case, with the vanadium mono-substituted undecamolybdate, $H_4Mo_{11}VO_{40}$, an improvement of literature results has been obtained through reaction optimization, thus giving: 17 % conversion of benzene at 50°C in CH_3CN, with selectivity = 90 % and TOF = 22.5 h^{-1}.

Processi catalitici innovativi per reazioni di ossidazione.

Tesi di Dottorato di Martino Gardan, Università degli Studi di Padova, Italia.

Lo studio e lo sviluppo di sistemi metallo-catalizzati innovativi per l'ossidazione di molecole organiche con ossidanti sostenibili, specialmente ossigeno molecolare, O_2, o acqua ossigenata, H_2O_2, è una prospettiva di grande attrazione per l'Industria Chimica.

Nel progetto di Tesi di Dottorato, sono state sviluppate diverse strategie allo scopo di effettuare trasformazioni ossidative di riferimento quali l'autoossidazione di derivati benzilici, l'idrossilazione di idrocarburi aromatici e l'epossidazione di olefine. In tutti i casi, l'approccio alla ricerca si è basato su alcuni aspetti chiave che prevedono l'utilizzo integrato di: i) ossidanti a basso impatto ambientale quali O_2 e H_2O_2; ii) catalizzatori multi-metallici ad elevata resistenza termica, idrolitica ed ossidativa; iii) tecniche di catalisi eterogenea per mezzo di materiali funzionali ibridi organici-inorganici costituiti da membrane catalitiche a matrice polimerica e protocolli che non prevedano l'impiego di solventi organici; iv) microonde o radiazioni fotochimiche quali tecniche di attivazione non convenzionali; v) tecniche di catalisi multipla con processi sequenziali e/o paralleli (Tandem Catalisi).

I catalizzatori impiegati appartengono alla classe degli ossidi polianionici metallici, detti poliossometallati (POMs), aventi formula generale $[X_xM_mO_y]^{q-}$, dove M è il componente metallico principale (Mo, V, W) e X è un eventuale eteroatomo (P o Si). Questi complessi sono molto vantaggiosi come catalizzatori perché di natura inorganica, resistenti e sono modulabili in termini di struttura, composizione chimica, densità elettronica e carica polianionica. Particolarmente interessante è la possibilità di funzionalizzare la porzione inorganica con domìni di natura organica, potendo così ottenere catalizzatori ibridi organici-inorganici dalle prestazioni catalitiche migliori. Poiché le fasi fluorurate sono di particolare interesse per ciò che concerne le trasformazioni ossidative, l'attività di ricerca si è focalizzata sulla sintesi, caratterizzazione e attività catalitica di nuovi poliossometallati fluorurati. Sono state seguite due strategie di sintesi differenti basate sulla metatesi di controcatione e sulla funzionalizzazione covalente di superfici di POM inorganici.

Con la prima strategia è stato isolato il polianione decatungstato $(W_{10}O_{32})^{4-}$ con un controcatione tetraalchilammonio fluorurato ottenedo il sale fluorofilico $\{[CF_3(CF_2)_7(CH_2)_3]_3CH_3N\}_4W_{10}O_{32}$, ($RfN_4W_{10}$). Il decatungstato è noto per la sua capacità di essere iniziatore di processi radicalici se fotoirradiato in atmosfera di ossigeno. L'ossidazione fotocatalitica di etilbenzene ed altri idrocarburi benzilici tramite RfN_4W_{10} e O_2 è stata condotta in 1,1,1,3,3,3-hexafluoroisopropanolo (HFIP), sia in omogeneo che in fase eterogenea. L'applicazione della tecnologia delle membrane per la catalisi eterogenea offre, in particolare, numerosi vantaggi in termini di combinazioni di avanzati processi di separazione molecolare con proprietà di trasporto selettive, insieme alla reattività su supporti solidi. L'eterogeneizzazione del fotocatalizzatore è stata così ottenuta per incorporazione di RfN_4W_{10} in film polimerici perfluorurati di HYFLON AD 60X, ottenendo così nuovi materiali ibridi da impiegare e reciclare in processi "*multi-turnover*" ed in assenza di solventi. Immagini di microscopia elettronica a

scansione (SEM) della superficie e della sezione del film evidenziano una distribuzione omogenea ed altamente dispersa dei domini catalitici che appaiono come particelle sferiche a dimensioni uniformi e di diametro pari a circa 2-3 μm. Inoltre, in condizioni controllate, è stato possibile ottenere una membrana porosa da poter utilizzare in un reattore a flusso continuo. Nelle condizioni testate, la fotoossigenazione con $(R_fN)_4W_{10}O_{32}$ dà benzilidroperossido ed il corrispondente alcool e chetone. E'importante evidenziare come la fotoossigenazione di tetralina ed indano proceda con TON>6000 e con una elevata selettività in alcool, fornendo così un' importante alternativa ad altri sistemi di ossigenazione basati su meccanismi di tipo radicalico.

Poliossometallati fluorurati sono stati sintetizzati anche tramite l'approccio di funzionalizzazione covalente. Questa strategia prevede l'impiego di poliossotungstati lacunari e organosilil cloruri $CF_3(CF_2)_7CH_2CH_2SiCl_3$ ($RfSiCl_3$) a dare derivati ibridi per mezzo dell'attacco covalente dei gruppi organici sulla superficie del POM. I complessi finali risultanti, con formula generale $Q_4[(RfSi)_xO_ySiW_wO_z]$, isolati come sali di tetrabutilammonio (Q^+) sono stati caratterizzati ed impiegati come catalizzatori per l'epossidazione di diverse olefine in presenza di H_2O_2. Studi cinetici e meccanicistici hanno fornito diverse indicazioni circa l'esistenza di un effetto sinergico fra i catalizzatori e il solvente per fluorurato utilizzato (HFIP). E'importante sottolineare come questa reazione attivata da microonde produca epossido in rese quantitative dopo soli 20 minuti anche per le olefine terminali. Ulteriori aspetti trattati riguardano le caratteristiche auto-assemblanti di questi complessi fluorurati anfifilici. Fenomeni di aggregazione in soluzione di HFIP sono stati studiati tramite DLS e tramite microscopia elettronica allo stato solido. Anche l'eterogeneizzazione di questo sistema è stata ottenuta tramite l'approccio di funzionalizzazione covalente. In questo caso, il poliossotungstato lacunare è stato fatto reagire con un silano che porta una catena alchilica insatura terminale: $CH_2=CH(CH_2)_6SiCl_3$ ($RSiCl_3$). La morfologia e la struttura del materiale ibrido risultante sono state modulate attraverso la variazione del rapporto dei solventi porogenici e dei comonomeri impiegati nella miscela di polimerizzazione. Il polimero ibrido finale presenta l'interessante proprietà di rigonfiare in alcool fluorurati, dove l'epossidazione di *cis*-cicloottene avviene con rese quantitative in 15 minuti.

Infine, è stato studiato il processo POM-catalizzato per la sintesi di fenolo: uno degli intermedi e *commodity* a più alto valore di mercato. A questo scopo l'attività di ricerca è stata incentrata sullo studio sia del processo autoossidativo, sia della mono-idrossilazione diretta del benzene. (i) L'applicazione di tecniche di Tandem Catalisi, allo scopo di sfruttare la produzione con sistema a membrana foto catalitica del cumilidroperossido da cumene, e promuoverne la sua decomposizione a fenolo in un secondo stadio con un catalizzatore POM-acido, (ii) lo screening di diversi molibdovanadati come catalizzatori da usare con H_2O_2 per l'idrossilazione di benzene. Nel primo caso, la Tandem Catalisi permette di ottenere una resa in fenolo pari a 63% rispetto alle moli iniziali di cumilidroperossido, nel secondo caso, con $H_4Mo_{11}VO_{40}$ si ha un miglioramento dei dati di letteratura per ottimizzazione della reazione con 17% di conversione, selettività = 90% e TOF = 22.5 h^{-1}.

Contents

Contents

Contents

1. General introduction.

1.1 Catalytic Oxidations: the importance from both industrial and synthetic point of view.

Oxidation reactions play an important role in organic chemistry[1][2] and there is an increasing demand for selective and mild oxidation methods in modern organic synthesis.

Historically, the observation that the degradation of several organic materials as rubber, oil and fat was due to the absorption of the atmospheric oxygen, goes back to the XIX century and the first scientific investigations were aimed to avoid such processes. During the 1940s, the first theory about autooxidation mechanism of simple hydrocarbons by oxygen, through a radicalic chain mechanism[3][4], was developed, and now an oxidative functionalization step is present in several important chemical processes.

During the last two decades, a significant progress has been achieved within the area of catalytic oxidations, which has led to a range of selective and mild processes from both industrial and synthetic point of view. These reactions may be based on organocatalysis, metal catalysis or biocatalysis. In this regard enantioselective catalytic oxidation reactions are of particular interest[5].

From an industrial point of view, the most important oxidation processes concern the oxidation of p-xylene to terephthalic acid and dimethyl terephthalate, the oxidation of ethylene to formaldehyde (Wacker Process), the oxidation of cyclohexane to cyclohexyl hydroperoxide or to cyclohexanol and cyclohexanone mixtures; the oxidation of cumene to cumyl hydroperoxide, which can give phenol through its acidic degradation (Hock Process, see also Chapter 4); and the oxidation of isobutane to tert-buthylhydroperoxide and tert-buthanol[6]. With regard to the production of high added value industrial and pharmaceutical intermediates, the most important reactions are the hydroxylation of saturated hydrocarbons and the olefins epoxidation[7]. Another field of application involving oxidative steps is within the *Advanced Oxidation Processes* (AOPs), where environmental remediation can be achieved through the oxidative degradation of pollutants, such as pesticides[8], aromatic molecules and phenol derivatives[9][10], aliphatic molecules and alcohols, amines, carboxylic acids, inorganic compounds (ammonia and nitrites), sulphur compounds[9][10].

A great emphasis is nowadays related to the use of environmentally friendly oxidants ("green" oxidants) that lead to a minimum amount of wastes. Table 1.1 list the most commonly used oxidants. They are classified comparing their active oxygen content, which is

the ratio between the weight of the oxygen atoms to be transferred to the substrate and the weight of the oxidant itself. By-products, formed during the oxidation reaction, are also reported.

Table 1.1 Oxidants (Oxygen donors) classifications on the basis of the active oxygen percentage and of the by-product formed.

Oxidant (OD)	% Active Oxygen	By-product (D)
O_2	100	-
H_2O_2	47	H_2O
N_2O	36.4	N_2
O_3	33.3	O_2
ClO^-	21.6	Cl^-
$(CH_3)_3COOH$ (TBHP)	17.8	$(CH_3)_3COH$
HSO_5^-	10.5	HSO_4^-
ClC_6H_4COOOH (m-CPBA)	10.2	ClC_6H_4COOH
IO_4^-	7.5	IO_3^-
C_6H_5IO (PhIO)	7.3	C_6H_5I

An oxidative process of interest from a sustainable point of view, should address economical benefits and green chemistry concerns, by:

i) providing the highest percentage of active oxygen, accordingly with the highest atom economy[11][12];

ii) avoiding the formation of toxic and difficult to eliminate by-products[11][12];

iii) using an oxidant with great availability and low cost.

From these considerations, it is obvious that the most attractive oxidant is molecular oxygen - dioxygen - (O_2)[13] because of: (i) its high active oxygen content (depending on the reaction, it can reach 50% or 100%, when one or two oxygen atoms are respectively introduced in the substrate; (ii) it does not give any oxidation by-products; (iii) it is cheap and abundant in the atmosphere. Hydrogen peroxide is also of interest, even if its cost is still quite high.

A major drawback, when using dioxygen as oxidant, is the low reactivity, because of the electronic state, involving spin conservation rules. Its triplet ground state is indeed not suitable for an interaction with organic substrates, commonly found in the singlet state. Thus, despite the favourable thermodynamic of the direct reaction between dioxygen and the organic molecules, an activation step for the substrate, dioxygen or both of them is required. (This, of course, prevent the complete oxidation of organic substances on Earth...)[14]. The

substrate activation is generally obtained by homolithic reactions in which a radical initiator provides organic radicals which are able to react with dioxygen, affording oxidized species. Such mechanism, reported in Scheme 1.1, foresees the presence of radical species in the initiation steps, as well as in the propagation and termination steps[15].

Initiation
$$In_2 \longrightarrow 2\ In\bullet$$
$$In\bullet + RH \longrightarrow InH + R\bullet$$

Propagation
$$R\bullet + O_2 \longrightarrow RO_2\bullet$$
$$RO_2\bullet + RH \longrightarrow RO_2H + R\bullet$$

Termination
$$R\bullet + RO_2\bullet \longrightarrow RO_2R$$
$$2\ RO_2\bullet \longrightarrow RO_4R \longrightarrow \text{non radical products} + O_2$$
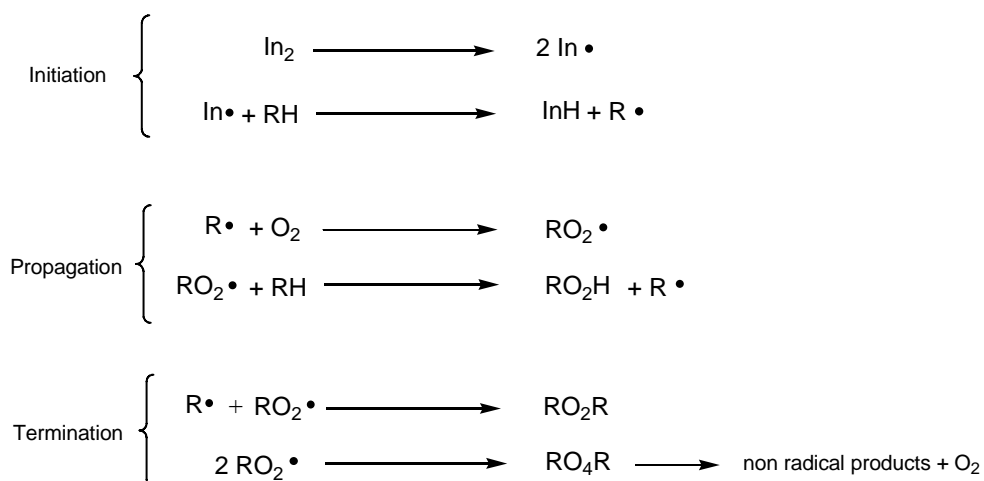
Scheme 1.1 Reaction mechanism in autooxidation reactions.

These kinds of reactions are known as *autooxidation*[3][4] and, despite they are not very selective, they are still used for the production of several important industrial chemical products[6].

The activation of the molecular oxygen can be obtained by means of photochemical or chemical processes (see Scheme 1.2).

Photochemical activation

Chemical activation

$$O_2 \xrightarrow{e^-} O_2\overset{\bullet}{\,\!^-} \underset{}{\overset{H^+}{\rightleftharpoons}} HOO\bullet \quad \text{Superoxide}$$

$$O_2\overset{\bullet}{\,\!^-} \xrightarrow{e^-} O_2^{2-} \underset{}{\overset{2H^+}{\rightleftharpoons}} HOOH \quad \text{Peroxide}$$

$$HOOH \longrightarrow 2\ HO\bullet \quad \text{Hydroxyl radical}$$
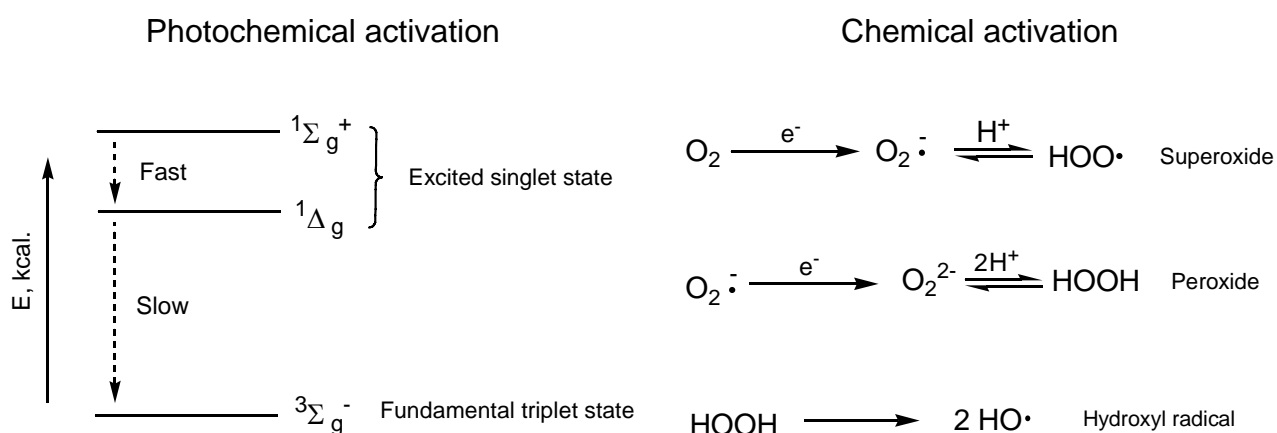
Scheme 1.2 Photochemical and chemical activation.

Photochemical activation (see Scheme 1.2 A) is obtained by exciting molecular oxygen from its fundamental triplet state to higher singlet energy levels. Generally only the lowest singlet energetic level ($^1\Delta_g$), commonly indicated as "singlet oxygen ($^1O_2$)", is involved in the oxidation reactions of organic substrates. While the higher singlet level ($^1\Sigma_g^+$) quickly converts to the lower singlet level $^1\Delta_g$, the lifetime of the latter is long enough to give reactions, since its decay to the fundamental state presents spin restriction.

The chemical activation (see Scheme 1.2 B) is obtained by mono- and bi-electronic reductive steps to produce reactive species like superoxides or peroxides. This activation can be promoted by different transition metal complexes, to be used in catalytic cycles[16]. Noteworthy, hydrogen peroxide can also be obtained in this way, starting from dioxygen.

The most interesting catalytic processes, from a selectivity point of view, are represented by the following general scheme:
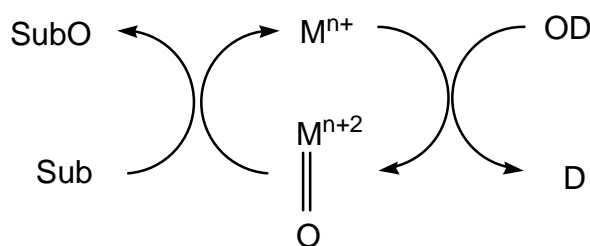
Scheme 1.3 Oxygen donor activation by a transition metal.

On the basis of this scheme, dioxygen or another suitable oxygen donor OD, interacts with the metal species M to form a metal-oxo species ("oxene") with high oxidation state, which is able to transfer the oxygen atom to a generic substrate Sub, in order to give the final oxidized species SubO, while returning to the metal initial oxidation state. This particular activation can be found in biological systems, where high efficiency and selectivity are achieved with metal-enzyme catalysis.[17][18][19] Iron and copper are commonly used in enzymatic systems, but it is also possible to find different metals such as manganese and vanadium. The study of the activity of such metal enzymes is often considered as a milestone for the design of innovative oxygenation processes.

A sustainable catalytic oxidation should present the following fundamental features[20]:

i) capability to activate O_2 and H_2O_2, in aqueous phase, with solvent-free protocols, or in environmentally friendly solvents, including perfluorinated environment, ionic liquids and carbon dioxide.;

ii) high selectivity;

iii) oxidative, hydrolytic and thermal stability in the reaction conditions.

4

The contemporary presence of these three features could provide the "ideal oxidation catalyst" (see Figure 1.1)[20].
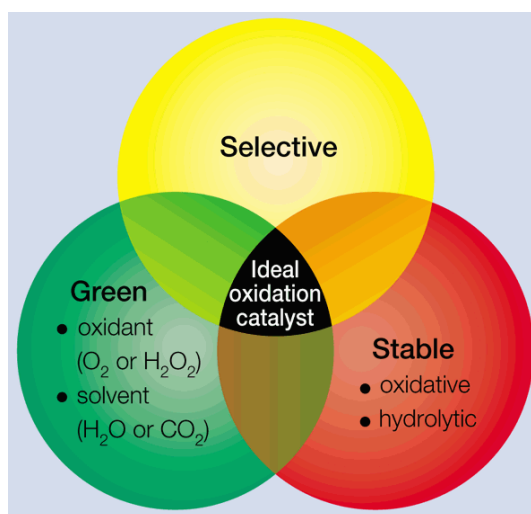
Figure 1.1. Schematization of the features of an "ideal" oxidation catalyst.

1.2 Polyoxometalates as catalysts for oxidation process.

1.2.1 Polyoxometalates: a general introduction.

The history of polyoxometalates (POM) goes back to early XIX century[21] when the discovery that metals belonging to early transition series such as niobium, vanadium, tantalum, molybdenum, and tungsten in their higher oxidation states (configuration d^o or d^1) can form in aqueous solution, at suitable pH, concentration and temperature, polynuclear oxoanions with variable dimensions, ranging from few Angstrom and tens of nanometers[22][23][24][25][26]. Such complexes are called polyoxometalates and a first classification of them is based on the chemical composition of these species, essentially represented by two types of general formula[22][23][24][25][26]:

a) $[M_mO_y]^{p-}$

b) $[X_xM_mO_y]^{q-}$

where M is the main transition metal constituent of the polyoxometalate, O is the oxygen atom and X can be a non-metal atom as P, Si, As, Sb, another element of the p block, or a different transition metal. In the first case (a), polyoxometalates are called isopolyanions; while in the second case (b), they are called heteropolyanions.

Listed below, are some examples of polyoxometalate structures.

5
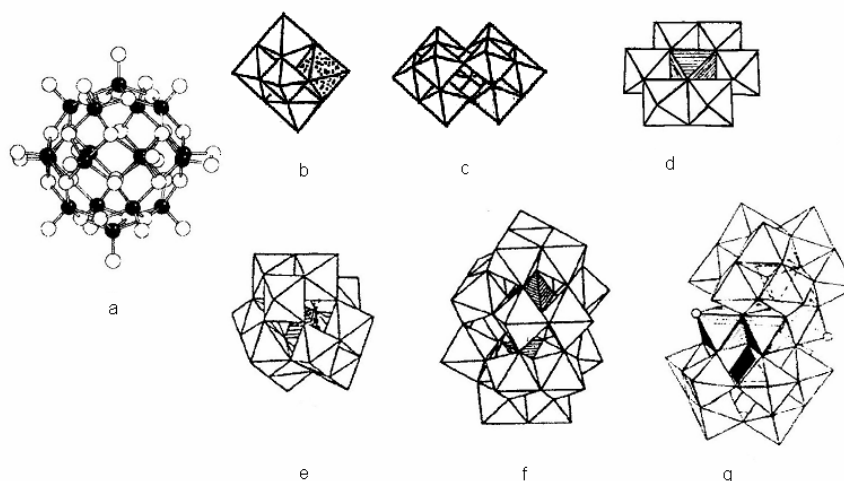
Figure 1.2. Some different structures of polyoxometalates: a) a ball-and-stick structure is reported for the isopolyvanadate [$V_{18}O_{42}$]$^{12-}$, with black spheres representing the V (IV) atoms. a-b) Lindqvist [M_6O_{19}]$^{2-}$ structure (M=Mo, W) and its dimeric decatungstate derivative [$W_{10}O_{32}$]$^{4-}$ (b), c) Anderson-Evans heteropolyanion [XMo_6O_{24}]$^{m-}$ (X=P, As). e) α-Keggin structure [$XM_{12}O_{40}$]$^{n-}$, (X = P, Si, B, Al, Ge; M = Mo, W). f) α-Well-Dawson structure [$X_2M_{18}O_{62}$]$^{n-}$ (X=P, Si; M = W, Mo). g) Krebs structure M'$_4$ (H_2O)$_y$](XW_9O_{33})$^{n-}$ (X=Bi, As, Sb, Te,; M'= Zn, Al, W)

In most cases, the structure of the polyoxometalates is derived from the aggregation of octahedral units MO_6 with a central metal atom M and the oxygen atoms placed on their corners.

In such octahedra, only one oxygen atom- or a maximum of two – present a double bond character with the central metal atom and they are not shared with other metal atoms within the complex (terminal oxygens, Lipscomb law[27]). Oxygen atoms exhibiting simple bonds with the metal allow the condensation between two octahedral units. In the following figure, two kinds of octahedra constituting POM structures are represented[22]: the first one is a terminal mono-oxo type presenting only one terminal oxygen atom, while the other five oxygens are shared with other atoms of the polyoxometalate; the second one is a terminal *cis*-di-oxo type and it presents two terminal oxygens, in cis position, while the remaining four oxygens are shared by other metals in the whole polyoxometalate structure.
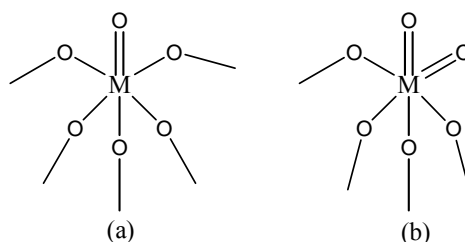
Figure 1.3. Octahedra constituting the most common structures of the polyoxometalates.

Two are the main characteristic features that a metal must possess to originate polyoxometalate complexes[22]:

i) dimensions (cationic radius) compatible with a octahedral coordination; ii) availability of empty and easy to access d orbitals, to form the terminal Metal – Oxygen double bond (withdrawing properties of pπ electrons from oxygen). This latter feature explains, for example, the absence of a polyanionic chemistry for Cr (VI): in fact its smaller dimensions (ionic radius = 0.58 Å) allow up to four coordinating oxygens.

The octahedra condensation takes place through shared oxygen atoms, with the formation of μ - oxo bridged bonds between two metals ions, by the following three different ways[23][28]: i) corner sharing; ii) edge sharing iii) face sharing (less frequent).

These sharing modes are represented in figure 1.4. The presence of terminal oxygen atoms is essential for the aggregation to take place in discrete structures and not in an extended material (as for most common metal oxides, silicates, germanates, tellurates). Since terminal oxygens are less basic, they are not suitable for the condensation with other monomeric units, thus providing a barrier towards the linear polymerization and finally favouring discrete molecular units[22].
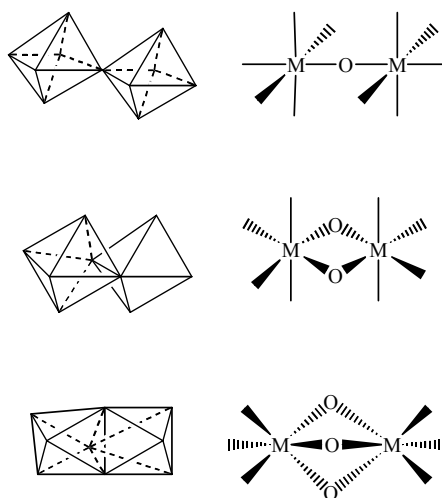
Figure 1.4. Condensation of the octahedron units in polyoxometalates.

General introduction.

One of the most important class of polyoxometalates, is that of Keggin heteropolyanions. Their general formula is: $[XM_{12}O_{40}]^{n-}$, with M = Mo (VI) or W (VI). Keggin obtained the structure of the hexahydrated dodecatungstophosphoric acid for the first time in 1934, by powder X-ray investigation[29]. This structure is called α-Keggin and consists of a central PO_4 tetrahedron surrounded by 12 octahedrons WO_6 belonging to the mono-oxo terminal type. Such octahedra are disposed in four groups (triplets M_3O_{13}), each of them constituted by the aggregation of three octahedral units by edge-sharing. The four different triplets are condensed each other by corner-sharing.
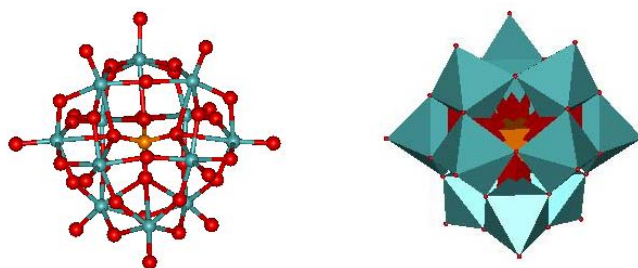
Figure 1.5. Two representation of the same α-Keggin structure of the $[PW_{12}O_{40}]^{3-}$ heteropolyanion. On the left side a ball-and-stick model is represented: the red spheres are oxygen atoms, the blue ones are tungsten atoms and the orange one is the central phosphorous atom. On the right side a polyhedral model is represented: blue octahedra are centred on tungsten atoms, while the red tetrahedron is centered on the central phosphorous atom.

Structure and symmetry of the α-Keggin polyanion have also been confirmed in solution by heteronuclear NMR spectroscopy (Table 1.2)[30] [31] [32] [33].

Table 1.2. Heteronuclear NMR characterization of heteropolyanions with α-Keggin structure.

Polyoxoanion	δ (^{183}W)[a]	δ (^{31}P)[b]	δ (^{29}Si)[c]	δ (^{17}O)[d]
α-$[PW_{12}O_{40}]^{3-}$	-99.4	-14.9		769 (O_t), 431, 405 (O_B, O_C), n.d. (O_A)
α-$[SiW_{12}O_{40}]^{3-}$	-103.8		-85.3	761 (O_t), 427, 405 (O_B, O_C), 27 (O_A)

a) ref.: WO_4^{2-}, 1M in D_2O; b) ref.: 85% H_3PO_4; c) ref.: $Si(CH_3)_4$; d) ref. H_2O.

The chemical equivalence of 12 tungsten atoms results into only one signal for ^{183}W-NMR[30]. One signal is also observed for the central atom[31] [32]; while for the oxygen nuclei is possible to observe four different spin systems[33]. Of the forty oxygen atoms present in the

Keggin structure, it is possible to distinguish four type of different oxygen atoms: i) 4 oxygens bonded to the central atom (O_A), ii) 12 terminal oxygens (O_t), iii) 12 oxygens bridging different triplets by corner-sharing (O_B), iv) 12 oxygens bridging octahedra which belong to the same triplet by edge-sharing (Oc).

Keggin polyoxometalates can also present structural isomers, which are formally obtained from the α structure by 60° rotation of one (β isomer), two (γ isomer), three (δ isomer) or four (ε isomer) triplets M_3O_{13}[22][23]. These isomers are characterized by lower symmetry and by a decreased thermodynamic stability with respect to the α structure.

1.2.2 Polyoxometalates as ligands for transition heterometals.

The properties of polyoxometalates are very interesting in different scientific fields as medicine, materials science and catalysis[24] (see also Section 1.2.4).

Polyoxometalates present a great variety of structures which can be obtained in particular synthetic conditions by tuning some specific parameters like concentration, stoichiometric ratio between the reagents, temperature and pH. Noteworthy, isostructural polyoxometalates may also present different properties depending both on the heteroatom X and the counterion associated with them. The choice of a suitable counterion for such complexes, allows indeed to solubilize them in a wide range of solvents; from apolar solvents (toluene, dichloromethane), by using a lipophilic cations such as tetraoctylammonium, to water, when using alkaline counterions or protons.

Furthermore, since they are made of metals in their higher oxidation states, polyoxometalates are more stable towards the oxidative degradation, than generic organic molecules.

One of the properties which makes polyoxometalates very appealing in catalysis, is their ability to act as ligands for different transition metals such as chromium, iron, manganese, cobalt and ruthenium. The coordination of an hetero-metal by a polyoxometalate complex takes place essentially in two ways[22][23][24]:

i)   through superficial coordination of the metal cation by electrostatic interaction with the anionic oxygens on the surface of the polyoxometalate (*Supported Complexes*);

ii)   incorporation of the transition metal in the polyoxometalate structure with formation of *Transition Metals Substituted Polyoxometalates* (*TMSP*).

While *Supported Complexes* are preferentially formed in organic solvents and in the presence of polyoxometalates with high charge through weak interactions, the *Transition*

Metals Substituted Polyoxometalates present higher stability since the transition metal is an effective constituent of the whole polyanion structure.

The synthesis of TMSP foresees the use of vacant or "lacunary" polyoxometalates[22][34]. Such complexes derives from the saturated original polyoxometalate, through the formal loss of one or more MO_6 tetrahedral units, thus affording vacancies on the surface. Synthetic procedures depend on the stability of the vacant complexes itself, which can be obtained from the precursors in suitable conditions and pH.

As an example, the structure of a monovacant tungsten complex (XM_{11}), derived from the α-Keggin structure is reported below[35]:
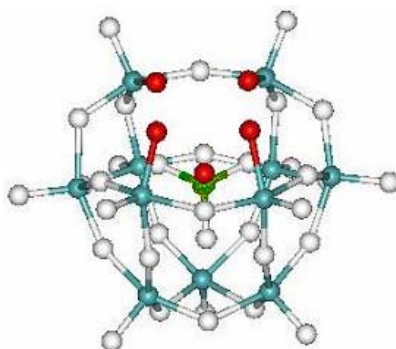
Figure 1.6. Ball-and-stick model for the structure of the monovacant α-Keggin $[XW_{11}O_{39}]^{n-}$. Blue spheres are W atoms, white ones represent oxygen atoms and red spheres are nucleophilic oxygen atoms around the vacant site. The green sphere is the X central heteroatom.

Such complex presents five "lacunary oxygens" highlighted in red colour in the figure 1.6. These oxygens form a "polydentate" site able to coordinate a multitude of transition metals M'. In this particular case, the vacant complexes $XW_{11}O_{39}^{n-}$ (X = P, Si) are stable and they can be isolated. Their synthesis can be obtained starting from $XW_{12}O_{40}^{(n-4)-}$, as well as by mixing stoichiometric amounts of mononuclear metal salts and adjusting the pH to a specific acidic value (see Scheme 1.4):

$$[XW_{12}O_{40}]^{p-} \xrightarrow{OH^-}$$

$$[XW_{11}O_{39}]^{(p+4)-}$$

$$11\ [WO_4]^{2-}\ +\ [XO_m]^{r-} \xrightarrow{H^+}$$
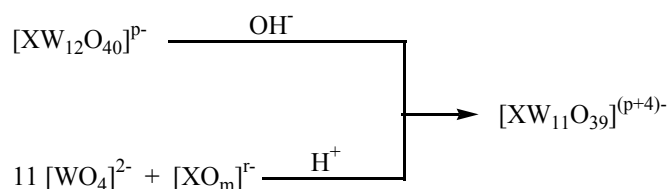
Scheme 1.4. General procedure for the synthesis of monovacant α-Keggin complexes $[XW_{11}O_{39}]^{p-}$.

The reaction between a vacant polyoxometalate with a suitable transition metal precursor M' gives the incorporation of such metal on the POM structure, giving the *Transition Metals Substituted Polyoxometalates* complex (see Scheme 1.5).
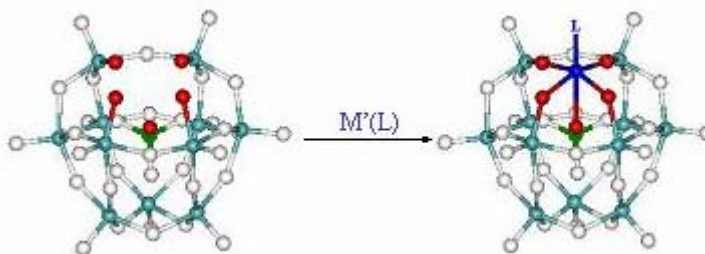
Scheme 1.5. Incorporation of a metal M' on the "lacuna" of the monovacant polyoxometalate [XW$_{11}$O$_{39}$]$^{p-}$.

The same considerations applies to di- (XM$_{10}$) and tri-vacant species (XM$_9$), resulting from the formal loss of two or three octahedra, respectively[36].

monovacant
α-Keggin

divacant
γ-Keggin
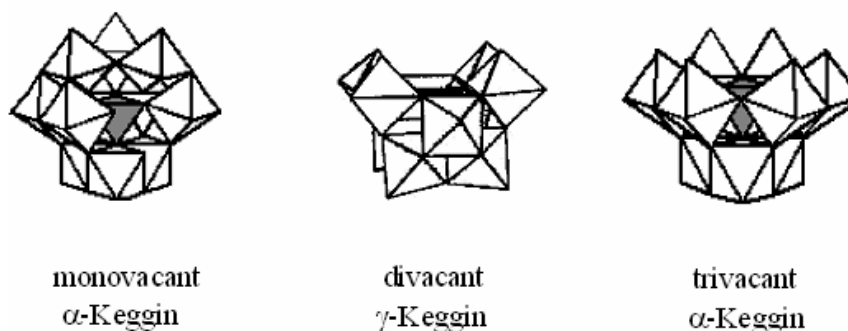
trivacant
α-Keggin

Figure 1.7. Polyhedral structures of mono-, di- and tri-vacant Keggin polyoxotungstates.

Beside the already presented "in pocket" coordination mode of transition metals, vacant polyoxometalates can be also obtained with the "out of pocket" structural motif, or as "Sandwich-like" dimeric structures.

General introduction.

a   b   c
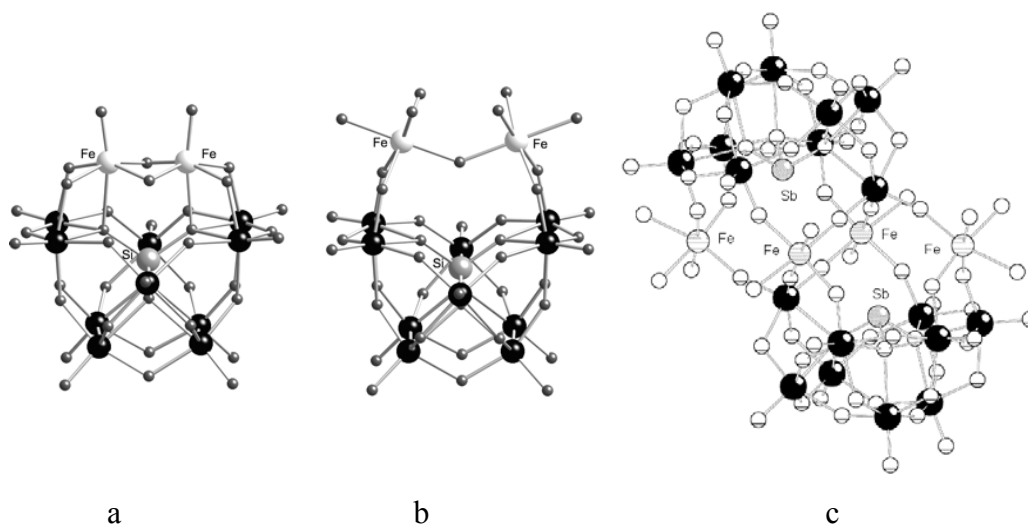
Figure 1.8 Structural motifs for iron-substituted polyoxotungstates: a) in pocket, b) out of pocket, c) sandwich-like.

Considering the high versatility in terms of structure, chemical composition, electron density and polyanionic charge, it is easy to explain why this complexes are good candidates as catalysts for oxidative processes.

1.2.3 Hybrid polyoxometalates as resistant catalysts and building blocks evolving to supramolecular aggregates.

As already introduced, vacant polyanionic complexes feature reactive terminal, coordinatively unsaturated, oxygen atoms. Their nucleophilicity can be exploited to obtain a reaction with electrophilic organic moieties to give organic - inorganic hybrid complexes[37][38][39].

In this Research Group, different synthetic procedure have been optimized to obtain organic – inorganic POM based hybrid complexes, starting from both organosilyl clorides and trialkoxysilanes as electrophilic reagents. The covalent functionalization has been obtained with yields ranging between 65 and 90%[40].

The use of $[\gamma\text{-SiW}_{10}\text{O}_{36}]^{8-}$ bi-vacant complex has shown to be convenient for these reaction, since it is characterized by a higher hydrolythic stability than other vacant complexes in the acid environment employed for these reactions. As in the case of the mono-vacant precursor, it presents four equivalent nucleophilic vacant oxygen atoms. These features allow to obtain silylated products with high selectivity: in the following figure, two adducts, obtained by reaction of decatungstosilicate with two or four equivalents of organosilane, are reported[41].
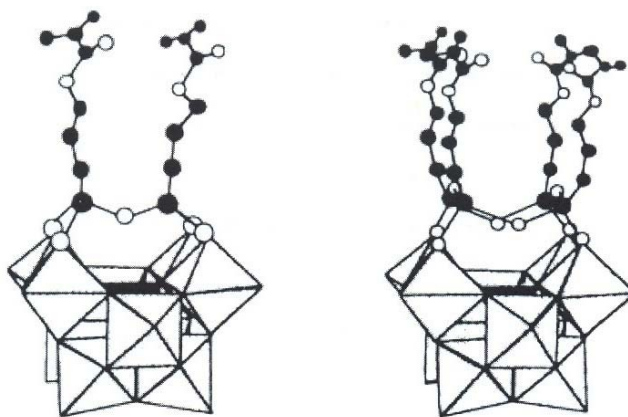
Figure 1.9 Structure of bi- and tetra-substituted decatungstosilicate derivatives.

The covalent functionalization of vacant polyoxoanion imparts a stabilization of the inorganic ligand, while generating further catalyst diversity that might also include the most desirable chiral upgrade. The derivatization of polyoxometalates is useful to: i) stabilize molecular structures which can otherwise give isomerization or decomposition[42], ii) support organic molecules and organometallic catalysts, for tuning their solubility in the reaction media, by using the vacant POM as a scaffold, iii) introduce polyfunctional groups to be used as spacers between polyoxometalates, so to result in the preparation of dendrimeric[39] or polymeric hybrid materials[41].

Moreover, they have been shown to be useful as building blocks evolving to self-assembled supramolecular aggregates and to nanostructured systems[43]. The aggregation has sometimes led to spherical vesicles, thus providing a microenvironment of interest for catalytic application, as well as a system to be exploited as molecular carrier[44]. (For more details, see Chapter 3).

1.2.4 Polyoxometalates as catalysts in oxidation reactions: general considerations.

The research about the applications of polyoxometalates has, over the past two decades, become very important, as reflected by the number of excellent papers and reviews[24 44a 45] devoted to this topic. The research diversity in the field of polyoxometalates is significant and it includes their application in materials science, analytical chemistry, surface chemistry, medicine, electrochemistry and photochemistry. However, the most extensive research on the application of polyoxometalates is the area of catalysis, where their use as Brönsted acid catalysts and as homogeneous oxidation catalysts has been firmly established since the late 1970s. The development of novel ideas and concepts, is moving the use of POMs towards

new frontiers, that could lead to important practical applications (hydrogenations[46], click chemistry[47], Suzuki coupling[48], etc.).

Polyoxometalates are generally stable in the presence of molecular oxygen, up to 350-450 °C. This, *a priori*, represents a distinct advantages over the widely investigated organometallic compounds, which are vulnerable to decomposition due to oxidation of the organic ligand bound to the metal center.

It is important to note that there are important polyoxometalate structure - reactivity and selectivity relationships, which represent fundamental studies to further improve their properties. and mechanistic knowledge[22-25]. Two oxidation catalytic processes, in which polyoxometalates are involved for the activation of dioxygen and hydrogen peroxide, are introduced in the next paragraphs; they will be developed and discussed in the following chapters of this Thesis.

1.2.5 Polyoxometalates as photocatalysts for the oxidation of organic molecules by O_2.

It has often been stated that polyoxometalates can be considered molecular models of semiconductor metal oxide surfaces[49]. At the same time, the possibility to undergo photoinduced multielectron transfers without changing their structure makes polyoxometalates very attractive catalysts for the oxidation of organic substrates in the presence of O_2[50] [51]. Moreover, their use in heterogeneous catalysis is attracting growing interest[52] [53].

Among polyoxometalates, tungstate derivatives are more convenient to use because they are easier to reoxidize by dioxygen, with respect to other polyoxomolybdates and vanadates[b] [54] [55].

As a general reaction mechanism involving polyoxotungstates, the following scheme reports the activity of the decatungstate $W_{10}O_{32}^{4-}$ [56] in homogeneous conditions[50]. Upon irradiation with wavelength < 350-400 nm, a *ligand to metal charge transfer* (LMCT) transition is obtained. The excited state is able to initiate the oxidation of the organic substrate through hydrogen abstraction (or electron abstraction), generating radical species which, in the presence of O_2, lead to the corresponding hydroperoxides. The reduced POM, the *heteropolyblu*e complex, shows an absorption in the visible region around at 700 nm: the typical blue colour is due to d→d transitions of the reduced ions containing d^1 electrons, and to the charge transfer transition between adjacent ions M^{5+}→M^{6+} [57] [58] [59]. Finally, dioxygen reacts with the *heteropolyblu*e complexes, restoring the initial form of the catalyst and forming reduced oxygenated species (superoxide radical, hydroxyl radical), that are able to directly react with the substrate and the reaction intermediates (see Scheme 1.6).

$$W_{10}O_{32}{}^{4-} \xrightarrow{h\nu} [LMCT\ O \rightarrow W] \rightarrow W_{10}O_{32}{}^{4-*}$$

$$W_{10}O_{32}{}^{4-*} + RH_2 \rightarrow HW_{10}O_{32}{}^{4-} + RH^\bullet$$

$$HW_{10}O_{32}{}^{4-} + RH^\bullet + O_2 \rightarrow W_{10}O_{32}{}^{4-} + RHOOH$$

$$RHOOH + HW_{10}O_{32}{}^{4-} \rightarrow$$
$$RHO^\bullet + W_{10}O_{32}{}^{4-} + H_2O$$

$$RHO^\bullet + RH_2 \rightarrow RHOH + RH^\bullet$$

$$RH^\bullet + O_2 \rightarrow RHOO^\bullet$$

$$RHOH + 2W_{10}O_{32}{}^{4-*} \rightarrow RO + 2HW_{10}O_{32}{}^{4-}$$

$$RHOOH + W_{10}O_{32}{}^{4-*} \rightarrow$$
$$[^\bullet ROOH + HW_{10}O_{32}{}^{4-}] \rightarrow RO + W_{10}O_{32}{}^{4-} + H_2O$$
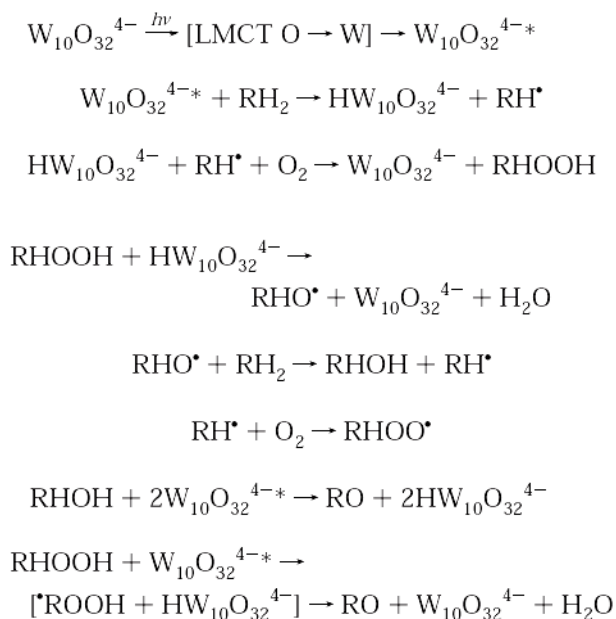
Scheme 1.6. General mechanism of $W_{10}O_{32}{}^{4-}$-mediated hydrocarbon photooxidation and radical intermediates species involved.

A very remarkable point in controlling the photoreactivity of polyoxotungstates in photocatalysis is the solvent effect, since its contribution gives radical species which react with the substrate and can elicit the autooxidation cycles. In water, the oxidation occurs through the production of highly reactive hydroxyl radicals OH· from the solvent activation routine, but it might override more selective pathways, originating within the substrate activation cycle, involving a direct interaction with the polyoxometalate photocatalyst[60][61][62]. The intervention of OH· as the dominant oxidant during photocatalysis in water is a matter of current debate, sustained by ESR experiments[63], product distribution and kinetic studies[54,64].

The main limit on the solvent choice is defined by its stability towards radicals. Acetonitrile is the most used, but acetone has also been employed[65]. Relative values of the rate constants for the reaction of the photocatalyst with propan-2-ol in acetone, acetonitrile, and water are 1/1.8/23[65].

In principle, the synthesis of photoactive polyoxometalate, can be controlled by a broad variety of parameters, among which are number and kind of metal addenda, central heteroatom, counterion. Despite the rich pool of complexes available, $W_{10}O_{32}{}^{4-}$ is the most extensively studied polyanion, even in heterogeneous conditions[53 a, b, d]. $(nBu_4N)_4W_{10}O_{32}$ has been successfully supported on silica, resulting in the immobilization of the polyoxoanion on the solid support through electrostatic interactions. The positive tetraalkylammonium cations likely act as a bridge between the negative surface of silica and the decatungstate.

Photoexcitation ($\lambda > 300$ nm) of powdered dispersion of the $(nBu_4N)_4W_{10}O_{32}/SiO_2$ system can promote the oxygenation of cyclohexane[53a] and cyclohexene[53d] at 20 °C and 1 atm. of O_2. Cyclohexane is oxidized to an equimolar mixture of cyclohexanol and cyclohexanone, while cyclohexene is converted into the corresponding cyclohexenyl hydroperoxide (about 90% of the overall oxidized substrate) and to cyclohex-2-en-1-one (about 6%).

Important aspects of the heterogeneous photocatalyzed process are the followings: (i) a broader range of dispersing medium can be employed; (ii) the photocatalyst can be reused several times without any significant loss of activity; (iii) the efficiency is comparable with that observed in homogeneous solution, sometimes with an even higher specific surface available; (iv) the catalytic support can drive the reaction selectivity through the occurrence of differential adsorption-desorption equilibria of reagents and intermediates.[66].

Polyoxometalates have also been used as a mean to heterogenieize cationic organic sensitizers (methylene blue (MB^+) and tris(2,2'-bipyridine)ruthenium(II) ($[Ru(bpy)_3]^{2+}$), by means of electrostatic interactions[38d]. The activity of such hybrid heterogeneous photocatalyst has been assessed in water, using visible light ($\lambda > 375$ nm) and oxygen (1 atm). To investigate the potential of the method for wastewater treatment, the photooxygenation of aqueous phenol solution (pH = 10.5) has been performed. With the complex $([Ru(bpy)_3])_2W_{10}O_{32}$[67], 84% of conversion of the initial phenol has been obtained with a turnover number (TON) = 45 and a loss of chemical oxygen demand (COD) = 29% in 150 minutes.

The use of multicomponent systems is an interesting strategy for controlling the photoreactivity of polyoxotungstates. As a further example, the presence of the porphyrin derivative $Fe^{III}(Cl)TDCPP$ dissolved, in catalytic amounts, in the reaction medium has been reported to improve yield and selectivity of cyclohexene oxidation by irradiated $(nBu_4N)_4W_{10}O_{32}$[68a]. In particular, the iron porphyrin induces an increase of quantum yield to give 1.6 ketone to alcohol ratio (instead of 4.1 with the decatungstate alone). The effect of the iron porphyrin has been ascribed to its ability to decompose allylic hydroperoxides to give the corresponding alcohols. As far as porphyrin stability is concerned, it has not been observed any appreciable bleaching of its UV-VIS spectrum, indicating that it does not undergo any significant degradation during the irradiation. This fact represents an important improvement with respect to the photocatalytic activity of the iron porphyrin alone[69].

In Chapter 2 of this Thesis, will be presented the use of an alternative and innovative medium as a fluorinated solvent and the heterogenization of the decatungstate in fluorinated

polymeric membranes to obtain a novel generation of heterogeneous photocatalysts with the ultimate aim to devise new selective systems for dioxygen activation.

1.2.6 Activation of hydrogen peroxide by polyoxometalates: the state of art.

Among oxygenation processes with hydrogen peroxide, those catalysed by high valent d^o transition metals are between the most important and selective[70].

Several research groups have studied the interaction between lacunary, transition metal substituted polyoxometalates or their parent Keggin anions and hydrogen peroxide[71]. Peroxotungstates have been used by Ishii and co-workers[72,73,74] who reported the use of a catalytic system employing polyoxoanions in phase transfer conditions, to perform selective epoxidations of olefins with hydrogen peroxide. In such conditions, the oxidant species in solution are dimeric peroxotungstate complexes like $\{PO_4[WO(O_2)_2]_4\}^{3-}$ [75], compounds also obtained by Venturello[76][77][78], Prandi[79] and Noyori[80,81]. Jacob presented a biphasic reaction with (aminomethyl) phosphonic and tungstic acids at pH 5 to epoxidize acid sensitive olefins[82]. A similar catalytic system has been recently used for heterogeneous sulfoxidations[83]. In contrast to monomeric or dimeric peroxo species, polynuclear peroxo species are expected to show specific reactivity and selectivity because of their electronic and structural characters. A number of Keggin type polyoxometalates were used to produce organic peroxides, with high selectivity, from cyclooctane, using lipophylic $XW_{12}O_{40}{}^{n-}$, $XW_{11}O_{39}{}^{n-}$, $XW_{11}VO_{40}{}^{n-}$, $XW_{11}M^{III}(H_2O)O_{40}{}^{n-}$ with X= Si, P, and M= Fe, Mn[84].

$(nBu_4N)_4W_{10}O_{32}$, was used to obtain the selective oxidation of alcohols to carboxylic acids and ketones with hydrogen peroxide[75f][85][86]. $H_2ZnSiW_{11}O_{40}{}^{6-}$ was used to oxidize alcohols in biphasic systems[87]. A polyfluorooxometalate complex, $[Ni(H_2O)NaH_2W_{17}O_{55}F_6]^{9-}$ [88] was also used to obtain epoxidation reactions with hydrogen peroxide.

In some cases, one or more peroxidic η^2-groups have been attached on a different transition metal ions: as in the case of $(Bu_4N)_5[PTi(O_2)W_{11}O_{39}]$, isolated by Poblet and Kholdeeva[89,90]. At variance, sandwich-like complexes containing Fe(III)[71d], Zn(II)[91], Pt(II), Pd(II), Rh(III)[92], Ru(III), Mn(II)[93], appeared stable and their reactivity, in the epoxidation of olefins and allyl alcohols, showed little dependence on the nature of the transition metal, so sustaining the hypothesis at the occurrence of W-peroxo groups. Peroxotungstic groups were indeed observed by FT-IR and ^{183}W-NMR analysis by Neumann and coworkers.

The most promising epoxidation catalysts belong to the vacant polyoxotungstates family. Acerete[94] and coworkers prepared and characterized by X-ray a peroxo-polyoxometalate: the

vacant Keggin polyanion $[CoW_{11}O_{39}]^{9-}$, grafted by four peroxo moieties to give $[CoW_{11}O_{35}(O_2)_4]^{10-}$.
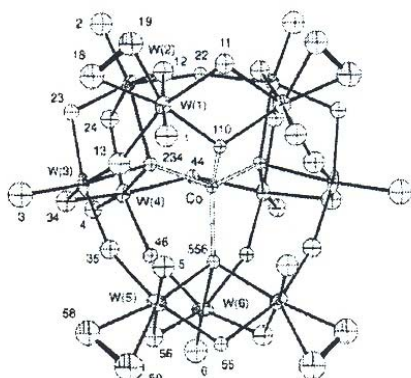
Figure 1.10. Structure of β_3-$[CoW_{11}O_{35}(O_2)_4]^{10-}$

This complex was used to epoxidize 2-cyclohexenol with hydrogen peroxide in a biphasic system.

| yield | 28.3% | 59.3% | 3.6% |
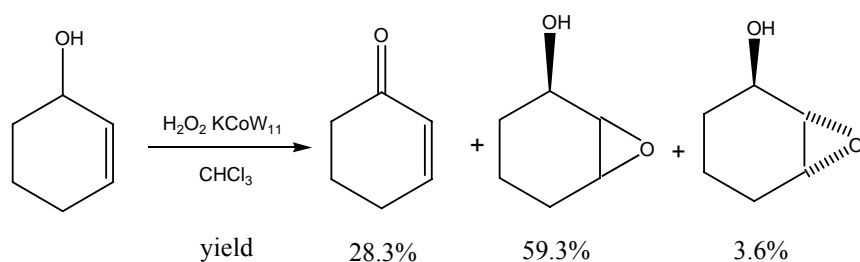
Recently, it has been reported that $Na_9[SbW_9O_{33}]$ in conjunction with a phase transfer catalyst (methyl tricapryl ammonium chloride) is a highly efficient catalytic system for the selective epoxidation of alkenes with aqueous H_2O_2 (yields up to 99%) in solvent-free conditions[95].

Mizuno and coworkers presented the benchmark performances of the decatungstosilicate[96] $[\gamma\text{-}SiW_{10}O_{34}(H_2O)_2]^{4-}$ for the epoxidation of olefins with high efficiency and selectivity, also giving an interesting regioselectivity when applied to diolefins[97]. The same complex has been used by Ren and coworkers to perform sulfoxidations, promoting the oxidation to sulfone in the presence of imidazole, and it has been heterogenized on ionic liquid-modified silica[98] [99].

Both cyclic olefins such cyclohexene, 1-methyl-1-cyclohexene, cyclooctene, cyclododecene, and 2-norbornene and non-activated terminal C_3-C_8 olefins such as propylene, 1-butene, and 1-octene could be transformed to the corresponding epoxides specifically with $\geq$ 99% selectivity and $\geq$ 99% efficiency of hydrogen peroxide utilization. 1,3-Butadiene was

epoxidized selectively to give the corresponding mono-epoxide, without the successive epoxidation of the other C=C fragment (i.e., no di-epoxide was formed).

Large-scale experiments (100 fold scaled-up) for propylene and 1-octene showed the same results as for the small-scale experiments.

The decomposition of hydrogen peroxide to form molecular oxygen was negligible, which reduces the risk of building an explosive atmosphere and simplifying the safety measures needed to insure it. Thus, the catalytic performance of this decatungstosilicate raises the prospect of an industrial application.

The functionality of lacunary polyoxometalates as a precursor of polynuclear peroxo species is an important issue since their vacant sites have the possibility to activate hydrogen peroxide[94]. The epoxidation of 1-octene with hydrogen peroxide catalyzed by a series of silicotungstates in acetonitrile at 32 °C has been examined. The vacant silicotungstates (*mono-*, *di-*, *tri-* and the saturated one, see Section 1.2.2) were converted to the corresponding tetra-*n*-butylammonium salts by the cation exchange reactions. A divacant lacunary silicodecatungstate $[\gamma\text{-SiW}_{10}\text{O}_{36}]^{8-}$ (**I**), showed moderate catalytic activity, whereas the other *mono-* and *tri*-vacant lacunary compounds, as well as a fully occupied dodecatungstosilicate, were almost inactive. The catalytic activity of **I** depended on the pH values upon the preparation of the corresponding tetra-*n*-butylammonium salts; the catalyst prepared at pH 2 (compound **I***) exhibited the highest activity, with the following yields after 6 h: 75% (pH 2), 52% (pH 1), >51% (pH 3, 4), >32% (pH 0). X-ray crystallographic structural analysis of **I*** was performed on a tetramethylammonium salt derivative, and the formulation of **I*** could be determined as $[\gamma\text{-SiW}_{10}\text{O}_{34}(\text{H}_2\text{O})_2]^{4-}$ involving two terminal W-(OH$_2$) (*aquo* ligand) fragments. Therefore, four protons are associated with the anionic cluster of **I***, as confirmed later by our research group by means of DFT calculations[100] (see Figure 1.11 A and B).

A   B
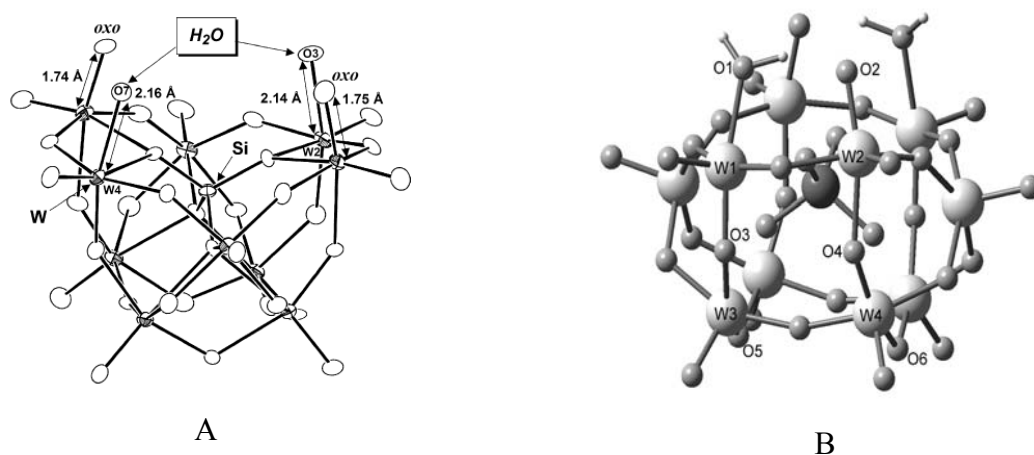
Figure 1.11.) X-ray crystallographic molecular structure determined by Mizuno et al.[96] (A) and DFT calculated optimized structure of $[\gamma\text{-SiW}_{10}\text{O}_{34}(\text{H}_2\text{O})_2]^{4-}$ [100] B).

19

Vacant phosphotungstates, as $Na_7PW_{11}O_{39}$, react with hydrogen peroxide to form $[PO_4\{WO(O_2)_2\}_4]^{3-}$. On the other hand, silicotungstates are rather stable in water compared with phosphotungstates and their chemistry has been well established by Tezé and Hervé[101].

The catalytic activity of **I*** for the epoxidation of 1-octene was compared with that of $[PO_4\{WO(O_2)_2\}_4]^{3-}$ and $[W_2O_3(O_2)_4(H_2O)_2]^{2-}$ with the same tungsten loading[75c, d, e 77 102]. In each case, the selectivity to 1,2-epoxyoctane was $\geq$ 99%, and **I*** showed the highest activity among the catalysts (yield after 10 h; **I***: 90%, $[PO_4\{WO(O_2)_2\}_4]^{3-}$: 38%, $[W_2O_3(O_2)_4(H_2O)_2]^{2-}$: 25%).

For the oxygenation of *cis-* and *trans-*2-octenes, the configuration around C=C moiety was retained in the corresponding epoxides. Moreover, in competitive reactions, *cis-*2-octene was oxygenated much faster than the *trans-* isomer. being the experimental ratio *cis/trans* 2,3-epoxyoctane 11.5. This value is higher than those obtained for the other tungstate-H_2O_2 systems[81] and for the stoichiometric epoxidation with organic oxidants such as *m*-CPBA[103] and dimethyldioxirane[104] as shown in Table 1.3.

Table 1.3. Comparison of R_{cis}/R_{trans} values for the competitive epoxidation of *cis-* and *trans-*olefins

System	Olefin	R_{cis}/R_{trans}
TBA- **I***/H_2O_2 [96]	*cis*-2-octene/*trans*-2-octene	11.5 [a]
$H_3PW_{12}O_{40}$/H_2O_2 [74]	*cis*-2-octene/*trans*-2-octene	3.7 [b]
$NH_2CH_2PO_3H_2$/WO_4^{2-}/H_2O_2 [81]	*cis*-3-octene/*trans*-3-octene	7.3
m-CPBA [103]	*cis*-2-octene/*trans*-2-octene	1.2
Dimethyldioxirane [104]	*cis*-3-hexene/*trans*-3-octene	8.3

[a] TBA- **I*** (8 µmol), *cis*-2-octene (5 mmol), *trans*-2-octene (5 mmol), 30% aq. hydrogen peroxide (1 mmol), CH_3CN (6 mL), 32 °C.
[b] $H_3PW_{12}O_{40}$ (8 µmol), cetylpyridinium chloride (24 µmol), *cis*-2-octene (1 mmol), *trans*-2-octene (1 mmol), 30% aq. hydrogen peroxide (3 mmol), $CHCl_3$ (5 mL), 60 °C.

Such a high stereospecific reactivity of **I*** suggests the contribution of a structurally rigid, non-radical oxidant generated on **I***. The authors were indeed able to isolate the di-peroxo species, where the two aquo ligands $W(H_2O)$ had been substituted by $W(O_2)$ groups[105].

The structural stability of **I*** was confirmed by observation of the reaction mixture with an in situ IR spectrometer. No substantial changes of spectral pattern were observed during the catalytic epoxidation by **I*** with hydrogen peroxide. On the other hand, a mixture of $H_3PW_{12}O_{40}$, hydrogen peroxide, and olefin exhibited a drastic change of spectral pattern due

to the conversion of $[PW_{12}O_{40}]^{3-}$ to $[PO_4\{WO(O_2)_2\}_4]^{3-}$. The contrast shows that a Si derivative of tetranuclear species (i.e. $[SiO_4\{WO(O_2)_2\}_4]^{4-}$) was not formed in the catalytic system of **I***, hydrogen peroxide, olefin, and acetonitrile. The kinetic study revealed the first-order dependence of the reaction rate on the concentration of **I*** (0.36 mM), supporting the idea. Finally, the catalyst **I*** could easy be recovered.

Another important approach in obtaining POM-based peroxidation catalysts is the complementary assembly of organic and inorganic molecular components. Beside the interest for their use to prepare novel hybrid frameworks with extended architectures[106], the merging of organic and inorganic domains produces a functional synergistic effect with the ultimate scope to improve the catalytic performance.

Our research group has reported on the screening of the reactivity of isostructural hybrid derivatives. The catalyst performance is strongly dependent on the structure/composition of the inorganic framework as well as on the nature of the organic moiety decorating the POM surface. Between the catalyst employed, the hybrid polyoxoanion $[(PhPO)_2SiW_{10}O_{36}]^{4-}$ has shown the oxidation of several class of substrates in halide-free solvent and in ionic liquids. Furthermore, the functionalization of the vacant site prevents the rearrangement of the POM structure[107]: stability studies by means of heteronuclear NMR and ESI-MS analyses have revealed that the complex is stable at higher temperature or under Microwave (MW) assisted activation[38a, b].

MW-induced dielectric heating is efficiently used by these poly-charged catalysts, behaving as MW-activated molecular heat carriers[108]. With $[(PhPO)_2SiW_{10}O_{36}]^{4-}$ and under MW irradiation, the oxidation scope has been expanded to include, in addition to highly reactive substituted olefins, alcohols, sulfides, and also electron-poor alkenes, ketones and sulfoxides. Indeed, the best performance has been obtained in the oxidation of internal olefins, secondary benzylic alcohols, and organic sulphur compounds with good to excellent yield of H_2O_2 conversion after 10-50 minutes of MW irradiation and 0.8% catalyst loading[38a].

A mechanistic study has been carried out to define the catalyst character. Competitive epoxidation of isomeric 2-hexenes have shown a reactivity ratio Z/E > 9. The Z preference speaks in favour of a POM-based peroxide as the competent oxidant[109]. Finally, the formation of a transient η^1-hydroperoxo intermediate via association equilibria of H_2O_2 to the POM precursor[110] has been suggested to explain the atypical biphilic behaviour found for Hammett linear free energy relationship[111 112].

The hybrid organic-inorganic catalytic complex $[(PhPO)_2SiW_{10}O_{36}]^{4-}$ has also been tested in ionic liquids (ILs) as alternative reaction media which can replaces hazardous volatile organic

solvents (VOCs)[38b]. ILs media have been successfully used for metal-catalyzed oxidations with peroxides[113][114][115], therefore the IL embedding of catalytically active polyanions, by a straightforward metathesis strategy, is expected to yield tailored functional phases[116].

Catalytic tests have been initially performed with *cis*-cyclooctene in both hydrophilic and hydrophobic ILs containing the 1-butyl-3-methylimidazolium cation [bmim$^+$], and different anions [BF$_4^-$], [CF$_3$SO$_3^-$], [PF$_6^-$], and [(CF$_3$SO$_2$)$_2$N$^-$] at 50 °C. The results obtained have revealed that a selective epoxidation with quantitative conversion of H$_2$O$_2$ (epoxide yields up to > 99%) is achieved in the more hydrophobic ILs, namely [bmim$^+$] [(CF$_3$SO$_2$)$_2$N$^-$] and [bmim$^+$] [PF$_6^-$], yielding respectively a maximum TOF of 5.7 and 3.5 TON/min, when the amount of water introuced into the reaction media is kept low. Since the presence of water is expected to impact the mass-transfer processes within the substrate/ILs/water multiphase system, a concentrated H$_2$O$_2$ solution has been used[38b].

A noteworthy implementation of the system has been achieved under MW irradiation. Indeed, the polyelectrolytic nature of the catalytic phase (hybrid-POM+IL) guarantees negligible vapour pressure, as well as fast and selective MW-induced heating by ionic conduction mechanism, even at low power (4-10 W). Under the condition explored, quantitative epoxidation has occurred in 1 minute, incrementing the TOF value by ca. 35 times with respect to the conventional heating, thus providing an innovative strategy for catalyst immobilization, activation and recovery[38b].

As a further steps towards the development of a novel generation of hybrid-POM-based catalysts, in Chapter 3 of this Thesis, it will be presented (i) the use of a fluorinated alcohol, as another alternative media, in the presence of a series of different fluorinated hybrid complexes; (ii) the heterogenization of such catalysts in a polymeric matrix, via the covalent grafting of unsaturated organic moieties on the polyanion.

1.3 Aim of the Ph. D. Thesis: Innovative oxidation processes.

The green chemistry revolution is providing a number of challenges to those who practice chemistry in industry, education and research, to develop new processes, products and services that achieve the social, economic and environmental benefits that are now required. With this challenges, there is also an equal number of opportunities to discover and apply new chemistry, to improve the chemical manufacturing and to enhance the much-tarnished image of chemistry.

This need a new approach to reduce materials and energy for chemical processes and products, through the discovery and the development of innovative synthetic pathways, using renewable feed–stocks and more selective chemistry, identifying alternative reaction conditions and solvents for improved selectivity and designing less toxic and inherently safer chemicals. In chemical synthesis, the ideal will be a combination of a number of environmental, health and safety, and economic targets (see Figure 1.12).
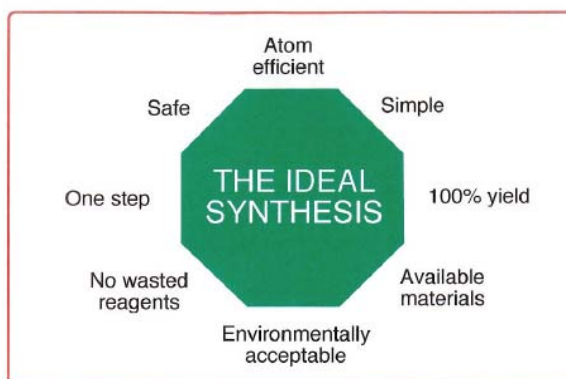
Figure 1.12. The ideal synthesis.

The drive towards clean technology in the chemical industry with an increasing emphasis on the reduction of waste at source will require a level of innovation and new technology that the chemical industry has not seen in many years; moreover mature chemical processes, that are often based on technology developed in the first half of the 20th century, may no longer be acceptable in these environmentally conscious days. This can be seen by considering the ever – escalating and various "costs of waste" (figure 1.13)[12].
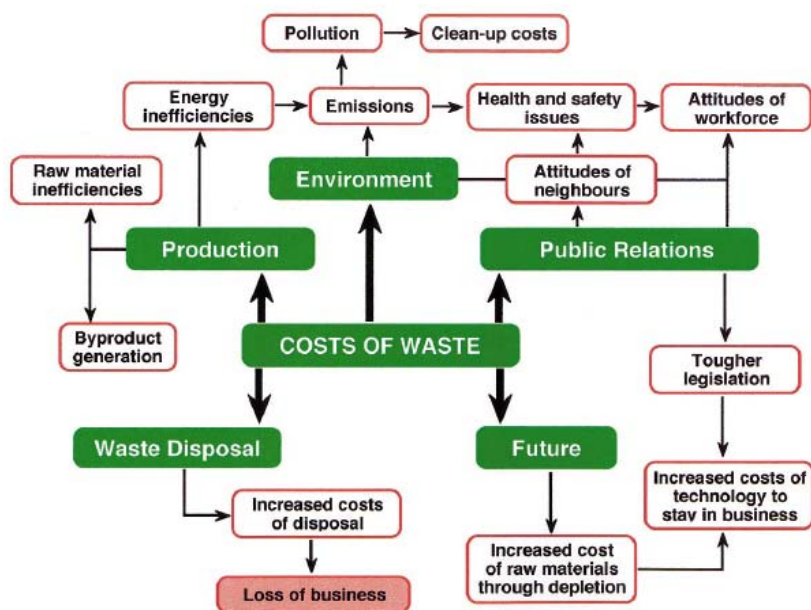
Figure 1.13. The costs of waste.

It is in this context that the study and development of innovative methodologies for chemical processes are very attractive perspectives for the industrial oxidation processes.

Different strategies have been used to implement benchmark oxidative transformations, and in all cases the research approach has been based on some key issues which involves not only the use of bulk oxidants with low environmental impact as dioxygen and hydrogen peroxide (see Section 1.1) but also:

i)   alternative reaction media such as perfluorinated environment,

ii)   non conventional techniques as microwave irradiation or photoirradiation,

iii) multiple catalysis technique, with sequential and/or parallel process (Concurrent Tandem Catalysis),

iv)   multi-metallic catalysts with thermal, hydrolytic and oxidative resistance, tailored functionality, solubility and prone to heterogenization on solid supports,

v)   heterogeneous catalysis techniques with polymeric or membrane-based hybrid organic – inorganic functional materials.

Developing new concepts or improving the existing ones is therefore more than just selecting the best of each field: it is the challenge to pick in each field those that will lead to the best possible combination and it is in this context that part of this Ph. D. Thesis will be developed (Chapter 2).

The project of the Thesis is aimed at design innovative oxidative routes as alternative to the traditional one (i.e.: those using stoichiometric amounts of permanganate, chromates, chlorine, or organic peracids). In particular, photocatalytic and catalytic systems, have been developed for the oxidation of different organic substrates, which are appealing in an industrial perspective, such as hydroxylation of saturated and aromatic hydrocarbons[117] or epoxidation of both terminal and internal olefins, using molecular oxygen[118] or hydrogen peroxide.

The use of polymeric films and supports has received particular attention, since selective affinity and mass-transport properties can be exploited to minimize or avoid the by-products formation[119]. The possibility to combine the membrane technology and the use of perfluorinated phases, as innovative reaction media for oxidative processes, is a very appealing issue, since the latter can promote the efficiency and selectivity of oxygen transfer reactions[120][121]. Moreover, the chemical inertness of perfluorinated reaction media and the easy way that they offer to separate reagents, products and catalytic species from the reaction mixture, are addition advantages to be considered[122]. Since the choice of the catalyst package has been established within the class of polyoxometalates (see Section 1.2), the research activity has been focused on the synthesis, characterization and catalytic activity of novel fluorous-tagged polyoxometalates by following two diverse synthetic approaches.

1.4 References and notes.

[1] C. Moreau, C. Dufraisse, *Chem. Rev.,* 7, **1926**, 113.

[2] N. A. Milas, *Chem. Rev.,* 10, **1932**, 295.

[3] J. L. Bolland, *Q. Rev., Chem. Soc.,* 3, **1949**, 1.

[4] L. Bateman, *Q. Rev., Chem. Soc.,* 8, **1954**, 147.

[5] J. –E. R. Bäckvall, in: *Modern Oxidation Methods,* WILEY-VCH, Weinheim, **2004**, Preface.

[6] A. K. Suresh, M. M. Sharma, T. Sridhar, *Ind. Eng. Chem. Res.,* 39, **2000**, 3958.

[7] W. F. Hoelderich, F. Kollmer, *Pure Appl. Chem.,* 72 (7), **2000**, 1273.

[8] S. Chiron, A. F. Alba, A. Rodriguez, E. G. Calvo, *Wat. Res.,* 34 (2), **2000**, 366.

[9] Y. I. Matatov-Meytal, M. Sheintuch, *Ind. Eng. Chem. Res.,* 37, **1998**, 309.

[10] F. Luck, *Catalysis Today,* 27, **1996**, 195.

[11] P. T. Anastas, J. C. Warner in: *Green Chemistry: Theory and Practice,* OXFORD UNIVERSITY PRESS, New York, **1998**.

[12] J. H. Clark, *Green Chemistry,* 1, **1999**, 1.

[13] C. L. Hill, I. A. Weinstock, *Nature,* 388, **1997**, 332.

[14] T. B. L. Kirkwood, *Nature,* 419, **2002**, 785.

[15] H. L. J. Bäckstrom, *J. Am. Chem. Soc.,* 49, **1927**, 1460.

[16] R. A. Sheldon, J. K. Kochi in: *Metal Catalyzed Oxidations of Organic Compounds,* ACADEMIC PRESS, New York, **1981**.

[17] I. Bertini, H. B. Gray, S. J. Lippard, J. S. Valentine in: *Bioinorganic Chemistry,* University Science Books: MILL VALLEY, CA, **1994**.

[18] J. S. Valentine, C. S. Foote, A. Greenberg, J. F. Liebman in: *Active Oxygen in Biochemistry,* St EDMUNDSBURY PRESS: London, **1995**.

[19] H. Sigel, A. Sigel in: *Metal Ions in Biological Systems,* MARCEL DEKKER Inc, New York, **1992**.

[20] C. L. Hill, *Nature,* 401, **1999**, 436.

[21] A. Hiskia, A. Mylonas, E. Papaconstantinou, *Chem. Soc. Rev.,* 30, **2001**, 62.

[22] M. T. Pope, A. Müller in *Heteropoly and Isopoly Oxometalates,* SPRINGER VERLAG, New York, **1983**.

[23] M. T. Pope, A. Müller, *Angew. Chem. Int. Ed.,* 30, **1991**, 34.

[24] C. L. Hill, *Polyoxometalates, Chem. Rev.* (Special Issue), 98, **1998**, 1.

[25] D. L. Kepert in: *The Early Transition Metals,* ACADEMIC PRESS Inc., London, **1972**.

[26] Y. P. Jeannin, *Chem. Rev.,* 98, **1998**, 51.

[27] W. N. Lipscomb, *Inorg. Chem.,* 4, **1965**, 132.

[28] O. Chen, J. Zubieta, *Coord. Chem. Rev.,* 114, **1992**, 107.

[29] J. F. Keggin, *Proc. R. Soc. London Scr. A.,* 144, **1934**, 75.

[30] R. Acerete, C. F. Hammer, L. C. W. Baher, *J. Am. Chem. Soc.,* 104, **1982**, 5384.

[31] R. Massart, R. Contant, J. M. Fruchart, J. P. Ciabrini, *Inorg. Chem.,* 11, **1977**, 2916.

[32] P. Judeinstein, C. Deprum, L. Nadjo, *J. Chem. Soc. Dalton Trans.,* **1991**, 1991.

[33] M. Filowitz, R. K. C. Ho, W. G. Klemperer, W. Shum, *Inorg. Chem.,* 18 (1), **1979**, 93.

[34] M. T. Pope in: *Comprehensive Coordination Chemistry,* G. Wilkinson, R. D. Gillard, J. A. McCleverty, Eds., PERGAMENON PRESS, New York, **1987**,Vol. 3, Chapter 38.

[35] F. Zonnevijlle, C. M. Tournè, G. F. Tournè, *Inorg. Chem.,* 21 (7), **1982**, 2742.

[36] J. Canny, A. Tézé, R. Thouvenot, G. Hervé, *Inorg. Chem.,* 25, **1986**, 2114.

[37] A. Müller, P. Kögerler, *Coord. Chem. Rev.,* 182, **1999**, 3.

[38] a) M. Carraro, L. Sandei, A. Sartorel, G. Scorrano, M. Bonchio, *Org. Lett.,* 8, **2006**, 3671. b) S. Berardi, M. Bonchio, M. Carraro, V. Conte, A. Sartorel, G. Scorrano, *J. Org. Chem.,* 72, **2007**, 8954. c) M. Bonchio, M. Carraro, G. Scorrano, E. Fontananova, E. Drioli, *Adv. Synth. Catal.,* 345, **2003**, 1119. d) M. Bonchio, M. Carraro, G. Scorrano, A. Bagno, *Adv. Synth. Catal.,* 346, **2004**, 648.

[39] H. Zeng, G. R. Newkome, C. L. Hill, *Angew. Chem., Int. Ed.,* 39, **2000**, 1772.

[40] P. Mason, *Degree thesis,* Università degli studi di Padova, A. A. **1998/1999.**

[41] C. R. Mayer, I. Fournier, R. Thouvenot, *Chem Eur.,* 6 (1), **2000**, 105.

[42] A. Proust, P. Gouzerh, F. Robert, *Inorg. Chem.,* 32, **1993**, 5291.

[43] M. Carraro, A. Sartorel, G. Scorrano, C. Maccato, M. H. Dickman, U. Kortz, M. Bonchio, *Angew. Chem. Int. Ed,.* **2008**, *47,* 7275 –7279.

[44] a) I. V. Kozhevnikov in: *Catalysis by Polyoxometalates,* WILEY-VCH, Chichester, **2002**. b) E. L. – M. Wong, R. W. –Y. Sun, N. P. –Y. Chung, C. –L. S. Lin, N. Yong, C. –M. Che, *J. Am. Chem. Soc.,* 128, **2006**, 4938.

[45] a) M. T. Pope in: *Isopoly and Heteropoly Anions,* SPRINGER, Berlin, **1983**. b) A. Müller in: *Polyoxometalate Chemistry,* KLUWER ACADEMIC, Dordrecht, **2001**. c) C. L. Hill, C. M. Prosser-McCartha, *Coord. Chem. Rev.,* 143, **1995**, 407. d) N. Mizuno, M. Misono, *Chem. Rev.,* 98, **1998**, 171. e) R. Neumann, *Prog. Inorg. Chem.,* 47, **1998**, 317.

[46] I. Bar-Nahum, R. Neumann, *Chem. Commun.*, **2003**, 2690.

[47] K. Yamaguchi, M. Kotani, K. Kamata, N. Mizuno, *Chem. Lett.*, 37 (12), **2008**, 1258.

[48] V. Kogan, Z. Aizenshtat, R. Popovitz-Biro, R. Neumann, *Org. Lett.*, 4 (20), **2002**, 3529.

[49] L. Emerson, L. G. Wistrand, *Acta Chem. Scand.*, 87, **1984**, 177.

[50] L. P. Ermolenko, C. Giannotti, *J. Chem. Soc. Perkins Trans.*, 2, **1996**, 1205.

[51] a) C. L. Hill, C. M. Prosser-McCartha in: *Photosensitization and Photocatalysis using Inorganic and Organometallic Compounds,* KLUWER ACADEMIC, Dordrecht, **1993**. b) E. Papaconstantinou, *Chem. Soc. Rev.*, 18, **1989**, 1. c) R. F. Renneke, M. Kadkbodayan, M. Pasquali, C. L. Hill, *J. Am. Chem. Soc.*, 113, **1991**, 8357. d) A. Maldotti, R. Amadelli, G. Varani, S. Tollari, F. Porta, *Inorg. Chem.*, 33, **1994**, 2968. e) D. C. Duncan, C. L. Hill, *J. Am. Chem. Soc.,* 119, **1997**, 243. f) C. Tanielan, K. Duffy, A. Jones, *J. Phys. Chem. B*, 101, **1997**, 4276.

[52] a) L. K. Kolkova, E. S. Rudakov, V. P. Tretyakov, *Kinet. Katal.*, 37, **1996**, 540. b) Y. Wu, X. Ye, X. Yang, X. Wang, W. Chu, Y. Hu, *Ind. Eng. Chem Res.*, 35, **1996**, 2546. c) R. Neumann, H. Miller, *Chem. Commun.* **1995**, 2277.

[53] a) A. Molinari, R. Amadelli, L. Andreotti, A. Maldotti, *J. Chem. Soc., Dalton Trans.* **1999**, 1203. b) A. Molinari, R. Amadelli, A. Mazzacani, G. Sartori, A. Maldotti, Langmuir, 18, **2002**, 5400. c) A. Maldotti, A. Molinari, G. Varani, M. Lenarda, L. Storaro, F. Bigi, R. Maggi, A. Mazzacani, G. Sartori, *J. Catal.*, 209, **2002**, 210. d) A. Molinari, R. Amadelli, V. Carassiti, A. Maldotti, *Eur. J. Inorg. Chem.,* **2000**, 91.

[54] E. Papaconstantinou, A. Mylonas, A. Hiskia, E. Androulaki, D. Dimotikali, *PCCP Phys. Chem. Chem. Phys.,* 1 (3), **1999**, 437.

[55] N. Mizuno, T. Watanabe, M. Misono, *J. Phys. Chem.,* 89, **1985**, 80.

[56] D. C. Duncan, T. L. Netzel, C. L. Hill, *Inorg. Chem.,* 34, **1995**, 4640.

[57] P. Argitis, E. Papaconstantinou, *E. Inorg. Chem.,* 25, **1986**, 4386.

[58] H. Soo, M. T. Pope, *Inorg. Chem.,* 11, **1972**, 1441.

[59] E. Papaconstantinou, A. Mylonas, *Polyhedron,* 15 (19), **1996**, 3211.

[60] M. A. Fox, R. Cardona, E. Gailard, *J. Am. Chem. Soc.,* 109, **1987**, 6347.

[61] C. L. Hill, D. A. Bouchard, *J. Am. Chem. Soc.,* 107, **1985**, 5148.

[62] M. Misono, H. Einaga, *Bull. Chem. Soc. Jpn.,* 70, **1997**, 1551.

[63] T. Yamase, R. Sasaki, T. Ikawa, *J. Chem. Soc., Dalton Trans.,* **1981**, 628.

[64] M. Bonchio, M. Carraro, V. Conte, G. Scorrano, *Eur. J. Org. Chem.,* **2005**, 4897.

[65] C. Tanielian, F. Cougnon, R. Seghrouchni, *J. Mol. Catal. A*, 262, **2007**, 164.

[66] A. Molinari, G. Varani, E. Polo, S. Vaccari, A. Maldotti, *J. Mol. Cat. A: Chem.*, 262, **2007**, 156.

[67] The crystal structure of $[Ru(bpy)_3]_2^{2+} [W_{10}O_{34}]^{4-}$ ·3 DMSO has been reported: Z. Han, E. Wang, G. Luan, Y. Li, C. Hu, P. Wang, N. Hu, H. Jia, *Inorg. Chem. Commun.,* 4, **2001**, 427-429.

[68] a) A. Maldotti, A. Molinari, P. Bergamini, R. Amadelli, P. Battioni, D. Mansuy, *J. Mol. Catal.,* 113, **1996**, 147. b) A. Molinari, A. Maldotti, R. Amadelli, A. Sgobino, V. Carassiti, *Inorg. Chim. Acta,* 272, **1998**, 197.

[69] a) A. Maldotti, C. Bartocci, G. Varani, A. Molinari, P. Battioni, D. Mansuy, *Inorg. Chem.*, 35, **1996**, 1126. b) A. Maldotti, L. Andreotti, A. Molinari, V. Carassiti, *J. Biol. Inorg. Chem.*, 4, **1999**, 154. c) A. Maldotti, A. Molinari, L. Andreotti, M. Fogagnolo, R. Amadelli, *Chem. Commun.* **1998**, 507.

[70] B. S. Lane, K. Burgess, *Chem. Rev.* 103, **2003**, 2457, and references therein cited.

[71] a) A. M. Khenkin, C.L. Hill *Mendeleev Commun.,* **1993**, 140. b) X. Zhang, Q. Chen, D.C. Duncan, R.J. Lachicotte, C.L. Hill, *Inorg. Chem.*, 36, **1997** 4381. c) X. Zhang, Q. Chen, D.C. Duncan, C.F. Campana, C.L. Hill, *Inorg. Chem.* 36, **1997**, 4208. d) X. Zhang, T.M. Anderson, Q. Chen, C.L. Hill, *Inorg. Chem.* 40, **2001**, 418. e) N. Mizuno,C. Nozaki,I. Kiyoto, M. Misono, *J. Am. Chem. Soc*, 120, **1998**, 9267. f) Y. Seki, J.S. Min, M. Misono, N. Mizuno, *J. Phys. Chem. B* 104, **2000**, 5940. g) N. Mizuno, Y. Seki, Y. Nishiyama, I. Kiyoto, M. Misono, *J. Catal.* 184, **1999**, 550. h) N.Mizuno, I. Kiyoto, C. Nozaki, M. Misono, *J.Catal.* 181, **1999**, 171.

[72] Y. Ishii, K. Yamawaki, T. Yoshida, T. Ura, H. Yamada, M. Ogawe, *J. Org. Chem.,* 52, **1987**, 1868.

[73] Y. Ishii, H. Tanaka, Y. Nishiyama, *Chem. Lett.,* 1, **1994**, 1.

[74] Y. Ishii, K. Yamawaki, T. Ura, H. Yamada, T. Yoshida, M. Ogawa, *J. Org. Chem.*, 53, **1988**, 3587.

[75] a) L.J. Csanyi, K. Jaky, *J. Mol. Catal.,* 61, **1990**, 75. b) L.J. Csanyi, K.Jaky, *J. Catal.,* 127, **1991**, 42. c) L. Salles, C. Aubry, R. Thouvenot, F. Robert, C. Dorémieux-Morin, G. Chottard, H. Ledon, Y. Jeannin, J.-M.Brégeault, *Inorg. Chem.,* 33, **1994**, 871. d) A.C. Dengel, W.P. Griffith, B.C. Parkin, *J. Chem. Soc. Dalton Trans.,* **1993,** 2683. e) A.J. Bailey, W.P. Griffith, B.C. Parkin, *J. Chem. Soc. Dalton Trans.,* **1995**, 1833. f) D.C. Duncan, R.C. Chambers, E. Hecht, C.L. Hill, *J. Am. Chem. Soc.*, 117, **1995**, 681.

[76] C. Venturello, E. Alneri, M. Ricci, *J. Org. Chem.,* 48, **1983**, 3831.

[77] C. Venturello, R. D'Aloisio, J.C. Bart, M. Riai, *J. Mol. Catal.,* 32, **1985**, 107.

[78] C. Venturello, R. D'Aloisio, *J. Org. Chem.,* 53, **1998**, 1553.

[79] J. Prandi, H. B. Kagan, H. Mimoun, *Tetrahedron Lett.,* 27, **1986**, 2617.

[80] K. Sato, M. Aoki, M. Ogawa, T. Hashimoto, R. Noyori, *J. Org. Chem.,* 61, **1996**, 8310.

[81] K. Sato, M. Aoki, M. Ogawa, T. Hashimoto, D. Panyella, R. Noyori, *Bull. Chem. Soc. Jpn.*, 70, **1997**, 905.

[82] A. L. Villa de P., B. F. Sels, D. E. De Vos, P. A. Jacobs, *J. Org. Chem.*, 64, **1999**, 7267.

[83] B. Karimi, M. Ghoreishi-Nezhad, J. H. Clark, *Org. Lett.*, 7, **2005**, 625.

[84] M.S. Balula, I.C.M.S. Santos, M.M.Q. Simões, M.G.P.M.S. Neves, J.A.S. Cavaleiro, A.M.V Cavaleiro *J. Mol. Catal. A: Chem.*, 222, **2004**, 159.

[85] Ming-Lin Guo, *Green Chem.* **2004**, *6*, 271.

[86] M. Schwegler, M. Floor, H. van Bekkum, *Tetrahedron Lett.*, 29, **1988**, 823.

[87] J. Wang, L. Yan, G. Li, X, Wang, Y. Ding, J. Suo *Tetrahedron Lett.*, 46, **2005**, 7023.

[88] R. Ben-Daniel, A.M. Khenkin, R. Neumann, *Chem. Eur. J.*, 6, **2000**, 3722.

[89] O.A. Kholdeeva, T.A. Trubitsina, R.I. A.V. Golovin, W.A. Neiwert, B.A. Kolesov, X. López, J.M. Poblet, *Inorg. Chem.*, 43, **2004**, 2284.

[90] T. Yamase, E. Ishikawa, Y. Asai, S. Kanai, *J. Mol. Catal. A: Chem.* **1996**,*114*, 237-245.

[91] P. T. Witte, P. L. Alsters, W. Jary, R. Mullner, P. Pochlauer, D. Sloboda-Rozner, R. Neumann, R., *Org. Process Res. Dev.,* 8, **2004**, 524.

[92] R. Neumann, A. M. Khenkin *J. Mol. Catal. A: Chem.*, 114, **1996**, 169.

[93] W. Adam, P. L. Alsters, R. Neumann, C. R. Saha-Möller, D. Sloboda-Rozner, R. Zhang, *J. Org. Chem.*, 68, **2003***, 1721.

[94] J. Server-Carrió, J. Bas-Serra, M. E. Gonzàlez-Nuñez, A. Garcìa-Gastaldi, G. B. Jameson, L.C. W. Baker, R Acerete *J. Am. Chem. Soc.*, 121, **1999**, 977.

[95] R. H. Ingle, N. K. Kala Raj, *J. Mol. Cat. A: Chem.*, 294, **2008**, 8.

[96] N. Mizuno, K. Kamata, K. Yonehara, Y. Sumida, K. Yamaguchi, S. Hikichi, *Science*, 300, **2003**, 964.

[97] K. Kamata, Y. Nakagawa, K.Yamaguchi, N. Mizuno, *J. Catal.*, 224, **2004**, 224.

[98] T. D. Phan, M. A. Kinch, J. E. Barker, T. Ren, *Tetrahedron Lett.*, 46, **2005**, 397.

[99] K. Yamaguchi, C. Yoshida, S. Uchida, N. Mizuno, *J. Am. Chem. Soc.*, 127, **2005**, 530.

[100] A. Sartorel, M. Carraro, A. Bagno, G. Scorrano, M. Bonchio, *Angew. Chem. Int. Ed.*, 46, **2007**, 3255.

[101] A. Tezé, G. Hervé, *Inorg. Synth.*, 27, **1990**, 85.

[102] K. Kamata, K. Yamaguchi, S. Hikichi, N. Mizuno, *Adv. Synth. Catal.*, 345, **2003**, 1193. b) K. Kamata, K. Yamaguchi, N. Mizuno, *Chem. Eur. J.*, 10, **2004**, 4728.

[103] S. Ueno, K. Yamaguchi, K. Yoshida, K. Ebitani, K. Kaneda, *Chem. Commun.*, **1998**, 295.

[104] A. L. Baumstark, P. C. Vasquez, *J. Org. Chem.*, 53, **1998**, 3437.

[105] N. Mizuno, K. Kamata,M. Kotani, K. Yamaguchi, S. Hikichi, *Chem. Eur. J.*, 13, **2007**, 639.

[106] a) M. Antonietti, M. Niederberger, B. Smarsly, *Dalton Trans.*, **2008**, 18. b) C. Sanchez, G. J. de A. A. Soler-Illa, F. T. Ribot, T. Lalot, C. R. Mayer, V. Cabuil, *Chem. Mater.,* 13, **2001**, 3061. c) C. Sterb, D. L. Long, L. Cronin, *Chem. Commun.,* **2007**, 471.

---

[107] Non functionalized lacunary POMs evolve to saturated W_{12}-derivatives under MW-assisted catalysis.

[108] B. A. Roberts, C. R. Strauss, *Acc. Chem. Res.,* 38, **2005**, 653.

[109] This value is similar to that obtained with the parent catalyst $[\gamma\text{-SiW}_{10}O_{34}(H_2O)_2]^{4-}$ (13.9) [97]. See also: Y. Goto, K. Kamata, K. Yamaguchi, K. Uehara, S. Hikichi, N. Mizuno, *Inorg. Chem.,* 45, **2006**, 2347.

[110] R. Prabhakar, K. Morokuma, C. L. Hill, D. G. Musaev, *Inorg. Chem.,* 45, **2006**, 5703.

[111] V. Conte, F. Di Furia, G. Modena in: *Organic Peroxides;* W. Ando, JOHN WILEY & SONS, Cheichester, **1992**, 559.

[112] a) M. Bonchio, S. Campestrini, V. Conte, F. Di Furia, S. Moro, *Tetrahedron,* 51, **1995**, 12363. b) K. A. Vassell, J. H. Espenson, *Inorg. Chem.*, 33, **1994**, 5491.

[113] J. Muzart, *Adv. Synth. Catal.*, 348, **2005**, 275 and references cited therein.

[114] V. Conte, B. Floris, P. Galloni, A. Silvagni, *Pure Appl. Chem.*, 77, **2005**, 1575.

[115] V. Conte, B. Floris, P. Galloni, A. Silvagni, *Adv. Synth. Catal.*, 347, **2005**, 1341.

[116] W. Miao, T. H. Chan, *Acc. Chem. Res.*, 39, **2006**, 897.

[117] G. Centi, S. Perathoner, *Catal. Today,* **2003,** *77*, 287-297.

[118] T. Punniyamurthy, S. Velusamy, J.Iqbal *Chem. Rev.* **2005,** 105; 2329.

[119] I. F. J. Vankelecom, *Chem. Rev.*, 102, **2002**, 10.

[120] A. Berkessel, J. A. Adrio *Adv. Synth. Catal.,* 346, **2004**, 275.

[121] a) K. Neimann, R. Neumann *Org. Lett.* **2000**, *2*, 2861-2863. b) S. P. de Visser, J. Kaneti, R. Neumann, S. Shaik, *J. Org. Chem.*, 68, **2003***,* 2903.

[122] C. Rocaboy, W.Bauer, J. A. Gladysz, *Eur. J. Org. Chem.*, **2000**, 2621.

2. Hybrid photocatalytic membranes embedding decatungstate for heterogeneous photooxygenation

2.1 Introduction.

Photocatalytic oxygenation represent a key strategy for the development of new sustainable methods for chemical transformations[1] [2]. They are of interest for the selective oxidation of organic substrates or for their full mineralization and therefore for the development of new photo-assisted synthesis or advanced oxidation processes (AOPs) applied to the environmental remediations[3] [4] [5].

The combined use of photoactivation techniques and dioxygen respond to environmental concerns, depending on the photocatalyst performance which, ideally, should:

  i)   undergo photoexcitation employing sunlight at room temperatures,

  ii)   promote fast and selective processes,

  iii)   activate dioxygen to form reactive oxygenated species,

  iv)   be stable, and easily recyclable for multi-turnover processes.

In this context, the design of innovative photooxygenation systems employing visible light, oxygen, mild temperatures, and aqueous or solvent-free conditions is a timely field of investigation[6] [7]. In particular, heterogeneous photooxidation on semiconductor surfaces like titanium dioxide (TiO_2) is receiving considerable attention[1] [2]. Related studies have been focusing on the advanced tuning of several parameters, ranging from crystallographic and morphological features, resulting in the preparation of nanostructured[8], doped and derivatized materials [2]. This latter approach aims at the invention of new hybrid systems where the merging of organic and inorganic domains exploits a functional synergistic effect for improving the catalytic performance[9] [10].

Polyoxometalates (POMs), have been referred to as "molecular fragments" or as the homogeneous analogues of photoactive semiconductor metal oxides[2] [11] [12] [13].

Furthermore, the activity of polyoxotungstates in promoting the photocatalytic oxygenation of organic substrates is well documented, both in organic solvents and in aqueous-phase[14] [15].

In particular, the photocatalytic properties of the decatungstate anion $W_{10}O_{32}{}^{4-}$ have been extensively studied in acetonitrile solution[16] [17] [18] [19] [20] and also applied to photooxygenations performed in water [19] [21] [22]. Its UV-Vis spectrum shows an absorption maximum at 324 nm, corresponding to a locally excited ligand – to – metal charge - transfer (LMCT) transition.

The overlap with the UV solar emission, opens the potential for environmentally benign solar-photoassisted applications[19][20].

Upon irradiation in the range of 350 – 400 nm, the complex is promoted to an excited state ($W_{10}O_{32}^{4-*}$) which decays in a very short time (less than 30 ps) to an extremely reactive transient ("wO") featuring a radical character. This latter happens to be the competent photoreactant[20], being able to initiate radical chain oxidations via hydrogen abstraction (HA) or electron transfer (ET) mechanism[23][24][25][26] (Scheme 1).
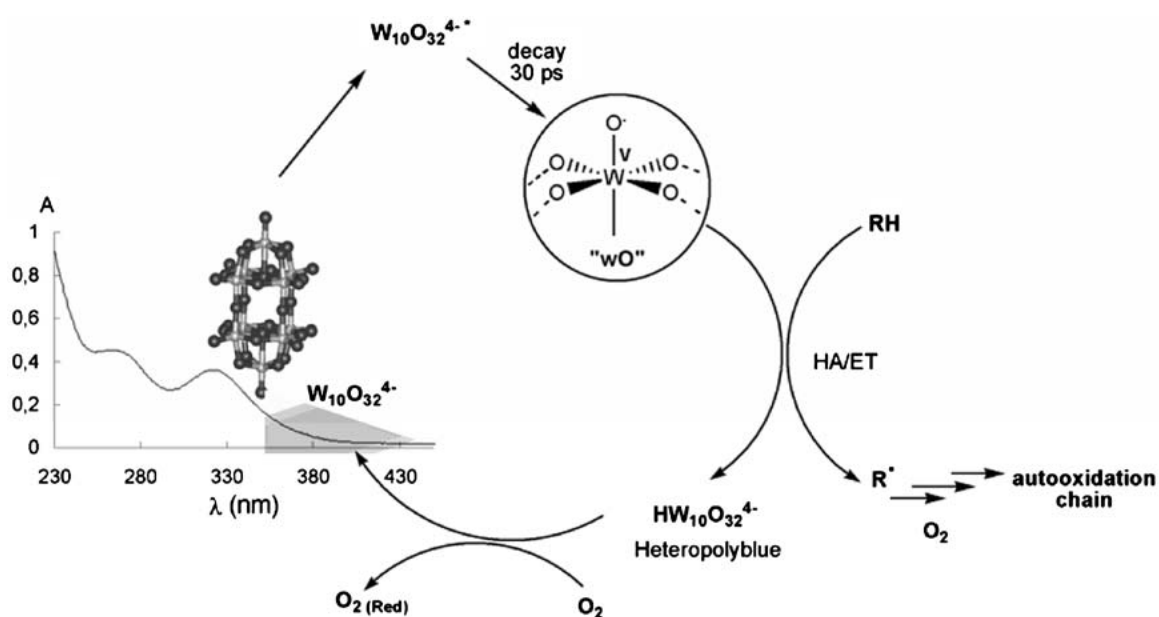
Scheme 2.1. Structure, UV-Vis spectrum, irradiation wavelength region and photocatalytic behavior of [$W_{10}O_{32}^{4}$].

In the catalytic scheme, dioxygen:
  i)   intercepts the organic radicals giving rise to autooxidation chains,
  ii) provides to the re-oxidation of the heteropolyblue complex ($W_{10}O_{32}^{5-}$ or $HW_{10}O_{32}^{4-}$),
  iii) evolves to reactive oxygenated species i.e.: hydroperoxide species (dioxygen reduction)[27][28][29].

The main drawback of POM-based photocatalysis lies in the low quantum yields Φ (in the range 0.1 - 0.5)[17][18], associated to a limited absorption in the most desirable visible range (Scheme 1). High photocatalyst/substrate ratios are thus generally required to obtain fast and efficient oxygenation cycles.

A point of interest in using POMs as photocatalysts is that, by counterion metathesis, the photo-assisted reaction can be easily performed in a wide range of different media, including aqueous phases.

The effect of the chemical environment assisting the photooxidation events of the catalytic cycle, is a key issue related to some fundamental aspects, such as:

i)   the lifetime of the photoactive transient,

ii)   the impact of solvent-derived reactive radicals (like hydroxyl radicals OH$^\bullet$ from water)[26],

iii)   dioxygen availability,

iv)   catalyst heterogenization.

This latter approach, has been recently pursued via the synthesis of hybrid materials. Three main classes of POM-based hybrids can be obtained depending on the linkage between the organic and inorganic components, specifically: a) covalent bonds, b) electrostatic anion/cation interactions, c) hydrogen bonds or Van der Waals contacts[30].

Hybrid POM-based photocatalysts belonging to the first two types, have been synthesized in our laboratories via the incorporation either of a covalently anchored fullerene moiety or cationic sensitizers like methylene Blue and tris-(2,2'-bipyridine) ruthenium (II) [Ru(bpy)$_3$]$^{2+}$ [31].

The third and last method, has been exploited to integrate the catalyst with target materials, as, for example, for the preparation of hybrid polymeric films or membranes with embedded polyoxometalates[32].

2.2. Hybrid photocatalytic membranes as new heterogeneous catalysts.

The design of new catalytic membranes retains a major interest. The application of membrane technology in catalysis offers the combination of advanced molecular separation, selective transport properties and reactivity. This opportunity, in addition to the obvious advantage of multi-turnover recycling, associated to heterogeneous supports, points to the design of innovative catalytic membrane reactors (CMRs), in order to allow catalyst compartmentalization, phase transfer catalysis, selective supply/removal of solvents, reagents, products and by-products[33].

Interesting examples of catalytic membranes have been reported for the heterogenization of catalysts like "zeozymes", Ti – Catalysts and heteropolyacids in selective red-ox processes and of several metal transition complexes[33].

POM immobilization on membranes can indeed be tuned by a proper choice of both the polymeric material and the catalyst precursor, in order to guarantee:

i)   structure integrity,

ii)   good dispersion,

iii)   active site accessibility,

iv)   transparency to UV-Vis irradiation,

v)   hydrothermal and chemical stability and resistance.

Moreover, the nature of the polymer and of the resulting hybrid membrane can be varied to tailor the hydrophobic/hydrophilic surface properties and its affinity towards target reagents.

The incorporation of decatungstate within polymeric membranes (polysulfone PS, polyether-etherketon PEEK-WC, polyvinylidene difluoride PVDF, polydimethylsiloxane PDMS), has been reported in order to obtain a novel class of heterogeneous photocatalysts with tunable composition and structural/surface properties[32].

These catalytic systems have been applied for the aerobic photooxidation of alcohols in aqueous media. A proper choice of the starting materials and of the blending parameters has been shown to impact the functional material in terms of hydrothermal and chemical stability, catalyst dispersion, transparency to UV-Vis irradiation, hydrophobic/hydrophilic surface character and selective mass transport of reagents and products including dioxygen[32].

2.2.1 Fluoro-polymeric membranes embedding a fluorous – tagged decatungstate.

Despite the remarkable advantages of perfluorocarbon inertness, the high solubility of oxygen in fluorinated solvents and the occurrence of fluorine-based peroxide activation [34], photocatalysis with POMs in fluorous environment is unprecedented.

Because of the environmental impact of perfluorinated solvents, along with their relative high costs, the innovations in this field are moving towards the concept of fluorous phase catalysis without fluorinated solvents[35].

In this context, perfluoropolymers offer several advantages when compared to other polymeric materials[36]. Besides their outstanding thermal and oxidative resistance, the peculiar nature of C-F bonds confers to these materials some unique physical-chemical properties that
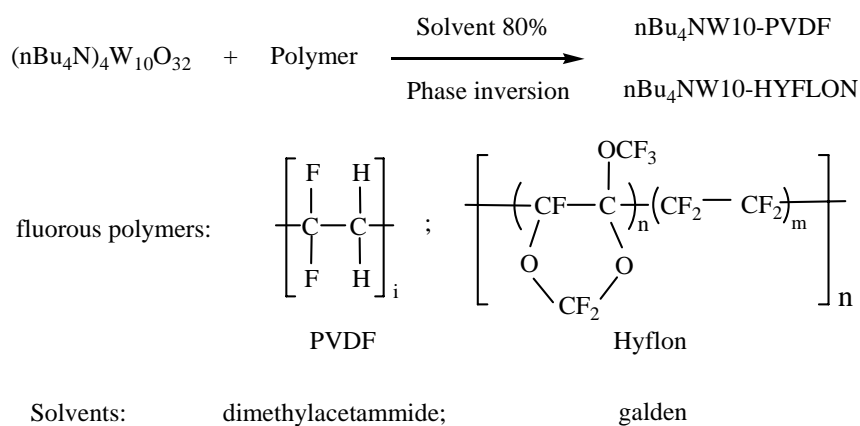
have been valuably exploited for gas separation and storage technologies[36]. In addition, the preferential permeability of dioxygen in fluorinated membranes has been reported[37].

In this Thesis, the preparation and characterization of new perfluorinated photocatalytic membranes incorporating decatungstate will be presented. The embedding of a fluorous-tagged decatungstate $(RfN)_4W_{10}O_{32}$, - where RfN is the ammonium fluorophilic counterion $[CF_3(CF_2)_7(CH_2)_3]_3CH_3N^+$ - within fluoropolymeric films, will be described as a method to optimize the membrane preparation. Results include stability studies under photoirradiation and the application of the resulting materials for heterogeneous photooxidation in the absence of organic solvents. A direct comparison between the membrane-based processes and the homogeneous counterpart will be addressed in terms of efficiency and selectivity. Moreover, the reactivity trend observed in the heterogeneous process will be correlated to the membrane structural and surface properties, as well as to the fluorine content.

2.3 Results and discussion

At first, the photooxygenation process has been studied using the lipophilic salt of decatungstate obtained by exchanging sodium cations in the presence of tetrabutylammonium bromide (nBu_4NBr). The resulting polyanion, with formula $\{[CH_3(CH_2)_3]_4N\}_4W_{10}O_{32}$, has been characterized both in solid state and in solution of CH_3CN and then it has been embedded in fluorinated membranes, obtained from polyvinylidene fluoride (PVDF) or from a co-polymer of 2,2,4-trifluoro-5-trifluoromethoxy-1,3-dioxole and tetrafluoroethylene (Hyflon AD 60X[®,] a copolymer of tetrafluoroethylene and 2,2,4-trifluoro-5-trifluoromethoxy-1,3-dioxole) by the inversion phase method (see Scheme 2), consisting in the preparation of a dense mixture of polymer and catalyst in the solvents, followed by the casting of such mixture on a surface and immersion in a water bath.

The hybrid polymeric films thus prepared (nBu_4NW10-PVDF and nBu_4NW10-Hyflon) have been analyzed by Scanning Electron Microscopy (SEM) in Back Scattered Electrons (BSE) mode. SEM images, collected both for the surface and the cross-section, highlight the clustering phenomena (white spots, with particles of different μm) due to the low solubility of the complex in the casting mixture[32 38], resulting in membranes with low catalytic activity .

$(nBu_4N)_4W_{10}O_{32}$ + Polymer $\xrightarrow[\text{Phase inversion}]{\text{Solvent 80\%}}$ nBu₄NW10-PVDF

nBu₄NW10-HYFLON

fluorous polymers:

$$\begin{bmatrix} F & H \\ | & | \\ C - C \\ | & | \\ F & H \end{bmatrix}_i \quad ; \quad \left[\left(CF - C \atop \substack{| \\ O} \right)_n (CF_2 - CF_2)_m \right]_n$$

PVDF   Hyflon

Solvents: dimethylacetammide;   galden

Scheme 2.2. Preparation of hybrid membrane embedding $(nBu_4N)_4W_{10}O_{32}$.

1-A   1-B

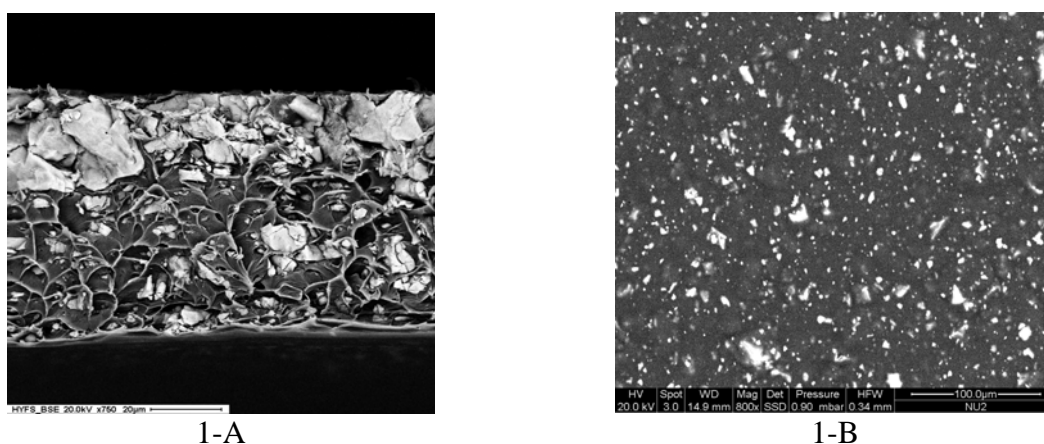**Figure 2.1. SEM-BSE images of the cross-section (A) and of the surface (B) of nBu₄NW10-Hyflon membrane.**

2.3.1 Hyflon® membranes characterizations.

In order to improve the affinity of the inorganic photocatalyst for the fluorinated phase used for the casting blend of the membrane, decatungstate has been isolated as a fluorophilic salt, by methatesis with a fluorous-tagged counterion, as reported on the following scheme:


$4 \ [CF_3(CF_2)_7CH_2CH_2CH_2]_3N^+CH_3$

counterion metathesis
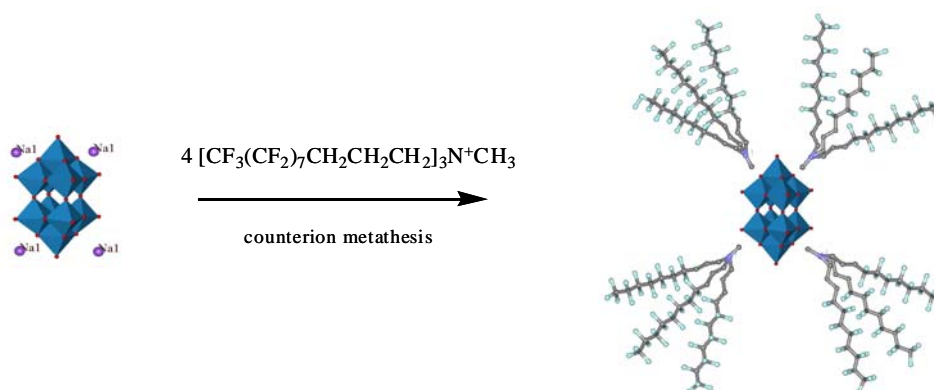
Scheme 2.3. Preparation of $\{[CF_3(CF_2)_7CH_2CH_2CH_2]_3NCH_3]\}_4W_{10}O_{32}$ (RfNW₁₀O₃₂) via counterion metathesis.

The fluorous-tagged cation RfN (see Section 2.2.1) has been synthesized following a literature procedure by reductive amination of the corresponding aldehyde[39] (see Experimental part at section 5.3.1).

As reported for $(nBu_4N)_4W_{10}O_{32}$, fluorophilic $(RfN)_4W_{10}O_{32}$ has been conveniently isolated from the sodium salt, by counterion metathesis with the fluorous ponytailed ammonium cation RfN, which allows its solubilization in 1,1,1,3,3,3-hexfluoro-2-propanol (HFIP) alone or in mixture with perfluorocarbons.

The fluorous-tagged photocatalyst has been characterized in solution and on membrane. In HFIP, the expected ^{183}W and ^{19}F NMR spin system have been obtained as showed in the Figure 2 here below:

A

B
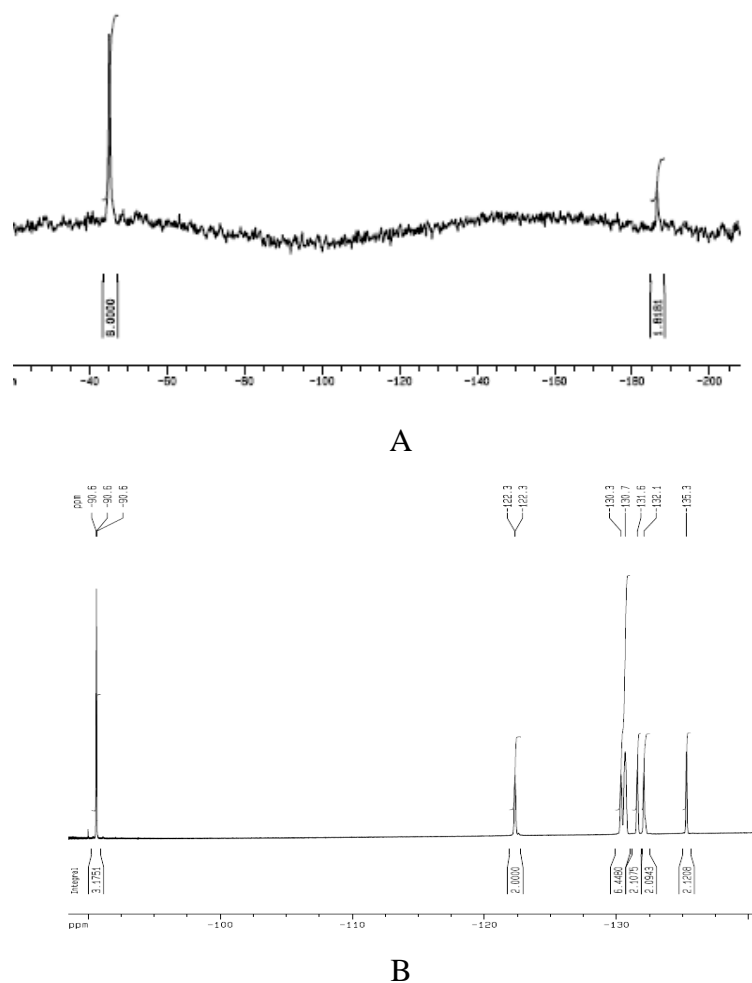
Figure 2.2. A) ^{183}W-NMR in HFIP/d2-HFIP and B) ^{19}F NMR in HFIP/d_2-HFIP with solvent suppression, of RfN$_4$W$_{10}$O$_{32}$. Structure of both the inorganic complex and the fluorinated cation are maintained in HFIP solutions.

It is possible to observe that [183]W-NMR presents two signals in ratio 8:2, in agreement with the D_{4h} symmetry of the decatungstate, while ^{19}F-NMR, presents the signals due to the eight non equivalent Fluorine atoms.

The resulting complex has been embedded in Hyflon®, upon dispersion with the polymer in a mixture HFIP-Galden, yielding flat hybrid membranes, RfNW10-Hyflon, by phase inversion techniques[32 38 40 41].
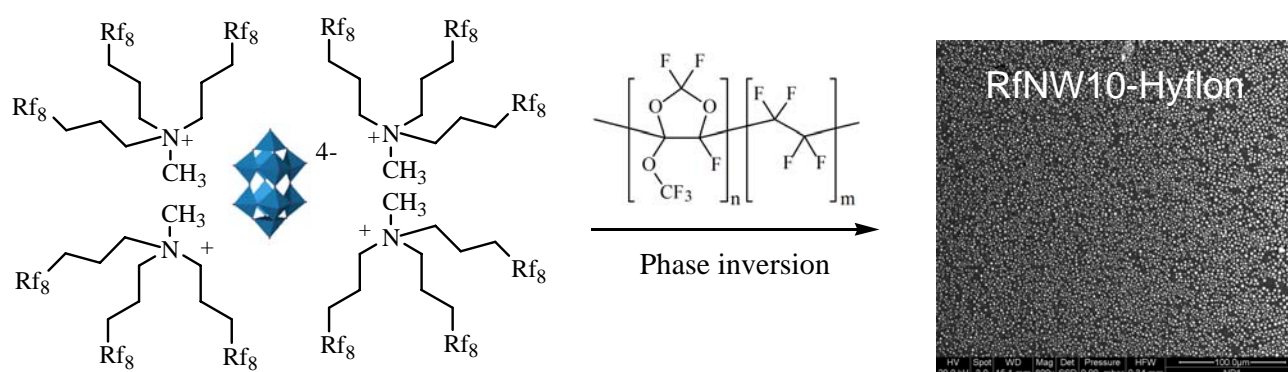
Scheme 2.4. Preparation of RfNW10-Hyflon membranes containing RfN$_4$W$_{10}$O$_{32}$ and surface BSE-SEM image.

Scanning electron microscopy (SEM) of the film surface and cross-section highlights a well dispersed, homogeneous distribution of the catalyst domains which appear as spherical particles of approximately 1-2 μm in diameter.(see Figure 3).

2-A   2-B
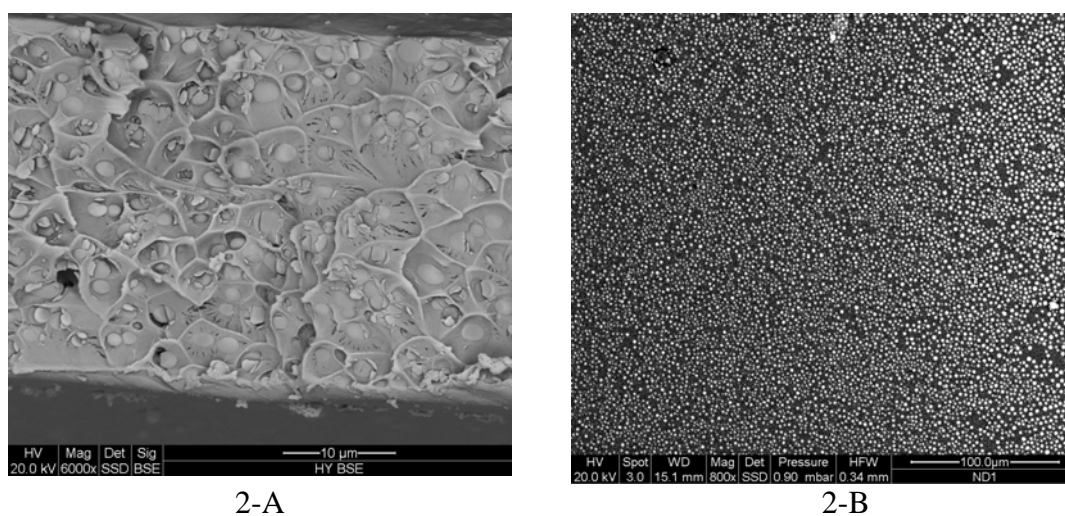
Figure 2.3. SEM-BSE images of the cross-section (A) and of surface (B) of RfNW10-Hyflon membrane.

This represents a remarkable improvement of the material morphology, in comparison with PVDF or Hyflon embedding the fluorous-free catalyst $(nBu_4N)_4W_{10}O_{32}$ [32][42].

UV-Vis spectra (Figure 4) have confirmed that the structural and spectroscopic features of the photoactive complex are preserved inside the polymeric film, where only a modest broadening of the charge transfer band (λ_{max} = 324 nm) is observed with respect to the homogeneous solution in HFIP or in CH_3CN.
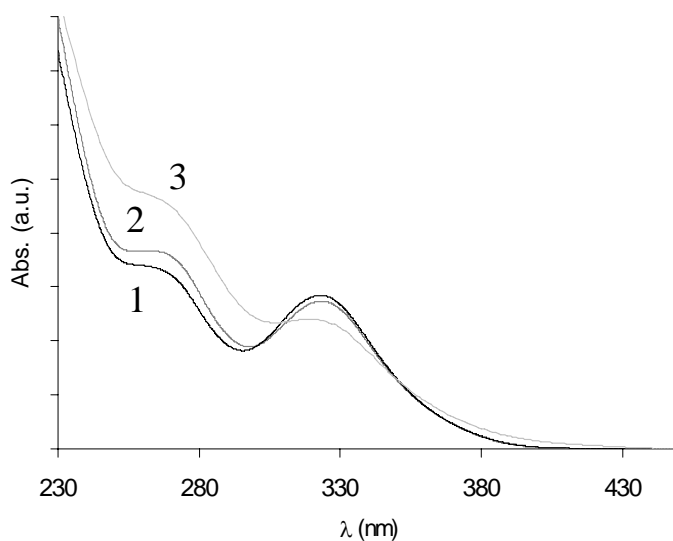
Figure 2.4. UV-Vis spectra of RfN$_4$W$_{10}$O$_{32}$ in HFIP 0.3 mM (1), in CH$_3$CN 0.3 mM (2) and of RfNW10-Hyflon with 25% w/w loading

The formation of such kind of macroaggregates observed by SEM-BSE analysis, has been described in the literature. Surfactant encapsulated polyoxometalates can indeed form spherical onion-like vesicles[43], through formation of alternate layers of polyanion and packed hydrophobic cations. In figure 5 it has been reported, as an example, the formation of regular aggregates with diameter of 500 μm, containing $SiW_{12}O_{40}{}^{4-}$ and dimethyldioctadecylammonium cation (DODA).

A   B
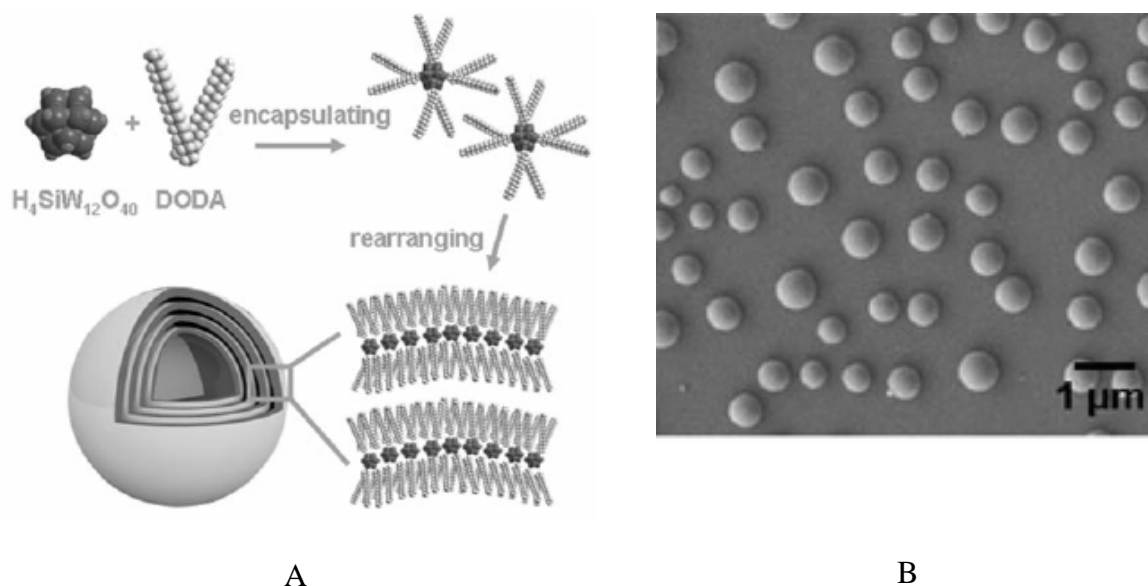
Figure 2.5. A) Assembly mechanism of amphiphilic POM/surfactant systems in organic solvents and at air/water interface. B) SEM characterization of the spherical assemblies.

Since the fluorophilic counterion is highly hydrophobic, it could promote a similar aggregation mechanism in the casting solution. The self-assembly of photoactive component in organized domains within the polymeric material is an important issue to understand and tune structural and superficial properties of the final hybrid membrane.

   Dynamic Light Scattering (DLS) measurements have thus been recorded to evaluate self-assembly phenomena for $RfN_4W_{10}O_{32}$ in HFIP solutions at different concentrations, but in conditions similar to those employed for the preparation of the casting mixture. Results are reported in Figure 6 and indicate the formation of spherical assemblies with hydrodynamic diameters ranging from 100 to 200 nm depending on the solution concentration.
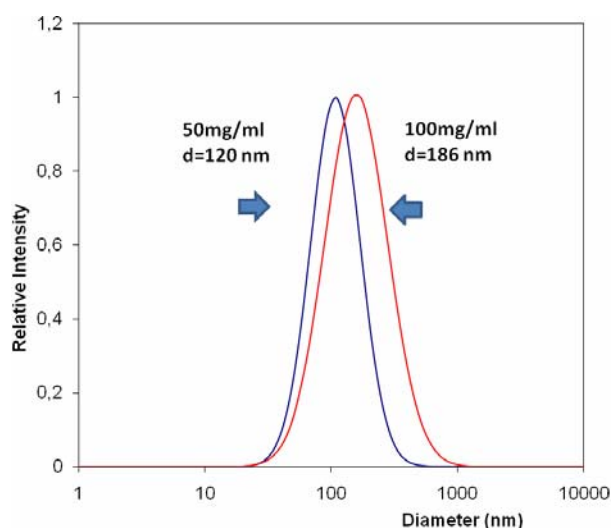
Figure 2.6. DLS results of $RfN_4W_{10}O_{32}$ in HFIP at different concentrations.

These spherical assemblies formed in solution are evolving to more extended inorganic domains during the separation process of the polymeric film. (See Figure 3B).

Furthermore, Atomic Force Microscopy (AFM) measurements recorded for RfNW10-Hyflon surface, reveals the porous morphology of the material, that shows cavities with average diameter of about 200 nm. (See. Fig. 7).

A

B

C

D
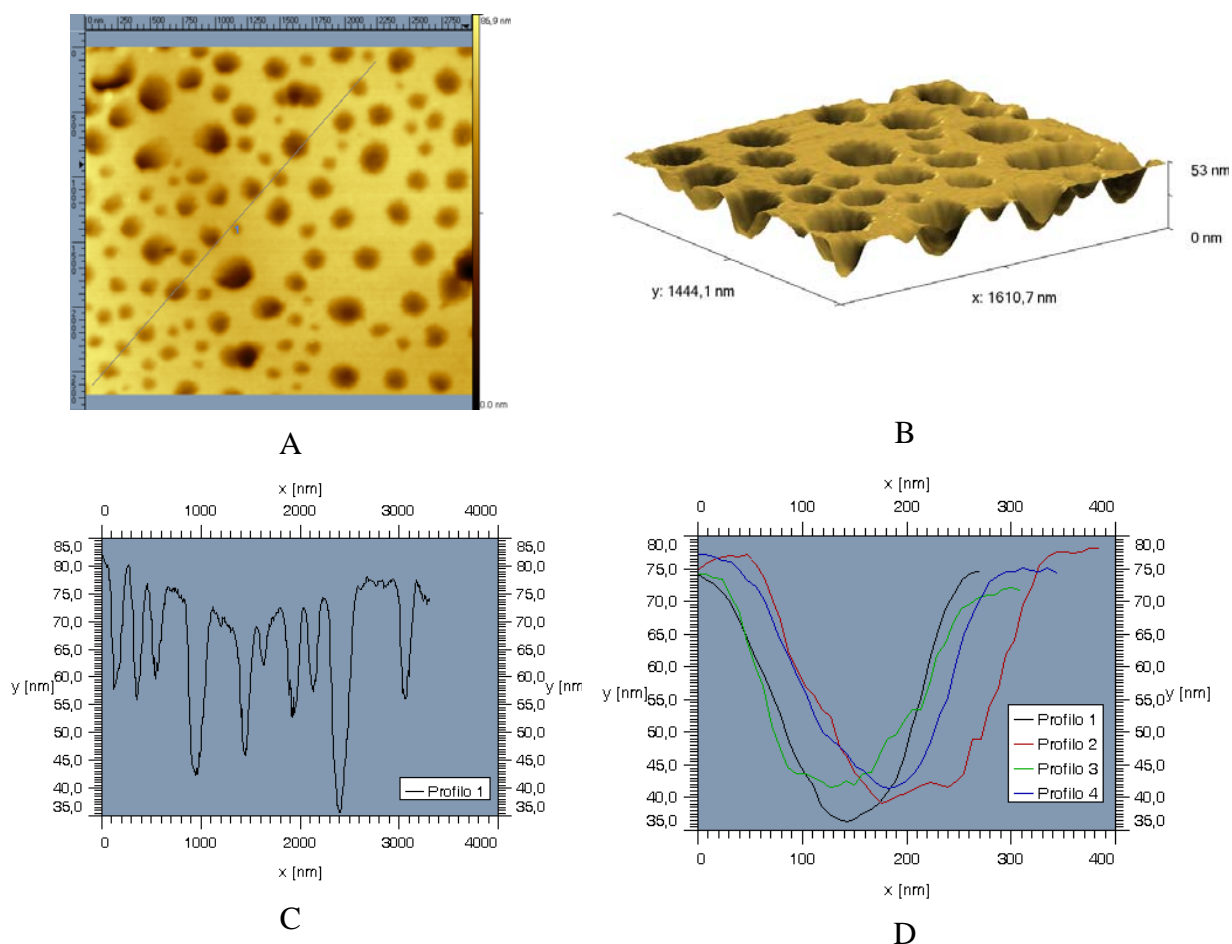
Figure 2.7. A-B) AFM measurements highlighting porous morphology of RfNW10-Hyflon membrane (thickness: 7 μm, 25% w/w loading) dimensional profiles C - D) for the superficial cavities recorded.

This behaviour can be explained admitting that water droplets may act as a template for the formation of self-organized microporous structures, before their evaporation. The process has already been described in the literature for a series of surfactant-encapsulated polyoxometalates complexes (SECs)[43] for which the formation of a porous film has been obtained through evaporation of a solution containing chloroform and POM, in a humidity-controlled atmosphere. Porous membranes can result from the condensation of water droplets on the polymeric film surface occurring upon evaporation of the casting solvent. In this case,

water droplets happen to be stabilized through a network of hydrogen bonds with the negatively charged oxygen atoms on the polyoxotungstate surface (hydrophilic domains). Slow evaporation of these aqueous micro-phases finally affords the microporous morphology of the resulting membrane (see Scheme 5).
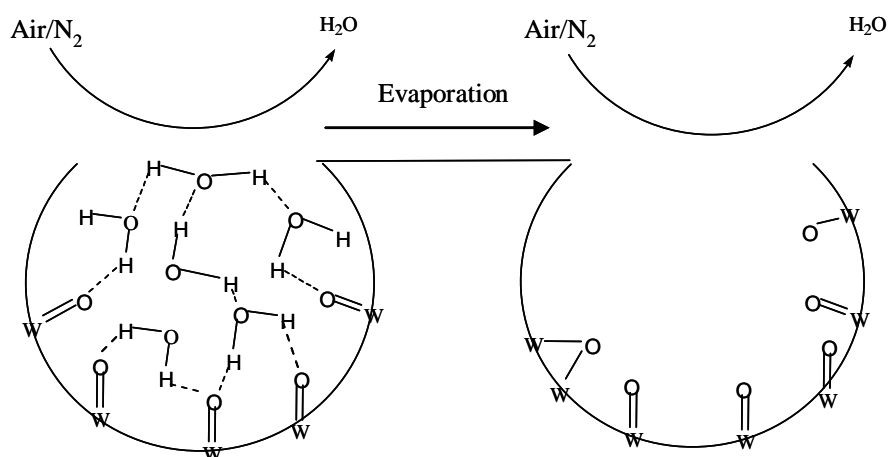
Scheme 2.5. Mechanism of micropores formation in the polymeric film. Water Droplets are stabilized by hydrogen bonds with the oxygenated surface of the polyoxometalates

According to this scenario, the photoactive inorganic catalyst should be more concentrated on the internal surface of the pores, so that they can be considered as functional structures or microreactors within the fluorinated polymeric film.

2.3.1.1 -Hyflon® photocatalytic hybrid membranes with microporous morphology,

In collaboration with ITM-CNR of Rende (CS - Italy), the approach described above[43] has been applied to obtain photocatalytic Hyflon-membranes with high porosity.

Figures 8A and 8B show SEM images of the surface and of the cross-section for a porous photocatalytic membrane obtained in this way, in a controlled humidity atmosphere (higher than 30% of relative humidity) as described in literature[43].

<div align="center">A   B</div>
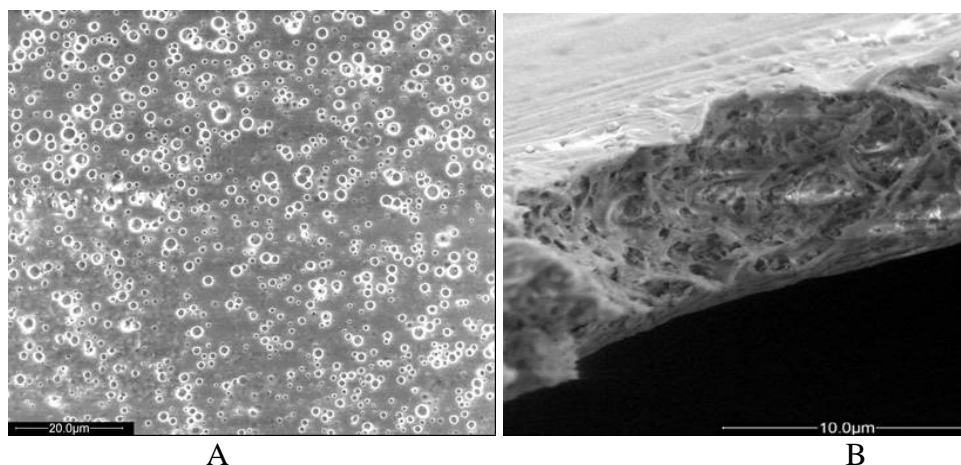
Figure 2.8. BSE-SEM images of A) Surface and B) cross-section of a porous RfNW10-Hyflon photocatalytic membrane obtained in a controlled humidity atmosphere.

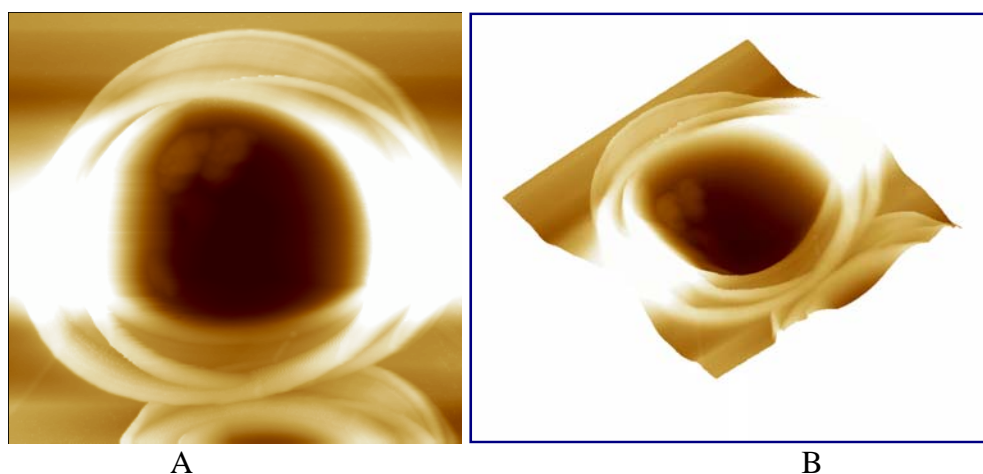AFM images of such membrane have also been recorded. Figures 9A and 9B, in particular, show the details of a single pore, with dimension of 0.6 μm.

<div align="center">A   B</div>

Figure 2.9. AFM analysis of a superficial pore.

The AFM evidence suggests that the photoactive inorganic species resides not only on the surface but also it decorates the inside walls of the pore, in the bulk-material. This is clearly shown in Figure 9, where the inorganic spherical domains, decorating the micro-channel walls, are seen as relief structures.

These finding supports the concept of the porous membrane displaying an extended array of catalytic micro-reactors, as the active components end up to accumulate on the internal surface of the material pores. Noteworthy, this result could be exploited to improve the photocatalytic process, by a continuos flow reaction, with the solution forced to permeate through these catalytic pores.

Moreover, the inclusion of polyanionic inorganic domains into hybrid Hyflon films has proved to be a straightforward technique to generate the porous structure, which is not

generally observed for the native polymer blend, giving final materials with dense morphology.

2.3.2 Catalytic activities.

Catalytic tests have been performed using different benzylic substrates to study the photooxygenation of the reactive C-H bonds under O_2 at atmospheric pressure.

Photooxygenation of ethylbenzene both in homogeneous and heterogeneous conditions by $(RfN)_4W_{10}O_{32}$ has been performed at first. The reaction yields the autoxidation products: hydroperoxide **(1)**, 1-phenylethanol **(2)** and acetophenone **(3)** as reported in the following scheme:
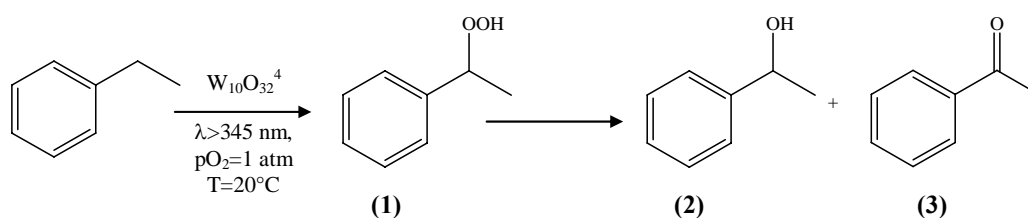
Scheme 2.6. Ethylbenzene photooxidation catalyzed by decatungstate.

Table 2.1. Photocatalytic oxygenation of ethylbenzene by decatungstate both in homogeneous and heterogeneous conditions with dense RfNW10-Hyflon membrane

#	Photocatalyst (thickness)	Solvent	Cat.,[b] μmol	Products,[c] mM (% **1:2:3**)	TON[d]
1[e]	$(nBu_4N)_4W_{10}O_{32}$	CH$_3$CN	0.60	20 (30:3:67)	50
2[e]	$(RfN)_4W_{10}O_{32}$	HFP	0.60	19 (47:7:46)	47
3[f]	$(nBu_4N)_4W_{10}O_{32}$	CH$_3$CN	0.20	64 (36:32:32)	351
4[f]	$(RfN)_4W_{10}O_{32}$	HFP	0.18	95 (56:23:21)	581
5	nBu$_4$NW10-PVDF (185 μm)	neat	0.32	23 (45:23:32)	78
6	nBu$_4$NW10-Hyflon (76 μm)[g]	neat	0.20	81 (14:66:20)	443
7	RfNW10-Hyflon (50 μm)	neat	0.18	196 (25: 41:34)	1198
8	RfNW10-Hyflon (7 μm)	neat	0.03	94 (16:46:38)	3447
9	RfNW10-Hyflon (94 μm)	neat	0.70	270 (15:48:37)	424
10	RfNW10-Hyflon/PTFE (124 μm)[h]	neat	0.05	99 (13:49:38)	2055

[a]Reaction conditions: ethylbenzene, 1.1 ml; pO$_2$ 1 atm; λ>345 nm; T=20°C; irradiation time: 4 h. [b]Photocatalyst content provided as homogeneous complex or embedded in membranes with 20-25% loading. [c]Total oxidation products and % distribution determined by GC-FID and GC-MS analyses. [d] TON: Turnover Number calculated as products (mol)/catalyst (mol). [e]Ethylbenzene, 0.02 M, t=2 h.; carboxylic acids and dimeric products have also been observed. [f]"Pseudo-neat" conditions obtained by addition of 20 μl of solvent. [g] Porous membrane. [h] RfNW10-Hyflon supported on PTFE. Support thickness = 117 μm, coating thickness = 7 μm, catalyst loading: 5.9% w/w.

The reactivity of $(RfN)_4W_{10}O_{32}$ has been compared with that of $(nBu_4N)_4W_{10}O_{32}$ in CH_3CN. Under homogeneous conditions, both in CH_3CN or in HFIP, the kinetic presents a bell-shaped profile for the hydroperoxide specie **(1)**, which is initially formed and then converts to the corresponding alcohol **(2)** and ketone **(3)** [44][45] (scheme 6).
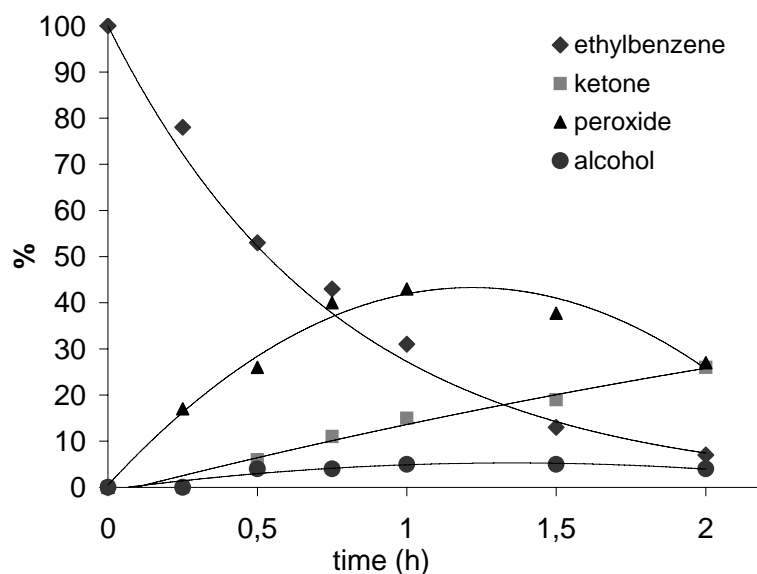
Figure 2.10. Bell-shape kinetic profile for the homogeneous photooxygenation of ethylbenzene in HFIP, catalyzed by $RfN_4W_{10}O_{32}$. (See entry 2, Table 1).

In both media, the poor alcohol selectivity depends on the competitive oxidation of 1-phenylethanol to acetophenone (see entries 1 and 2 in Table 1)[46].

In fluorinated phase a modest increase of the hydroperoxide concentration has been observed, likely because of a higher availability of O_2, which can be trapped by the benzylic radical intermediate (see entry 2, Table 1). In a substrate enriched liquid phase, the over-oxidation to ketone is sensibly reduced (entries 3 and 4 in Table 1), in such conditions, the product distribution reveals an increased alcohol selectivity.

Solvent-free conditions have thus been conveniently adopted for heterogeneous photocatalysis with hybrid membranes (entries 5-10 in Table 1). As proved by UV-Vis, FT-IR and reactivity test (Figure 11), the polymeric films do not present leaching of the photoactive component in hydrocarbon media.

A   B
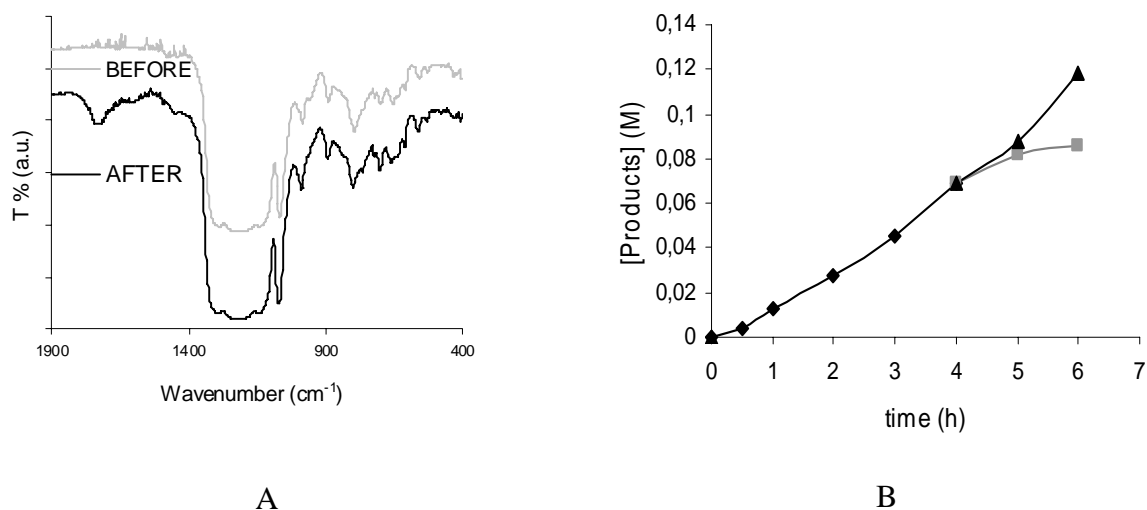
Figure 2.11. A) FT-IR of hybrid RfNW10-Hyflon membrane before and after the photocatalytic process (W-O stretching mode vibrations bands are visible in the 970-800 cm^{-1} region). B) control test for leaching. Upon removal of the catalytic film from neat ethylbenzene after 4h, quenching of the reaction has been observed,.

The impact of the fluorous-tagged decatungstate on the material performance, is highlighted by Figure 12, where the turnover efficiency of three different membranes, with equal photocatalyst content, but increasing fluorous character has been compared. While catalysis by nBu$_4$NW10-PVDF is negligible (entry 5, Table 1 and profile 1 on Figure 12), the Hyflon – based systems, show a remarkable activity with peak performance depending on the fluorous content of the photocatalyst counterion (see Figure 12, profile 2 and 3; Table 1, entries 6-7).
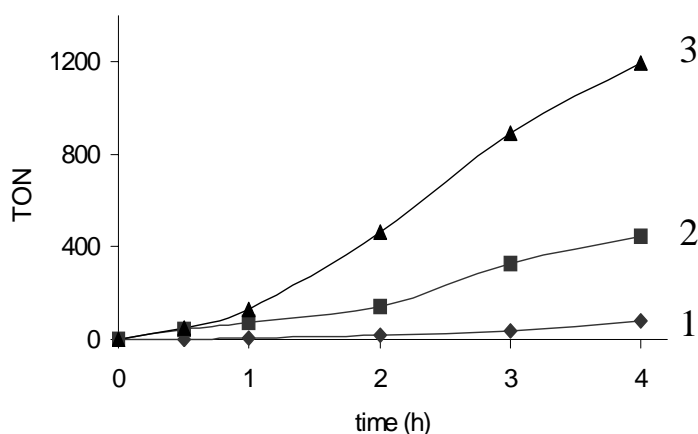
Figure 2.12. Fluorine content dependence of the total turnover number for ethylbenzene photooxygenation by nBu$_4$NW10-PVDF (1), nBu$_4$NW10-Hyflon (2), RfNW10-Hyflon (3) (entries 5-7 in Table 1).

This observation is likely ascribed to the optimized dispersion of the fluorophilic catalyst within the perfluorinated polymeric film, fostering an enhanced on-membrane reactivity also with respect to the homogeneous solution (compare entries 4 and 7 in Table 1).

The turnover dependence on the film thickness has been studied by using membranes with 25% loading and cross-section in the range 7-94 µm (entries 7-9 in Table 1). Although a steady increase in the total oxidation products is observed as a function of the overall photocatalyst content, an inverse correlation between the turnover and the membrane thickness has been observed, revealing a preferential activity of the surface with respect to the deeper catalyst (Figure 13).
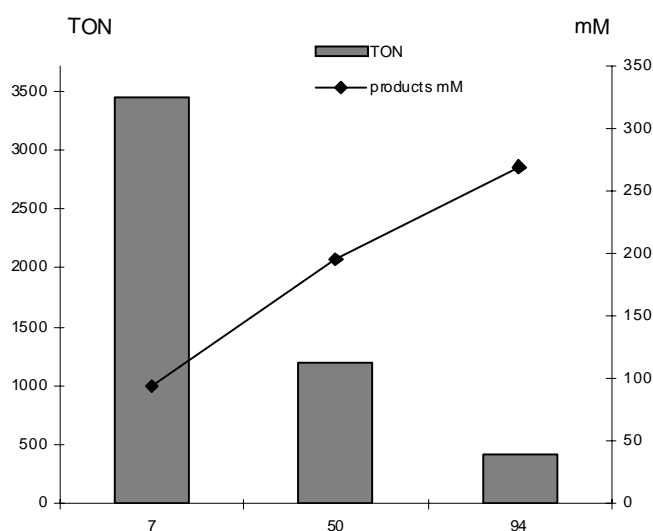
Figure 2.13. Turnover number and total concentration of the oxidation products (mM) calculated after the photooxygenation of ethylbenzene by RfNW10-Hyflon with thickness between 7 and 94 µm.

A low hydrocarbon penetration is indeed expected for Hyflon-based materials, thus fostering surface catalysis.

The mechanical properties of the thinner Hyflon membranes has been improved by using a secondary polytetrafluoroethylene or Teflon® (PTFE) support, without affecting the catalytic efficiency (entry 10 in Table 1)[47].

As mentioned before, the reactivity studies have been extended to other benzylic substrate and the corresponding results have been reported in the following Table:

Table 2.2. Photocatalytic oxygenation of benzili hydrocarbons by RfNW10-Hyflon membrane[a].

Substrate	Products, (% distribution)[b]	mM[c] (TON)
Tetralin	1-Tetralin hydroperoxide (14) 1-Tetralol (58) 1-Tetralone (6)	167[d] (6124)
Indane	1-Indane hydroperoxide (31) 1-Indanol (48) 1-Indanone (10)	165[d] (6051)
Cumene	Cumene hydroperoxide (47) Cumyl alcohol (53)	91 (3337)
2-Ethylnaftalene	1-(2-Naphtyl)-ethane-1-hydroperoxide (21) 1-(2-Naphtyl)-ethan-1-ol (26) 1-(2-Naphtyl)-ethan-1-one (53)	30 (1100)

[a]Reaction conditions: substrate 1.1 ml; pO_2=1 atm, λ>345 nm, T=20 °C, irradiation time: 4 h., heterogeneous catalyst: RfNW10-Hyflon (7 μm, 25% w/w catalytic loading). [b]% distribution determined by GC-FID and GC-MS analysis. [c]mM concentration of total oxidation products and TON calculated as products (mol)/catalyst (mol). [d]10-20% of dimerization products have also been observed.

Noteworthy, tetraline and indane photooxygenation proceeds with TON higher than 6000 and remarkable alcohol selectivity, thus providing a convenient alternative to other radical-based oxygenation systems [44] [45] [48]. Furthermore, the production of alkyl hydroperoxides might be exploited in a coupled tandem catalytic path, as oxygen transfer intermediates[49]. In the case of cumene, it could be possible to develop a consecutive catalytic system in which the acid catalyzed decomposition of cumyl-hydroperoxide yields phenol and acetone as final products. (Hock's process, see also Chapter 4).

It is important to underline that the reaction selectivity can be strongly affected by the reaction conditions. A different affinity of the polymeric material with respect to the substrates and reaction intermediates, in terms of swelling, absorption, hydrophobicity, may result in an increased selectivity towards high value-added products.

In order to understand better this fact, the hydrophobicity parameter (LogP = partition coefficient 1-octanhol/water) of ethylbenzene and its oxidation products have been correlated with the swelling percentage (defined as the weight increase of the swollen membrane in contact with the substrate) of Hyflon and polyvinylidenefluoride (PVDF) membranes (Figure 14).

The more hydrophobic polymeric material, Hyflon, has a higher affinity towards the more hydrophobic (higher LogP value) liquid: ethylbenzene. On the contrary it has a lower affinity for the more hydrophilic liquid: 2-phenylethanol.

The catalytic results is thus in agreement with the higher hydrophobic features of the Hyflon, which shows a decreased affinity from ethylbenzene to acetophenone and 1-phenylethanol. The lower affinity of the latter with the polymeric material limits its over-oxidation to ketone specie.
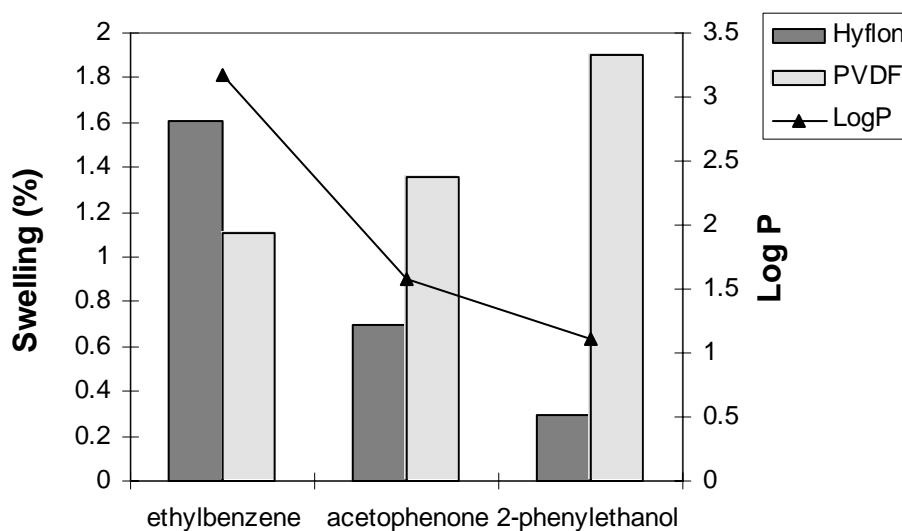
Figure 2.14. Swelling of a dense Hyflon and a dense PVDF membrane in pure liquid at 30°±1 and logarithm of the partition coefficient between n-octanol and water (LogP) of the pure testing liquid.

Further research work will be focused on a better understanding of the recycle of these Hyflon photocatalytic membranes. Preliminary results highlight loss of activity of about 20% after each cycle. Since leaching or degradation phenomena of the catalyst embedded in membrane can be excluded, it is possible that a partial poisoning of the catalyst can occur upon absorption of oxidized or over-oxidized products (*fouling*). This problem could be solved using a countinuos system with tangential and trans-membrane flows so to avoid fouling phenomena.

2.3.2.1 Continuous flow process: catalytic tests.

As reported in the § 2, the combination of advanced molecular separation and selective transport properties, with the obvious advantage of multi-turnover recycling, associated to heterogeneous supports, points to the design of innovative catalytic membrane reactors (CMRs) allowing the catalyst compartmentalization, phase transfer catalysis, selective supply/removal of solvents, reagents, products and by-products.

In this sense, a photocatalytic reactor has been designed to operate in a continuous process, in order to minimize pollutants and by-products accumulations by tangential flow, while

providing a better contact of the active sites with the substrates within the porous, by means of a permeation flow.

The reactor is characterized by (i) the presence of a cell (1,5 ml vol), equipped with a quartz window with 1 cm of diameter, to allow the focalized radiation to enter and irradiate the membrane, (ii) a minimum volume of the channels, to minimize the unproductive time spent by the reaction mixture to reach the membrane and to be recycled, (iii) a pump to supply and force the mixture in the tubes and through the membrane, (iv) a manometer with a valve , to tune the trans-membrane flow and pressure (in the range 1 to 10 bar).
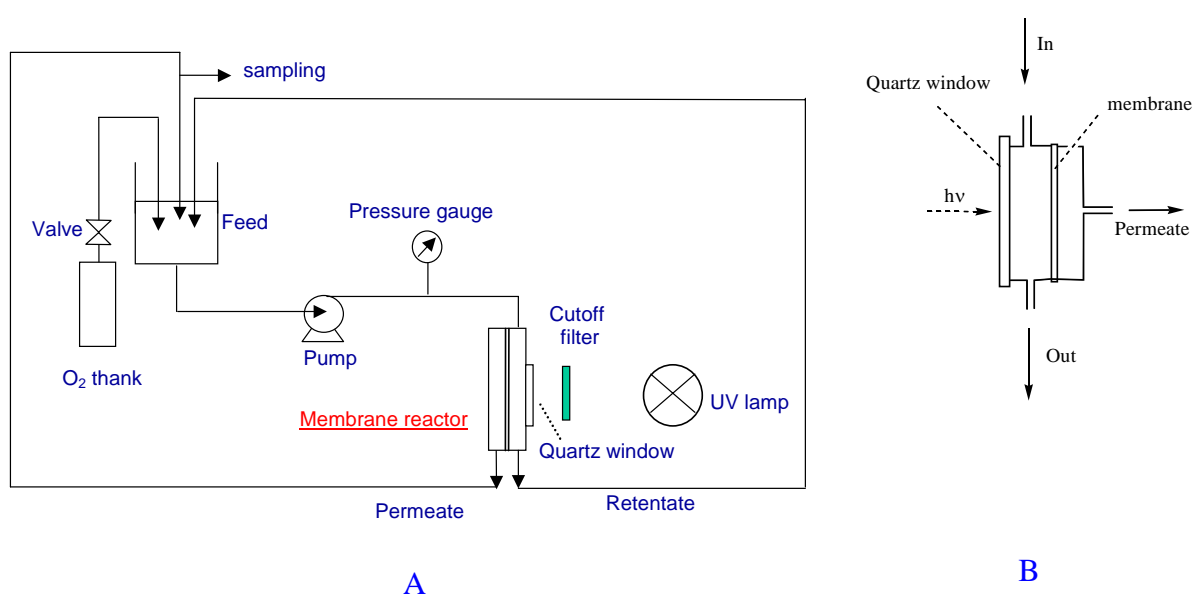
Scheme 2.7. A) Scheme of Catalytic membrane Photoreactor used for continuous catalytic tests . B) Detail of the irradiated cell.

Figure 2.15. Photoreactor working in continuous with trans-membrane flow collecting.

With a new batch of porous RfNW10-Hyflon photocatalytic membrane (see also section 2.3.1.1) it has been possible to compare its activity both in static and in flow processes, as highlighted by the results presented in the following Table:

Table 2.3. Catalytic activity of porous RfNW10-Hyflon membrane both in static and in continuous process

#	Catalyst	System	mM [products]	μmol. products	TON	% C-OOH	% C-OH	% C=O
1	-	static	25	28		48	25	27
2	RfNW10Hyflon	static	85	93	2049	11	69	20
3	-	flow	15	30		49	30	21
4	RfNW10Hyflon	flow	30	60	1170	32	37	31
5	"	*Permeate*	*47*			*26*	*42*	*32*
6	"	*Retentate*	*32*			*50*	*23*	*27*

Reaction conditions. pO_2 = 1 atm., λ > 345 nm, T = 25°C, irradiation time: 4 h. Oxidation prodoucts were analyzed and determined by GLC e GC/MS. TON = mmol total products/mmol of catalyst; loading: 20-22% w/w; thickness: 18-25 μm. Volume of ethylbenzene: 1mL in static process; 2 mL in flow-continuous process; Flow: 0,3 mL/min.

Under flow conditions, the contact-time of reagents/catalyst during irradiation turns out to be ill-defined and therefore it is difficult to trace a direct comparison with the static process in terms of efficiency or total turnover number. Apparently, the static process seems more efficient than the flow one, despite the improved interaction of ethylbenzene with the catalytic sites upon membrane permeation. This is likely due to a shorter contact time between the mixture and the membrane, which is of crucial importance during photo-oxidation. The larger volume required to fill the continuous reactor affects indeed the residence time which requires a careful optimization.

Nevertheless, by analyzing the permeate composition, a higher concentrations of the oxidation products **(2)** and **(3)** has been observed, suggesting that the catalytic sites are effectively present in the cross-section and available during the permeation into the bulk-material. Hence improvement of the continuous process could be obtained by increasing the ratio between the permeate and the retentate flows.

2.4 Conclusions.

The protocol employed to prepare the catalytic membranes embedding the decatungstate polyanions has given new insights for the optimization of such hybrid functional material with the aim to improve the catalyst selectivity.

The results achieved include the photocatalyst characterization in fluorinated media, in solution or within the membrane, and a reactivity screening focusing on the impact of membrane parameters on the oxidation efficiency and selectivity. Scanning electron microscopy (SEM) of the film surface and cross-section highlights a highly dispersed, homogeneous distribution of the catalyst domains which appear as spherical particles with uniform size of approximately 2-3 μm in diameter. This is a remarkable improvement of the material morphology, in comparison with Hyflon membranes embedding the fluorous-free tetrabutylammonium decatungstate. Catalysis results have been obtained and compared with different benzylic hydrocarbons both in the homogeneous and in the heterogeneous system. Under the conditions explored, photooxygenation by fluorinated decatungstate yields the benzylic hydroperoxide and the corresponding alcohol and ketone. Noteworthy, tetraline and indane photooxygenation proceeds with TON > 6000 and remarkable alcohol selectivity, thus providing a convenient alternative to other radical-centred oxygenation systems.

The solvent-free use of dioxygen under mild temperature and pressure conditions, for multi-turnover hydrocarbon oxygenation represents an encouraging step forward in sustainable catalysis. To investigate the material morphology and the distribution of the catalytic domains, the aggregation phenomena of fluorinated decatungstate in HFIP have been studied by Dynamic Light Scattering. The presence of spherical aggregates with average hydrodynamic diameter ranging from 100-200 nm, is generally observed and it is responsible for the nucleation of the micrometric POM-based domains ultimately embedded within the polymeric membrane. The self-assembly behaviour of surfactant encapsulated POMs evolving to nano-structured, onion-like vesicles, has been observed for the fluorous-tagged POMs, and it has been exploited for the construction of novel functional materials with application in catalysis. The POM-based amphiphile can indeed template the formation of a micro-structured porous film under humidity-controlled casting conditions. The resulting membrane shows a pattern of regular and no-coalesced pores, thus creating an extended array of channels where the inorganic catalytic domains are exposed along the sidewalls. Therefore, the POM-templated membrane can be considered as a multichannel micro-reactor to be used under flow conditions, implementing the substrate/catalyst contact, along the membrane

cross-section. A Catalytic membrane Reactor (CMR) has finally been designed, so as to monitor the reaction progress and catalyst activity, by sampling the product distribution in the permeate and retentate fractions. The results obtained provide a clear evidence of substrate/hydroperoxide transformation along the catalytic membrane micro-channels.

2.5 References and notes.

[1] K. Szaciłowski, W. Macyk, A. Drzewiecka-Matuszek, M. Brindell and G. Stochel, *Chem. Rev.,* 105, **2005**, 2647.

[2] A. Maldotti, A. Molinari and R. Amadelli, *Chem. Rev.,* 102, **2002**, 3811.

[3] B. Meunier and A. Sorokin, *Acc. Chem. Res.,* 30, **1997**, 470.

[4] O. Legrini, E. Oliveros and A. M. Braun, *Chem. Rev.,* 93, **1993**, 671.

[5] Y. G. Adewuvi, *Environ. Sci. Technol.,* 39, **2005**, 8557.

[6] A. G. Griesbeck and A. Bartoschek, *Chem. Commun.*, **2002**, 1594.

[7] M. Bonchio, T. Carofiglio, M. Carraro, R. Fornasier and U. Tonellato, *Org. Lett.*, 4, **2002**, 4635.

[8] T. Peng, D. Zhao, K. Dai, W. Shi and K. J. Hirao, *J. Phys. Chem. B.* , 109, **2005**, 4947.

[9] A. P. Wight and M. E. Davis, *Chem. Rev.,* 102, **2002**, 3589.

[10] S. O. Obare, T. Ito, M. H. Balfour and G. J. Meyer, *Nano Lett.* 3, **2003**, 1151 and reference therein.

[11] M. T. Pope, *Heteropoly and Isopoly Oxometalates* (Springer-Verlag, New York, **1983**).

[12] C. L. Hill, *Chem. Rev.*, 98, **1998**, 1-390.

[13] M. T. Pope and A. Müller, *Polyoxometalate Chemistry. From Topology Via Self-assembly to Applications* (Kluwer Academic Publishers, Dordrecht, The Netherlands, **2002**).

[14] M. A. Fox, R. Cardona and E. Gaillard, *J. Am. Chem. Soc.*, 109, **1987**, 6347.

[15] A. Hiskia, A. Mylonas and E. Papaconstantinou, *Chem. Soc. Rev.,* 30, **2001**, 62.

[16] D. C. Duncan, T. L. Netzel and C. L. Hill, *Inorg. Chem.,* 34, **1995**, 4640.

[17] C. Tanielian, K. Duffy and A. Jones, *J. Phys. Chem. B* 101 **1997**, 4276.

[18] C. Tanielian, *Coord. Chem. Rev.* 178-180, **1998**, 1165.

[19] I. Texier, J. A. Delaire and C. Giannotti, *Phys. Chem. Chem. Phys.* 2, **2000**, 1205.

[20] C. Tanielian, R. Seghrouchni and C. Schweitzer, *J. Phys. Chem. A,* 107, **2003**, 1102 and references therein.

[21] Y. Nosaka, T. Takei and N. Fujii, *J. Photochem. Photobiol. A: Chem.,* **1995**, 173.

[22] R. R. Ozer and J. L. Ferry, *J. Phys. Chem. B,* 104, **2000**, 9444.

[23] C. L. Hill, *Synlett.,* **1995**, 127.

[24] C. L. Hill and Z. Zheng, *Chem. Commun.,* 6, **1998**, 2467.

[25] R. C. Chambers and C. L. Hill, *Inorg. Chem.,* 28, **1989**, 2509.

[26] A. Mylonas, A. Hiskia, E. Androulaki, D. Dimotikali and E. Papaconstantinou, *Phys. Chem. Chem. Phys.,* 1, **1999**, 437.

[27] D. Dimotikali and E. Papaconstantinou, *Inorg. Chem. Acta,* 87, **1984**, 177.

[28] H. Hiskia and E. Papacostantinou, *Inorg. Chem.,* 31, **1992**, 163.

[29] R. Akid and J. R. Darwent, *J. Chem. Soc. Dalton Trans.,* **1985**, 395.

[30] C. Sanchez, G. J. A. A. Soler-Illia, F. Ribot, T. Lalot, C. R. Mayer and V. Cabuil, *Chem. Mater.,* 13, **2001**, 3061 and references therein.

[31] M. Bonchio, M. Carraro, G. Scorrano and A. Bagno, *Adv. Synth. Catal.,* 346, **2004**, 648.

[32] M. Bonchio, M. Carraro, G. Scorrano, E. Fontananova and E. Drioli, *Adv. Synth. Catal.,* 345, **2003**, 1119.

[33] I. F. Vankelecom, *Chem. Rev.,* 102, **2002**, 3779, and references therein.

[34] a) K. Neimann and R. Neumann, *Org. Lett.,* 2, **2000**, 2861; b) S. P. de Visser, J. Kaneti, R. Neumann and S. Shaik, *J. Org. Chem.,* 68, **2003**, 2903; c) A. Berkessel and J. A. Adrio, *Adv. Synth. Catal.* 346, **2004**, 275; d) M. Vazylyev, D. Sloboda-Rozner, A. Haimov, G. Maayan and R. Neumann, *Top. Catal.,* 34, **2005**, 93 and references therein.

[35] a) M. Wende and J. A. Gladysz, *J. Am. Chem. Soc.*, 125, **2003**, 5861, b) L. V. Dinh and J. A. Gladysz, *Angew. Chem., Int. Ed.,* 44, **2005**, 4095.

[36] a) V. Arcella, P. Colaianna, P. Maccone, A. Sanguineti, A. Gordano, G. Clarizia and E. Drioli, *J. Membr. Sci.*, 163, **1999**, 203; b) V. Arcella, C. Troglia and A. Ghielmi, *Ind. Eng. Chem. Res.*, **2005**, 44, 7646.

[37] a) J. C. Jansen, F. Tasselli, E. Tocci and E. Drioli, *Desalination,* 192, **2006**, 207; b) R. S. Prabhakar, B. D. Freeman and I. Roman, *Macromolecules*, 37, **2004**, 768.

[38] M. Mulder, *Basic Principles of Membrane Technology* (Kluwer Academic Publishers, Dordrecht, The Netherlands, **1996**).

[39] a) C. Rocaboy, W. Bauer, J. A. Gladysz, *Eur. J.Chem.,* **2000,** 2621-2628. b) G. Maayan, R. H. Fish, R. Neumann, *Org. Lett.*, 20, **2003**, 3547.

[40] M. Carraro, M. Gardan, G. Scorrano, E. Drioli, E. Fontananova, M. Bonchio, *Chem. Commun.,* **2006,** 4533.

[41] M. Carraro, M. Gardan, L. Donato, G. Scorrano, E. Drioli, E. Fontananova, M. Bonchio, *Desalination*, *200*, **2006**, 705.

[42] M. Bonchio, M. Carraro, M. Gardan, G. Scorrano, E. Drioli, E. Fontananova *Top. Catal., 40*, **2006**, 133.

[43] a) H. Li, H. Sun, W.Qi, M. Xu, L. Wu, *Angew. Chem. Int. Ed.,* 46, **2007**, 1300, b) W. Qi, H. Li, L. Wu, *J. Phys. Chem. B*, 112, **2008**, 8257, c) H. Sun, H. Li, W. Bu, M. Xu, L. Wu, *J. Phys. Chem. B, 110,* **2006**, 24847.

[44] I. N. Lykakis, M. Orfanopoulos, *Tetrahedron Lett.,* 45, **2004**, 7645.

[45] I. N. Lykakis, C. Tanielian, M. Orfanopoulos, *Org.Lett.,* 5 ,**2003**, 2875.

[46] D. Attanasio, L. Suber, K. Thorslund, *Inorg. Chem.,* 30, **1991**, 590.

[47] A. Gordano, V. Arcella, E. Drioli, *Desalination*, 163, **2004**, 127.

[48] G. Yang, Q. Zhang, H. Miao, X. Tong, J. Xu, *Org. Lett.,* 7, **2005,** 263.

[49] a) R. Neumann and M. Dahan, *Chem. Commun.*, **1995**, 171, b) J. C. Wasilke, S. J. Obrey, R. T. Baker and G. C. Bazan, *Chem. Rev.*, 105, **2005**, 1001; c) J. M. Lee, Y. Na, H. Han, S. Chang, *Chem. Soc. Rev.*, 33, **2004**, 302.

3. Hydrogen peroxide activation by hybrid polyoxotungstates in fluorinated alcohol.

3.1 Introduction.

The activation of aqueous hydrogen peroxide has captivated researchers interested in the use of this environmentally friendly oxidant with high oxygen content (47% of active oxygen) and for oxidative transformations in synthetic chemistry. Hydrogen peroxide may be basically activated in three ways. First, hydroxy and hydroperoxy radicals may be formed by a Haber-Weiss mechanistic scheme in the presence of several metal compounds[1]. These radicals lead to non-selective transformations of organic substrates. Second, under basic conditions, the strong nucleophile HOO^- is formed, which is active for the epoxidation of electrophilic alkenes such as β-unsaturated ketones or carboxylic acid derivatives. The third and likely most important synthetic application of hydrogen peroxide is in the area of electrophilic and heterolytic oxidation as the epoxidation of alkenes.

Olefin epoxidation is a key transformation in organic synthesis, both on laboratory and industrial scale[2] [3]. The method of choice- in fine chemical production – is usually the Prilezhaev reaction of olefins with stoichiometric amount of percarboxylic acids, such as peracetic and *m-* chloroperbenzoic acid[4]. Even if H_2O_2 has been frequently used for the separate or *in situ* production of organic peroxides and peracids, environmental and safety concerns, the high cost, the need for large amounts of organic solvents and the presence of the corresponding carboxylic acid[5], urge for the use of alternative processes, mainly based on catalysis with high valent (d°) metal complexes of Ti, V, Mo, W, and Re.

Among the most effective catalysts, worthy of note are: titanium silicates[6], peroxo-phosphotungstates[7], manganese triazacyclononane[8] and methyl trioxorhenium[9]. From a mechanistic point of view, both the carboxy group in the peracid and the high valent metal centers lead to the formation of a peroxo group bearing an electrophilic oxygen atom. It is well established that the subsequent oxygen transfer to a nucleophile such as an alkene takes place via a butterfly type transition state[10].
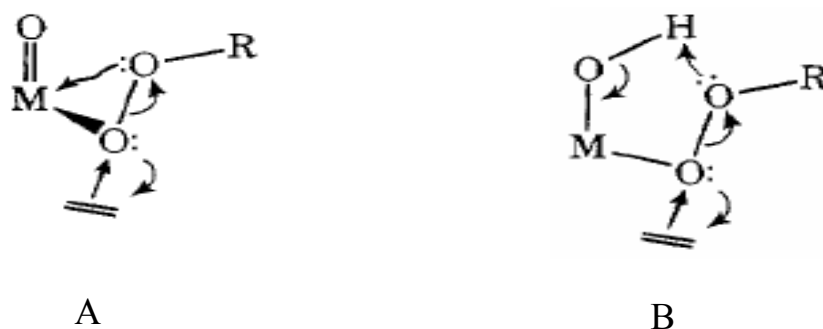
Figure 3.1. Two butterfly-type transition state proposed by Chong and Sharpless[10].

Briefly, it seems clear that any compound that reduces the electron density at one of the oxygen atoms of the hydrogen peroxide will lead to a facilitated nucleophilic attack by the substrate with heterolytic oxygen transfer. Recently, it has been found that one can simply carry out oxidation reactions with hydrogen peroxide in perfluorinated alcohols as solvent, *without* the addition of any other catalyst[11] [12] [13]. The possibility to use perfluorinated media in oxidation catalysis is of special interest because of the higher dioxygen solubility. Fluorinated alcohols, in additions, exhibit strong hydrogen donor power, high ionising power, low nucleophilicity, and they are able to template hydrogen peroxide, leading to the activation of the pertinent oxidant and, likely, to the stabilization of the transition state. Fluorinated alcohols have been indeed applied as a *non innocent* solvent to perform epoxidations[11] [14] [15] [16] [17], lactonizations[18], and sulfoxidations[19]. From ^{1}H and ^{17}O NMR spectra, it has been deduced that the strong electron-withdrawing properties of fluorine, along with the hydrogen bonding properties of the O-H hydrogen atom, lead to the formation of an electrophilically activated intermediate, as depicted in the following Scheme:
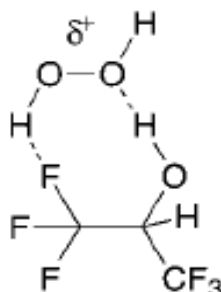
Scheme 3.1. Electrophilic activation of hydrogen peroxide by the "Fluorine" inductive effect.

Moreover, the reactivity seems to increases with fluorine content: 1,1,1,3,3,3-hexafluoroisopropyl alcohol (HFIP) has been found to be more active than 2,2,2-trifluoroethanol (TFE)[14] in activating the peroxidic intermediates.

This "booster effect" is thus explained on the basis of a double effect, both structural and electronic, mediated by bridging hydrogen bonds, that allows the electrophilic activation of hydrogen peroxide and promotes the oxygen transfer to the organic substrate[11 14 15 16 17 18 19].

3.2 Hybrid polyoxotungstates as catalysts in hydrogen peroxide activation.

Among catalytic protocols using hydrogen peroxide as terminal oxidant, those involving competent W(VI)-peroxides are generally characterized by negligible decomposition pathways and good to excellent selectivities[20]. Tungstate-based systems, using H_2WO_4 or Na_2WO_4 as catalyst precursors, have advanced into efficient synthetic methods for alkene oxidation[21 22].

However, because of the complexity of H_2O_2 equilibria with mono- or polynuclear tungsten precursors, speciation of the competent intermediates and their dynamic behaviour is a major issue[23 24]. This hampers both a precise understanding of the mechanistic scenario and a reliable drawing of structure-reactivity correlations spanning the diverse catalytic routines[21 23].

In this light, an appealing alternative is represented by polyoxotungstates (POM), displaying stable structures under oxidation turnovers[21 25 26 27].

Worthy of notice is the catalytic performance of $[\gamma\text{-SiW}_{10}O_{34}(H_2O)_2]^{4-}$ with selectivity > 99% in the epoxidation of internal and terminal double bonds (2-10 h at 32°C)[26]. This catalyst is characterized by a divacant structure, featuring a tetra-oxygenated nucleophilic site on POM surface and four W(VI) atoms capable of H_2O_2 coordination[27 28]. In this system, two major drawbacks are represented by protonation equilibria, likely engaging the lacunary site, which alter the POM solubility and reactivity[27 29], and by a thermally induced catalyst deactivation (for more details see Section 1.2.6 in General introduction).

Recent results obtained in our research group[30] have shown that a convenient remedy can be provided by the functionalization of the POM vacant site through the covalent graphting of organic moieties[31 32]. The higher stability of hybrid structures, in comparison to lacunary species, can be ascribed to the graphted organic functions, acting as protecting groups of the nucleophilic oxygenated site on the POM lacuna. Therefore, undesired parallel reactions, such as condensation or isomerisation of the vacant POMs, are inhibited, thus increasing their

stability in different solvents and at higher temperatures. The presence of an organic moiety, moreover, offers the possibility to modulate the stereoelectronic features of the resulting POM and can influence the reactivity of the proximal metallo-peroxides formed on the POM surface[30]. As already discussed in the general introduction, polyoxometalates are thus good candidates as inorganic scaffolds to develop new hybrid molecular materials with catalytic activity, giving both high oxidation yields and selectivities with a broad range of substrates, in the presence of hydrogen peroxide[30][33].

Functional amphiphilic molecules have been prepared by using the combination of polyanionic metallo-oxo clusters and organic domains with lipophylic character[34]. Following this approach, fluorous-tagged cationic surfactants have been used to improve the affinity of polyanions towards fluorinated solvents[35] and fluorinated polymers[36] (see also Chapter 2).

In our research group, new synthetic procedures for the covalent graphting of vacant silicon- and phosphorous-Keggin polyoxotungstates, have been optimized using, as electrophilic reagents, both organosilyl clorides ($RSiCl_3$) and trialkoxysiloxanes ($RSi(OR')_3$), where R = Et, n-Pr, Ph, in order to obtain functionalized derivatives containing W-O-X bridged bonds with X = P or Si[30], with yields ranging from 65 to 90%[37].

The general mechanisms for the derivatisation of lacunary polyanions with organosilanes are reported in the following scheme. The process requires the hydrolysis of the organic reagent: even if these derivatives may give easy polymerization (to form $RSiO_n$ species), the condensation with oxygen atom on POM defect site, occurs smoothly. Tetraalkylammonium or tetraarylphosphonium salts can be added to the reaction mixture as phase transfer agents, in order to isolate the product in polar organic solvents.
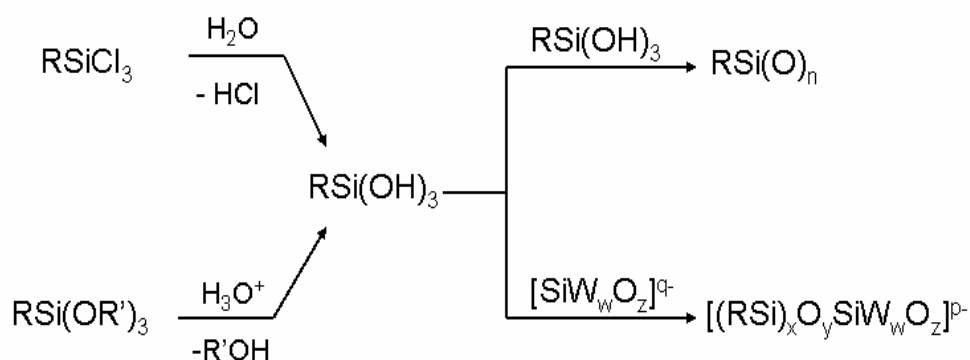
Scheme 3.2. General procedure for the preparation of hybrid organic-inorganic derivatives.

To exploit and combine the ability of fluorinated phases for the electrophilic activation of hydrogen peroxide with the use of POM-based catalysts, fluorous-tagged hybrids have been prepared, starting from vacant Keggin polyoxotungstates. To this aim, the organic reagents

have been properly chosen, bearing extended fluorinated alkyl chains. The resulting hybrid POM features both the catalytic properties of a vacant polyoxotungstate, and the stereo-electronic effects induced by the fluorinated moiety.

3.3 Results and discussion.

The design, synthesis and characterization of three different fluorophilic POMs, resulting from three different vacant Keggin polyoxotungstates are presented herein.

3.3.1 Preparation and characterization of lacunary polyoxotungstates precursors.

Inorganic precursors with defect structure, have been synthesized following literature procedures[38] and used for the covalent graphting with organic residues. In this work three different vacant polyoxotungstates have thus been prepared, respectively mono- $[\alpha\text{-}SiW_{11}O_{39}]^{8-}$, di- $[\gamma\text{-}SiW_{10}O_{36}]^{8-}$ and trivacant $[\alpha\text{-}SiW_9O_{34}]^{10-}$, as convenient precursors for the synthesis of hybrid organic-inorganic derivatives[30].

^{183}W NMR has been used as a fundamental technique to confirm the structure of both the POM precursors and of the resulting hybrids: the structure and the spectra are briefly described in the following paragraphs.

$[\alpha\text{-}SiW_{11}O_{39}]^{8-}$

The mono-vacant precursor has been isolated as hydrosoluble potassium salt. The ^{183}W-NMR spectrum is reported in the following Figure 2: the corresponding spin-system consists of six signals with integration ratio 2:2:2:2:2:1, in agreement with a C_s symmetry featuring six non equivalent tungsten atom groups[38].
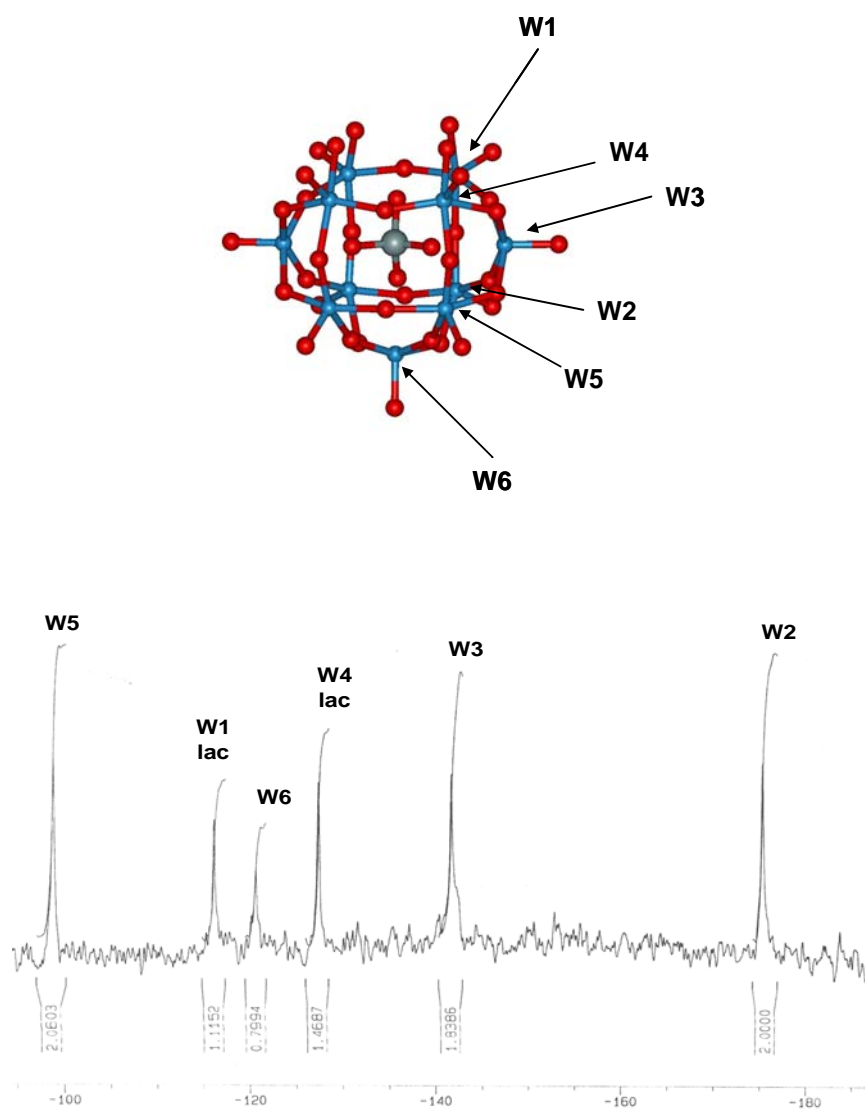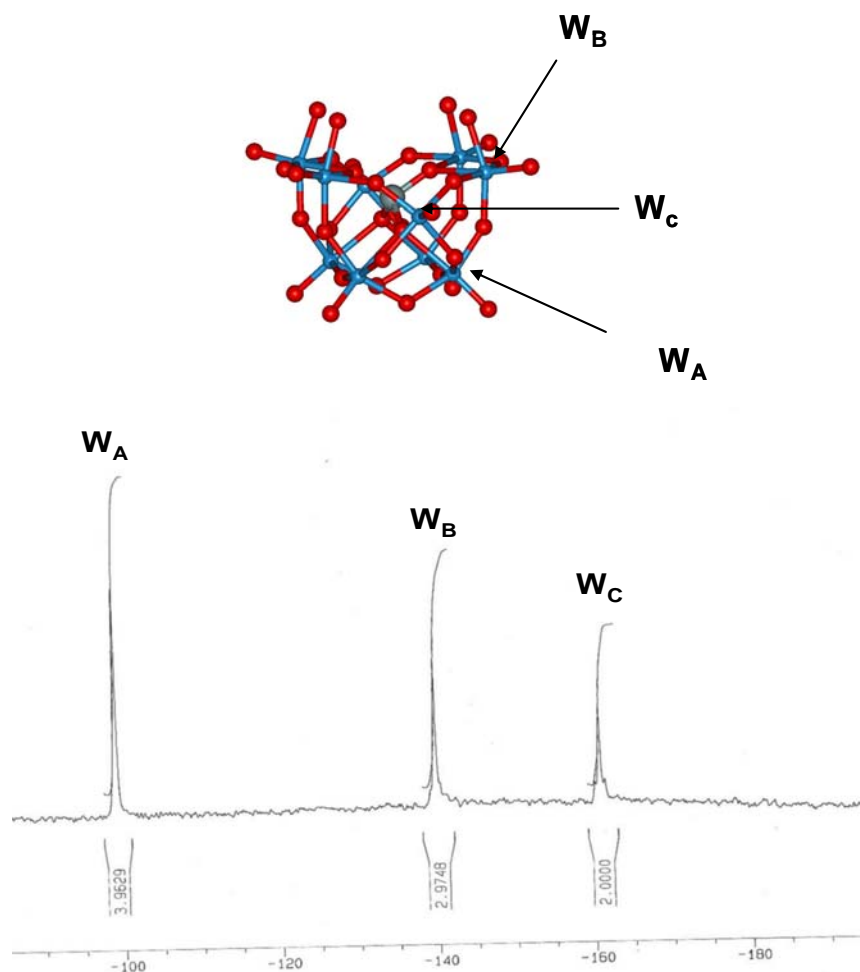
Figure 3.2. Mono-vacant precursor and its ^{183}W-NMR spectrum as potassium salt.

$[\gamma\text{-}SiW_{10}O_{36}]^{8-}$

The di-vacant precursor has been synthesized through a two steps procedure. The mono-vacant precursor $[\beta_2\text{-}SiW_{11}O_{39}]^{8-}$ has been obtained at first as potassium salt, then this complex has been converted to the divacant derivative in presence of K_2CO_3 at pH = 9.1 (See also the Experimental Part on Section 5.4.1). In Figure 3.3 the ^{183}W-NMR spectrum, recorded for the potassium salt of $[\gamma\text{-}SiW_{10}O_{36}]^{8-}$, is reported: the corresponding spin-system consists of three signals with integration ratio 2:2:1, in agreement with the anion symmetry (C_{2v})[38].

Figure 3.3. Di-vacant spectrum and its ^{183}W-NMR spectrum as potassium salt.
A difference in integral ratio is due to spin relaxations.
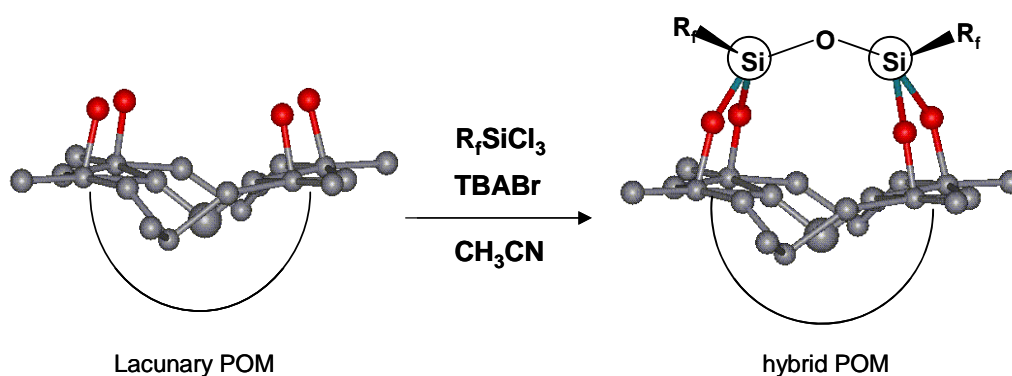
$[\alpha\text{-SiW}_9\text{O}_{34}]^{10-}$

The tri-vacant precursor has been isolated as sodium salt, exhibiting insolubility in aqueous media. The C_3v symmetry, as shown by the structural representation in Figure 3.4, indicates that a spin-system, consisting of two signals should be expected with integration ratio 1:2[38].
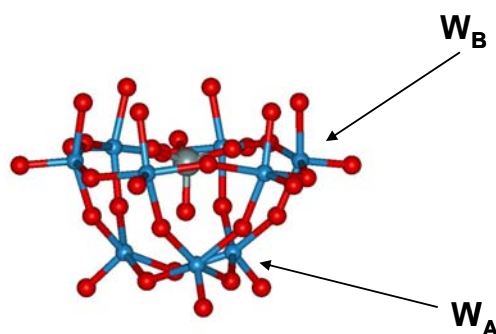
Figure 3.4. Tri-vacant precursor.

3.3.2 Preparation and characterization of fluorous-tagged hybrids.

The synthetic strategies presented on scheme 3.2 at Section 3.2, have been used to synthesize the fluorous-tagged hybrids **(1)**, **(2)**, **(3)**, with general formula: $[(RfSi)_xO_ySiW_wO_z]^{4-}$, as tetrabutylammonium (TBA) salts. The vacant precursors have been reacted with two or more equivalents of the fluoroalkyl derivatives $CF_3(CF_2)_7CH_2CH_2SiX_3$, with X= OCH_3 or Cl, abbreviated as R_fSiX_3 (see Scheme 3.3).


Lacunary POM $\qquad$ hybrid POM

Scheme 3.3. Synthesis of hybrid complexes 1-3.
1 $[(CH_3CH_2CH_2CH_2)_4N]_4[(CF_3(CF_2)_7(CH_2)_2Si)_2O(SiW_{11}O_{39})]$
2 $[(CH_3CH_2CH_2CH_2)_4N]_4[(CF_3(CF_2)_7(CH_2)_2Si)_2O(SiW_{10}O_{36})]$
3 $[(CH_3CH_2CH_2CH_2)_4N]_4[(CF_3(CF_2)_7(CH_2)_2Si)_4O_3(SiW_9O_{34})]$

Noteworthy, the resulting products are soluble in polar solvents, namely, acetonitrile (CH_3CN) and dimethylsulfoxide (DMSO), but also in hexafluoro *iso*-propanol (HFIP).

Each complex was characterized in the solid state (FT-IR spectroscopy, elemental analysis) and in solution (ESI-MS, ^{29}Si-, ^{183}W-, ^{19}F-NMR).

As already introduced, among the characterization techniques, the spin-systems observed by means of ^{183}W-NMR spectra, are particularly diagnostic because they allow to recognize the expected signal patterns, in agreement with the structural hypothesis, and with different chemical shifts with respect to the corresponding POM precursors[39]. In the following figures, the ^{183}W-NMR spectra are reported for each hybrid complex together with their structures.

TBA$_4$[(RfSi)$_2$O(SiW$_{11}$O$_{39}$)] **(1)**
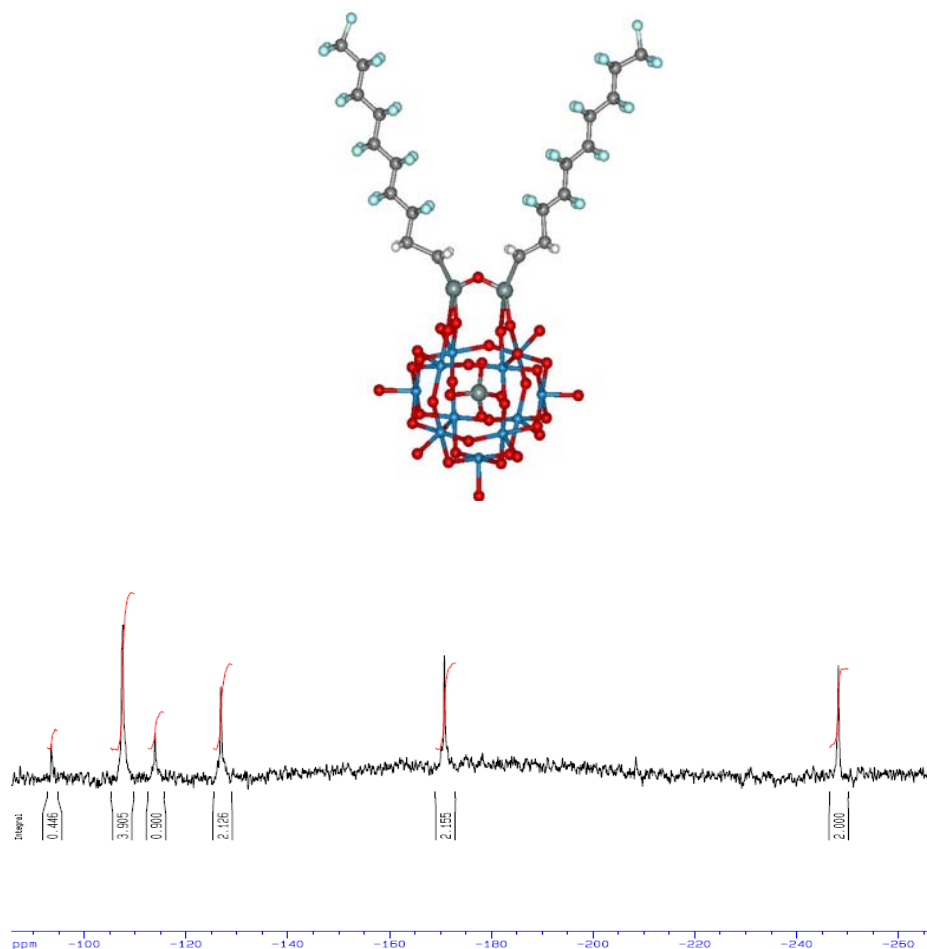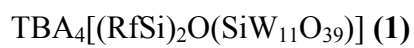
A

Figure 3.5. A) ^{183}**W-NMR spectrum of (1) in CD$_3$CN/ CH$_3$CN. The signal at 98 ppm is attributed to [SiW$_{12}$O$_{40}$]$^{4-}$ obtained as a by-product.**

TBA$_4$[(RfSi)$_2$O(SiW$_{10}$O$_{36}$)] **(2)**
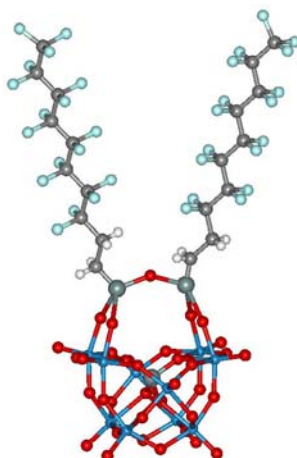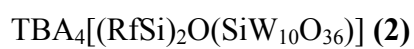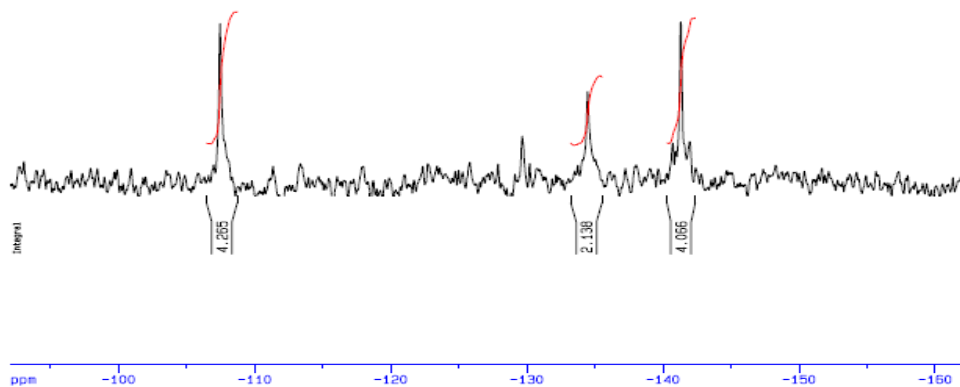
A

Figure 3.6. ^{183}W-NMR spectrum of (2) in CD$_3$CN/ CH$_3$CN.

TBA$_4$[(RfSi)$_4$O$_3$(SiW$_9$O$_{34}$)] **(3)**
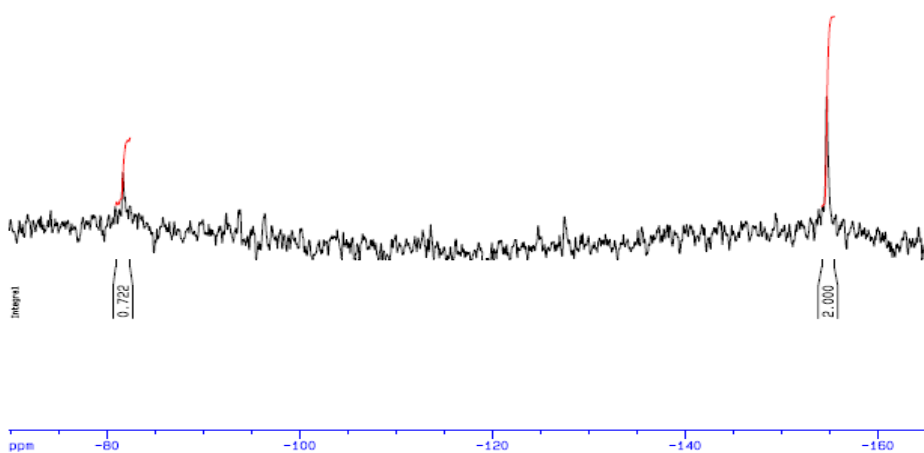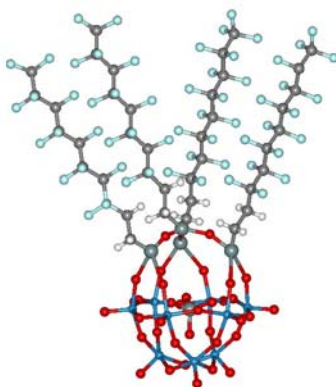
A

Figure 3.7. ^{183}W-NMR spectrum of (3) in CD$_3$CN/ CH$_3$CN.

Furthermore, ^{19}F-NMR spectra allows to confirm the presence of the fluorinated alkyl chains graphted on the vacancies of the inorganic scaffolds.

As an example, it is here reported the ^{19}F-NMR spectrum of the hybrid complex **1,** whose surface is decorated by two fluoroalkyl residues. Spectra have been recorded for complexes **2** and **3,** incorporating two and three, fluorinated chains, respectively.
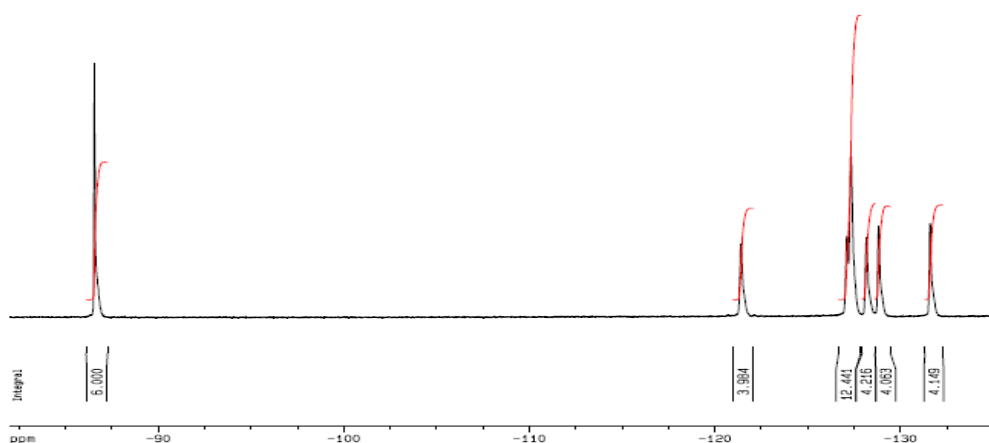
Figure 3.8. ^{19}F-NMR spectrum of (1) in CD$_3$CN/ CH$_3$CN.

To check the outcome of the POM surface silylation, FT-IR analyses are particularly useful: upon covalent functionalization of the defects on the polyoxotungstates, changes are expected within the POM absorbance region. FT-IR spectra, in the wavenumbers range 500-1200 cm^{-1}, show vibrational stretching bands [ν_{as} (W-O$_B$-W) and ν_{as} (W=O$_t$)] which are shifted to higher frequencies with respect to those of the corresponding precursors (see Figure 3.9 and also the Experimental part on Section 5.4.1 and 5.4.2). The occurrence of C-F bond is finally revealed by the strong band at 1200-1250 cm^{-1}.

A

B

C
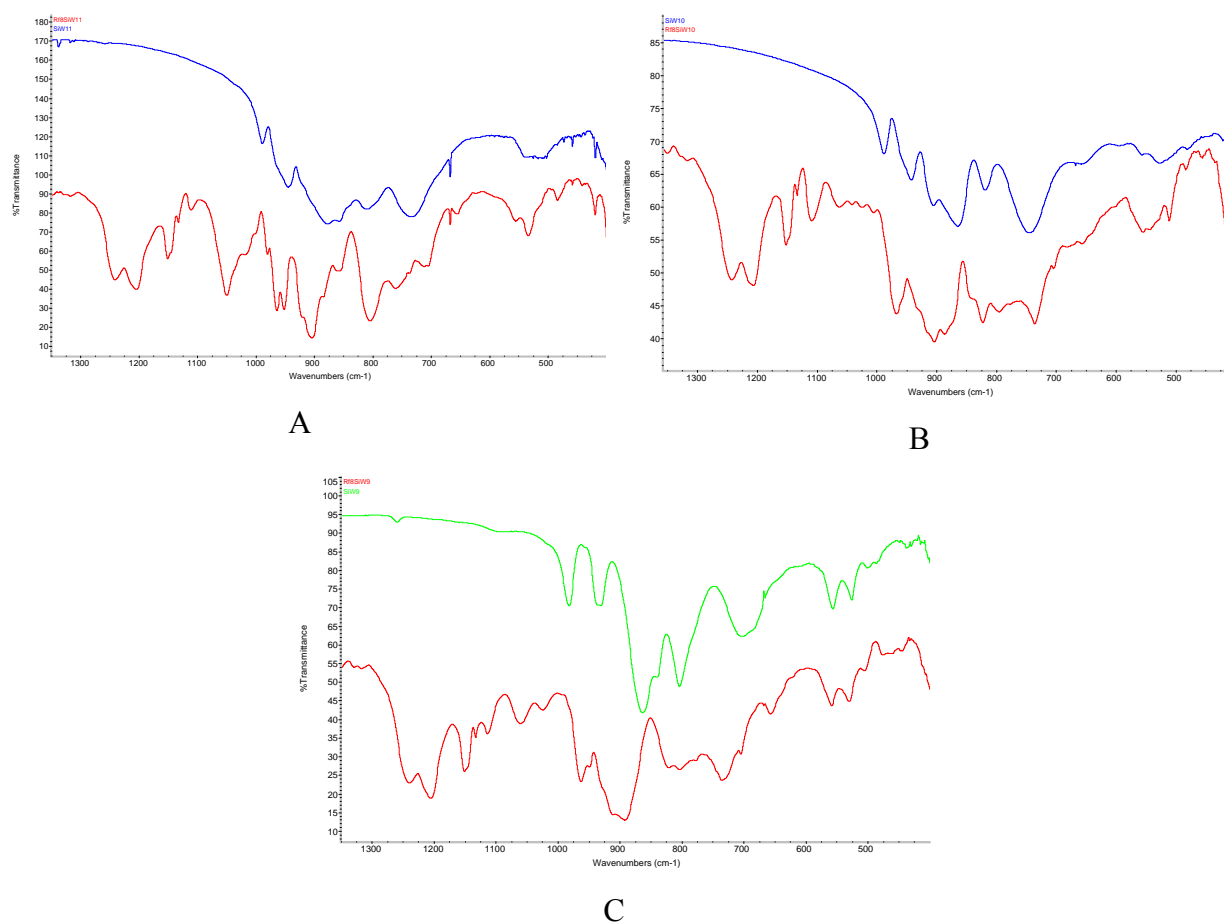
**Figure 3.9. Comparison of FT-IR spectra (KBr) of hybrid complexes 1 − 3 with respect to those of their precursor. A) FT-IR of [α-SiW$_{11}$O$_{39}$]$^{8-}$ and hybrid complex (1) (blue line and red line respectively). B) FT-IR of [γ-SiW$_{10}$O$_{36}$]$^{8-}$ and (2) (blue line and red line respectively). C) F-IR of [α-SiW$_9$O$_{34}$]$^{10-}$ and (3) (green line and blue line respectively).**

Hybrids **1-3** share an analogous amphiphilic behaviour. These are molecules incorporating both an inorganic polyoxoanionic and hydrophilic surface together with a highly hydrophobic domain, which is localized on the covalently graphted fluoroalkyl pendants (**1-3**).

3.3.3. Catalytic activity of fluorous-tagged hybrids.

Hybrid-fluorinated polyoxotungstates **1-3** have been used as catalysts for the epoxidation of different olefins, both internal and terminal ones, in fluorous media (HFIP) and in the presence of H$_2$O$_2$ as oxidant. For comparison purposes, catalytic epoxidations have also been performed with: (i) CH$_3$CN, as conventional organic solvent, (ii) the isocharged fluorous-tagged salt (RfN)$_4$W$_{10}$O$_{32}$ **(4)**, bearing fluorinated moieties associated by electrostatic interactions (see Chapter 2), (iii) no catalyst in HFIP solvent. These reactions can be conveniently schematized as follow:
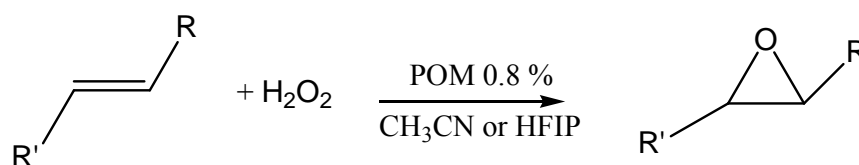
Catalytic results are listed in Table 3.1:

Table 3.1. Catalytic tests in olefins epoxidation with H_2O_2. Reaction conditions: POM 0,8 µmol; substrate 0,5 mmol; H_2O_2 0,1 mmol, 0,6 ml of HFIP, T=70°C.

#	Alkene	T(°C)	yield % HFIP (min)	yield % CH_3CN/**2** (min)	yield % HFIP/**2** (min)	yield % CH_3CN/**3** (min)	yield % HFIP/**3** (min)	yield % HFIP/**4** (min)
1	Cyclooctene	70	84 (15)	6 (15)	99 (15)	6 (15)	79 (15)[b]	89 (15)
		25	23 (15)	-	-	-	>99 (15)	-
2	Cyclohexene	70	59 (15)	18 (15)	97 (15)	<5 (15)	98 (15)	42 (15)
		25	30 (60)	-	>99 (60)	-	>99 (30)	-
3	*trans*-2-octene	70	86 (15)	38 (15)	99 (15)	<5 (15)	92 (15)	78 (15)
		25	45 (180)	-	99(180)	-	96(120)	-
4	1-octene[a]	70	6 (25)	<5 (25)	77 (25)	<5 (25)	79 (25)	56 (15)
		40	<5(180)	-	98(180)	-	98(180)	-
5	1-hexene[a]	70	<5 (25)	<5 (25)	68 (25)	<5 (25)	47 (25)	73 (25)
		25		-	98(420)	-	98(420)	-
6	1-decene[a]	70	5 (25)	9 (25)	85 (25)	< 5 (25)	75 (25)	99 (25)
		40	<5 (120)	-	92 (120)	-	84 (60)	-
7	1-dodecene[a]	70	< 5 (25)	<5 (25)	80 (25)	< 5 (25)	78 (25)	76 (25)

[a] Carboxylic acids in traces are also observed. [b] Presence of cyclooctanone is also observed.
All yields are calculated with respect to H_2O_2.

Since the catalytic activity of **1** was found to be negligible in HFIP, the screening of activity has been reported for complexes 2, 3, 4 in Table 3.1.

Results can be discussed as follows:

(i)   Epoxidation of **internal olefins** (entries 1-3 in Table 3.1) occurs smoothly in HFIP at 70 °C in the absence of POM catalysts. However, a remarkably efficient process results from the combined system, integrating both the fluorous-tagged catalysts **2** or **3** and the HFIP medium. Under these conditions, epoxide yields > 99% and excellent selectivities are obtained at 25°C, in 15-30 min. Noteworthy, the activity of the fluorous-tagged, non-lacunary derivative **4** turns out to be negligible, indicating a dominant role of the defect site on the POM surface.

(ii)   The synergistisc effect of the fluorous binary systems is striking in the case of the less nucleophilic **terminal olefins** (see entries 4-7 in Table 3.1). In all cases the composite system HFIP/Hybrid-POMs **2-4** features a strong reactivity enhancement, in comparison with the isolated counterparts (HFIP or hybrid complexes in CH₃CN). The increase of the reaction efficiency by the HFIP/**3** catalyzed process is also unequivocally demonstrated by the column graph in Figure 3.10.

(iii)   Reactions performed at 25°C, are more selective, because any secondary reaction, including the overoxidation and epoxide cleavage and/or H_2O_2 decomposition, are minimized.
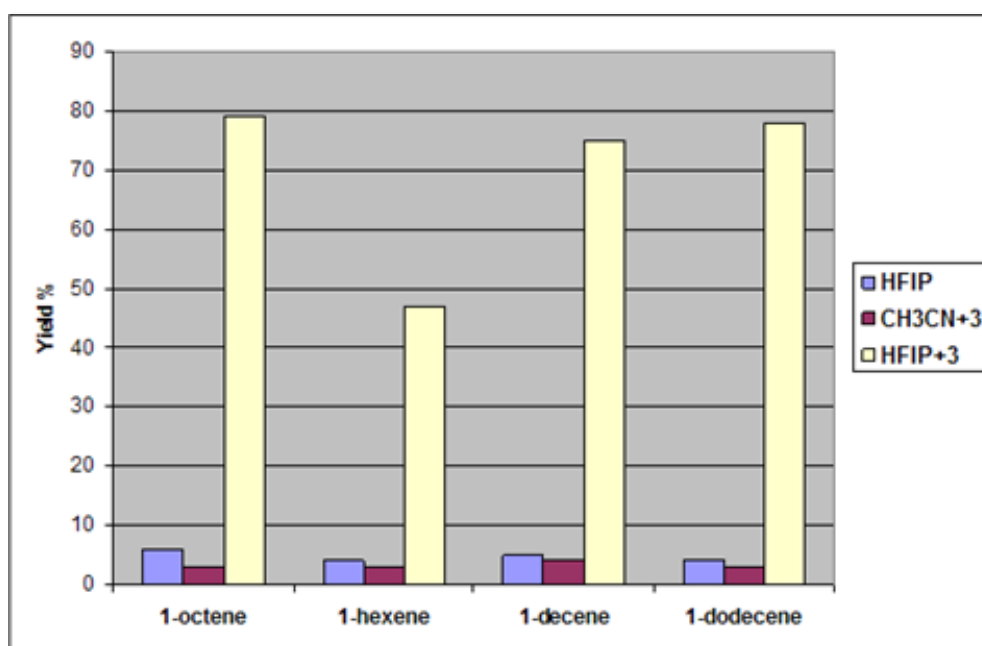
Figure 3.10. Synergistic effect for the composite system HFIP/3 with respect to the isolated counterparts: HFIP or 3/CH₃CN for different terminal olefins. Similar series have been obtained for complexes 2 and 4.

The reactions have also been performed under microwave (MW) assisted conditions[30][40]. Even if HFIP has a dielectric constant relatively low (ε = 16.7), the polyanionic nature of the catalysts is pivotal to exploit the MW absorption[41]. Under the conditions adopted (Table 3.2) epoxidation of 1-octene, chosen as a model substrate, occurs with yields up to 99% in 20 min., in the presence of catalyst **3**. Good results are also obtained in the presence of **2**, yielding 90 % epoxide (see Table 3.2, entries 3, 4). Noteworthy, These results have to be compared with the 5% conversion obtained when only HFIP is present (see Table 3.2, entry 1), again showing the remarkable synergistic effect of the composite system.

Table 3.2. Oxidation experiments of 1-octene with H_2O_2 in the presence of fluorous-tagged hybrids-**1-4**. Reaction conditions: POM 0,8 µmol; 1-ottene 0,5 mmol; H_2O_2 0,1 mmol; 0,6 ml of HFIP, 70°C.

Entry	POM	Reaction conditions	yield %[a] 1,2-epoxyoctane (time, min)
1	-	MW[b]	5 (20)
2	**1**	MW[c]	22 (20)
3	**2**	MW[c]	90 (20)
4	**3**	MW[c]	99 (20)
5	**4**	MW[c]	67 (20)

a. Yield calculated respect H_2O_2, carboxylic acids and diols are detected in trace.
b. Irradiation power = 100 W, T_{bulk} = 70-80°C.
c. Irradiation power = 100 W, T_{bulk} = 75-85°C.

Evidence on the character of the competent oxidant formed in solution under turnover conditions, and of its stereo-electronic features, have been derived from the competitive oxidation of hexene isomers.

Table 3.3. Competitive epoxidations of different hexene isomers with H_2O_2. Reaction conditions: POM 0.8 µmol; substrates 0.25+0.25 mmol; H_2O_2 (70%) 0,1 mmol; 0.6 ml of HFIP, T=70°C.

Hexenes	Reactivity Ratio			
	HFIP[b]	HFIP/**2**[a]	HFIP/**3**[a]	HFIP/**4**[a]
trans-2-hexene/1-hexene	19	3.3	3.1	2.0
cis-2-hexene/*trans*-2-hexene	1.4	2.0	2.4	4.9
cis-2-hexene/1-hexene	18	7.6	7.9	6.1

[a] t=15'; [b] t=1h;

Results in Table 3.3 address the reactivity ratios of the epoxidation performed under different conditions, with or without the fluorous-tagged catalyst. Inspection of data in Table highlights some key points as follows:

(i) Epoxidation promoted by HFIP alone is dominated by electronic effects. This is clearly indicated by the superior reactivity of *cis*/*trans* internal hexenes compared to the terminal one (reactivity ratio >18) and by the reactivity ratio close to 1, observed for the *cis*/*trans* isomers.

(ii) Epoxidation promoted by the hybrid catalysts in HFIP undergoes to a different selectivity behaviour. Indeed, a remarkable activation of the terminal olefin is observed, when compared to the electron-richer *cis*/*trans* isomers. In this case the

selectivity ratio drops in the range 2-8. Also, the *cis/trans* hexenes react with a selectivity factor in the range 2-5. This fact rules out the participation of solvent-based intermediates, like dioxiranes or geminal hydroxo-hydroperoxo species, and points to the involvement of a POM-based peroxide. This latter is expected to show an increased reactivity and sensitivity to steric effects[26a 26b]

A working hypothesis on the structural formulation of the oxidant shall take into consideration the following factors: (i) a POM-based peroxide, (ii) its formation on the defect surface site, (iii) a strong activation by interaction with the fluorinated alcohol. In this light, a convincing scenario depicts a tungsten hydroperoxide interacting through a network of hydrogen bonds with the donor/acceptor sites of the HFIP solvent. This supramolecular assembly is likely responsible for the synergistic action leading to a remarkable reactivity enhancement, observed in the binary system HFIP/POM catalyst (Scheme 3.4).

Amsterdam Density Functional (ADF)[42] calculations have been performed to address the stereo-electronic properties of a selected molecular fragment representing the surface inorganic hydroperoxide, hydrogen bonded to HFIP (See Scheme 3.4). The optimized geometry of the supramolecular complex yields a distinct elongation of the metal-peroxo bond, compared to the isolated species, as fostered by the H-bond ligation with the solvent.


A

B
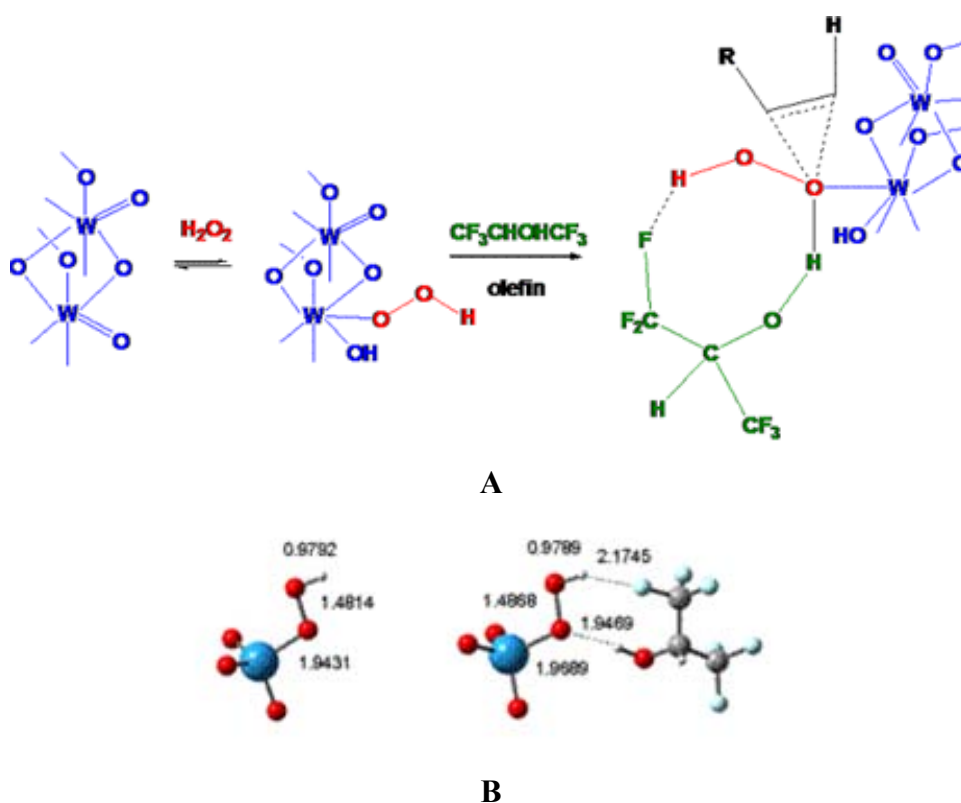
Scheme 3.4. A) Hypothesis about possible transition state and B) calculated structure for the W-peroxo moiety activated by HFIP.

Moreover, the oxygen transfer to the olefin acceptor is likely to occur via a transition state which happens to be favoured by a double effect, including the electronic activation of the peroxide LUMO by the ligation with the d^o tungsten atom, and the specific H-bond interaction with the perfluorinated solvent.

3.3.4. Amphiphilic and structural properties of fluorous-tagged hybrids.

Such hybrid amphiphiles can aggregate in solution. In this regard, the POM molecular unit provides a versatile *tecton,* being a building block with structure/composition/charge features to be tailored in order to control the *packing parameters* and then finally, the aggregate morphology. This latter is expected to be influenced by the overall tungsten content – length, volume and number- of the fluorophilic chains[43].

Dynamic Light Scattering (DLS) measurements carried out for **1-4** in HFIP at catalytic concentration, indicate the presence of spherical assemblies, while, in CH_3CN, the solution gives very poor signals. Such assemblies, with average hydrodynamic diameter ranging from 100 to 150 nm, are formed in a very short time after the sample is dissolved. Corresponding DLS results are shown in figure 3.11:
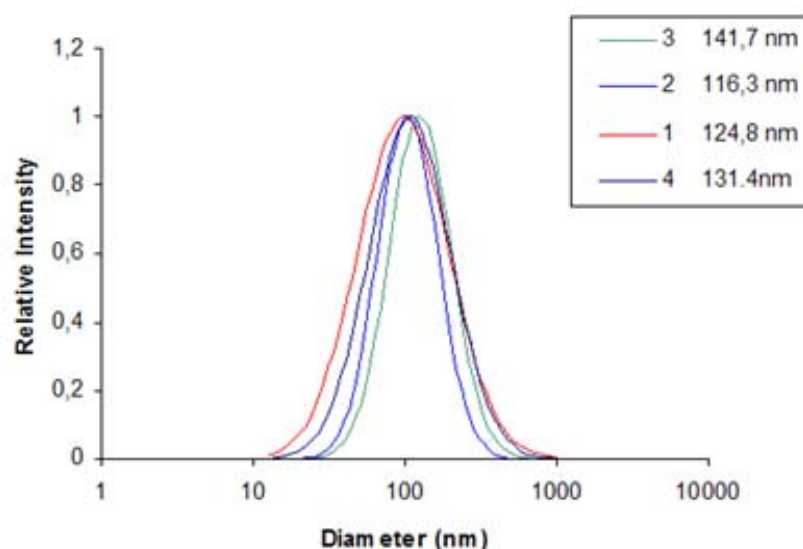
Figure 3.11. DLS measurements of complexes 1-4 in HFIP at catalytic concentration (1.33 mM). The legend shows the diameters at maximum of statistical distributions for each of four studied systems.

It is worth to mention that the acceleration effect observed for H_2O_2 mediated oxidation in HFIP, has been recently addressed on the basis of the formation of H-bonded clusters involving the fluorinated alcohol and the peroxide moiety[11]. This aspect is of particular

relevance when considering the synergistic action of the POM catalysts and the eventual formation of vesicle/micelle like supremolacular aggregates, where the solvent/peroxide reagent can exist in a confined state. The effect of catalyst aggregation on the epoxidation kinetics has thus been examined by performing the oxidation of *cis* – cyclooctene at 25 °C and in the presence of increasing concentration of the POM hybrids. To this aim, the most reactive catalysts **2** and **3** have been selected for screening, and the resulting traces are reported in Figure 3.12. In both cases, the oxidation rate shows a saturation behaviour startingwhen more than 0.2 μmol of POM are present in the reactor ([POM] > 0.33 mM). A possible explanation would imply that POM aggregation is making the catalytic sites less available to activation, in terms of exposition/solvation of the fluorinated alcohol.
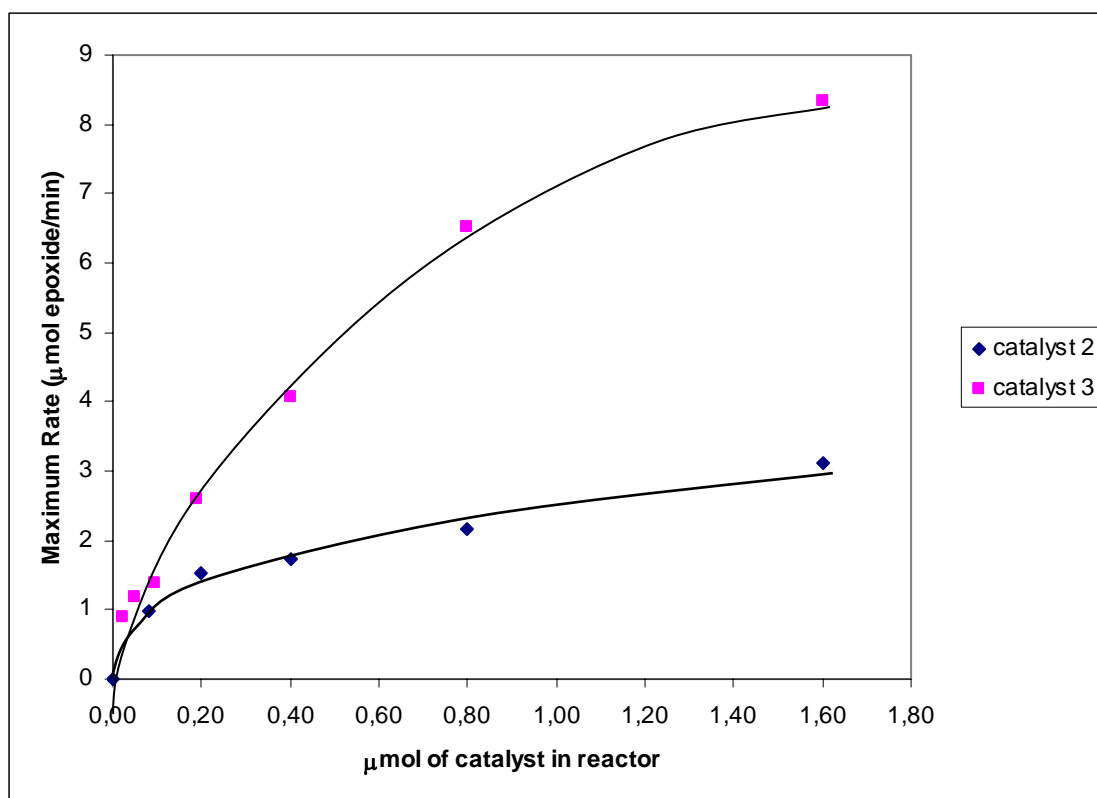

Figure 3.12. Graph reporting maximum rates vs μmol of catalyst. Rates have been calculated for linear steps of the kinetic trace, subtracting solvent contribution.

This issue can be addressed by studying the morphology of the nanostructured assemblies evolving in solution as a result of the aggregation of the amphiphilic POM[44]. To this aim, the diverse systems under investigation have been studied by Scanning Electron Microscopy (SEM) and Transmission Electron Microscopy (TEM), applied to solid-state samples prepared from HFIP solutions of **1-4** after solvent evaporation on a silicon plate.

74

Indeed, SEM images show the presence of spherical vesicles with dimensions ranging from 160 to 260 nm, as reported in Figure 3.13 for **3**.
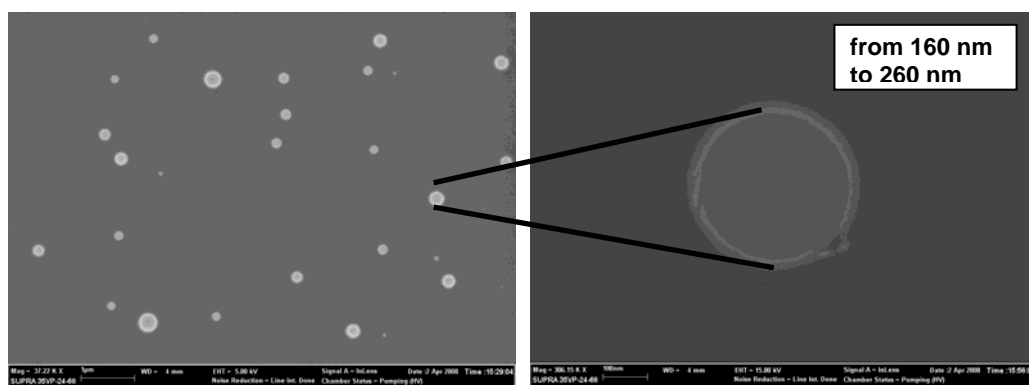
Figure 3.13. SEM images of complex (3) in the solid state. Sample has been obtained starting from a solutions 1.33 mM (catalytic conc.) in HFIP.

TEM images[45] suggest that such aggregates bear a multilamellar structure, as expected for a hybrid assembly based on surfactant-encapsulated polyoxometalates[34].

A   **B**
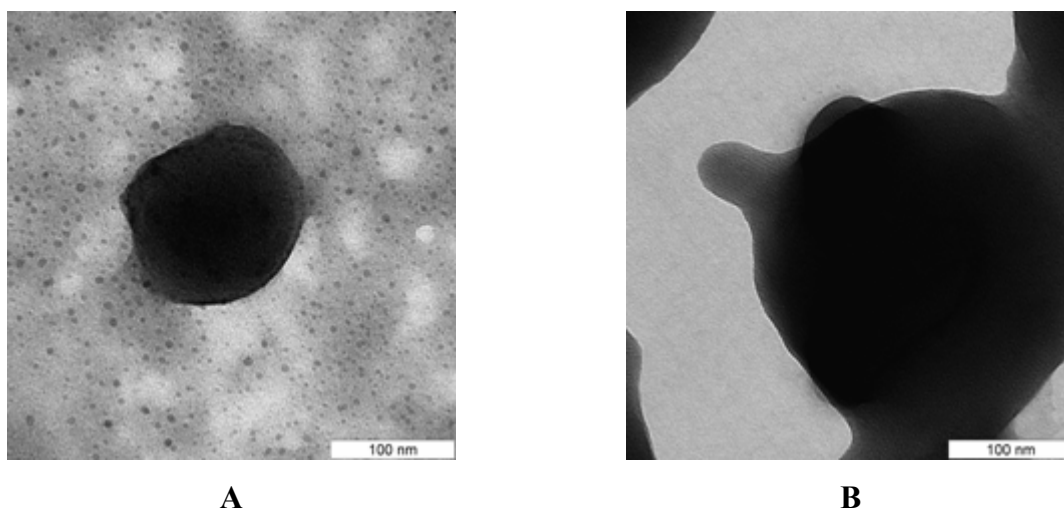
Figure 3.14. TEM images from CH$_3$CN 1mM solutions of: (3) A and (1) B.

A possible explanation is that a layered structure arises from the regular packing of the amphiphilic POM units in which fluorinated chains (F) are faced to shield two polyanionic layers, while TBA cation (Q) are faced each other on opposite sides, as in the following model:

HFIP--F-**POM**-Q--Q-**POM**-F--F-**POM**-Q-

HFIP
interface
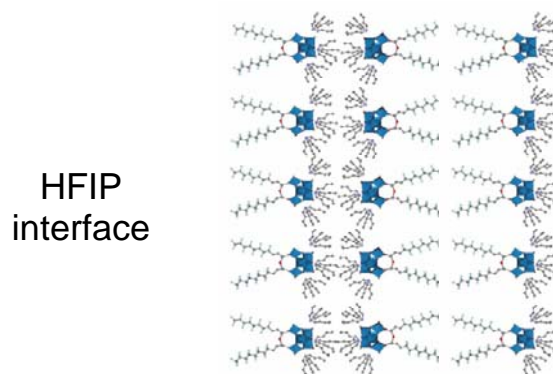
Fig 3.15 Scheme of a layered structure from the regular packing of the amphiphilic POM units.

The exact morphology of such aggregates will be established by Small Angle X-ray Spectroscopy (SAXS), to detect the presence and the orientation of multiple layers of ordered *tectons*.

3.3.5 Catalyst heterogenization in co-polymeric networks.

The catalyst up-grade has been realized through heterogenization of these hybrid catalysts within a suitable support. In the previous chapter, a successful approach has been presented, exploting membrane-based technology and fluorous polymers. In the present case, the combined use of fluorinated membranes with fluorous alcohols is not possible, because of the solubility of the heterogeneous material in this medium, and the corresponding extensive leaching of the catalyst in solution.

To overcome this problem, strategies for the covalent graphting of the POM hybrid to the polymeric material, have been devised herein. The synthetic approach exploits the intoduction of terminal unsaturated alkyl chains, by covalent functionalization of the lacunary POM precursor. Polyoxotungstates containing vinyl, allyl, methacryl, styryl moieties have been reported in the literature[46].

These complexes have been used as molecular cross linking agents in the presence of acrylates to prepare new hybrid polymers with hydrogel behaviour, with swelling properties[47] or to be used for catalytic applications[48].

3.3.5.1 Synthesis and characterization of functionalized hybrid polyoxotungstates as monomers.

Two different hybrid complexes (**5** and **6**), derived respectively from monovacant $[\alpha\text{-}SiW_{11}O_{39}]^{8-}$ and divacant $[\gamma\text{-}SiW_{10}O_{36}]^{8-}$ polyoxotungstates precursors (see section 3.3.1) have been synthesized by covalent graphting of two 1-octenyl alkyl chains (R). The synthetic strategy adopted is exactly the same as that reported for the fluorophilic hybrid complexes in Scheme 3.3.

Derivatives **5** and **6** have been characterized in solution by ESI-MS, ^{1}H, ^{13}C, ^{29}Si and ^{183}W-NMR and in the solid state by FT-IR and elemental analysis (see Experimental part, Section 5.4.3).

Among their characterization, particularly diagnostic are ^{183}W-NMR and ^{13}C-NMR spectra because they allow to recognize the expected signals for the inorganic moiety as well as the presence of the unsaturated alkyl chains in the final product.

In the following figures, ^{183}W-NMR of complexes **5** and **6** are reported and the resulting spectra are very similar to those reported for complexes **1** and **2**:

TBA$_4$[(CH$_2$=CH(CH$_2$)$_6$Si)$_2$O(SiW$_{11}$O$_{39}$)] **(5)**
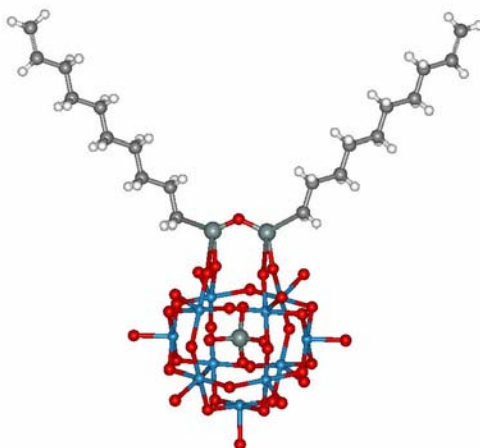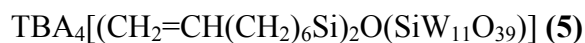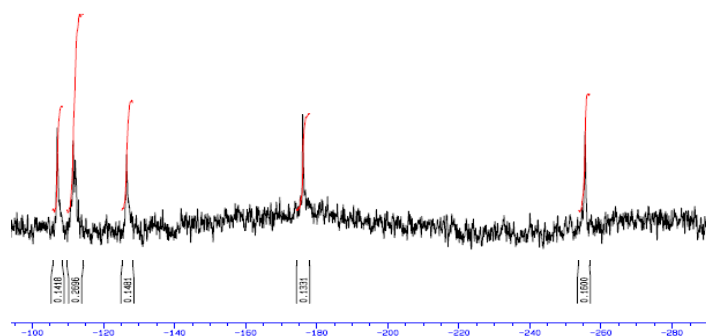
Figure 3.16. ^{183}W-NMR spectrum of (5) in CD$_3$CN/ CH$_3$CN and its representation.

TBA$_4$[(CH$_2$=CH(CH$_2$)6Si)$_2$O(SiW$_{10}$O$_{36}$)] **(6)**
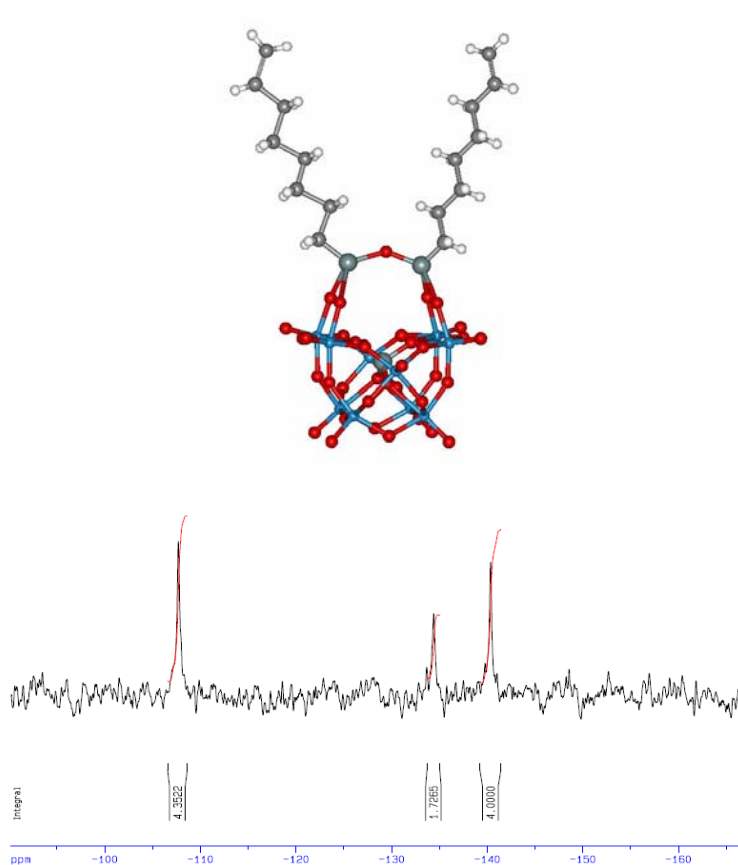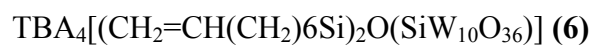
Figure 3.17. ^{183}W-NMR spectrum of (6) in CD$_3$CN/ CH$_3$CN and its representation.

Similar ^{13}C-NMR have been collected for both complexes **5** and **6,** with the latter reported below. It accounts for the octenyl alkylic residues graphted on the lacunary oxygens and for the butyl chains of the counterion.
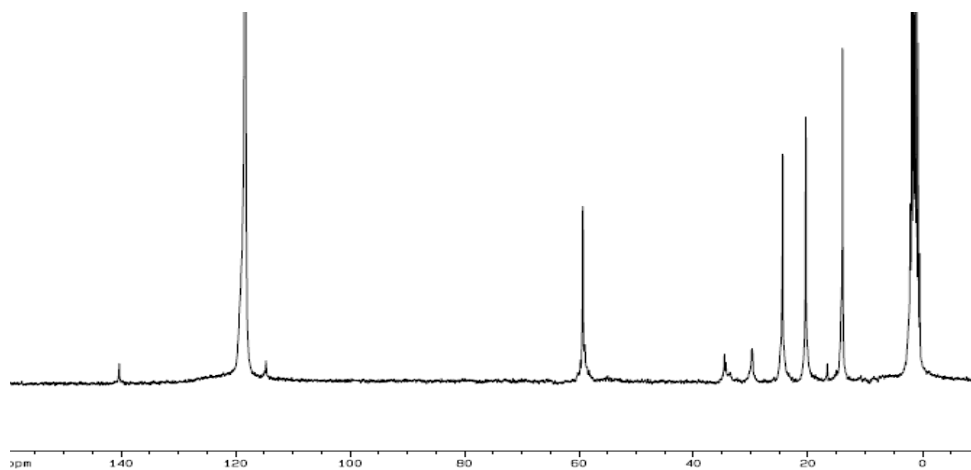
Figure 3.18 ^{13}C-NMR of complex 6.

As previously reported for fluorinated hybrid complexes **1 – 3**, FT-IR analysis confirm the successful POM functionalization.

A

B
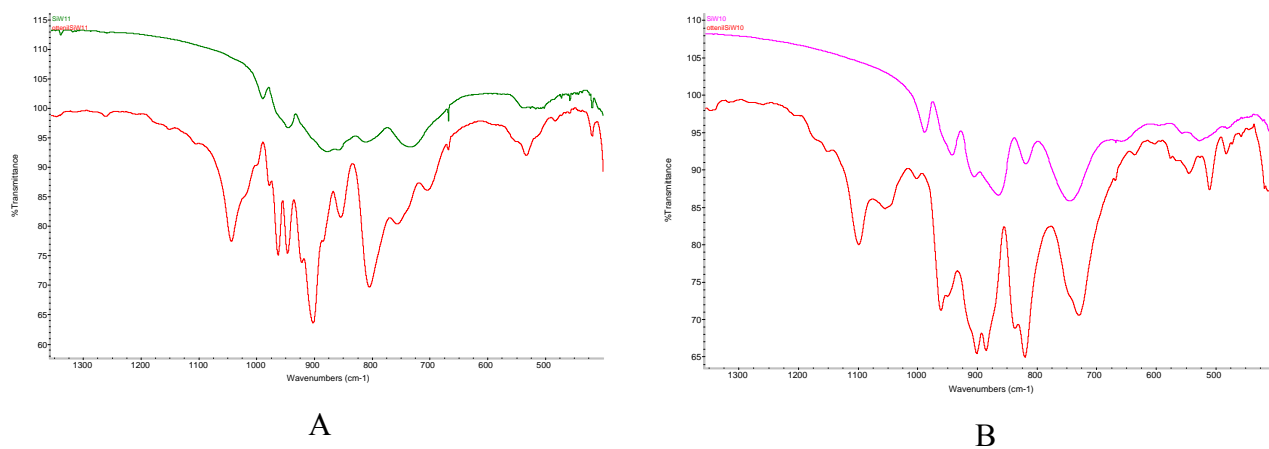
Figure 3.19. Comparison of FT-IR spectra (KBr) of hybrid complexes 1 – 3 with respect those of their precursor A) FT-IR of [α-SiW$_{11}$O$_{39}$]$^{8-}$ and hybrid complex (5) (green line and red line respectively). B) FT-IR of [γ-SiW$_{10}$O$_{36}$]$^{8-}$ and (6) (purple line and red line respectively).

3.3.5.2 Hybrid polyoxotungstates cross-linked in co-polymeric networks:.

POM bearing terminal olefin functions can be cross-linked in the presence of different co-monomers.

The choice of 1-octenyl residues to be graphted in the vacant polyoxoanion, rather than a shorter vinylic or acrylic residues, fosters an efficient polymerization reaction. Polymerization process have been thus performed at 70°C with methyl methacrylate (MMA) as co-monomer, ethylene glycol dimethacrylate (EDM) as the main cross-linking agent, in the presence of bis (tertbutyl-cyclohexyl) peroxodicarbonate as radical initiator, together with the porogenic solvents 1,4-butanediol and 2-propanol[49]. CH_3CN has been added in minimum amount, in order to completely solubilise the POM in the reaction mixture.
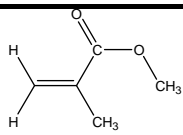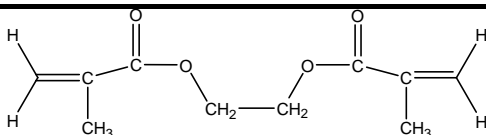
Different ratios of the individual components have been tested, with **5** or **6** hybrid monomers, in order to obtain polymeric materials with different structure and morphology, to be correlated with their catalytic activities with the final aim to get informations to optimize the properties of the resulting materials.

Polymerization conditions and the ratios between components in the polymerization mixture have been reported in the following Table 3.4:

Table 3.4. Polymerization conditions. Radicalic initiator: bis (tertbutyl-cyclohexyl) peroxodicarbonate (1%). Porogenic solvents:1,4-butanediol, 2-propanol, CH_3CN in minimum amount to homogenize polymerization mixture, P Ar = 1 atm. T = 70°C. All % are w/w.

Polymer	MMA	EDM	POM-monomer
PMMA-1[a]	25%	15%	0%
PMMA-2[a]	25%	11,3%	3,7%
PMMA-3[a]	25%	7,5%	7,5%
PMMA-4[a]	25%	3,7%	11,3%
PMMA-5[a]	10%	18%	12%
PMMA-6[b]	10%	10%	12%

[a] 1,4-butanediol e 2-propanol are in ratios 25% e 35% w/w respectively.
[b] 1,4-butanediol e 2-propanol are in ratios 28% e 40% w/w respectively.

Final polymers containing both polyoxotungstates **5** and **6** have been isolated in good yields (80-85%), upon precipitation, washing with a mixture of organic solvents (tetrahydrofurane/acetonitrile 4/1 vol/vol) and then vacuum drying.

These materials can be thus conveniently represented as in the following figure, which highlights how the POM is cross-linked in the final copolymeric network, together with four tetrabutylammonium counterions:
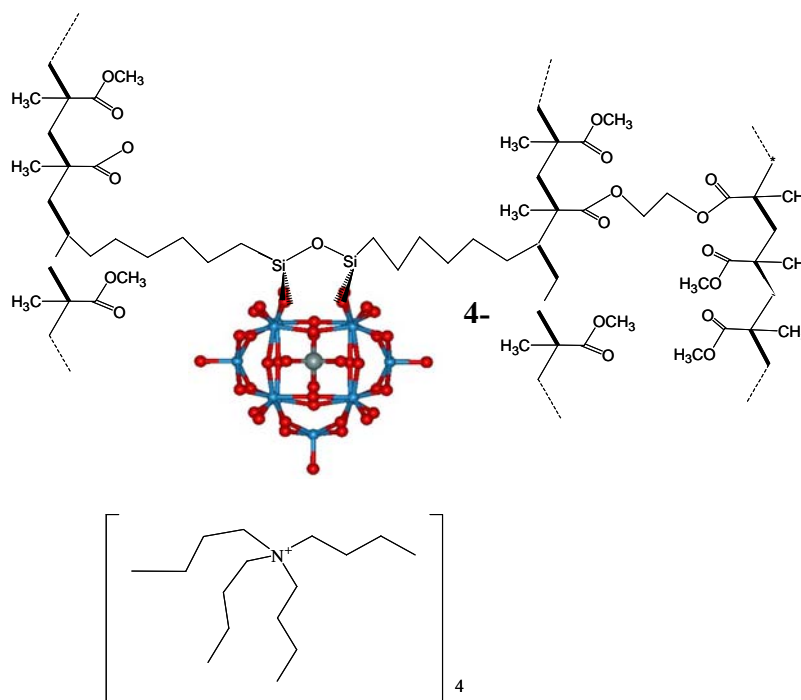
Figure 3.20. Hypothetic structure for hybrid copolymer.

The solubility in CH₃CN depends on the [MMA]/[EDM]/[**POM**] ratio, and in particular on the weight percentage of the cross-linking monomer (EDM) added in the polymerization mixture. When its percentage is higher than 15%, the resulting material is completely insoluble, while at lower ratios, a hybrid polymer with *swollen-gel* behaviour is obtained.

To obtain a highly porous polymers, the polyanion and porogenic solvents have been added in higher weight ratios while keeping EDM below 15% (see Table 3.4, entry 6).

The resulting materials have been characterized in the solid state by means of FT-IR spectroscopy, thermal analysis and electronic microscopy.

FT-IR analysis show that the polyoxotungstate vibrational bands in the region between 750 and 1100 cm^{-1} (νSiO$_2$ 1044 cm^{-1}, νW=O$_t$ 903 cm^{-1}, νW-O$_b$-W 854, 805 cm^{-1}) are maintained in the hybrid material, confirming both its presence and its stability after radical polymerization, as reported in the following figure:
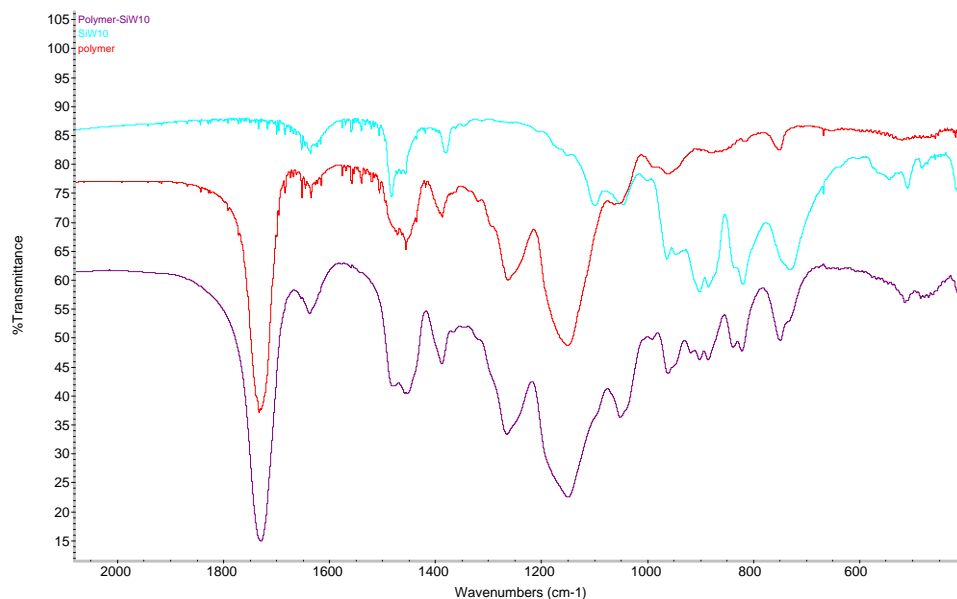
Figure 3.21. FT-IR of a) only POM: [(CH$_3$CH$_2$CH$_2$CH$_2$)$_4$N]$_4$[CH$_2$CH(CH$_2$)$_6$Si]$_2$OSiW$_{11}$O$_{39}$ (6) *top (green spectrum);* **b) PMMA (copolymer of MMA and EDM)** *in the middle (red spectrum);* **c) PMMA-(5)POM** *bottom (blue spectrum).*

TGA and DSC measurements show that 14% of the material is likely made of inorganic components. This reveals that only 53% of the initial polyoxometalate has been cross – linked into the final polymer or, as suggested by the elemental analysis, a significant amount of solvent is still trapped within the polymeric lattice.

A

B
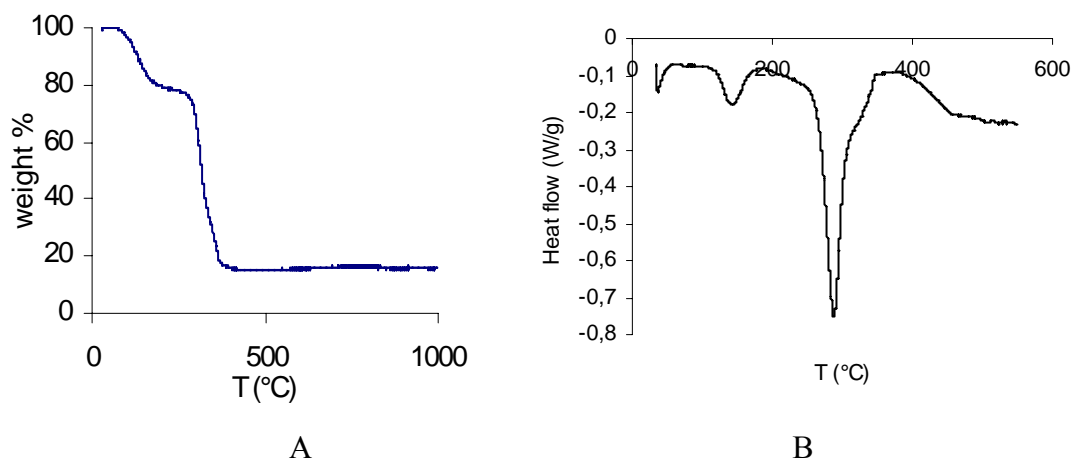
Figure 3.22. A) TGA of porous PMMA-6 polymer, obtained in the condition shown in Table 3.4. Analysis has been carried out under air, 10°C/min. B) DSC of the same polymer, showing endothermic transformations.

The morphology of these materials has been investigated by SEM analysis. In particular, for the porous polymer (see entry 6 in Table 3.4), a comparison with a similar copolymer of MMA and EDM without POM, reveals that the presence of the inorganic complex enhance

the porosity of the final material. A network with pores with width of 200-500 nm has been observed both in presence of **5** or **6** while PMMA shows compact aggregates larger than 1 μm (see Figure 3.23A and B, here below).
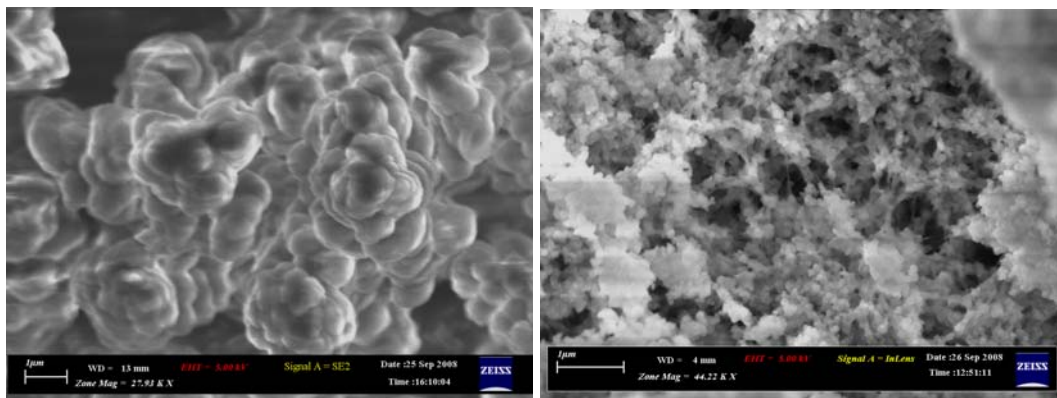
A   B

Figure 3.23. SEM images of PMMA e PMMA-(6).

The investigation on the morphology of such materials has also been completed by TEM images[45]. For the denser regions of the hybrid polymer, packed irregular aggregates (dimensions ranging from 80 to 100 nm) are observed.
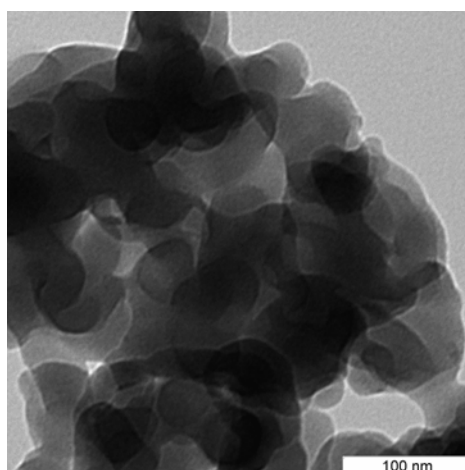
Figure 3.24. TEM image of PMMA-5 obtained at the conditions shown in entry 5 of Table 3.4.

The characterization of such materials have to be completed with an accurate study on pores dimension and the swelling behaviour when mixed with CH_3CN, dimethylformamide (DMF), dimethylsulfoxide (DMSO) and perfluorinated solvents like HFIP and 2,2,2-trifluoroethanol

(TFE). Finally, EDX analysis will be instrumental to confirm the composition the hybrid material.

3.3.5.3 Catalytic activity of polyoxotungstates in co-polymeric networks.

The activity of such heterogeneous catalytic systems has been initially investigated by performing the epoxidation of *cis*-cyclooctene in the presence of hydrogen peroxide in acetonitrile.

The different polymeric materials have been screened for catalytic activity in the epoxidation of both internal and terminal olefins, by using an analogous reaction protocol as described for the homogeneous oxidation in HFIP (see previous paragraph). The results obtained are reported in the following Table 3.5:

Table 3.5. Cyclooctene epoxidation. Reaction conditions: POM (estimated in polymeric material) 0,8 µmol; *cis*-cyclooctene 0,5 mmol; H_2O_2 0,1 mmol; 0,6 ml of CH_3CN, T = 70°C.

Entry	catalyst	(w/w %)[a]	Solubility in CH_3CN	2h	4h	overnight
1	**5**		YES	<5	<5	<5
2	**MMA:EDM:5**	25:11,3:3,7	Swollen gel	<5	<5	<5
3	**MMA:EDM:5**	25:7,5:7,5	Swollen gel	<5 %	<5	<5
4	**MMA:EDM:5**	25:7,5:11,3	Swollen gel	<5	<5	5
5	**MMA:EDM:5**	10:18:12	NO*	<5	<5	7
6	**6**		YES	28	37	70
7	**MMA:EDM:6**	25:7,5:7,5	Swollen gel	<5	<5	42
8	**MMA:EDM:6** [b]	25:7,5:7,5	Swollen gel	<5	6	51
9	**MMA:EDM:6**	10:10:12	NO*	<5	6	45
10	**MMA:EDM:6** [b]	10:10:12	NO*	9	18	85
11	**MMA:EDM:6** [c]	10:10:12	NO*	< 5	< 5	9

Yields were calculated with respect to H_2O_2. **a** weight ratios are referred to the polymerization mixture, the difference to 100% is represented by the porogenic solvents contribute. **b** 2µmol catalyst on polymeric matrix, **c** 2µmol catalyst on polymeric matrix; 1-octene were used as substrate rather than *cis*-cyclooctene.
* The catalytic polymer is insoluble in CH_3CN but give swelling.

Results in Table 3.5 allow to observe that complex **6** is more active than **5**, both in heterogeneous phase (85% of maximum yield after 24 hours) and in homogeneous phase, in agreement with the experimental results obtained with the hybrid fluorinated complexes (see Section 3.3.3).

Yields obtained with the heterogeneous systems are generally lower than those calculated for the corresponding homogeneous systems with the same catalytic loading (compare entry 1

with 2-5 and entry 6 with 7 and 9 on Table 3.5): it is thus required a higher catalyst content in the reaction mixture to reach synthetically interesting yield (compare entries 7 with 8, and 9 with 10 on Table 3.5).

Since the catalytic system [MMA]/[EDM]/[**6**] = 10:10:12% w/w, with higher porosity, has shown the best performance, it has also been used in perfluorinated alcohols (1,1,1,3,3,3-hexafluoro-2-propanol - HFIP - and 2,2,2-trifluoroethanol – TFE -), in the presence of hydrogen peroxide. Results reported in table 3.6 shows that quantitative yields for the epoxidation of *cis*-cyclooctene and 1-octene have been obtained after 15 and 60 minutes, respectively. This reveals that the expected synergistic effect is maintained also under heterogeneous conditions. At variance with the acetonitrile mixture, catalytic results obtained with **6** in HFIP are better for the heterogeneous system. As a final remark, it is interesting to observe that the fluorophilic complex **2** is much more efficient than **6** (see Table 3.1), suggesting that the fluorinated chains are also important for its enhanced efficiency. It should be noted, however, that the free olefinic functional group can be oxidized to give terminal epoxides, likely affecting both the catalytic activity and the aggregation behaviour.

Table 3.6. Catalyitc epoxidation reactions with **6**: 0,8 μmol estimated in polymeric material: **MMA:EDM:6**=10:10:12; substrate 0,5 mmol; H_2O_2 0,1 mmol; 0,6 ml of perfluorinated solvent, T = 70°C. Yields were calculated with respect to H_2O_2.

Catalyst	Substrate	Solvent	Yield %(minutes)
MMA:EDM:6		HFIP	99 (15)
6	*cis*-cyclooctene		61 (15)[a]
MMA:EDM:6		TFE	93 (30); 99 (60)
MMA:EDM:6		HFIP	21 (25); 70 (60)
6	1-octene		23 (25)[a]; 42 (60)[a]
MMA:EDM:6		TFE	10 (30); 80 (180)

[a] Yields obtained in homogeneous conditions.

After the reaction, the polymeric catalyst can conveniently be recovered by filtration from the reaction mixture and then recycled. Control experiments have been made to exclude catalyst leaching or polymer loss by solubilisation or degradation phenomena. These experiments are presented in the following graph in Figure 3.25:
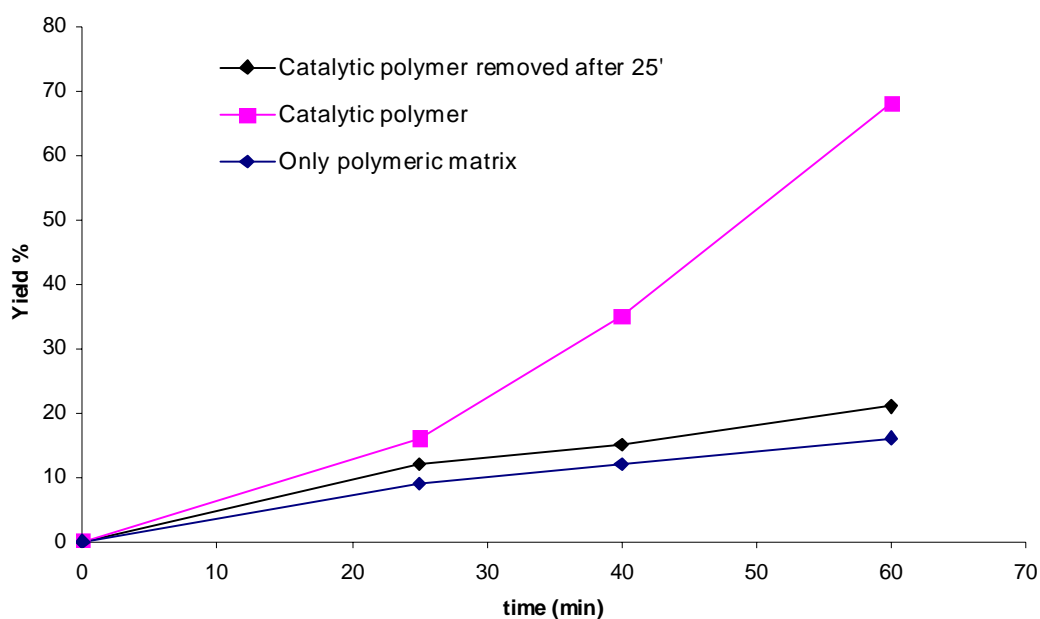
Figure 3.25. Control experiment performed with the polymeric matrix without the active specie and leaching test for the polymeric catalyst. Oxidant: H$_2$O$_2$ 70% in HFIP.
Polymer MMA:EDM:6=10:10:12 was pre-treated in HFIP a 70°C before use.

These kinetic profiles reveal that:

- The polymeric matrix (*blue line*) alone is not providing any catalytic activity, since the epoxidation profile overlaps with that observed in HFIP without added catalyst (compare the black line, and see Table 3.1, Section 3.3.3).

- In the presence of the catalytic polymer (*purple line*) a remarkable acceleration of the epoxidation rate is observed. The kinetic profile is reproducible, even for different batches of the hybrid polymeric material, or when it is pre-treated at high temperatures in the reaction medium.

- Upon removal of the heterogeneous catalyst (black line) from the solution, after 25 minutes, the epoxidation undergoes a sudden slowdown, and the reaction slope becomes that of the uncatalyzed process.

FT-IR analysis of the recovered material has revealed a partial structural change (see the region of polyoxoanion bands between 1100 and 800 cm^{-1} in the Figure below).

Future experiments will address the recycling behaviour and the design of continuous-flow epoxidation systems. The possibility to use these material inside "monolithic" columns, in

which the polymer is also covalently bonded with the internal walls of the reactor will also be explored[50].
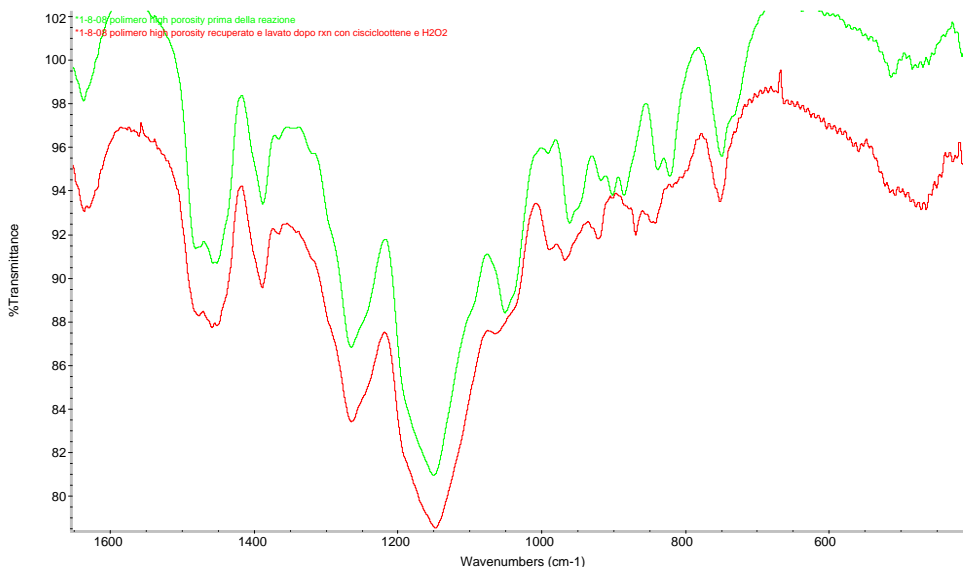
Figure 3.26. FT-IR Comparison for the polymeric catalyst MMA:EDM:(5)=10:10:12 with high porosity. **Top: FT-IR spectrum before reaction**, **Bottom: FT-IR spectrum of recovered catalyst.**

3.4 Conclusions.

In summary, innovative fluorous-tagged POMs have been synthesized and used for catalytic epoxidation in fluorous alcohols. A synergistic effect on catalysis has been discovered that fosters unprecedented catalytic rates, almost quantitative yields and high selectivity also for terminal epoxides, (yields up to 90-99%; TON = 125, TOF 500 h^{-1}) These POM hybrids were synthesized employing mono-, di-, or tri-lacunary Keggin polyoxotungstates and fluorinated organosilyl derivatives (RfSiCl$_3$), to afford covalently grafted complexes, isolated as tetrabutylammonium salts and characterized both in solid state and in solution. Noteworthy, under microwave irradiation, the epoxide is produced in quantitative yield after 20 minutes (TON: 124, average TOF: 6.2 min^{-1}). A very interesting issue, is that, being amphiphilic molecules with an extended fluorophilic domain and a polar inorganic head, they assemble in solution giving nanoaggregates in solution, which have also been observed by SEM and TEM analysis. The upgrade to heterogeneous catalysis has also been achieved exploiting the covalent functionalization approach. In this case, the lacunary polyoxotungstates have been reacted with an organo silyl chloride bearing a terminal olefinic group. The resulting di-

substituted complex has been successfully heterogenized by cross linking in a co-polymeric network. The morphology and the structure of the resulting hybrid materials can be tuned upon variation of copolymers and porogenic solvents ratio. FT-IR spectra show the integrity of the inorganic structure.

These materials can swell in fluorinated alcohols and exhibit interesting reactivity towards olefins epoxidation. (Yield > 99% for cis-cyclooctene epoxidation, TON > 124, TOF > 6.2 min^{-1}).

3.5 References and notes.

[1] a) F. Haber, J. Weiss, *Naturwissenschaften,* 20, **1931**, 948. b) J. K. Kochi (Ed.), Free Radicals, vol. II, WILEY, New York, **1973**, Chapters II-IV, pp. 5-37. c) H. Weiner, A. Trovarelli, R. G. Finke, *J. Mol. Catal. A,* 191, **2003**, 217-252 and references therein.

[2] R. A. Sheldon, in *Applied Homogeneous Catalysis with Organometallic Compounds,* eds. B. Cornils, W. A. Herrmann, VCH, Weinheim, **1996**, vol. 1, p. 411.

[3] G. Sienel, R. Rieth and K. T. Rowbottom, in *Ullmann's Encyclopedia of Organic Chemical,* WILEY-VCH, Weinheim, **1999**, vol. 4, p. 1987.

[4] D. Swern in *Organic Peroxides,* ed. D. Sweren, Wiley Interscience, New York, 1971, vol. 2, p. 355.

[5] Peroxomonocarbonate has been suggested as an environmentally attractive anionic peracid. a) H. Yao, D. E. Richardson, *J. Am. Chem. Soc.,* 122, **2000**, 3220. b) D. E. Richardson, H. Yao, H., K. M. Frank, D. A. Bennett, *J. Am. Chem. Soc.,* 122, **2000**, 1729.

[6] M. G. Clerici, G. Bellussi, U. Romano, *J. Catal.,* 129, **1991**, 159.

[7] C. Venturello, E. Alneri, M. Ricci, *J. Org. Chem.* 48, **1983**, 3831

[8] D. E. De Vos, B. F. Seles, M. Reynaers, Y. V. S. Rao, P. A. Jacobs, *Tetrahedron Lett.,* 39, **1998**, 3221.

[9] W. A. Herrmann, R. W. Fischer, M. U. Rauch, W. Scherer, *J. Mol. Catal.,* 86, **1994**, 243.

[10] a) P. D. Bartlett, J. E. Leffler, *J. Am. Chem. Soc.,* 72, **1950**, 3030. b) A. O. Chong, K. B. Sharpless, *J. Org. Chem.,* 42, **1977**, 1587.

[11] A. Berkessel, J. A. Adrio, *Adv. Synth. Catal.,* 346, **2004**, 275.

[12] A. Berkessel, J. A. Adrio, D. Hüttenhain, J. M. Neudörfl, *J. Am. Chem. Soc.,* 128, **2006**, 8421.

[13] There are reports of trifluoroethanol as a "magic" solvent for *catalytic* epoxidation reactions. a) M. C. A. Van Vliet, I. W. C. E. Arends, R. A. Sheldon, *Chem. Commun.,* **1999**, 821-822. b) M. C. A. Van Vliet, I. W. C. E. Arends, R. A. Sheldon, *Chem. Commun.,* **1999**, 263. c) T. M. Shryne, L. Kim, US Patent 4024165, **1977.**

[14] K. Neimann, R. Neumann, *Org. Lett.,* 2, **2000**, 2861.

[15] a) M. C. A. Van Vliet, I. W. C E. Arends, R. A. Sheldon, *J. Chem. Soc. Perkin Trans.,* 1, **2000**, 377. b) G.-J. ten Brink, B. C. M. Fernandes, M. C. A. van Vliet, I. W. C. E. Arends, R. A. Sheldon, *J. Chem. Soc. Perkin Trans.,* 1, **2001**, 224.

[16] M. C. A. van Vliet, I. W. C. E. Arends, R. A. Sheldon, *Synlett,* 2, **2001**, 248.

[17] S. P. de Visser, J. Kaneti, R. Neumann, S. Shaik, *J. Org. Chem.,* 68, **2003**, 2903.

[18] A. Berkessel, M. R. M. Andreae, H. Schmickler, J. Lex, *Angew. Chem. Int. Ed.,* 41, **2002**, 4481.

[19] J.-P. Bégué, D. Bonnet-Delpon, B. Crousse, *Synlett,* 1, **2004**, 18.

[20] a) *Modern Oxidation Methods;* J. - E. Bäckvall Ed. Wiley Weinheim, **2004.** b) B. S. Lane, K. Burgess, 103, **2003**, 2457.

[21] P. T. Witte, P. L. Alsters, W. Jary, R. Mullner, P. Pochlauer, D. Sloboda-Rozner, R. Neumann, 8, *Org. Process Res. Dev.* **2004**, 524 and references therein.

[22] a) J. Prandi, H. B. Kagan, H. Mimoun, *Tetrahedron Lett.* 27, **1986**, 2671. b) C. Venturello R. D'Aloisio, *J. Org. Chem.,* 53, **1988**, 1553. c) With $H_3PW_{12}O_{40}$ as precursors: Y. Ishii, K. Yamawaki, T. Ura, H. Yamada, T. Yoshida, M. Ogawa, *J. Org. Chem.,* 53, **1988**, 3587. d) K. Sato, M. Aoki, M. Ogawa, T. Hashimoto, R. Noyori, *J. Org. Chem.,* 61, **1996**, 8310. e) A. L. Villa de, B. F. Seles, D. E. De Vos, P. A. Jacobs, *J. Org. Chem.,* 64, **1999**, 7267.

[23] Prandi and Ishi-Venturello systems have been shown to evolve to reactive di- or tetra-nuclear peroxides such as $\{[WO(O_2)_2]_2O\}^{2-}$ and $\{PO_4[WO(O_2)_2]_4O\}^{3-}$. In Noyori's proposal, the aggregation state is unknown.

[24] a) L. Salles, C. Aubry, R. Thouvenot, F. Robert, C. Dorémieux-Morin, G. Chottard, H. Ledon, Y. Jeannin, J.-M. Brégeault, *Inorg. Chem.,* 33, **1994**, 871. b) A. J. Bailey, W. P. Griffith, B. C. Parkin, *J. Chem. Soc., Dalton Trans.* **1995**, 1833. c) D. C. Duncan, R. C. Chambers, E. Hecht, C. L. Hill, *J. Am. Chem. Soc.,* 117, **1995**, 681. d) J. Y. Piqumal, L. Salles, G. Chottard, P. Herson, C. Ahcine, J. M. Bregeault, *Eur. J. Inorg. Chem.,* 5, **2006**, 939.

[25] a) W. Adam, P. L. Alsters, R. Neumann, C. R. Saha-Möller, D. Sloboda-Rozner, R. Zhang, *J. Org. Chem.,* 68, **2003**, 1721. b) D. Sloboda-Rozner, P. L. Alsters, R. Neumann, *J. Am. Chem. Soc.,* 125, **2003**, 5280. c) D. Sloboda-Rozner, P. Witte, P. L. Alsters, R. Neumann, *Adv. Synth. Catal.,* 346, **2004**, 339.

[26] a) N. Mizuno, K. Kamata, K. Yonehara, Y. Sumida, *Science,* 300, **2003**, 964. b) N. Mizuno, K. Yamaguchi, K. Kamata, *Coord. Chem. Rev.,* 249, **2005**, 1944. c) K. Kamata, Y. Nakagawa, K. Yamaguchi, N. Mizuno, *J. Catal.,* 224, **2004**, 224.

[27] A. Sartorel, M. Carraro, A. Bagno, G. Scorrano, M. Bonchio, *Angew. Chem. Int. Ed,.* **2007**, *46,* 3255.

[28] The tetraperoxo complex derived from addition of H_2O_2 to the four lacunary W(VI) of α-Keggin $[CoW_{11}O_{39}]^{9-}$ has been characterized by X-ray analysis and found to be reactive in the epoxidation of 2-cyclohexenol. See: J. Server-Carrió, J. Bas-Serra, M. E. Gonzàlez-Nuñez, A. Garcia-Gastaldi, G. B. Jameson, L. C. W. Baker, R. Acerete, *J. Am. Chem. Soc.,* 121, **1999**, 977.

[29] The catalytic activity of the lacunary complex is highly dependent on the pH at which it is isolated. For a discussion on the speculated structure of the active catalyst see: D. G. Musaev, K. Morokuma, Y. V. Geletii, C. L. Hill, *Inorg. Chem.,* 43, **2004**, 7702.

[30] a) M. Carraro, L. Sandei, A. Sartorel, G. Scorrano, M. Bonchio, *Org. Lett.,* 8, **2006**, 3671. b) S. Berardi, M. Bonchio, M. Carraro, V. Conte, A. Sartorel, G. Scorrano, *J. Org. Chem.,* 72, **2007**, 8954.

[31] H. Zeng, G. R. Newkome, C. L. Hill, *Angew. Chem. Int. Ed.,* 39, **2000**, 1772.

[32] a) M. Bonchio, M. Carraro, G. Scorrano, E. Fontanaova, E. Drioli, *Adv. Synth. Catal.,* 345, **2003**, 1119. b) M. Bonchio, M. Carraro, G. Scorrano, A. Bagno, *Adv. Synth. Catal.,* 346*,* **2004**, 648.

[33] a) M. Antonietti, M. Niederberger, B. Smarsly, *Dalton Trans.,* **2008**, 18. b) C. Sanchez, G. J. de A. Soler-Illia, F. T. Ribot, T. Lalot, C. R. Mayer, V. Cabuil, *Chem. Mater.*, 13, **2001**, 3061. c) C. Streb, D. L. Long, L. Cronin, *Chem. Commun.,* **2007**, 471.

[34] H. Li, H. Sun, W. Qi, M. Xu, L. Wu, *Angew. Chem. Int. Ed.*, 46, **2007**, 1300.

[35] G. Maayan, R. H. Fish, R. Neumann, *Org. Lett.,* 5, **2003**, 3547.

[36] a) M. Carraro, M. Gardan, G. Scorrano, M. Bonchio, E. Fontanaova, E. Drioli, *Chem. Commun.,* **2006**, 4533. b) M. Bonchio, M. Carraro, M. Gardan, G. Scorrano, E. Drioli, E. Fontananova, *Top. Catal.,* 40*,* **2004**, 133.

[37] P. Mason, *Degree thesis,* Università degli studi di Padova, A. A. **1998/1999.**

[38] a) A. Tézé, G. Hervé, *Inorg. Synth.,* 27, **1990**, 85-96. b) A. Tezè, G. Hervè, *J. Inorg. Nucl. Chem.,* 39, **1977**, 999. c) J. Canny, A. Tezè, R. Thouvenot, G. Hervè, *Inorg. Chem.,* 25, **1986**, 2114. d) see also M. Carraro, *Ph. D. Thesis,* Università degli studi di Padova, **2001** and A. Sartorel, *Ph. D. Thesis,* Università degli Studi di Padova, **2002** in the Experimental Parts.

[39] M. S. Weeks, C. L. Hill, R. F. Schinazi, *J. Med. Chem.,* 35, **1992**, 1216.

[40] M. Bonchio, M. Carraro, G. Scorrano, U. Kortz, *Adv. Synth. Catal.,* 347, **2005**, 1909.

[41] a) M. Larhed, C. Moberg, A. Hallberg, *Acc. Chem. Res.,* 35, **2002**, 717. b) A. Loupy, *CR Chemie,* 7, **2004**, 103. c) A.de la Hoz, A. Diaz-Ortiz, A. Moreno, *Chem. Soc. Rev.,* 34, **2005**, 164. d) B. Ahmed, D. Barrow, T. Wirth, *Adv. Synth. Catal.,* 348, **2006**, 1043 and references cited therein. e) T. N. Glasnov, C. O. Kappe, *Macromol. Rapid Commun.,* 28, **2007**, 395. f) B. P. Mason, K. E. Price, J. L. Steinbacher, A. R. Bogdan, D. T. Mc Quade, *Chem. Rev.,* 107, **2007**, 2300.

[42] Relativistic DFT calculations have been carried out using the Amsterdam Density Functional (ADF) code. Scalar relativistic effects were taken into account by means of the Zero-Order Regular Approximation (ZORA) method. BP86 function has been adopted. The basis set were triple – zeta quality, doubly polarized (TZ2P). The solvent effect was considered by means of the COSMO method.

[43] C. J. Faul, M. Antonietti, *Adv. Mat.,* 15, **2003**, 673.

[44] a) D.-P. Hong, M. Hoshino, R. Kuboi, Y. Goto, *J. Am. Chem. Soc.,* 121, **1999**, 8427. b) H. Schaal, T. Häber, M. A. Suhm, *J. Phys. Chem. A,* 104, **2000**, 265. c) M. Fioroni, K. Bruger, A. E. Mark, D. Roccatano, *J. Phys. Chem. B,* 105, **2001**, 10967.

[45] TEM images were recorded tanks to the collaboration with Prof. Markus Antonietti at Max Planck Institute of Colloids and Interfaces, Potsdam, Germany.

[46] P. Judeinstein, *Chem. Mater.*, 4, **1992**, 4.

[47] a) C. R. Mayer, R. Thouvenot, T. Lalot, *Macromolecules,* 33, **2000**, 4433. b) C. R. Mayer, I. Fournier, R. Thouvenot, *Chem. Eur. J.,* 1, **2000**, 105.

[48] T. Hasegawa, H. Murakami, K. Shimizu, Y. Kasahara, S. Yoshida, T. Kurashina, H. Seki, K. Nomiya, *Inorg. Chim. Acta,* 36, **2008**, 11385.

[49] J. Urban, P. jandera, P. Schoenmakers, *J. Chromatogr. A,* 1150, **2007**, 279.

[50] O. Nuñez, T. Ikegami, W. Kajiwara, K. Miyamoto, K. Horie, N. Tanaka, *J. Chromatogr. A,* 1156, **2007**, 35.

4. Synthesis of phenol by POM-based catalytic methods.

4.1 Introduction.

Phenol is one of the most important intermediates of the chemical industry with a global production estimated around 8 Mt/year[1]. Its application in the manufacture of fine chemicals has been growing recently. Nowadays, the main industrial processes involving phenol concerns: i) the production of phenol-formaldehyde resins (PF), which absorb almost a third of the whole phenol demand in the world scale; ii) the production of bisphenol A (BPA), that absorb about 25% of phenol demand and it is actually growing due to the strategic importance that this product assumes in the synthesis of epoxy resins and other high added-value materials production; iii) the caprolactam production, through the transformation of phenol to cyclohexanone .

The existing technology of phenol production is based on the Hock process which also co-produces acetone in 1:1 molar ratio with respect to phenol. According to this process, the decomposition of cumyl hydroperoxide to phenol occurs by acid-catalysis, while the peroxide is produced by cumene autooxidation at high temperature and pressure. This two-step process has a number of disadvantages, one of which is the low selectivity of sulfuric acid as a catalyst, together with its high corrosive potential. Alternatively, the direct oxidation of benzene with nitrous oxide does not produce co-products such as acetone. The use of zeolitic catalysts provides phenol selectivities as high as 97–100% at 100% N_2O conversion. However, the process at present requires frequent regeneration and the manufacture economics are strongly dependent on obtaining a cheap supply of N_2O (usually obtained as a by-product from adipic acid production).

Alternative methods are thus desirable, especially to maximize efficiency and selectivity. With this aim, the research activity has been focused on:

(i)   Tandem Catalysis techniques by polyoxometalates (POMs)-based processes. This implies the photocatalytic production of cumene hydroperoxide by the hybrid membranes described in the previous chapters (see previous discussion, on Chapter 2), followed by its *in situ* rearrangemet to phenol by a second acid POM co-catalyst (Figure 4.1);

(ii)   The screening of several molybdovanadate catalysts for the direct benzene mono-hydroxylation, with H_2O_2 as bulk oxidant (Figure 4.2).
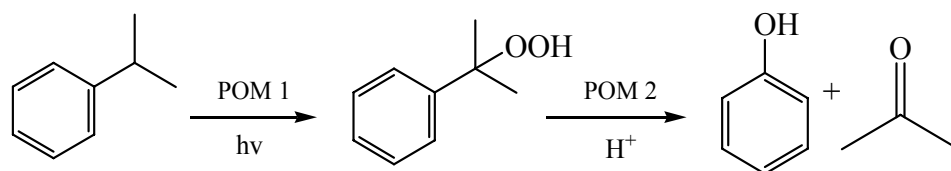
Figure 4.1. Scheme representing the reactions studied. Equation 1: POMs-based Tandem Catalysis.
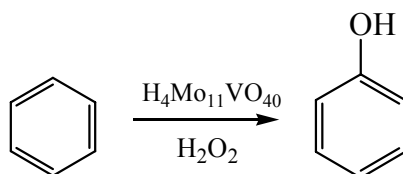
Figure 4 2: Direct benzene hydroxylation.

4.2 Results and discussion.

4.2.1 Conversion of cumyl-hydroperoxide to phenol, with cumene as a starting reagent. (POM-mediated Tandem catalysis).

The liquid phase, aerobic photooxidation of cumene by membrane embedded decatungstate, has been shown to yield cumyl-hydroperoxide, accumulating in solution with a concentration higher than 10^{-2} M (see Chapter 2).

Cumyl-hydroperoxide can be further decomposed to phenol and acetone in 1:1 molar ratio in the presence of an acid catalyst, as in the case of the Hock process (see the following Scheme).
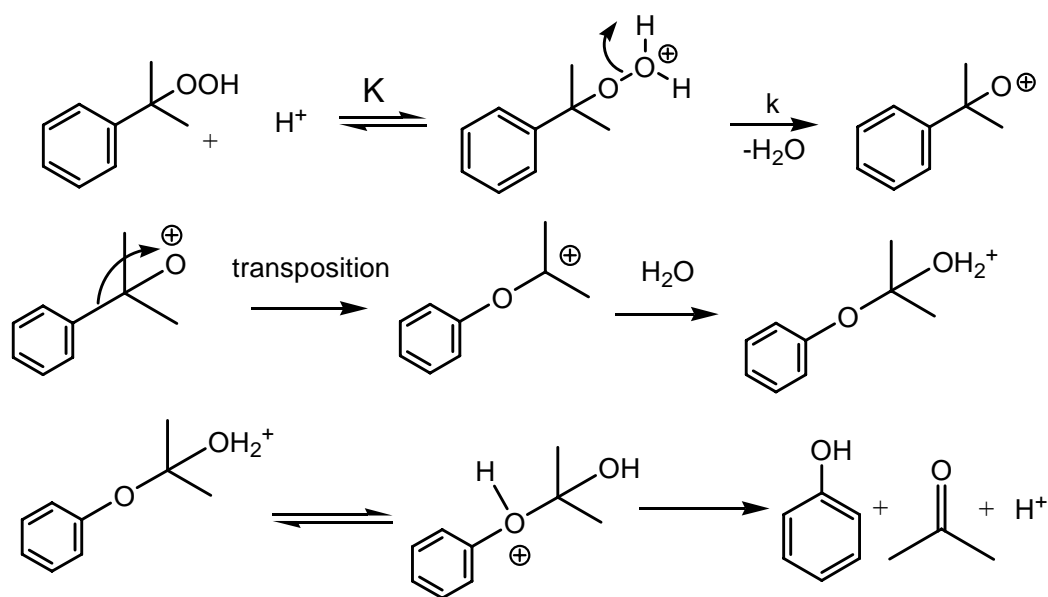
Scheme 4.1. Acid catalyzed decomposition of cumyl - hydroperoxide to phenol and acetone.

However, the latter process is always accompanied by the parallel formation of by-products as: acetophenone, 2-phenyl-2-propanol (cumylic alcohol), α- methyl-styrene (by cumylic alcohol dehydration) and its oligomers.
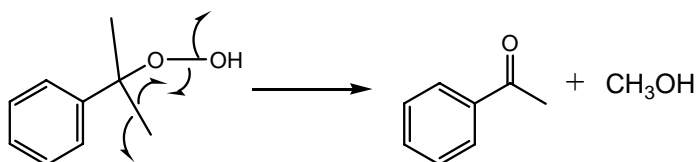
Scheme 4.2. Suggested mechanism for the parallel formation of acetophenone from cumyl – hydroperoxide.
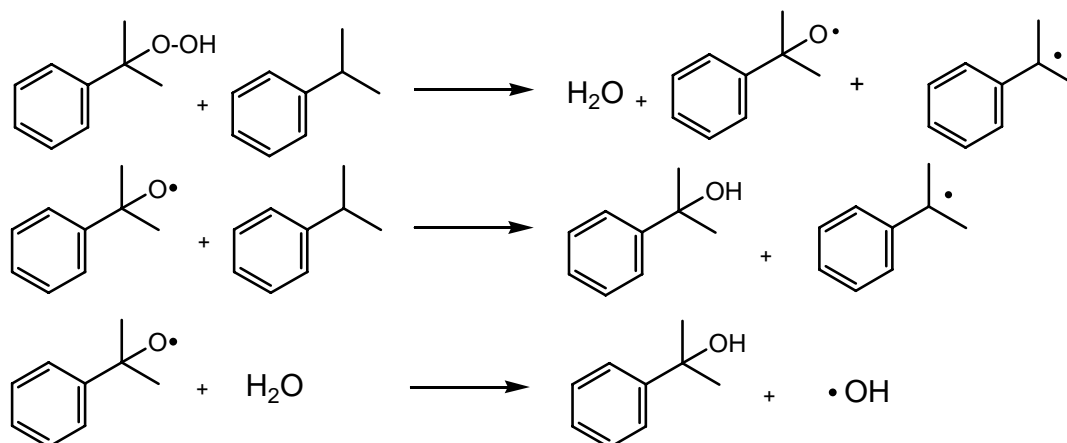
Scheme 4.3. Suggested mechanism for the formation of cumylic alcohol from cumyl – hydroperoxide.

dehydratation;
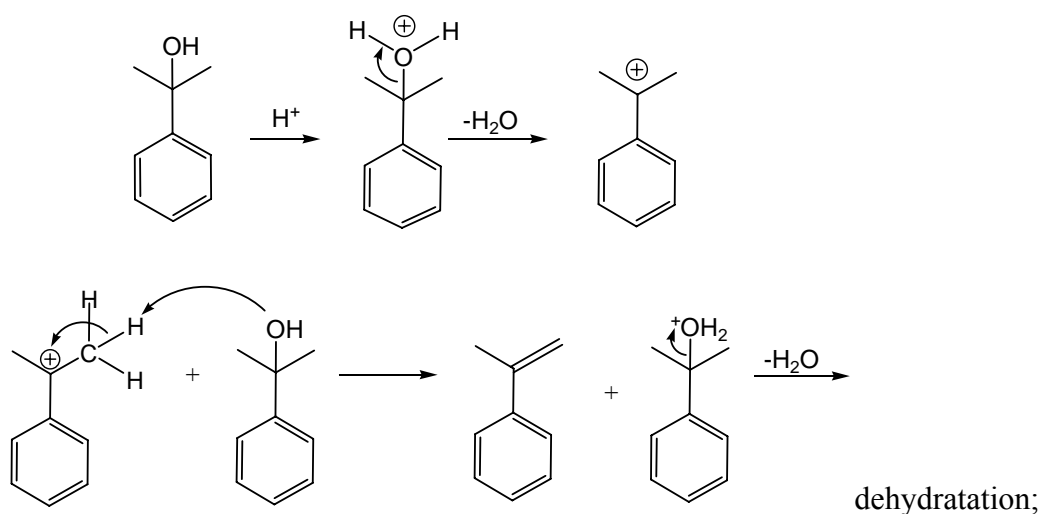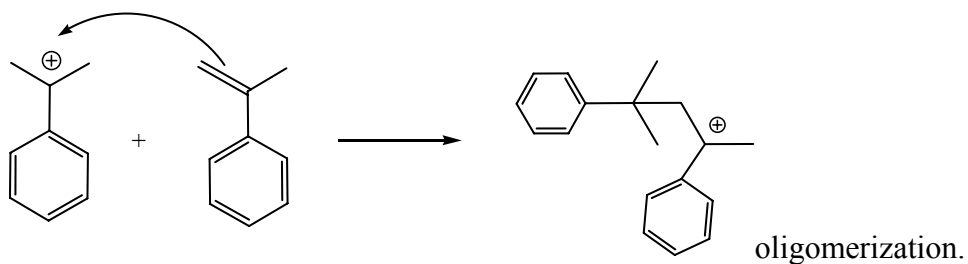
oligomerization.

Scheme 4.4. Mechanism of cumylic – alcohol dehydratation to α - methyl-styrene followed by its oligomerization

As highlighted by this *scenario*, a careful optimization of reaction conditions should be thus pursued to increase the selectivity of the acidic decomposition of the cumyl-hydroperoxide to phenol.

In this sense, the properties of dodecametalate-polyanionic complexes with formula: $H_3PW_{12}O_{40}$ (**1**) and $H_4SiW_{12}O_{40}$ (**2**) (Figure 4.3) as solid acids is well known in the literature[2] [3].

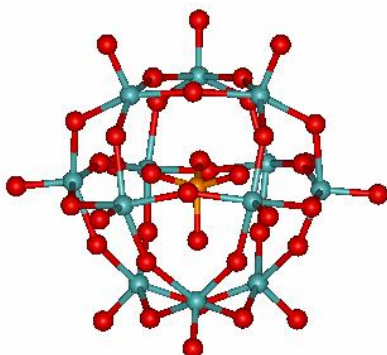**Figure 4.3. Structure of acidic Keggin-polyoxometalate complexes employed.**

Complexes **1** and **2** are heteropolyacids (HPAs) exhibiting purely Brönsted-type acidity, which is stronger than that of other solid acids such as SiO_2-Al_2O_3, zeolites, and H_3PO_4/SiO_2[2] [3] [4]. According to literature data[3], HPAs exhibit super-acid properties in the solid state and in the following order: $H_3PW_{12}O_{40}$ > $H_4SiW_{12}O_{40}$ >$H_3PMo_{12}O_{40}$ > $H_4SiMo_{12}O_{40}$. The strong acidity is due to the large size of the polyanion, which has a low and delocalized surface charge density, that results in weak interactions between the polyanions and the proton, as found for liquid superacids (typically SbF_6^-)[5]. The advantages of using solid heteropolyacids as catalysts are related also to their low volatility, low corrosiveness, activity and flexibility. Upon comparison of HPAs with sulphuric acid, vis-à-vis their reactivity in Brönsted acid-

catalysed liquid phase reactions, it has been found that the activity/mole proton of HPA is higher by a factor of 3-100, depending on the reaction conditions[3].

The use of a solid inorganic support has been reported to further increase selectivity, active surface area, recycling of the catalyst[2b]. 20% w/w montmorrilonite-K-10 clay has been used as support for $H_3PW_{12}O_{40}$, with partial substitution of protons with Cs^+, in order to obtain a catalytic specie with higher surface area and improved thermal stability[2a]. With this system, 77.5% of cumyl hydroperoxide conversion and 100% selectivity towards phenol and acetone has been obtained in 30 minutes, using $4 \cdot 10^{-3}$ g/cm^3 of catalyst loading, and a temperature of 40°C.

Data in Table 4.1 are referred to the phenol production by cumyl hydroperoxide decomposition in the presence of such complexes under heterogeneous conditions, upon dispersion in the hydrocarbon phase. For comparison purposes, these data include the activity of the monomeric tungstic acid and sulphuric acid. The reactivity has also been evaluated towards the dehydration of 2-phenyl-2-propanol to α-methyl-styrene, (see Scheme 4.4).

Table 4.1. Cumyl hydroperoxide (CHP) and 2-phenyl-2-propanol decomposition in cumene and in presence of acidic catalysts.

Acidic catalyst	Substrate (mM)	time (h)	Product (Yield %)
Phosphotungstic acid $H_3PW_{12}O_{40}$ (**1**)	CHP (40)	2	phenol (62)
Tungstosilicic acid $H_4SiW_{12}O_{40}$ (**2**)	CHP (40)	48	phenol (64)
Tungstic acid H_2WO_4 (**3**)	CHP (40)	168	phenol (65)
Sulphuric acid H_2SO_4 98%	CHP (40)	2	phenol (62)
Phosphoungstic acid $H_3PW_{12}O_{40}$ (**1**)	2-phenyl-2-propanol (45)	2	α-methyl-styrene (62)
Tungstosilicic acid $H_4SiW_{12}O_{40}$ (**2**)	2-phenyl-2-propanol (45)	24	α-methyl-styrene (56)
Sulphuric acid H_2SO_4 98%	2-phenyl-2-propanol (45)	2	α-methyl-styrene (> 99)

Reaction condition: CHP or 2-phenyl-2-propanol: 40 mM in 10 mL of cumene, H^+ 10% mol.

In such reactions, catalyst (**1**) presents higher reactivity than (**2**), while performing like H_2SO_4 for the cumyl hydroperoxide conversion to phenol. Morover, HPAs tested are less reactive towards the dehydration of 2-phenyl-2-propanol with respect to sulphuric acid, since the latter seems to yield a complete conversion to α-methyl-styrene.

In a preliminary Tandem catalysis experiment, a mixture containing cumyl hydroperoxide and other cumene photooxidation products, has been directly treated with solid $H_3PW_{12}O_{40}$ (Table 4.2)[2]. In particular, after 4 hours of cumene photooxygenation with the heterogeneous catalyst "RfNW10-HYFLON/PTFE" – Step 1 - (see also Table 2.1, entry 10 on chapter 2), 2.5 mg of hydrated phosphotungstic acid (< 1 μmol) have been added to the reaction mixture. After 24 hours under stirring, phenol was produced with 63% yield with respect to the initial cumyl hydroperoxide content– Step 2 –, as expected on the basis of the previous independent reactions (Table 4.1). The production of α-methyl-styrene has also been observed, together with its correlated oligomers and tars which accounted for the remaining 40% of the cumyl-hydroperoxide.

Table 4.2. Photocatalytic Cumyl hydroperoxide production and its following decomposition in the presence of hydrated phosphotungstic acid.

Products after photocatalysis **Step 1** [a]	Conc. (mM) (t = 4h)	Products after acidic catalysis **Step 2** [b]	Conc.(mM)[c] (t= 24 h)
Cumyl hydroperoxide	12	Cumyl hydroperoxide	2.4
2-phenyl-2-propanol	10	2-phenyl-2-propanol	3.9
acetophenone	0.4	**PHENOL**	7.5
		α-methyl-styrene	6.1
		acetophenone	0.4

[a]Reaction conditions: substrate: 1.1 ml; pO_2=1 atm, λ>345 nm, T=25 °C, irradiation time: 4 h., catalyst 1: R_fNW_{10}-HF/Teflon (124 μm, 25% in peso di loading catalitico). [b]Reaction conditions: p = 1 atm, T=25°C, cat.: 20% mol H^+. c) Oligomers and tars have to be added at the final material balance.

Further developments will be focused to obtain a faster acidic hydroperoxide decomposition to phenol (route b, Scheme 4.5), with respect to the parallel route yielding the undesired radical decompostion to alcohol (and styrene).
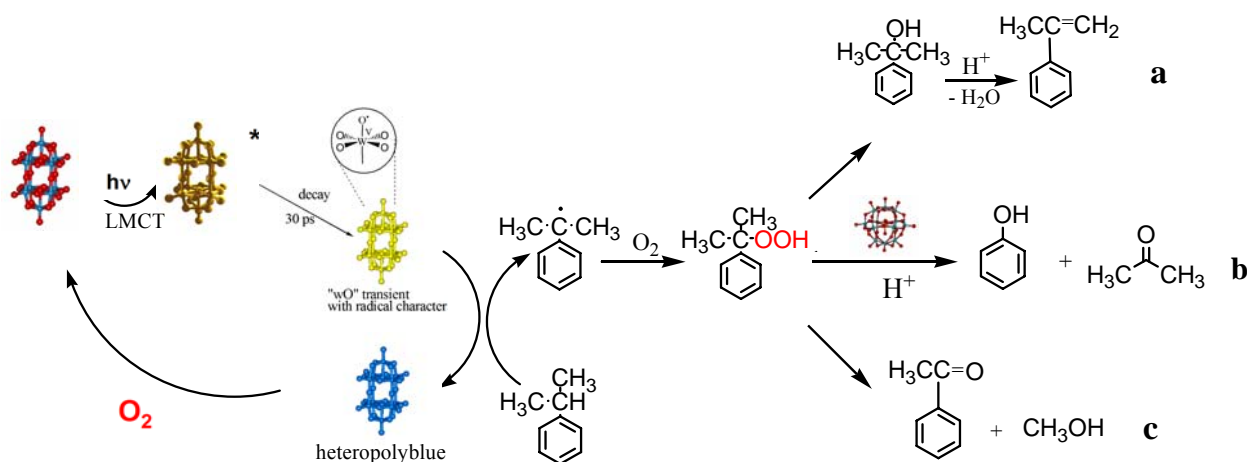
Scheme 4.5. POM mediated "Tandem-catalysis" for the conversion of cumene to phenol.

This aspect requires cumylhydroperoxide production and its decomposition to phenol to occur without time separation between the events. Since heteropolyacids are well known photocatalysts,[6] [7] [8] their use as heterogenous bifunctional catalysts to achieve both photooxidation and acid catalysis will be investigated. The immobilization on inorganic inert supports of HPA will be also considered to decrease poisoning phenomena while increasing the catalyst's active surface[2] [9].

4.2.2 Direct oxidation of benzene to phenol catalyzed by vanadium substituted polyoxometalates.

Since the expected market growth is much larger for phenol than for acetone, the development of a process based on the direct oxidation of benzene to phenol is an important goal in organic chemistry from the industrial perspective. Unfortunately, the oxidation of benzene is usually affected by a poor selectivity due to the lack of kinetic control: indeed, phenol is more easily oxidized than benzene itself and substantial amounts of over-oxygenated by-products (catechol, hydroquinone, benzoquinone, benzoquinones, and tars) can also form. Because of this, the oxidation is often stopped at low conversions, generally <10%. Moreover, only few oxidants are environmentally acceptable, the most promising among them appearing to be nitrous oxide (exploited in the Solutia process, based on iron catalysis on zeolites)[10] and hydrogen peroxide.

With the latter oxidant, remarkable results (benzene conversion: 8.6%, phenol selectivity: 91% and 98% of H_2O_2 conversion) have been recently obtained by combining the use of a peculiar co-solvent (sulfolane) and a modified titanium silicalite (TS-1B) as the catalyst, at 100 °C[1] [11].

Among molecular catalysts, vanadium peroxo complexes are known to promote the hydroxylation of aromatic compounds to the corresponding phenols under very mild conditions. Depending on the nature of the metal coordination sphere, tuned by the associated ligand system, vanadium peroxo complexes may indeed act either as very selective electrophilic oxygen transfer reagents or as efficient radical oxidants. The hydroxylation of aliphatic and aromatic hydrocarbons are examples of homolytic reactivity. Complexes like $VO(O_2)Pic(H_2O)_2$ (with Pic = picolinate) have been reported to be particularly effective for the hydroxylation of benzene and substituted benzene. The bidendate picolinate ligand (pic) may indeed inhibit the electrophilic reactivity while enhancing the homolytic pathways[12]. A typical radical chain kinetic has also been observed for the vanadium peroxo picolinate

decomposition in CH_3CN, in the absence of organic substrates, yielding dioxygen together with a vanadium(V) dimeric oxo species.
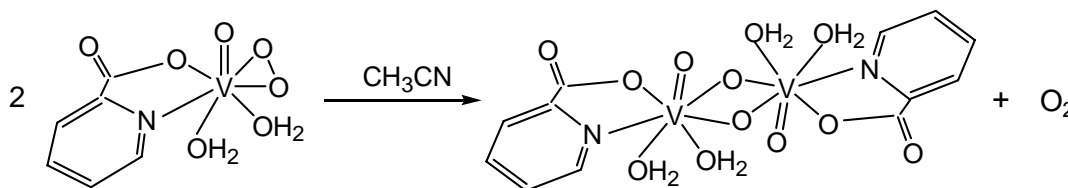
Scheme 4.6 decomposition of peroxo picolinate to dimeric oxo species and molecular oxygen.

In such system, the -chain carrier and the metal-based competent oxidant, derives from the monoreduction of the vanadium peroxide itself. Since in the presence of an excess of benzene, the decomposition reaction is not completely suppressed, it has been suggested that the intermediate (Scheme 4.7)[12] may react with the starting complex to give phenol or dioxygen (see Scheme 4.6).
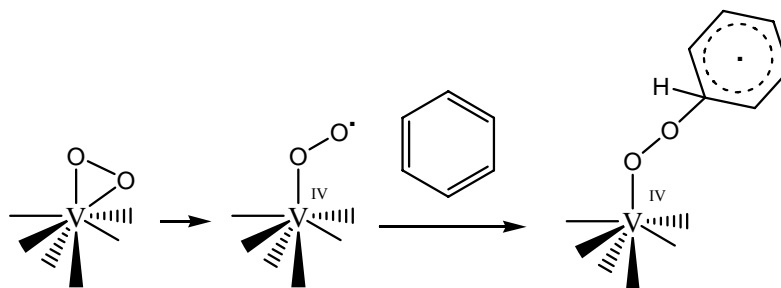
Scheme 4.7. V(IV) peroxocomplex as the active hydroxylating agent.

The analogue reaction, catalyzed by Keggin – polyoxomolybdates, mono - and di - substituted with vanadium has been explored in literature[13], but several points lack an accurate investigation, such as: (i) the speciation of the pertinent catalyst in the reaction mixture, (ii) the role of the inorganic and polyoxoanionic ligand on the activity of the V(V) reactive centre, and (iii) reaction optimization[14].

4.2.2.1 Synthesis of Vanadium substituted polyoxometalates.

As previously introduced, the occurrence of a vanadium (V) centre, in the polyoxometalate complexes, is the key factor to achieve the catalytic hydroxylation of benzene, but a coordination environment turn out to be essential.

With this aim, some vanadium polyoxometalate complexes, with different structures, charges and nuclearities have been investigated. Their general structures are here reported below in Figure 4.4, and they are attributable to the following formulas: $VPMo_{11}O_{40}^{4-}$ (**3**), $V_2PMo_{10}O_{40}^{5-}$ (**4**), $V_2SiW_{10}O_{40}^{6-}$ (**5**), $V_3P_2W_{15}O_{62}^{9-}$ (**6**), $V_3Te_2W_{18}O_{69}^{7-}$ (**7**), e $V_3Se_2W_{18}O_{69}^{7-}$ (**8**). These complexes belong to different POM classes, i.e. Keggin (structures a, b), Dawson (structure c), and Hervè (structure d)[15] [16] [17] (See Experimental part, Section 5.5.1). For comparison purposes, the monomeric precursor $NaVO_3$ has also been used.

a   b   c   d
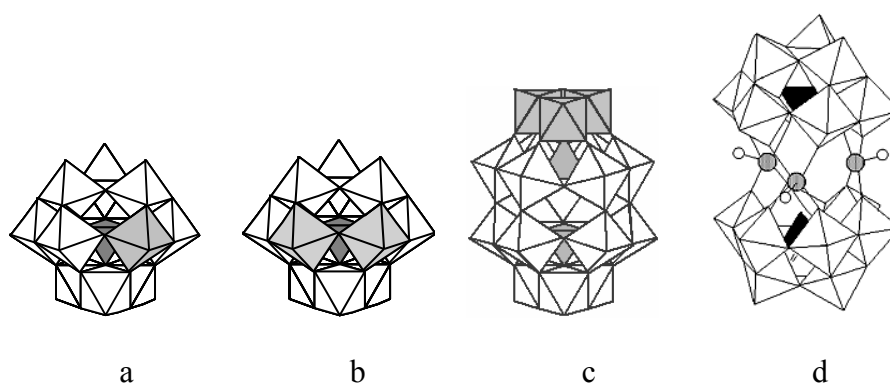
Figure 4.4. Structure of a) $VXM_{11}O_{40}^{n-}$; b)$V_2XM_{10}O_{40}^{n-}$; c) $V_3P_2W_{15}O_{62}^{9-}$; d) $V_3X_2W_{18}O_{69}^{7-}$.

4.2.2.2 Catalytic tests.

Table4. 3 shows the activity of these different systems, compared in terms of phenol yield and turnover number (TON), calculated per vanadium centre.

Table 4.3. Benzene oxidation in the presence of vanadium substituted POM and H_2O_2. Reaction conditions: Room T., Benzene: 2.7 mmol (240 μL), H_2O_2: 5.8 mmol (539 μL of H_2O_2 10.8 M), $3.6\cdot10^{-2}$ mmol of each complex in 3 mL of solvent.

#	POM	cation	solvent	t (h)	Yield % Phenol [a]	TON/V
1	$\mathbf{VPMo_{11}O_{40}^{4-}}$	H	CH_3COOH	21	3.9	2.9
2		**H**	**CH_3CN**	**24**	**18.5**	**14.8**
3	$V_2PMo_{10}O_{40}^{5-}$	Na	CH_3COOH	24	6.1 [b]	2.3
4		Na	CH_3CN	24	4 [b]	1.5
5	$V_2SiW_{10}O_{40}^{6-}$	TBA_4H_2	CH_3CN	24	0	0
6	$V_3P_2W_{15}O_{62}^{9-}$	K_8H	CH_3COOH	24	0	0
7	$V_3P_2W_{15}O_{62}^{9-}\cdot$	TBA_4H_5	CH_3CN	24	4.4	1.1
8	$V_3Te_2W_{18}O_{69}^{7-}$	TBA	CH_3CN	120	7	1.7
9		K	CH_3COOH	24	0	0
10	$V_3Se_2W_{18}O_{69}^{7-}$	TBA	CH_3CN	120	5.2	1.3
11	VO_3^-	Na	CH_3COOH	96	4.1 [b]	3.1

a) Yields calculated with respect the initial benzene. Benzoquinone is generally also observed by GLC-FID until 6% with respect phenol, which evolves to other products not detected through GLC-FID. b) Induction time >5 h. c) Induction time = 24 h.

A major role on the catalytic activity seems to be played by: (i) the nuclearity of the vanadium inside the polyoxometalate; (ii) the type of metal addendum in the polyoxoanion (Mo or W); (iii) the counterion associated; (iv) the solvent.

In general these reactions present low catalytic efficiency and they are affected by the parallel decomposition of H_2O_2. Kinetic profiles show a plateau when phenol conversion reaches values between 4 and 18%. This behaviour is reported in Figure 4.5 for the vanadium monosubstituted polyoxomolybdate $H_4PVMo_{11}O_{40}$, which resulted the most active catalyst among those tested, accordingly with studies reported in the literature[17]. On the other hand, polynuclear species, with vanadium atoms in vicinal positions, show low reactivity. In particular, the complex $V_2SiW_{10}O_{40}{}^{6-}$ (**5**), known as efficient epoxidation catalyst[15], has found to be inactive for the benzene hydroxylation, likely because of the absence of active radical intermediates.
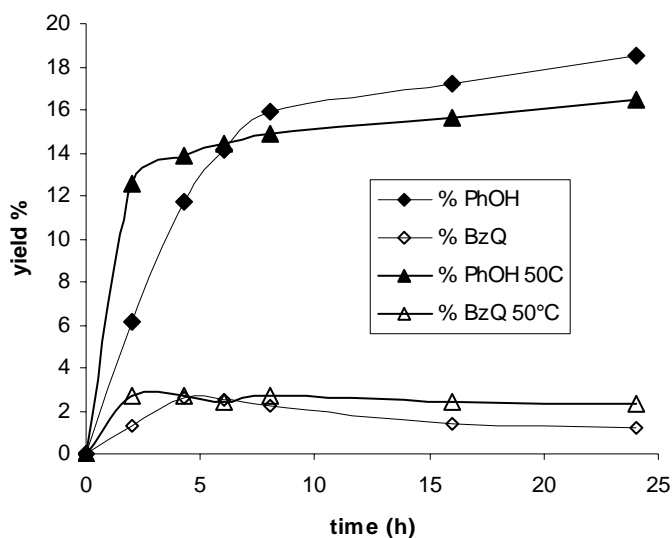
Figure 4.5. Direct benzene hydroxylation with H_2O_2 and $H_4PMo_{11}VO_{40}$ (H-**3**) at 25°C and 50°C.

To collect insights about the catalyst speciation in reaction solutions and its evolution in the presence of H_2O_2, the reaction mixture has been monitored by ^{1}H- and [51]V-NMR spectroscopy. The kinetic profile, obtained by ^{1}H-NMR following benzene and phenol signals, shows a regular trend with no induction time. This evidence suggests that the catalyst should not undergo any substantial transformation during the course of reaction.
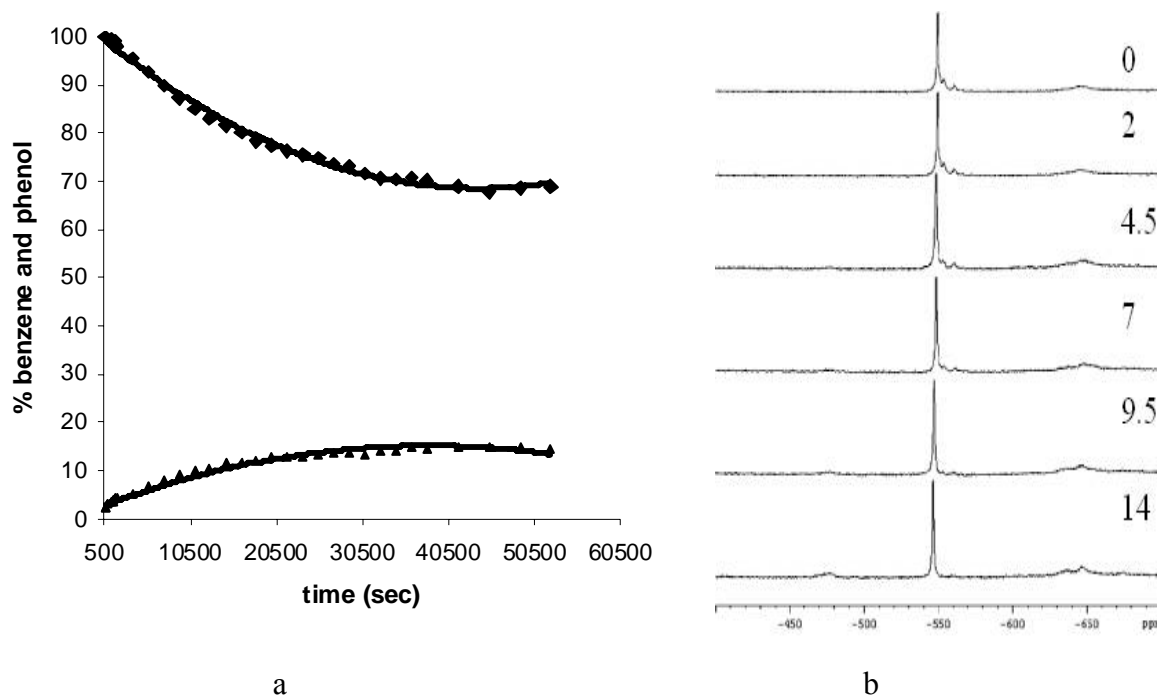
Figure 4.6. Kinetic profile of the reaction followed by: a) ^{1}H NMR and b) ^{51}V NMR (conditions are those described in entry # 2 on Table 3, solvent: CD$_3$CN).

By ^{51}V-NMR, it is has been observed that the main catalyst signal (-540 ÷ -550 ppm), is not sensitively modified during the reaction. Broad signals are also observed in the region of vanadium(V) peroxidic complexes around -600 ÷ -650 ppm. This last observation is likely ascribable to the formation, *in situ*, of paramagnetic intermediates of V(IV) responsible of the parallel decomposition of H$_2$O$_2$ in the system.

The stability of the whole system, during turnover regime, is a crucial issue, since it allows to face optimization studies of the process with respect to some important parameters, such as temperature, dilution, multiple recharging of the bulk oxidant, as described in the following Table 4.4:

Table 4.4. Hydroxylation of benzene with H_2O_2 and $H_4PMo_{11}VO_{40}$ (H-**3**) at 50°C. Reaction conditions: 36 µmol of (H-**3**) in 3 mL of CH_3CN.

#	Benzene (mmol)	charging H_2O_2 x mmol (% in H_2O)	Δt (h)[a]	t (h)	Phenol produced (mmol)	Yield % phenol: benzoquinone[b]	TON	TOF[c]
0[d]	2.7	1 x 5.8 (35%)	-	24	0.5	18.5 : 1.2	15	2.8
1	2.7	1 x 5.8 (35%)	-	24	0.4	16.5 : 2.3	14	5.8
2	2.7	2 x 5.8 (35%)	4	24	0.6	20.6 : 1.0	16	5.8
3	2.7	5 x 3.6 (35%)	0.5	2.5	0.7	24.5 : 5.1	22	9.0
4	5.6	5 x 3.6 (35%)	0.5	3	0.8	15.0 : 1.7	41	15.0
5	11.2	5 x 3.6 (35%)	0.5	3	1.7	15.4 : 1.8	80	22.5
6	5.6	5 x 3.6 (70%)	0.5	3	0.4	7.5 : 1.8	33	10.5
7	11.2	5 x 3.6 (70%)	0.5	3	1.3	11.8 : 2.2	53	17.0

a. Time interval between the addition of two portions of H_2O_2.
b. (TON/h) calculated for the first 2 hours of the reaction.
c. Yields are calculated with respect the initial benzene amount. Benzoquinone is formed as byproduct and evolves to other products not detected through GLC-FID.
d. Temperature: 25 °C.

As reported in Table 4.4, an increasing of temperature to 50°C allows to obtain a sensitive increase of the turnover frequency (TOF at 25°C = 2.8; TOF at 50°C = 5.8, see entries 0 and 1 in Table 4.4 and Figure 4.5). The problem concerning the peroxide decomposition has been partially solved by the stepwise addition of hydrogen peroxide aliquots[12c], in order to limit the excess of H_2O_2 introduced at once. In particular, it was useful to add H_2O_2, in a ratio of 100:1 with respect the vanadium complex, each 30' and for a total reaction time of 3 hours (see entries 3-7 on Table 4.4). The rate of the whole process also depends on the initial benzene concentration, as it appears from the kinetic profiles shown in Figure 4.7 (compare reactions 3-5, Table 4.4). For substrate/catalyst ratios greater than 1500, a linear zero order kinetic profile, sustained by a constant concentration of active and stable specie, is thus obtained.

In a such system it is possible to reach a turnover frequency of 22.5 h^{-1} which is comparable with the activity observed in the case of the titanium silicalite[1][11].
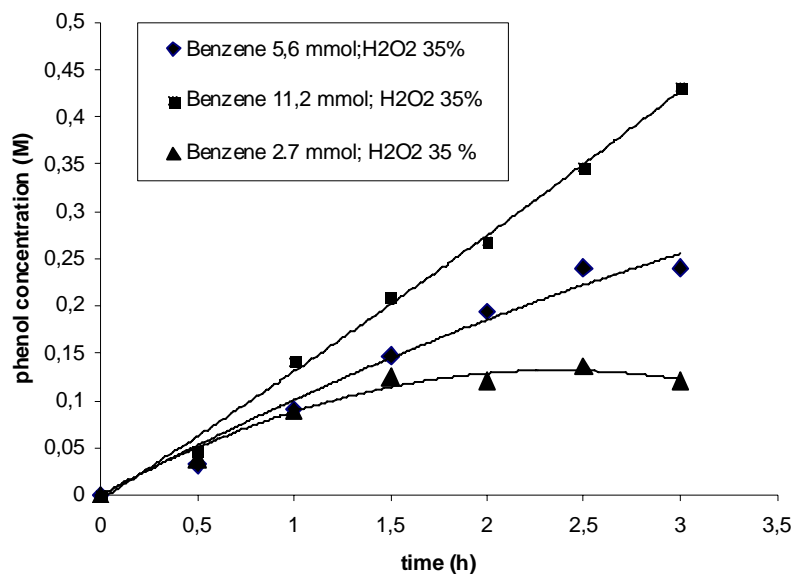
Figure 4.7 Benzene oxidation catalyzed by H$_4$PVMo$_{11}$O$_{40}$. Reactivity comparison at 50 °C: initial concentration effect.

4.3 Conclusions.

POM-based catalysis has been applied to the synthesis of phenol, one of the most valuable intermediate and commodity chemical on the market. The most widely employed industrial process for the synthesis of phenol is by the decomposition of cumene hydroperoxide. With the aim to implement both the cumyl autooxidation pathway, and the direct mono-hydroxylation of benzene , the following studies on the process have been carried out:

i.   the application of Tandem Catalysis techniques, so to exploit the membrane-based photocatalytic production of the cumene hydroperoxide (see previous discussion), and foster its decomposition to phenol through a second step by a acid POM catalyst (Scheme 4.3);

ii. (ii) the screening of several molybdovanadate catalyst to be used with H$_2$O$_2$ for benzene hydroxylation (Scheme 4.4).

In the first case, the POM mediated tandem catalysis yields 63% phenol with respect to the initial amount of cumyl-hydroperoxide. In the second case, with the vanadium mono-substituted undecamolybdate, H$_4$Mo$_{11}$VO$_{40}$, reaction optimization[13] [14] [17] has been obtained

,thus yielding: 17 % conversion of benzene at 50°C in acetonitrile, TOF = 22.5 h^{-1} and selectivity = 90%.

4.4 References and notes.

[1] D. Bianchi, L. Balducci, R. Bortolo, R. D'Aloisio, M. Ricci, G. Spanò, R. Tassinari, C. Tonini, R. Ungarelli, *Adv. Synth. Catal.,* 349, **2007**, 979.

[2] a) G. D. Yadav, N. S. Asthana, *Appl. Catal. A: Gen.,* 244, **2003**, 341. b) G. D. Yadav, *Catal. Surv. From Asia,* 9, **2005**, 117 and references therein.

[3] M.N. Timofeeva, *Appl. Catal. A: Gen.* 256, **2003***,* 19*,* and references therein cited.

[4] J. Arichi, M. Eternot, B. Louis, *Catal. Today,* 138, **2008**, 117.

[5] G. A. Olah, G. K. S. Prakash, J. Sommer, *Superacids,* Wiley, New York, NY, **1985**.

[6] a) E. Papaconstantinou, A. Hiskia, *Inorg. Chem.,* 31, **1992**, 163. b) E. Papaconstantinou, *Chem. Soc. Rev.*, 18, **1989,** 1. c) E. Papaconstantinou, A. Mylonas, A. Hiskia, E. Androulaki, D. Dimotikali, *PCCP Phys. Chem. Chem. Phys.,* 1 (3), **1999**, 437.

[7] C. L. Hill, C. M. Prosser-McCartha, *Photosensitization and Photocatalysis Using Inorganic and Organometallic Compounds,* KLUVER ACAD. PUBL., Netherlands, **1997**, 307.

[8] N. Mizuno, T. Watanabe, M. Misono, *J. Phys. Chem.,* 89, **1985**, 80.

[9] J. Macht, M. J. Janik, M. Neurock, E. Iglesia, *Angew. Chem. Int. Ed.,* 46, **2007**, 1.

[10] G. I. Panov, A. S. Kharitonov, V. I. Sobolev, *Appl. Catal. A,* 98, **1993**, 1.

[11] L. Balducci, D. Bianchi, R. Bortolo, R. D'Aloisio, M. Ricci, R. Tassinari, R. Ungarelli, *Angew. Chem. Int. Ed.,* 42, **2003**, 4937.

[12] a) M. Bonchio, V. Conte, F. Di Furia, G. Modena, *J. Org. Chem.,* 54, **1989**, 4368. b) M. Bonchio, V. Conte, F. Di Furia, G. Modena, S. Moro, *J. Org. Chem.,* 59, **1994**, 6262. c) M. Bianchi, M. Bonchio, V. Conte, F. Coppa, F. Di Furia, G. Modena, S. Moro, S. Standen, *J. Mol. Catal.,* 83, **1993**, 107.

[13] K. Nomiya, Y. Nemoto, T. Hasegawa, S. J. Matsuoka, *J. Mol. Catal. A: Chem.* 152, **2000**, 55.

[14] K. Nomiya, H. Yangibayashi, C. Nozaki, K. Kondoh, E. Hiramatru Y. Shimizu, *J. Mol. Catal.,* 114, **1996**, 181.

[15] Y. Nakagawa, K. Kamata, M. Kotani, K. Yamaguchi, N. Mizuno *Angew. Chem. Int. Ed.,* 44, **2005**, 5136.

[16] K. Nomiya, S. Matsuoka, T. Hasegawa, Y. Nemoto, *J. Mol. Catal. A: Chemical,* 156, **2000**, 143.

[17] Y. Tang, J. Zhang, *Trans, Met. Chem.,* 31, **2006**, 299–305 and references therein.

5 Experimental part.

5.1 Instruments and apparatus.

^{1}H-NMR spectra were recorded with a Bruker AC 250 spectrometer operating at $\nu = 250.18$ MHz. Chemical shifts were determined using $Si(CH_3)_4$ as reference (δ ^{1}H-NMR = 0 ppm). For protonic spectra, the following symbolism has been used: s: singlet; d: doublet; t: triplet; q: quartet; m: multiplet.

^{13}C-NMR spectra were recorded with a Bruker Avance AX 330 spectrometer operating at $\nu = 75.47$ MHz. Chemical shifts were determined using $Si(CH_3)_4$ as reference (δ ^{13}C-NMR = 0 ppm).

^{29}Si-NMR spectra were recorded with a Bruker Avance DRX 400 spectrometer operating at $\nu = 79.49$ MHz, using a 10 mm tube. Chemical shifts were determined using $Si(CH_3)_4$ as reference (δ ^{29}Si-NMR = 0 ppm).

^{183}W-NMR spectra were recorded with a Bruker Avance DRX 400 spectrometer operating at $\nu = 16.67$ MHz. using a 10 mm tube. Na_2WO_4 2M in D_2O was used as external reference (δ ^{183}W-NMR = 0 ppm).

^{19}F-NMR spectra were recorded with a Bruker Avance DRX 400 spectrometer operating at $\nu = 376.45$ MHz with trifluorotoluene in benzene-d_6 as external reference. For ^{19}F-NMR the same symbolism of protonic spectra has been used.

^{31}P-NMR spectra were recorded with a Bruker Avance DRX 300 spectrometer operating at $\nu = 121.49$ MHz with H_3PO_4 85% as external reference (δ ^{31}P-NMR = 0 ppm).

^{51}V-NMR spectra were recorded with a Bruker Avance DRX 300 spectrometer operating at $\nu = 78.28$ MHz MHz, using solution of $5 \cdot 10^{-3}$ M of vanadium (V) monoperoxo picolinate (see Section 5.5.6) as reference: δ ^{51}V-NMR = -600 ppm.

FT-IR spectra were recorded with a Nicolet 5700-Thermo Electron Corporation instrument. For FT-IR spectra following symbolism has been used: w: weak signal; s: strong signal; b: broad band signal.

UV-Vis spectra were recorded with a Lambda 45 Perkin-Elmer spectrophotometer, subtracting polymers absorption. Molar extinction coefficients ε are expressed in $M^{-1} \times cm^{-1}$.

Atomic Force Microscopy (AFM) images and measurements were obtained using an AFM MT-MDT Ntegra Instrument. Scanning mode: by-sample mode/no-contact mode. Scanner Volume: $75 \times 75 \times 6 \ \mu m^3$. Probe: NT-MDT NSG01 type, silicon tip (dimensions: $130 \times 35 \ \mu m$) operating at typical frequency of 150 kHz which coincides with a force constant k = 55 N/m.

Scanning Electronic Microscopy (SEM) were obtained using a Cambridge Instrument Stereoscan 360 and a Quanta 200F FEI Philips on Back Scattered Electrons (BSE) mode and with a Zeiss SUPRA 40VP instrument, using an accelerating voltage of 1-5 kV.

Transmission Electronic Microscopy (TEM)[1] were obtained using a ZEISS EM 912 Omega, transmission electron microscope at an acceleration voltage of 120 kV. Samples grids were prepared by applying one droplet of the sample solution onto a carbon – coated 400 - mesh copper grid and left to dry.

GLC analysis were performed on a Hewlett Packard 6890 series instrument equipped with a flame ionisation detector (FID) using a 30 m (0.32 mm internal diameter, 0.25 μm film thickness) HP-5 capillary column; with a Hewlett Packard 5890 series II instrument equipped with FID using a 60 m (0,53 mm internal diameter, 1 μm film thickness) Alcohols Stabilwax® (Restek) capillary column or with a Shimadzu GC-2100 instrument for GLC-flash chromatography equipped with FID, using a 15 m (0.10 mm internal diameter, 0.10 μm film thickness) Equity™-5 capillary column whose composition is: 5% biphenyl and 95% dimethylsiloxane.

GC-MS spectra were recorded on a Agilent GC6850 series coupled with a Agilent 5973 Network Mass Selective Detector. GC system is equipped with a 30 m (0.32 mm internal diameter, 0.25 μm film thickness) HP-5 capillary column.

ESI-MS spectra were recorded on a Agilent 1100 series instrument with a LC/MSD Trap SL. (+3500 V capillary potential, -20 V skimmer potential and −100 V Cap. Exit potential).

Thin Layer Cromatography (TLC) were performed using DC *Fertigplatten-Durasil-25* UV_{254} sheets (Machery-Nagel).

Chromatography Column purifications were performed on gravity column using Sigma-Aldrich silica gel, mesh grade 10184, granulometry 70-230 mesh, 100 Angstrom.

For Photocatalytic experiments, continuous irradiation was performed with a light source housing (Oriel instruments) equipped with a 500 W Hg-Xe arc lamp, (200-500 W) power supply, F/1.5 UV grade fused silica condenser to collect the radiations from the emitting source, a 5 cm path length liquid (water) filter with fused silica windows to absorb IR radiations, a secondary focusing lens to maximise the incident light on the membrane and the irradiated cell. The distance between the cell, both for heterogeneous process and homogeneous process, and cut-off filter ($\lambda > 345$ nm) is 3.5 cm; distance between focusing lens and cut-off filter is 5 cm. Cut-off filters ware used to prevent the direct photolysis of the organic substrates.

   Oxygen was supplied inside the reaction mixture through a balloon collected with a Teflon tube immersed in the solution.
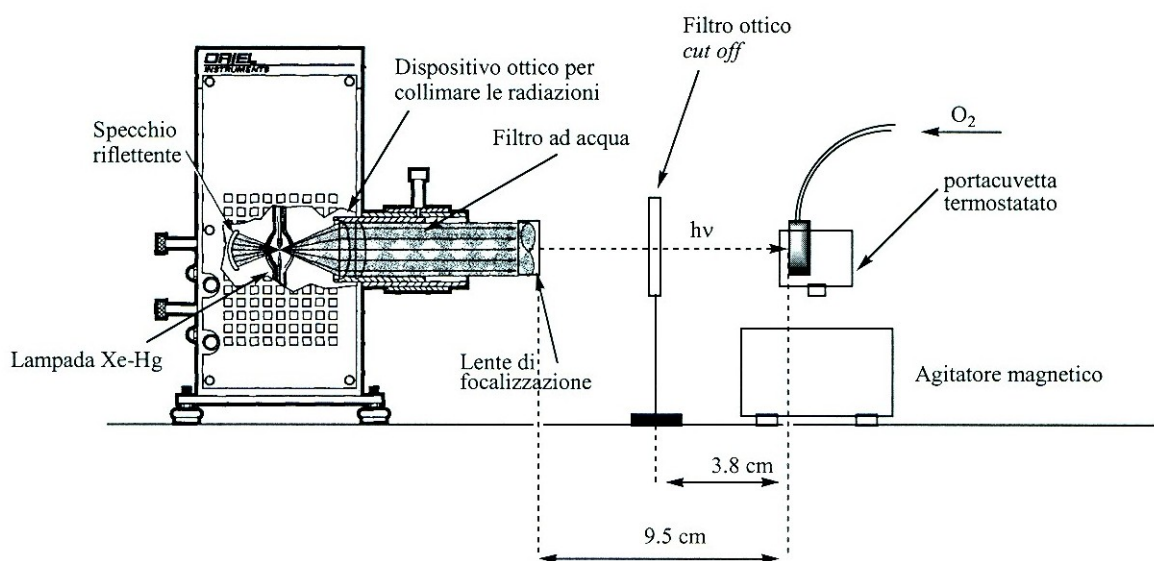
Figure 5.1. Schematization of the optical apparatus used for the photocatalytic experiments.

Temperature was controlled by means of a Haake L thermostat with external circulation with a 0.05 °C of precision.

MW assisted reactions were performed with a MW-lab-station Discover (CEM instruments).

Dynamic Light Scattering (DLS) measurements were performed with NICOMP 170 – Spectra Physics instrument.

pH meter: pH lab 827, Metroohm – Swiss.

TGA measurements were recorded with a TGA Q500 TA instrument. Program: 1°C/min, under nitrogen flow.

DSC measurements were recorded with a DSC Q100 TA instrument. Program: 1°C/min, under nitrogen flow.

Elemental Analysis were performed at microanalysis laboratory of Chemical Science Department, University of Padova.

5.2 Solvents and chemicals.

General Remarks. Commercially available reagents and solvents were used as received without further purification.

MilliQ-deionised water (Millipore) was used as solvent for spectrometric measurements.

Table 5.1. Solvents.

Solvent	Chemical company
Ethylic Ether	Sigma-Aldrich
Anhydrous hexane	
1,4-butanediol	
1,1,1,3,3,3-hexafluoro-2-propanol	

Deuterated chloroform	Sigma-Aldrich
Deuterated acetonitrile	
D$_2$O	
Anhydrous Dichloromethane	Fluka
Anhydrous Tetrahydrofuran	
Ethanol	
2,2,2-trifluoroethanol	
Acetonitrile	Prolabo
2-propanol	
Trifluorotoluene	Miteni S.p.A.
Galden HT 55®	Solvay-Solexis

Table 5.2. Chemicals.

Chemical	Chemical company
Dess-Martin periodinane	Sigma-Aldrich
10% Pd/C	
Tetrabuthylammonium Bromide	
Dodecane	
Decane	
2-phenyl-2-propanol	
Acetophenone	
2-ethylnaphtalene	
Triphenylphosphine	
H$_2$O$_2$ 35%	
Na$_2$SiO$_3$ Cis-cyclooctene	
Trans-2-octene	
Cis-2-hexene	
Trans-2-hexene	
Methyl methacrylate	
Ethylenglycol dimethacrilate (EDM)	
Benzene	

Phenol	Sigma-Aldrich
p-benzoquinone	
Na_2HPO_4	
$Na_2MoO_4 \cdot 2H_2O$	
$NaVO_3$	
$[(n-C_4H_9)N]Br$	
Benzyl amine	Fluka
Dimethylsulphate	
$(NH_4)MoO_4 \cdot 4H_2O$	
Ethylbenzene	
Tetraline	
Indane	
Cumene	
$CH_2CH(CH_2)_6SiCl_3$	
Cyclohexene	
1-octene	
1-hexene	
1-decene	
1-dodecene	
Cumyl hydroperoxide 80%	
Phosphotungstic acid $H_3PW_{12}O_{40}$	
Tungstosilicic acido $H_4SiW_{12}O_{40}$	
Tungstic acid	
V_2O_5	
$Na_2S_2O_3$	Carlo Erba
$KHCO_3$	
KIO_3	
Acetic Acid Glacial	
Starch indicator for iodometry	
Sulphuric Acid 98%	
HCl 37%	
MoO_3	
$MgSO_4$	Prolabo
NaOH	

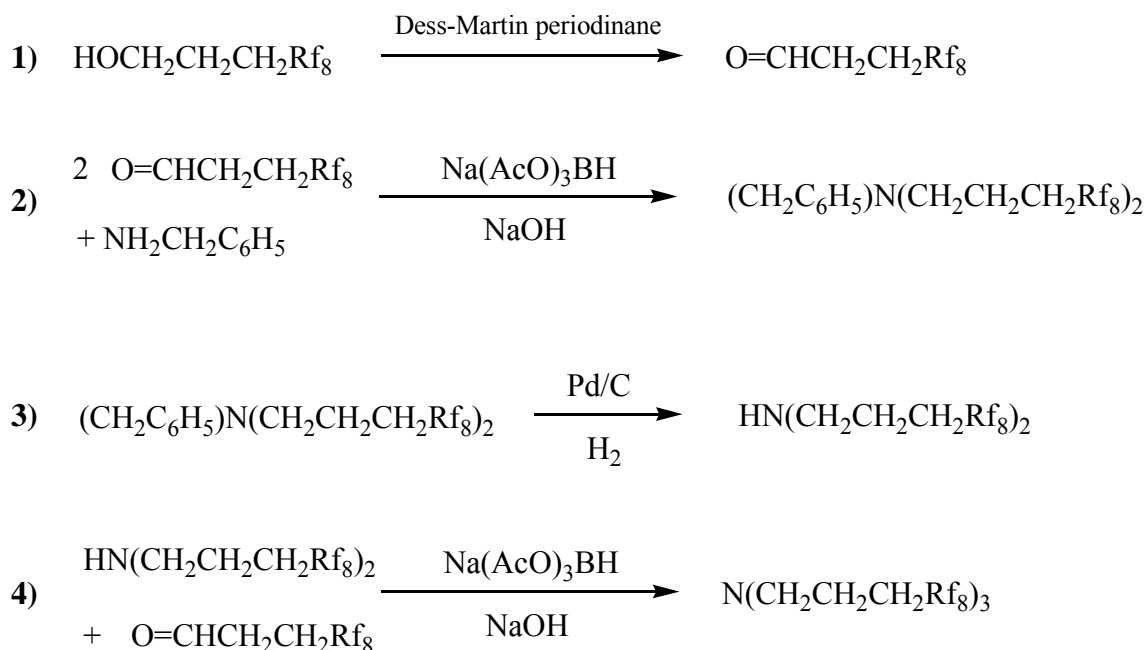|	
3(perfluoroctyl)propanol $CF_3(CF_2)_7(CH_2)_2SiCl_3$	Fluorochem
Na(AcO)$_3$BH	Acros
Celite	Merck
Na$_2$WO$_4$·2H$_2$O	Riedel-de-Haën
KI	J. T. Baker
H$_2$O$_2$ 70%	Ausimont
bis (tertbutyl-cyclohexyl) peroxodicarbonate	Ineos-Vinyls
Na$_2$CO$_3$	Janssen Chimica
Hyflon® AD 60X polymer	Solvay Solexis

5.3 Hybrid photocatalytic membranes embedding decatungstate for heterogeneous photooxidation.

5.3 1 Synthesis of the fluorinated counterion $[CF_3(CF_2)_7(CH_2)_3]_3CH_3N^+$.

$[CF_3(CF_2)_7(CH_2)_3]_3CH_3N^+$ counterion was synthesized following a literature procedure[2].

The preparation is a multi-step synthesis and yields the cation as a methylsulphate salt[3], starting from the 3-perfluorooctylpropanol as (33 % mol/mol).

The procedure can be schematized as follow:

1) HOCH$_2$CH$_2$CH$_2$Rf$_8$ $\xrightarrow{\text{Dess-Martin periodinane}}$ O=CHCH$_2$CH$_2$Rf$_8$

2) 2 O=CHCH$_2$CH$_2$Rf$_8$ + NH$_2$CH$_2$C$_6$H$_5$ $\xrightarrow[\text{NaOH}]{\text{Na(AcO)}_3\text{BH}}$ (CH$_2$C$_6$H$_5$)N(CH$_2$CH$_2$CH$_2$Rf$_8$)$_2$

3) (CH$_2$C$_6$H$_5$)N(CH$_2$CH$_2$CH$_2$Rf$_8$)$_2$ $\xrightarrow[\text{H}_2]{\text{Pd/C}}$ HN(CH$_2$CH$_2$CH$_2$Rf$_8$)$_2$

4) HN(CH$_2$CH$_2$CH$_2$Rf$_8$)$_2$ + O=CHCH$_2$CH$_2$Rf$_8$ $\xrightarrow[\text{NaOH}]{\text{Na(AcO)}_3\text{BH}}$ N(CH$_2$CH$_2$CH$_2$Rf$_8$)$_3$

113

5) $N(CH_2CH_2CH_2Rf_8)_3$ $+ CH_3OS(O)_2OCH_3$ $\xrightarrow{\text{reflux}}$ $(Rf_8CH_2CH_2CH_2)_3N^+CH_3\ CH_3OSO_3^-$
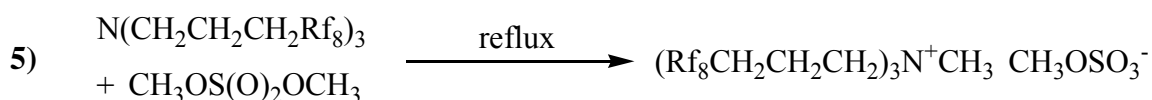
Each step is described in detail in the following paragraphs.

5.3.1.1 Synthesis of O=CHCH₂CH₂Rf₈.

A 250 mL flask was charged with the Dess-Martin reagent (4.84 g, 11.40 mmol)[4] and anhydrous CH_2Cl_2 in minimum volume required to solubilize it. A solution of $HOCH_2CH_2CH_2Rf_8$ (5.00 g, 10.45 mmol) in CH_2Cl_2 (minimum volume) was added under stirring in 10 minutes. Once the oxidation was completed (monitoring by GLC analysis), 50 mL of diethylether was added. The white suspension was poured into a solution of $Na_2S_2O_3$ (12.62 g, 79.8 mmol; 7 equiv./Dess-Martin reagent) in saturated aqueous $KHCO_3$ (200 mL). The organic phase was separated, washed with 200 mL of saturated $KHCO_3$ and then with water until neutrality (pH 7), finally it was dried with $MgSO_4$. The solvent was removed by rotary evaporation to give $O=CHCH_2CH_2Rf_8$ as a clear oil.

MW: 478.5 g/mol. Yield: 4.57 g of aldehyde, 92% mol/mol.

^{1}H-NMR (CDCl₃): δ = 2.37-2.52 (m, 2H, **CH₂**Rf8), 2.83 (t, $^3J_{HH}$ = 7 Hz, 2H, O=CHC**H₂**), 9.84 (br s, 1H, O=C**H**).

5.3.1.2 Synthesis of [(C₆H₅)CH₂]N(CH₂CH₂CH₂Rf₈)₂.

A 100 mL flask was charged with the aldehyde synthesized at step 1 (see § 5.3.1.1, 3.20 g; 6.72 mmol, 2.5 eq., excess), 25 mL of anhydrous tetrahydrofuran (THF), and benzyl amine $NH_2CH_2C_6H_5$ (0.29 g, 2.68 mmol). Solid $Na(AcO)_3BH$ (2.20 g, 10.08 mmol) was added under vigorous stirring. The reaction was monitored by GLC analysis. The reaction was stirred overnight. When the aldehyde was completely reacted with benzyl amine, 1 M NaOH (15 mL) was added to the waxy solution. The mixture was extracted with diethylether (3 x 25 mL), washed with water until neutrality and dried with $MgSO_4$. Solvent removal gave a crude colorless oil that was purified by column cromatography on silica gel (1/9 v/v ether/hexanes).

MW: 1027.4 g/mol. Yield: 2.01 g, 73% mol/mol.

^{1}H-NMR (CDCl₃): δ = 1.72-1.79 (m, 4H, **CH₂**CH₂Rf8), 2.03-2.16 (m, 4H, **CH₂**Rf₈), 2.50 (t, $^3J_{HH}$ = 7 Hz, 4H, NC**H₂**), 3.55 (s, 2H, **CH₂**C₆H₅), 7.25-7.35 (m, 5H, C₆**H₅**).

5.3.1.3 Synthesis of HN(CH$_2$CH$_2$CH$_2$Rf$_8$)$_2$.

A 100 mL flask was charged with a solution of (C$_6$H$_5$CH$_2$)N(CH$_2$CH$_2$CH$_2$Rf$_8$)$_2$ obtained in the previous step (see § 5.3.1.2, 2.01 g, 1.96 mmol) in reagent grade ethanol/anhydrous hexane (1/1 v/v, 40 mL). 10% Pd/C (0.342 g, 0.319 mmol) was added, than the mixture was purged with N$_2$ for 10 minutes and fitted with a balloon filled with H$_2$ (1 atm). The mixture was checked by GLC analysis, stirred for 2 hours and filtered through a Celite® plug (2 cm). Solvent was removed by rotary evaporation to give HN(CH$_2$CH$_2$CH$_2$Rf$_8$)$_2$ as a white solid.

MW: 937.3 g/mol. Yield: 1.67 g, 91% mol/mol.

^{1}H-NMR (CDCl$_3$): 1.26 (br s, 1H, N**H**), 1.74-1.81 (m, 4H, C**H$_2$**CH$_2$Rf$_8$), 2.09-2.24 (m, 4H, C**H$_2$**Rf$_8$), 2.70 (t, ^{3}J$_{HH}$ = 7 Hz, 4H, NC**H$_2$**).

5.3.1.4 Synthesis of N(CH$_2$CH$_2$CH$_2$Rf$_8$)$_3$.

A 100 mL flask was charged with HN(CH$_2$CH$_2$CH$_2$Rf$_8$)$_2$ obtained in the previous step (see § 5.3.1.3, 1.67 g, 1.78 mmol), anhydrous THF (25 mL) and a solution of O=CHCH$_2$CH$_2$Rf$_8$ (obtained in the step 1, see § 5.3.1.1, 1.03 g, 2.15 mmol; 1.2 eq.) in anhydrous THF (20 mL). Solid Na(AcO)$_3$BH (0.584 g, 2.68 mmol) was then added under vigorous stirring. The reaction was monitored by GLC and when aldehyde was completely reacted with amine (overnight stirring), NaOH 1 M (25 mL) was added to the waxy solution. Mixture was extracted with diethylether 3 x 25 mL), washed with water until neutrality and dried with MgSO$_4$. Solvent removal gave a solid residue that was purified by column cromatography on silica gel (1/9 v/v ether/hexanes).

MW: 1397.4 g/mol. Yield: 1.82 g, 73% mol/mol.

Total yield (with respect to the initial perfluorinated alcohol): 33% mol/mol.

^{1}H-NMR (CDCl$_3$): 1.68-1.77 (m, 6H, C**H$_2$**CH$_2$Rf$_8$), 2.03-2.21 (m, 6H, C**H$_2$**Rf$_8$), 2.47 (t, ^{3}J$_{HH}$ = 7 Hz, 4H, NC**H$_2$**).

5.3.1.5 Precipitation of (Rf$_8$CH$_2$CH$_2$CH$_2$)$_3$NCH$_3$$^+$ CH$_3$OSO$_3$$^-$ salt.

A 100 mL flask was charged with N(CH$_2$CH$_2$CH$_2$Rf$_8$)$_3$ obtained in the previous step (see § 5.3.1.4, 1.82g, 1.30 mmol), 20 mL of trifluorotoluene and 0.400 mL of dimethylsulfate. The mixture was refluxed overnight. The precipitate formed was collected by a fritted funnel, washed with diethylether, dried by means of rotary evaporation.

The solid appear as a white salt. MW: 1524.0, Yield: 1.76 g, 89% mol/mol.

^{1}H-NMR: (CF$_3$COOD): δ = 2.0-2.4 (bm, 12H, CF$_2$**CH$_2$CH$_2$**), 3.19 (s, 3H, **CH$_3$**N), 3.35-3.6 (bm, 6H, **CH$_2$**N), 3.87 (s, 3H, **CH$_3$**O).

FT-IR: analysis (KBr, ν< 1300 cm^{-1}): 1237 (s), 1202 (s), 1146 (s), 1117 (w), 1064 (w) , 1026 (w), 662 (w), 576 (w), 558 (w), 529 (w) cm^{-1}.

ESI-MS (positive mode): m/z = 1413 ([CF$_3$(CF$_2$)$_7$(CH$_2$)$_3$]$_3$CH$_3$N$^+$), negative mode: m/z = 111 (CH$_3$OSO$_3^-$).

5.3.2 Synthesis of Na$_4$W$_{10}$O$_{32}$ [5].

To a boiling solution containing Na$_2$WO$_4$·2H$_2$O (33 g, 0.1 mol) in deionized water (200 mL) were added 200 mL of a boiling aqueous solution of 1 M HCl . The resulting solution was boiled for other 10 sec. and *quickly* cooled at 30°C in a dry ice/acetone bath under stirring.

Solid NaCl was added to near saturation, and the mixture was further cooled to 0°C for 1 h.

A precipitate formed, which was collected and dried on a fritted funnel. This precipitate was suspended in hot acetonitrile (100 mL), the suspension was filtered, and the filtrate was placed in a freezer overnight. Large pale-lime crystalline rectangular blocks of Na$_4$W$_{10}$O$_{32}$ were collected on fritted funnel and dried under vacuum. (8 g, 32.8 % yield).

FT-IR (KBr, ν< 1300 cm^{-1}): 961 (s), 903 (s), 797 (s,b), 579 (w).

^{183}W-NMR (D$_2$O) δ: -43.0 (8W, s), -173.7 (2W, s).

UV (H$_2$O, conc. 10^{-4}M, 200-500 nm), λmax 322.4 nm, shoulder at 258 nm; logε$_{322.4}$=4.94.

5.3.3 Fluorinated photocatalyst preparation and characterization.

The fluorophilic salt of decatungstate [[CF$_3$(CF$_2$)$_7$(CH$_2$)$_3$]$_3$CH$_3$N]$_4$W$_{10}$O$_{32}$ - (RfN)$_4$W$_{10}$O$_{32}$ − has been isolated by mixing a solution containing 4.3 equivalents of (Rf$_8$CH$_2$CH$_2$CH$_2$)$_3$NCH$_3^+$ CH$_3$OSO$_3^-$ (0.882 mmol) in 2,2,2-trifluoroethanol and a solution containing 0.205 mmol of Na$_4$W$_{10}$O$_{32}$ in water. The resulting complex was recovered by centrifugation, dried under vacuum and recrystallized from HFIP/water.

Yield: 70% mol/mol.

FT-IR analysis (KBr, ν< 1300 cm^{-1}): 1237 (s), 1202 (s), 1149 (s), 1134 (w), 1117 (w), 961 (m), 895 (w), 810 (m), 705 (w), 659 (w) cm^{-1}. ^{19}F-NMR: (376.45 MHz, CF$_3$CH(OH)CF$_3$/CF$_3$CD(OD)CF$_3$, solvent suppression, 298K) : -90.6 (48F, s), -122.3 (32F, s), -130.3 (32F, s), -130.7 (64F, m), -131.6 (32F, s), -132.1 (32F, s), -135.3 (32F, s). ^{183}W-NMR: (16.67 MHz, CF$_3$CH(OH)CF$_3$, 298K) -45.1 (8W, s), -186.5 (2W, s). Elemental Analysis, calculated: C 20.4%; N 0.70%; found: C 21.0%; N 0.66%.

**5.3.4 Preparation of Hyflon membrane incorporating decatungstate.**

Flat sheet were prepared by following the phase inversion process obtained by immersion precipitation technique. The work has been carried out by Dr. Annarosa Gugliuzza (ITM-CNR, section of Rende (CS))

A solution of Hyflon AD 60X® (Hyflon) in Galden HT 55® (2.4 wt%) was mixed with a solution of $(RfN)_4W_{10}O_{32}$ in HFIP (6.8 wt%) in suitable ratio, in order to provide the desired catalyst loading in the membrane. The solutions were cast on an inert support or on a PTFE porous support (pore diameter 0.22 μm) by setting the knife gap at the desired thickness. After 1 min. of air exposure (or air with controlled % of humidity in the case of porous membranes), the casted film was immersed for 2 h. in a coagulation bath containing deionised water at 20 °C. The membranes were then removed from the coagulation bath and dried in a oven at 60 °C under vacuum for 24 h [6]. At variance, phase inversion techniques induced by solvent evaporation was applied at 25±1 °C [6,7].

The same procedure was applied to prepare PVDF membrane containing decatungstate both with the fluorinated counterion and tetrabuthylammonium counterion.

Hyflon® and Galden HT 55® were kindly supplied by Solvay Solexis (see also § 5.2).

Hyflon®: copolymer of tetrafluoroethylene and 2,2,4-trifluoro-5-trifluoromethoxy-1,3-dioxole.
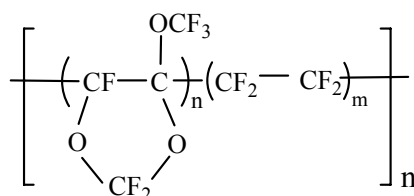
Figure 5.2. Scheme of copolymer: Hyflon®

Galden HT 55®: commercial name for a copolymer of Perfluoropolyether with boiling point = 55°C and general formula: $-(CF_2-CF_2O)_n-(CF_2O)_m-$.

5.3.5 Membrane characterization and analysis.

Characterization of RfNW10-Hyflon membranes was performed by FT-IR, UV-Vis, SEM spectroscopy in back scattered electrons mode (BSE), AFM by-sample mode/no-contact mode.

5.3.6 General homogeneous photooxidation procedure.

The photocatalytic experiments were carried out in a quartz cell hosted in a termostatted holder at 20°C.

The reaction solutions (2 mL of HFIP or CH_3CN) containing the substrate (0.02 M) and the $W_{10}O_{32}^{4-}$ photocatalyst (0.3 mM) were placed in the cell, under magnetic stirring, and dioxygen was supplied through a small Teflon tube connected with a balloon-tank.

Reaction aliquots (25 μL) were diluted with a dichloromethane solution (500 μL) containing C_{12} or C_{10} as internal standard. The reaction was monitored over time by quantitative GLC-analysis. Peroxide content was determined using the triphenylphosphine (PPh_3) quencher method[8]. Carboxylic acids were revealed by silylation with BSTFA before GLC-MS analysis. Dimers accounted for 30-40% of total oxidation products at high percentages of substrate conversion.

An example of reaction kinetic recorded for the ethylbenzene oxidation in HFIP solution is reported on Chapter 2 at Section: 2.3.2.

5.3.7 General heterogeneous static photooxidation procedure.

The photocatalytic experiments were carried out in a photoreactor composed of a quartz window and a rubber ring to host the membrane retail, that was placed on the internal wall of the cell opposite to the light source (8.5 cm distance from the focusing lens), to collect all the focalized radiation. The hydrocarbon (1.1 mL) was placed in the cell, under magnetic stirring, and oxygen was supplied through a small Teflon tube connected with a tank. Reaction aliquots (25 μL) were diluted with a dichloromethane solution (500 μL) containing C_{12} as internal standard. The reaction was monitored over time by quantitative GLC-analysis. Peroxide content was determined using the triphenylphosphine quencher method. At the end of irradiation, the membrane was separated from the reaction mixture, washed with hexane, exposed to oxygen atmosphere to complete oxidation of the reduced heteropolyblue complex, and dried under vacuum. FT-IR analysis was used to assess the membrane integrity after catalysis (see the following figure). In the FT-IR spectrum of the used membrane, the presence of an absorption band at 1700 cm^{-1} might be ascribed to retention of oxidation products which could affect the catalytic membrane efficiency in successive runs. A drop of about 20-25% was indeed observed upon membrane recycling.

5.3.8 General heterogeneous continuous photooxidation procedure.

The photocatalytic experiments in continuous mode were carried out in a proper photoreactor composed of a quartz window and a rubber ring to host the membrane retail, that was placed on the internal wall of the cell opposite to the light source (8.5 cm distance from the focusing lens), to collect all the focalized radiation. The reactor has been designed in order to minimize the "dark" volume of reaction mixture circulating outside the irradiated window in contact with the excited photocatalyst, and to collect a trans-membrane permeate flow through a porous-sinterized steel-septum. The hydrocarbon (2.0 mL) was placed in the reactor tank, and oxygen was supplied through a small Teflon tube connected with a balloon. The optimized flow of the reaction mixture (0.3 mL/min) has been obtained through a peristaltic pump. As for the static process, reaction aliquots (25 µL) were diluted with a dichloromethane solution (500 µL) containing C_{12} as internal standard. The reaction was monitored over time by quantitative GLC-analysis and peroxide content was determined using the triphenylphosphine quencher method.

Scheme and picture of both the design and the photoreactor with circulating photoirradiated mixture are showed at Chapter 2 on Section 2.3.2.1.

5.3.9 GC-analysis procedure and conditions.

Both reagents and oxidation products have been analyzed by GLC-Flame Ionisation Detector (FID) technique.

Analysis were obtained with a 30 m (0.32 mm internal diameter, 0.25 µm film thickness) HP-5 capillary column and with a 60 m (0,53 mm internal diameter, 1 µm film thickness) Alcohols Stabilwax® (Restek) capillary column when a better separation between the oxidation products of a specific reaction mixture was required.

Solutions injected in the column were prepared by sampling reaction aliquots (25 µL) diluted with 500 µL of CH_2Cl_2 containing C_{12} or C_{10} ($8.8 \cdot 10^{-4}$ M) as internal standard and an excess of triphenyphosphine as quencher.

Analysis were performed with the following conditions and programs:

For 30 m HP-5 capillary column:

T injector =180°C;

T detector = 250°C;

Flow rate: 1 mL/min;

Chapter 5.

Analysis program:

Initial Temperature: 55°C for 3 min.; Rate: 15°C/min.; Final Temperature 250°C for 2 min.

For 60 m Alcohols Stabilwax column:

T injector: = 200°C;

T detector = 280°C;

Flow rate: 6 mL/min;

Analysis program:

Initial Temperature: 55°C for 5 min.; Rate: 12°C/min.; Final Temperature 250°C for 10 min.

Retention times of different products were identified by injecting standard solutions and confirming them through GC-MS analysis.

5.3.10 GC Response Factor: general calculation procedure.

For each substrate and their corresponding products, three solutions at different concentration have been prepared through consecutive dilutions .

Aliquots of these solutions (25 μL) were sampled and diluted with 500 μL of internal standard solution.

Each sample has been analyzed three times, thus obtaining average values for the ratio between the analyte and internal standard areas.

Average values ($A_{analyte}/A_{standard}$) were plotted versus concentration ratios ($C_{analyte}/C_{standard}$), thus obtaining a linear interpolation. Calculated slopes corresponds to the Response Factor of the product of interest, as in following equation:

$$A_{analyte}/A_{standard} = F_{analyte} (C_{analyte}/C_{standard})$$

5.3.10.1 GC Response Factor: calculation procedure for ethylbenzene and its oxidation products.

As example, calculation procedure for Response Factors of ethylbenzene and its oxidation products are here reported .

A mother solution of ethylbenzene, 1-phenyl-ethanol and acetophenone (each at concentration $1.0 \cdot 10^{-1}$ M) has been prepared and, by consecutive dilutions, other three diluted

120

solutions $(4.0 \cdot 10^{-2}$ M, $2.0 \cdot 10^{-2}$ M and $1.0 \cdot 10^{-2}$ M) , have been obtained, thus giving four solutions at known concentration for each analyte.

Internal standard solution, in concentration $8.8 \cdot 10^{-4}$ M, has been prepared by dissolving 10 μL of n-dodecane (C_{12}) in 50 mL of CH_2Cl_2.

Final samples have been prepared by sampling 25 μL of each solution, diluted with 500 μL of internal standard C_{12} solution. (Diluting Factor D: 21). Analysis were repeated three times for each sample and the ratios between the analyte and internal standard peak areas was obtained. From the known concentration of the internal standard ($8.4 \cdot 10^{-4}$ M) and that of each analyte for each sample injected, it was possible to interpolate the following results:

Table 5.3. Analytical results for determining Response Factor of Ethylbenzene and its oxidation products.

Solution	$C_{analyte}^{a}/C_{standard}$	Average $A_{analyte}/A_{standard}$		
		Ethylbenzene	1-phenyl-ethanol	Acetophenone
1	5.6667	2.420	1.998	2.220
2	2.2667	0.856	0.698	0.797
3	1.1333	0.498	0.394	0.459
4	0.5667	0.239	0.199	0.246

a. Analyte concentration is that of each solutions divided by the Diluting Factor.
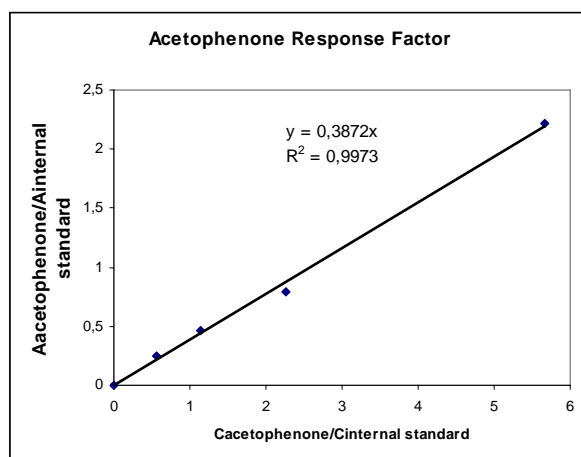
Response Factors are the slopes of the following plots:
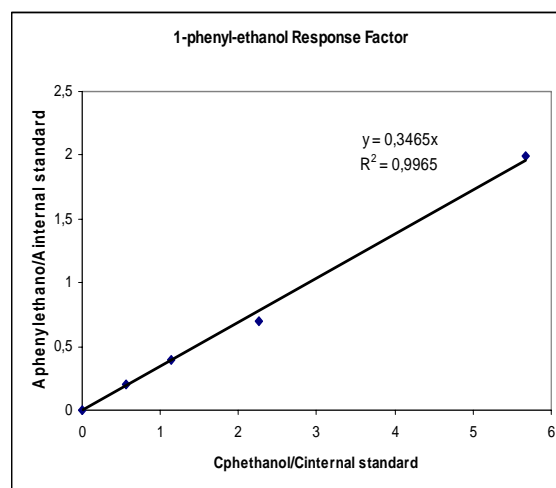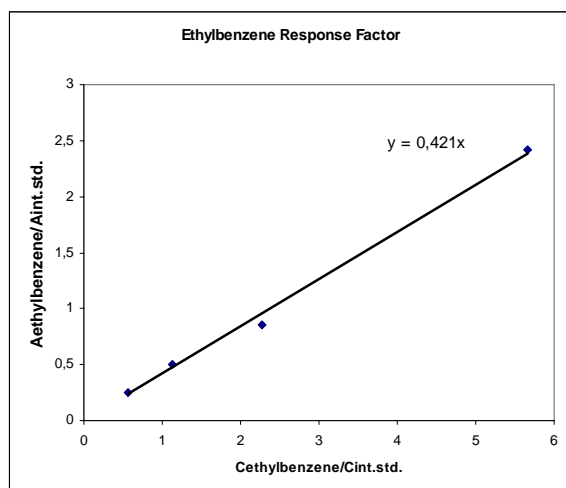
Figure 5.5: Plots of Analytical data for Response Factors calculations.

Thus giving:

Table 5.4. Response Factor for Ethylbenzene and its photooxidation products.

Analyte	Response Factor
Ethylbenzene	0.421
1-Phenylethanol	0.347
Acetophenone	0.387

Similar procedures have been applied for other substrates used and their photooxidation products.

5.3.11 Quantitative analysis calculations.

Quantitative evaluation of a determined product or substrate in solutions analyzed have been calculated with the internal standard method through the following relations:

$$C_{analyte} = (A_{analyte}/A_{standard})\cdot(C_{standard}/F_{standard})$$

and finally:

$$C_{analyte} \text{ in reaction mixture: } (A_{analyte}/A_{standard})\cdot(C_{standard}/F_{standard})\cdot D$$

Where $F_{analyte}$ is the calculated Response Factor (see previous paragraph), and D is the Dilution Factor used in preparing the sample to analyze.

5.4 Hydrogen peroxide activation by hybrid polyoxotungstates in fluorinated alcohols.

5.4.1 Synthesis and characterization of precursors vacant polyoxotungstates.

Vacant polyoxotungstates were synthesized following literature procedures[9].

Synthesis of $K_8[\alpha\text{-}SiW_{11}O_{39}]$[10]

$$11WO_4^{2-} + SiO_3^{2-} + 16H^+ + 8K^+ + 6H_2O \longrightarrow K_8[\alpha_2\text{-}SiW11O_{39}]\,14H_2O$$

Na_2SiO_3 (sodium metasilicate, 1,51 g, 12.4 mmol) was dissolved with magnetic stirring at room temperature in 12 mL of distilled water (if the solution is not completely clear, it must be filtered – Solution A).
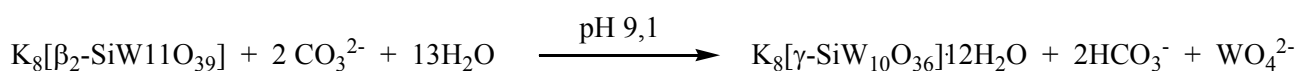
In a 250 mL beaker, containing a magnetic stirring bar, $Na_2WO_4\cdot2H_2O$ (Sodium tungstate bihydrate, 45.48 g, 0.138 mol) was dissolved in 75 mL of boiling water (Solution B).

To the boiling Solution B, a solution of 4M HCl (40 mL, 0.164 mol) was added dropwise in ~ 30 minutes, with vigorous stirring to dissolve the precipitate of tungstic acid. Solution A was then added and, quickly, 12 mL of 4M HCl (49.3 mmol) were also added. The pH was ~ 5 to 6. The solution was kept boiling for 1h. After cooling to room temperature, the solution must be filtered if it is not completely clear. Solid KCl (solid potassium chloride 37 g, 0.496 mol) was added to the solution, while stirring. The white solid product was collected on a fritted funnel (medium porosity), washed with 2 x 12 mL of aqueous KCl solution 1M, then with cold water (1 x 12 mL), and finally dried under vacuum.

Yield: 30.4 g, 82%.

FT-IR<1000 cm^{-1} (KBr, cm^{-1}): 996, 959, 893, 797, 731, 537, 514, 475.

Synthesis of $K_8[\gamma\text{-}SiW_{10}O_{36}]$

$$K_8[\beta_2\text{-}SiW11O_{39}] + 2\,CO_3^{2-} + 13H_2O \xrightarrow{\text{pH 9,1}} K_8[\gamma\text{-}SiW_{10}O_{36}]12H_2O + 2HCO_3^- + WO_4^{2-}$$

This synthesis requires accurate pH readings on a calibrated pH meter.

The potassium salt of the β_2 isomer of undecatungstosilicate (9 g, 2.78 mmol), -recently synthesized as described below -, was dissolved in 140 mL of water maintained at 25°C.

123

Impurities in the $K_8[\beta_2\text{-}SiW_{11}O_{39}]$ salt (mainly paratungstate) give insoluble materials, which are removed quickly by filtration on a fine frit or through Celite® plug. The pH of the solution was quickly adjusted to 9.1 by addition of a 2M aqueous solution of K_2CO_3. The pH of the solution was kept at this value by addition of the K_2CO_3 solution for exactly 16 minutes. The potassium salt of the γ-decatungstosilicate was then precipitated by addition of solid KCl (potassium chloride 24.42 g). During the precipitation (10 minutes), the pH was maintained at 9.1 by addition of small amounts of the K_2CO_3 solution. The solid was removed by filtration, washed with 1M KCl solution, and dried under vacuum.

Yield: 2.94 g, 25%.

Properties: the potassium salt of $[\gamma\text{-}SiW_{10}O_{36}]^{8-}$ is soluble in water and stable below pH 8 while, in strongly acidic solution, pH <1, it converts slowly into $[\beta\text{-}SiW_{12}O_{40}]^{4-}$.

FT-IR (KBr, cm^{-1}): 987 (m), 942 (s), 905 (s), 866 (s,b), 820 (s,b), 742 (s,b), 656 (sh), 556 (w), 530 (m).

^{183}W-NMR (0,45 g dissolved in 2 mL hot D_2O) δ: -99.4 (4W), -140.4 (4W), -161.4 (2W).

Synthesis of $K_8[\beta_2\text{-}SiW_{11}O_{39}]$

$$11WO_4^{2-} + SiO_3^{2-} + 16H^+ + 8K^+ + 6H_2O \longrightarrow K_8[\beta_2\text{-}SiW11O_{39}]\ 14H_2O$$

Sodium metasilicate (1.50 g, 12.3 mmol) was dissolved in 25 mL of water (Solution A).

Sodium tungstate bihydrate (45.44 g, 0.138 mol) was dissolved in ~ 75 mL of water in a separate 250 mL beaker containing a magnetic stirrer bar. This solution was immersed in an ice/water bath and then cooled at ~ 5°C. To this solution, 40 mL of 4.1M HCl (0.16 mmol) were added dropwise in ~ 30 minutes, under vigorous stirring, in order to dissolve the hydrated tungstic acid that is locally formed.

When the tungstate solution returned at room temperature, the solution A was added, and the pH was adjusted at 5.5 by addition of the 4M HCl solution (~ 10 mL). This pH was maintained by addition of small amounts of 4M HCl for 100 minutes. Solid potassium chloride (22.1 g, 0.296 mol) was then added to the solution with gentle stirring. After 15 minutes, the precipitate was collected by filtration through a sintered glass filter. Purification was achieved by dissolving the product in 210 mL of water. The insoluble material was quickly removed by filtration on a fine frit, and the salt was precipitated again by addition of solid KCl (19.7 g, 0.264 mol). The precipitate (white solid) was separated by filtration, washed with 2M KCl solution (2 x 12 mL), and dried under vacuum.
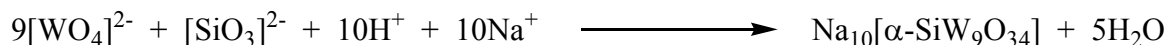
Yield: 17.00 g, 45%.

FT-IR<1000 cm^{-1} (KBr, cm^{-1}): 993 (w), 949, 878 (s), 805 (s), 731(s), 536 (w), 517 (w).

UV (4·10^{-5} M in H$_2$O): λ_1 = 298 nm, logε = 5.16, λ_2 = 283 nm, logε = 5.92.

Synthesis of Na$_{10}$[α-SiW$_9$O$_{34}$]

$$9[WO_4]^{2-} + [SiO_3]^{2-} + 10H^+ + 10Na^+ \longrightarrow Na_{10}[\alpha\text{-}SiW_9O_{34}] + 5H_2O$$

Sodium tungstate dihydrate (50 g, 0.15 mol) and sodium metasilicate (1.67 g, 13.7 mmol) were dissolved in 55 mL of hot water (80-100°C) in a 250 mL beaker containing a magnetic stirring bar. To this solution were added dropwise 35.7 mL of 6M HCl in ~ 30 min under vigorous stirring. The solution was boiled until the volume decreased to ~ 80 mL. Unreacted silica was removed by filtration over a fine frit or over Celite® plug or by centrifugation.

Anhydrous sodium carbonate (13.7 g) was dissolved in 41.2 mL of water in a separate beaker. This solution was slowly added to the first solution with gentle stirring. A precipitate formed slowly, and it was removed by filtration, using a sintered glass filter, after 1 h. The solid was stirred with 270 mL of 4M NaCl solution and filtered again. It was then washed successively with two 30 mL portions of ethanol and 30 mL of diethyl ether and dried under vacuum.

Yield: 19.23g; 47%

FT-IR <1000 cm^{-1} (KBr, cm^{-1}): 981 (m), 935 (m), 929 (sh), 859 (s), 804 (s), 686 (s,b), 554 (m), 525 (m), 499 (w), 484 (sh).

5.4.2 Synthesis and characterization of fluorinated hybrid polyoxotungstates 1-3.

5.4.2.1 General procedure for the synthesis of tetrabutylammonium salts of fluorinated hybrid lacunary polyoxotungstates:

$$Mm[SiWwOz] \xrightarrow[\text{CH}_3\text{CN}]{\substack{R_fSiCl_3 \\ TBABr}} TBA_4[(RfSi)xOySiWwOz]$$
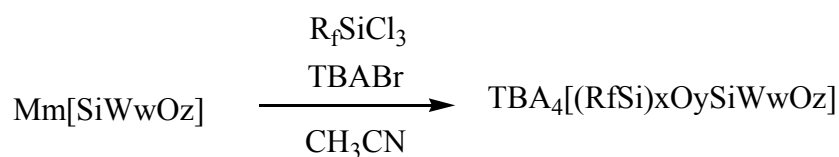
M = Na, K.

Rf = CF$_3$(CF$_2$)$_7$(CH2)$_2$-

TBA = (CH$_3$CH$_2$CH$_2$CH$_2$)$_4$N$^+$

Chapter 5.

Polyoxotungstates graphted with fluorinated alkyl chains were prepared by adding 2 (products **1** and **2**) or 4 (product **3**) equivalents of $CF_3(CF_2)_7(CH_2)_2SiCl_3$ to a suspension containing 4 equivalents of n-Bu$_4$NBr and 0.2 mmol of vacant polyoxotungstate in 10 ml of CH_3CN and let overnight at room temperature under efficient stirring. After removal of the insoluble material, the product was collected by evaporation of the solvent and washing with water on a fritted funnel. Yield: 65-75%. The identity of products **1-3** was demonstrated by FT-IR, ^{19}F-NMR, [183]W-NMR, ^{29}Si-NMR, ESI-MS (-) and elemental analysis, as follow in the next section.

5.4.2.2 Characterizations.

$((CH_3CH_2CH_2CH_2)_4N)_4[(CF_3(CF_2)_7(CH_2)_2Si)_2O(SiW_{11}O_{39})]$ **(1).**

FT-IR (KBr): 2964(s), 2876(s), 1630(w), 1484(m), 1473(w), 1457(w), 1382(w), 1242(s), 1206(s), 1152(s), 1134(m), 1112(w), 1051(s), 981(w), 965(m), 953(m), 905(s), 805(s), 761(w), 721(w), 668(m), 656(w), 534(m) cm^{-1} . ^{29}Si-NMR (79.49 MHz, CD$_3$CN/CH$_3$CN, 298 K): -58.83 (2Si, s); -80.31(1Si. s); ^{19}F-NMR (376.45 MHz, CD$_3$CN/CH$_3$CN, 298 K): -86.3 (6F, s), -121.4 (4F, s), -127.2 (12F, m), 128.5 (8F, m), 131.6 (4F, s);.[183]W-NMR (16.67 MHz, CD$_3$CN/CH$_3$CN, 298 K): -107.6 (4W, s), -113.8 (1W, s), -126.9 (2W, s), -170.8 (2W, s), -248.2 (2W, s); ESI-MS(-), (CH$_3$CN): m/z= 910.0 (calculated for $[(CF_3(CF_2)_7(CH_2)_2Si)_2O(SiW_{10}O_{39})]^{4-}$: 909); Elemental Analysis for $C_{84}H_{152}F_{34}N_4O_{40}Si_3W_{11}$ (%): found C 21.79, H 3.30, N 1.18; calculated C 21.88, H 3.32, N 1.21.

$((CH_3CH_2CH_2CH_2)_4N)_4[(CF_3(CF_2)_7(CH_2)_2Si)_2O(SiW_{10}O_{36})]$ **(2).**

FT-IR (KBr): 2965(s), 2876(s) 1630(w), 1483(m), 1383(w), 1243(s), 1207(s), 1152(s), 1134(m), 1109(m), 968(m), 904(s), 823(m), 736(m), 555(w), 511(w) cm^{-1}. ^{29}Si-NMR (79.49 MHz, CD$_3$CN/CH$_3$CN, 298 K): -64.39 (2Si, s), -88.08 (1Si, s); ^{19}F-NMR (376.45 MHz, CD$_3$CN/CH$_3$CN, 298 K): -86.2 (6F, s), -120.8 (4F, s), -127.0 (12F, m), 127.8 (8F, m), 131,3 (4F, s); [183]W-NMR (16.67 MHz, CD$_3$CN/CH$_3$CN, 298 K): -106.7 (4W, s), -133.2 (2W, s), -140.5 (4W, s); ESI-MS(-), (CH$_3$CN): m/z= 851.5 (calculated for $[(CF_3(CF_2)_7(CH_2)_2Si)_2O(SiW_{10}O_{36})]^{4-}$ 851.2); Elemental Analysis for $C_{84}H_{152}F_{34}N_4O_{37}Si_3W_{10}$ (%): found C 21.99, H 3.17, N 2.07; calculated C 23.04, H 3.50, N 1.28.

$((CH_3CH_2CH_2CH_2)_4N)_4[(CF_3(CF_2)_7(CH_2)_2Si)_4O_3(SiW_9O_{34})]$ **(3).**

FT-IR (KBr) 2965(s), 2876(s) 1630(w), 1485(m), 1473(w), 1457(w), 1382(w), 1240(s), 1206(s), 1152(s), 1134(m), 1115(m), 1062(m), 963(w), 950(w), 893(s), 824(m), 736(m),
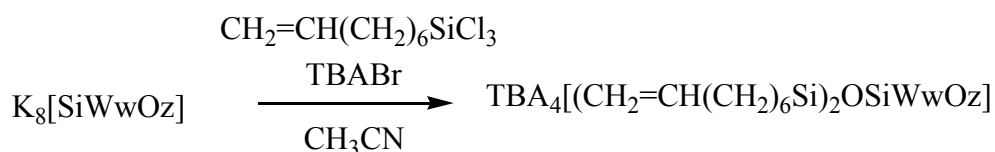
668(w), 657(w) cm^{-1}. ^{29}Si-NMR (79.49 MHz, CD$_3$CN/CH$_3$CN, 298 K): -62.18 (3Si, s), -83.65 (1Si, s), -88.42 (1Si, s), ^{19}F-NMR (376.45 MHz, CD$_3$CN/CH$_3$CN, 298 K): -87.4 (12F, m), -121.8 (8F, m), -127.7 (24F, m), -128.7 (16F, m), -132.2 (8F, m). ^{183}W-NMR (16.67 MHz, CD$_3$CN/CH$_3$CN, 298 K): - 78.84 (3W, s), -154.29 (6W, s). ESI-MS(-), (CH$_3$CN): m/z= 1043.6 (calculated for [(CF$_3$(CF$_2$)$_7$(CH$_2$)$_2$Si)$_4$O$_3$(SiW$_9$O$_{34}$)]$^{4-}$ 1042.9); Elemental Analysis for C$_{104}$H$_{160}$F$_{68}$N$_4$O$_{37}$Si$_5$W$_9$ (%): found C 23.05, H 2.88, N 1.12; calculated C 24.28, H 3.13, N 1.09.

[[CF$_3$(CF$_2$)$_7$(CH$_2$)$_3$]$_3$CH$_3$N]$_4$W$_{10}$O$_{32}$ **(4).**
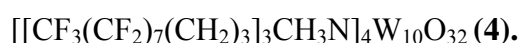
For this salt see synthetic procedure and characterization on Section 5.3.3.

5.4.3 Synthesis and characterization of hybrid polyoxotungstates monomers 5-6[11].

5.4.3.1 General procedure for the synthesis of tetrabutylammonium salts of hybrid lacunary polyoxotungstates monomers.

$$
\begin{array}{c}
\text{CH}_2\text{=CH(CH}_2)_6\text{SiCl}_3 \\
\text{TBABr} \\
\text{K}_8[\text{SiWwOz}] \xrightarrow{\hspace{2cm}} \text{TBA}_4[(\text{CH}_2\text{=CH(CH}_2)_6\text{Si})_2\text{OSiWwOz}] \\
\text{CH}_3\text{CN}
\end{array}
$$

TBA = (CH$_3$CH$_2$CH$_2$CH$_2$)$_4$N$^+$

Hybrid polyoxotungstates **(5)** or **(6)** were prepared by adding 2 equivalents of CH$_2$CH(CH$_2$)$_6$SiCl$_3$ and 6 equivalents of 4 M HCl to a stirred suspension containing 4 equivalents of n-Bu$_4$NBr and 0.2 mmol of mono- or divacant Keggin polyoxotungstate in 10 ml of CH$_3$CN and 1 ml of H$_2$O. The mixture was stirred overnight, and the insoluble material was removed by filtration. The product was collected after evaporation of the solvent and washing with water (4 x 5 ml) on a fritted funnel. Yield: 65-75% . The identity of products **5, 6** was demonstrated by FT-IR, ^{13}C NMR, ^{183}W NMR, ^{29}Si NMR, ESI-MS (-) and elemental analysis, as follow in the next section.

5.4.3.2 Characterizations.

((CH$_3$CH$_2$CH$_2$CH$_2$)$_4$N)$_3$H[(CH$_2$CH(CH$_2$)$_6$Si)$_2$O(SiW$_{11}$O$_{39}$)] **(5).**
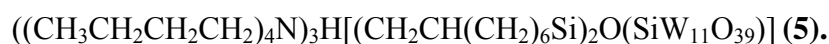
FT-IR (KBr): 2962(s), 2930(s), 2874(s), 1636(m), 1484(m), 1473(w), 1465(w), 1458(w), 1044(s), 978(w), 963(s), 947(s), 922(w), 903(s), 854(m), 805(s), 757(w), 705(w), 668(w), 534(m) cm^{-1} . ^{29}Si{H} NMR (79.49 MHz, CD$_3$CN/CH$_3$CN, 298 K): -51.58 (2Si, s); -

84.17(1Si. s); ^{13}C{H} NMR (75.47 MHz, CD$_3$CN/CH$_3$CN, 301 K): 140.4, 114.6, 59.1, 34.6, 33.6, 24.4, 23.8, 20.4, 13.9. ^{183}W NMR (16.67 MHz, CD$_3$CN/CH$_3$CN, 298 K): -111.2 (2W, s), -114.2 (3W, s), -129.1 (2W, s), -176.8 (2W, s), -255.4 (2W, s); ^{1}H NMR (CD$_3$CN, 301K) 5.82 (2H, m), 4.94 (4H, m), 3.16 (24H, m), 2.05 (4H, m), 1.50-1.70 (28H, m), 1.41 (28H, m), 0.99 (36H, t, J=7.30Hz), 0.51 (4H, t, J=7.83Hz); ESI-MS(-), (CH$_3$CN): m/z= 741.7 (calculated for [(CH$_2$CH(CH$_2$)$_6$Si)$_2$O(SiW$_{11}$O$_{39}$)]$^{4-}$: 741.2); Elemental Analysis for C$_{64}$H$_{174}$N$_4$O$_{40}$Si$_3$W$_{11}$ (%): found C 23.75, H 4.56, N 1.39; calculated C 24.39, H 4.45, N 1.42.

((CH$_3$CH$_2$CH$_2$CH$_2$)$_4$N)$_3$H[(CH$_2$CH(CH$_2$)$_6$Si)$_2$O(SiW$_{10}$O$_{36}$)] **(6).**

FT-IR (KBr): 2961(s), 2928(s) 2874(s), 1636(m), 1484(s), 1465(m), 1382(m), 1100(s), 1047(s), 964(s), 947(m), 902(s), 885(s), 821(s), 731(s), 668(w), 544(m), 510(m), 483(w), 458(w), 407(m) cm^{-1}. ^{13}C{H} NMR (75.47 MHz, CD$_3$CN/CH$_3$CN, 301 K): 140.4, 114.7, 59.4, 34.6, 34.3, 29.7, 24.4, 20.4, 16.6, 13.9. ^{29}Si{H} NMR (79.49 MHz, CD$_3$CN/CH$_3$CN, 298 K): - 61.93 (2Si, s), - 88.49 (1Si, s); ^{183}W NMR (16.67 MHz, CD$_3$CN/CH$_3$CN, 298 K): - 108.7(4W, s), -134.4(2W, s), -140.4 (4W, s); ^{1}H NMR (CD$_3$CN, 301K) 5.83 (2H, m), 4.94 (4H, m), 3.17 (24H, m), 2.20 (4H, m), 2.03 (4H, m), 1.63 (24H, m), 1.41 (36H, m), 0.98 (36H, t, J=7.29Hz), 0.51 (4H, m); ESI-MS(-), (CH$_3$CN): m/z=683.7 (calculated for [(CH$_2$CH(CH$_2$)$_6$Si)$_2$O(SiW$_{10}$O$_{36}$)]$^{4-}$ = 683.3); Elemental Analysis for C$_{64}$H$_{139}$N$_3$O$_{37}$Si$_3$W$_{10}$ (%): found C 24.23, H 4.45, N 1.29; calculated C 22.18, H 4.04, N 1.21.

5.4.4 General procedure of polyoxotungstates polymerization in cross-linked networks.

Complexes (**5**) or (**6**) were copolymerized with different ratios of methyl-methacrylate (MMA) and ethylenglycol dimethacrylate (EDM), in the presence of porogenic solvents (2-propanol, 1,4-butanediol) and a minimum amount of CH$_3$CN in order to obtain an homogeneous mixture. Bis-(tertbuthyl-cyclohexyl) peroxodicarbonate was used as radical initiator. After 24h at 343K, the white and swollen polymers were recovered, washed with a THF/CH$_3$CN 4/1 mixture, dried and then characterized (see § 5.4.5).

5.4.5 Polymeric networks characterization.

Final hybrid polymeric materials were characterized on solid state by FT-IR, SEM and TEM analysis. TGA and DSC measurements were also recorded. (See Chapter 3).

5.4.6 Hydrogen peroxide titration procedure.

5.4.6.1 Na$_2$S$_2$O$_3$ standardization by iodometric titration.

$$IO_3^- + 6H^+ + 5I^- \longrightarrow 3I_2 + 3H_2O$$

$$6S_2O_3^{2-} + 3I_2 \longrightarrow 6I^- + 3S_4O_6^{2-}$$
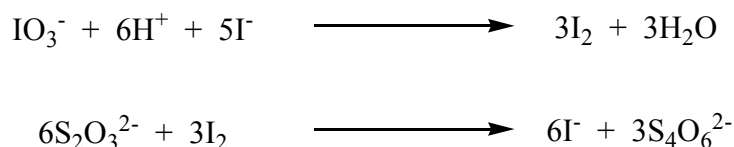
Sodium tiosulphate is not a primary standard, hence its titration is necessary.

The procedure for iodometric method is described below:

10 mL of both deionised water and glacial acetic acid were poured in a 100 mL conical flask with 10 mL of a 10% KI aqueous solution and 1 mL of a 0.25M KIO$_3$ standard solution. (The latter solution was prepared by dissolving in 10 mL of milliQ water 535 mg of KIO3 previously dried in oven at 110°C, for at least 1 hour, and then cooled in a desiccator).

The flask was kept in the dark for at least 2 minutes, to allow the I$_2$ formation (the solution become yellow-orange). This solution was then titrated with the thiosulphate solution (3.40 g in 250 mL of water, prepared at least one week before, and stored in the dark), until the iodine colour becomes very faint. At this point starch indicator, which forms an intensely blue compound with free iodine, was then added and the titration was continued until the colour disappeared completely at the end point.

Iodometric titration were repeated three times. The average concentration of the thiosulphate solution resulted: 0.0863 M.

Caution: starch indicator has not to be added too early because, otherwise, iodine is strongly adsorbed onto it and accuracy is reduced.

5.4.6.2 H$_2$O$_2$ titration.

$$H_2O_2 + 2I^- + 2H^+ \longrightarrow I_2 + 2H_2O$$

$$2S_2O_3^{2-} + I_2 \longrightarrow 2I^- + S_4O_6^{2-}$$
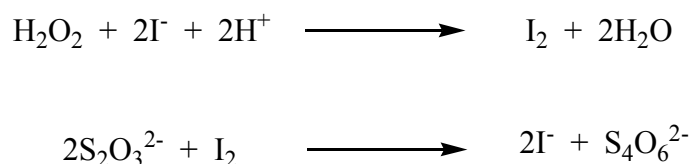
Both solution of 35% and 70% of H$_2$O$_2$ were titrated.

40 µL of H_2O_2 solution were poured in a conical flask with 10 mL of water, 10 mL of 10% KI, 10 mL of glacial acetic acid and a small amount of $(NH_4)_2MoO_4\cdot4H_2O$ as catalyst for I_2 formation.

The flask was closed with a plug and kept in the dark for two minutes and then titrated with a standard thiosulfate solution, until the colour of iodine solution becomes very faint. Starch indicator was then added and the titration was continued until the colour disappears completely at the end point.

Titration was repeated three times for both 35% and 70% H_2O_2 giving the following average concentrations:

H_2O_2 35%: 11.35 M

H_2O_2 70%: 24.93 M.

5.4.7 General homogeneous oxidation procedure.

$CF_3CH(OH)CF_3$ or CH_3CN (0.6 ml), POM (0.8 µmol) and the substrate (0.5 mmol) were mixed, and 0.1 mmol of 70% hydrogen peroxide was added, in a closed glass reactor. (Caution: The uncontrolled heating of large amount of peroxides must be avoided. Care must be taken to avoid possible explosion).

The reaction mixture was heated at 70°C. Sample aliquots were taken (20 µl), diluted with 500 µl of CH_2Cl_2 containing dodecane as internal standard and triphenylphosphine as quencher, and analysed by GLC-FID. Hydrogen peroxide content was verified by iodinated paper, and the reactions were generally monitored until oxidant consumption. Carboxylic acids were revealed by silylation procedure with BSTFA, before GC-MS analysis.

POMs stabilities were assessed by comparison of their FT-IR spectra before the reaction and after it upon precipitation and washing with methanol.

5.4.8 General heterogeneous oxidation procedure.

Solvent ($CF_3CH(OH)CF_3$, CF_3CH_2OH or CH_3CN; 0.6 ml), catalytic polymer (estimated POM cross linked: 0.8 µmol) and substrate (0.5 mmol) were stirred with 0.1 mmol of hydrogen peroxide (70% aqueous solution) in a closed glass reactor. (Caution: The uncontrolled heating of large amount of peroxides must be avoided. Care must be taken to avoid possible explosion).

The reaction mixture was heated at 70°C and mixed under magnetic stirring. Sample aliquots were taken (20 µl) after filtration, diluted with 500 µl of CH_2Cl_2 containing dodecane as internal standard and triphenylphosphine as quencher, and analysed by GC-FID. Hydrogen

peroxide content was verified by iodinated paper, and reaction were generally monitored until oxidant consumption. Carboxylic acids were revealed by silylation procedure with BSTFA, before GC-MS analysis.

Polymers integrity and polyanions stability were assessed by comparison of FT-IR spectra before and after the reaction, upon precipitation and washing with methanol. For recycling tests, catalyst were filtered and collected from the reaction mixture, washed with THF/CH$_3$CN 4/1 v/v, dried and then re-used.

5.4.9 GC-analysis procedure and conditions.

Both olefins and epoxides-oxidation products have been analyzed through GLC-Flame Ionisation Detector (FID) technique.

Analysis were obtained with a 15 m (0.10 mm internal diameter, 0.10 μm film thickness) Equity-5 (Supelco) capillary column.

Solutions injected to the column were prepared by sampling reaction aliquots (20 μL) diluted with 500 μL of CH$_2$Cl$_2$ containing C$_{12}$ (8.8·10^{-4} M) as internal standard and an excess of triphenylphosphine as quencher.

Analysis were performed with the following conditions and program:

T injector =180°C;

T detector = 250°C;

Flow rate: 69.5 mL/min, flash GLC;

Analysis program:

Initial Temperature: 55°C for 3 min. (30°C for the same time for hexenes); Rate: 15°C/min.; Final Temperature 250°C for 2 min.

Response Factors and quantitative evaluations of products and reagents were calculated and done following the same procedure described at section 5.3.9-11.

5.5 Synthesis of phenol by POM-based catalytic methods.

5.5.1 Synthesis and characterization of Vanadium substituted polyoxometalates.

Synthesis of $[(CH_3CH_2CH_2CH_2)_4N]_4[\gamma\text{-}1,2\text{-}H_2SiV_2W_{10}O_{40}]\cdot H_2O$[12]

1 g (0.33 mmol) of $K_8[\gamma\text{-}SiW_{10}O_{36}]$, synthesized following the procedure described on section 5.4.1, was quickly dissolved in 1M HCl (3.5 mL). $NaVO_3$ (0.5M, 1.4 mL, 0.69 mmol) was added, and the mixture was gently stirred for 5 minutes. The solution was filtered off, and followed by the addition of $[(n\text{-}C_4H_9)_4N]Br$ (1 g, 3.13 mmol) in a single step. The resulting yellow precipitate was collected by the filtration and then washed with an excess amount of water ($\sim$ 40 mL). The crude product was purified twice with the precipitation method (addition of 125 mL of H_2O into acetonitrile solution of the crude product (8 mL)). Analitically pure $[(CH_3CH_2CH_2CH_2)_4N]_4[\gamma\text{-}1,2\text{-}H_2SiV_2W_{10}O_{40}]\cdot H_2O$ was obtained as a pale yellow powder. Yield: 0.93 g (76%).

FT-IR: 2961(s), 2935(s, sh) 2873(s), 1630 (m) 1484(s), 1380(m), 1151(w), 1006(m), 995(m, sh), 966(s), 916 (s), 904(s), 876(s), 840(m), 790(s), 691(m), 550(m), 519(w), 482(w), 457(w), 405(m)

^{29}Si NMR (79.49 MHz, CD_3CN/CH_3CN, 298 K): - 84.24(1Si, s); ^{183}W NMR (16.67 MHz, CD_3CN/CH_3CN, 298 K): - 82.2(4W, s), -96.9(2W, s), -129.4(4W, s).

Synthesis of $Na_5[PMo_{10}V_2O_{40}]\cdot 14H_2O$[13]

3.18 g (30 mmol) of Na_2CO_3 were added to a suspension of 5.46 g (30 mmol) of V_2O_5 in 50 mL water in 10 minutes and the solution was heated at 50°C in a water bath. The solution was refluxed for 1 h, resulting in a green solution. 25 µL of 30% aqueous H_2O_2 solution were added. After 1 h reflux of the dark-red solution, the solution was cooled to room temperature. Brown powder formed was filtered off by filtration through a folded filter paper. To the yellow-green filtrate, 43.18 g (300 mmol) of MoO_3 were slowly added under stirring, followed by refluxing for 15 minutes. To the yellow suspension, 4.77 g (45 mmol) of Na_2CO_3 were added over 10 minutes, and then 3.42 g (30 mmol) of 85% H_3PO_4 were added. The orange suspension obtained was refluxed for 3 h, and the resulting dark-orange clear solution was cooled to room temperature. The solution was evaporated by rotary evaporator to deposit

orange crystals. The crystals, collected on a fine glass frit, were dried thoroughly by suction, and then for 3 h under vacuum. Orange crystals obtained in 26.38 g (44.2%) yield were soluble in water, acetone, acetonitrile, methanol, ethanol and ethyl acetate, but insoluble in benzene, chloroform and dichloromethane.

FT-IR: 1627(s), 1075(s), 1063(s), 1053(m, sh), 951(s), 868(s), 781(s), 594(m), 503(m).

^{51}V NMR: (16.67 MHz, D_2O, 298 K): major peak at: -534.7.

^{31}P NMR: (79.49 MHz, D_2O, 298 K): major peak at: -3.29.

Synthesis of $H_4[PMo_{10}VO_{40}]$[14]

1.8 g of Na_2HPO_4 $12H_2O$ were dissolved in 25 mL of distilled water and 0.46 g of V_2O_5 were dissolved in 10 mL of Na_2CO_3 2M solution. The substances were then mixed and heated until boiling. 30 minutes later, 13.3 g $Na_2MoO_4·2H_2O$ were dissolved in 40 mL of deionized water and added to the mixture while keeping the temperature at 90°C for 30 minutes. Then 1:1 H_2SO_4 was added (dropwise with stirring) to the solution until the pH attained 2. Stirring was continued until room temperature was reached, and then 15 mL of diethyl ether were added to the mixture. After thoroughly shaking, 1:1 H_2SO_4 was added, until three layers appeared in the solution. The middle oil-like red material (heteropolyacid-ether compound) was removed with diethyl ether. Then some distilled water was added and the product was placed in a vacuum desiccator. The resulting orange fine powder was characterized by FT-IR . Yield: 7.09 g, 77%.

FT-IR. 1618(m), 1063(s), 961(s), 867(s), 779(s), 595(m).

^{51}V-NMR: (16.67 MHz, D_2O, 298 K): major peak at: -533.4.; (CD_3CN, 298 K): major peak at: -565.0.

^{31}P NMR: (79.49 MHz, D_2O, 298 K): major peak at: -3.87.

Following complexes: $K_8HV_3P_2W_{15}O_{62}$; $Q_4H_5V_3P_2W_{15}O_{62}$; $Q_7V_3Te_2W_{18}O_{69}$; $K_7V_3Te_2W_{18}O_{69}$; $Q_7V_3Se_2W_{18}O_{69}$ were all already synthesized and available in this laboratory[15].

$Q^+ = [(n-C_4H_9)_4N]^+$.
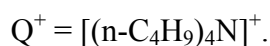
5.5.2 General procedure for cumylhydroperoxide decomposition.

Solvent (Cumene, 10 mL), cumylhydroperoxide 80% w/w in Cumene (CHP, 74 μL were required to obtain a solution 40 mM of CHP in Cumene) and acid catalyst (10% mol. H$^+$) were stirred in a closed glass reactor at room temperature. (Caution: The uncontrolled heating of large amount of peroxides and acid must be avoided. Care must be taken to avoid possible explosion).

Sample aliquots were taken (25 μl) and filtered if required, they where then diluted with 500 μl of CH$_2$Cl$_2$ containing dodecane as internal standard and triphenyphosphine as quencher, and analysed by GC-FID. The consumption of cumylhydroperoxide was verified by iodinated paper, and the reactions were generally monitored until its complete consumption. Formation of tars and oligomers were observed in the reactor during the reaction.

5.5.3 General procedure for phenol production by POM-mediated Tandem catalysis process.

Process 1. Cumylhydroperoxide weas produced from *neat* Cumene photooxygenation following exactly the same procedure described on Section 5.3.7.

Process 2. After irradiation time (4 hours), 2.5 mg of solid phosphotungstic acid (< 0.9 μmol;) were added under vigorous magnetic stirring in the reaction solution (1.1 mL). After 24 hours, 25 μL of sample aliquot were taken, diluted with 500 μl of CH$_2$Cl$_2$ containing dodecane as internal standard and triphenylphosphine as quencher, and then analysed by GC-FID. Phenol was detected in yield: 63% mol/mol with respect to the initial cumylhydroperoxide content. The difference between the concentration of 2-phenyl-2-propanol calculated before and after the process 2, allows to estimate approximately the amount of such product dehydrated to α-methyl-styrene and its oligomers in the presence of the acidic catalyst.

5.5.4 General procedure for the catalytic benzene oxidation to phenol.

The oxidation of benzene in the liquid-phase was performed in a glass reactor. Typically, 0.036 mmol of catalyst and 240 μL of benzene (5.8 mmol) were added to 3 mL of solvent. 539 μL of H$_2$O$_2$ 10.8 M (35 % w/w, titrated as reported in section 5.4.6) were added through the neck of the reactor. (In some reactions H$_2$O$_2$ was added in stepwise aliquots each 30 minutes). A magnetic stirrer was provided to stir (~ 600 rpm) the reaction mixture. Aliquots

of 50 µL of sample were taken, diluted with 500 µl of CH_2Cl_2 containing dodecane as internal standard and triphenyphosphine as quencher, and then analysed by GC-FID.

5.5.5 GC-analysis procedure and conditions.

Both reagents and products have been analyzed through GLC-Flame Ionisation Detector (FID) technique.

- In the case of acidic decomposition of cumylhydroperoxide to phenol and Tandem catalysis process POM-mediated, analysis were obtained with a 60 m (0,53 mm internal diameter, 1 µm film thickness) Alcohols Stabilwax® (Restek) capillary column in order to obtain a better separation between products and by-products formed.

Analysis were performed with the following conditions and program:

Solutions injected into the column were prepared by sampling reaction aliquots (25 µL) diluted with 500 µL of CH_2Cl_2 containing C_{10} ($8.8 \cdot 10^{-4}$ M) as internal standard and an excess of triphenylphosphine as quencher.

T injector: = 200°C;

T detector = 280°C;

Flow rate: 6 mL/min;

Analysis program:

Initial Temperature: 55°C for 5 min.; Rate: 12°C/min.; Final Temperature 250°C for 15 min.

- In the case of the direct oxidation of benzene with H_2O_2 analysis were performed with a 15 m (0.10 mm internal diameter, 0.10 µm film thickness) Equity-5 (Supelco) capillary column.

Analysis were performed with the following conditions and program:

Solutions injected to the column were prepared by sampling reaction aliquots (50 µL) diluted with 500 µL of CH_2Cl_2 containing C_{12} ($8.8 \cdot 10^{-4}$ M) as internal standard and an excess of triphenylphosphine as quencher.

T injector =180°C;

T detector = 250°C;

Flow rate: 69.5 mL/min;

Analysis program:

Initial Temperature: 55°C for 3 min.; Rate: 15°C/min.; Final Temperature 250°C for 2 min.

Retention times of different products were identified by injecting standard solutions and confirming them through GC-MS analysis.

Response Factors and quantitative evaluations of products and reagents were calculated as described in section 5.3.9-11.

As an example, the calculations for phenol Response Factors obtained by the Shimadzu GC-2100 equipped with a 15 m Equity^{TM}-5 capillary column are reported below:

A mother solution of phenol, ($1.48 \cdot 10^{-2}$ M) was prepared and, by consecutive dilutions, other two diluted solutions with concentration $7.4 \cdot 10^{-3}$ M and $1.5 \cdot 10^{-3}$ M respectively, were obtained, thus giving 3 solutions at known title for each analyte.

An internal standard solution, with concentration $8.8 \cdot 10^{-4}$ M, was prepared by dissolving 10 μL of n-dodecane (C_{12}) in 50 mL of CH_2Cl_2.

Final samples have been prepared by sampling aliquots of 50 μL from each solution, successively diluted with 500 μL of internal standard C_{12} solution. (Diluting Factor D: 11). Analysis were repeated three times for each sample and the ratios between the analyte and internal standard peak areas were obtained and averaged. From the known concentration of the internal standard ($8.4 \cdot 10^{-4}$ M) and of each analyte in each sample injected, it was possible to obtain the following results:

Table 5.5. Analytical results for determining Response Factor of Phenol.

Solution	$C_{phenol}^{a}/C_{standard}$	Average $A_{phenol}/A_{standard}$
1	16.0091	4.524
2	8.0046	2.132
3	1.6009	0.287

a. Phenol concentration is that of each prepared solutions divided per Diluting Factor.

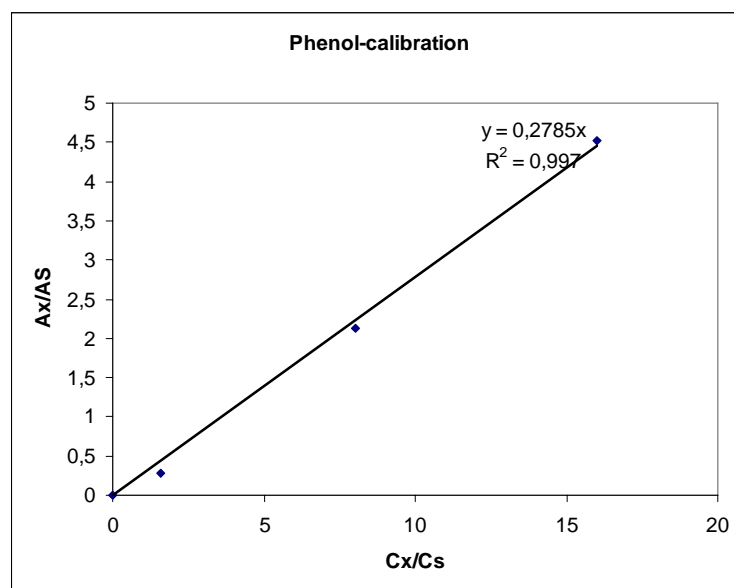The Response Factors is the slope of the following plot: 0.279.

Figure 5.6: Plot of Analytical data for Respose Factor of phenol.

5.5.6 General procedure for the preparation of vanadium (V) monoperoxo picolinate for [51]V-NMR.

A solution 5×10^{-3} M of vanadium (V) monoperoxo picolinate, used as external reference for [51]V-NMR (see Section 5.1), was prepared by dissolving 2.8 mg of NH_4VO_3 in 5 mL of milliQ water ($4.992 \cdot 10^{-3}$ M), 70% $HClO_4$ dropwise until pH = 1 and 3.12 mg of picolinic acid ($5.069 \cdot 10^{-3}$ M). H_2O_2 ($5 \cdot 10^{-3}$ M) was finally added (2.19 µL of 35% w/w) to the solution.

5.6 References and notes.

[1] TEM images were recorded tanks to the collaboration with Prof. Markus Antonietti at Max Planck Institute of Colloids and Interfaces, Potsdam, Germany.

[2] C. Rocaboy, W. Bauer, J. A. Gladysz, *Eur. J.Chem.,* **2000,** 2621-2628.

[3] G. Maayan, R. H. Fish, R. Neumann, *Org. Lett.*, 20, **2003**, 3547-3550.

[4] D. B. Dess, J. C. Martin, *J. Am. Chem. Soc.,* 113, **1991**, 7277-7287. b) M. Frigerio, M. Santagostino, S. Sputore, *J. Org. Chem.,* 64, **1999**, 4537-4538.

[5] a) D. C. Duncan, T. L. Netzel and C. L. Hill, *Inorg. Chem.,* 34, **1995**, 4640-4646. b) See also M. Carraro, *Ph. D. Thesis,* Università degli studi di Padova, **2001** page 144.

[6] M. Bonchio, M. Carraro, G. Scorrano, E. Fontananova and E. Drioli, *Adv. Synth. Catal.,* 345, **2003**, 1119-1126.

[7] I. F. Vankelecom, *Chem. Rev.,* 102, **2002**, 3779-3810.

[8] G. B. Shul'pin, *CR Chemie,* 6, **2003**, 163-178.

[9] a) A. Tézé, G. Hervé, *Inorg. Synth.,* 27, **1990**, 85-96. b) A. Tezè, G. Hervè, *J. Inorg. Nucl. Chem.,* 39, **1977**, 999. c) J. Canny, A. Tezè, R. Thouvenot, G. Hervè, *Inorg. Chem.,* 25, **1986**, 2114. d) see also M. Carraro, *Ph. D. Thesis,* Università degli studi di Padova, **2001**, pages 140-141.

[10] C. Rocchiccioli-Deltcheff, R. Thouvenot, *J. Chem.Research,* 46, **1977.**

[11] Mayer, C.R.; Fournier, I.; Thouvenot, R. *Chem. Eur. J.,* 6, **2000**, 105-110.

[12] Y. Nakagawa, K. Kamata, M. Kotani, K. Yamaguchi, N. Mizuno, *Angew. Chem.*, 44, **2005**, 5136-5141.

[13] K. Nomiya, S. Matsuoka, T. Hasegawa, Y. Nemoto, *J. Mol. Catal. A: Chemical,* 156, **2000**, 143-152.

[14] Y. Tang, J. Zhang, *Trans Met. Chem.,* 31, **2006**, 299-305.

[15] Synthesis of $K_8HV_3P_2W_{15}O_{62}$: R.G. Finke, B. Rapko, R.J. Saxton, P.J. Domaille, *J.Am.Chem.Soc.* 108, **1986**, 2947; Synthesis of $K_7V_3Se_2W_{18}O_{69}$ and $K_7V_3Te_2W_{18}O_{69}$: these V-substituted POMs were prepared by modifying a procedure reported for $K_{12}[(VO)_3(BiW_9O_{33})_2]\cdot30H_2O$ (T. Yamase, B. Botar, E. Ishikawa, K. Fukaya, *Chem Lett.,* **2001**, 56). $V_3Se_2W_{18}$: 2.20 g (6.66 mmol) of $Na_2WO_4\cdot2H_2O$ were dissolved in 20 ml of deionized water and placed in a beaker. 204.1 mg (1.11 mmol) of Na_3VO_4 and 95.4 mg (0.74 mmol) of H_2SeO_3 were then added; the solution is light yellow and pH is 9.5. The pH was quickly set to 1.0 by addition of HCl 4 M, resulting in a colour change to orange. The solution was then kept at 90°C for 1 h and filtered after cooling. Addition of 400 µl of CsCl 2 M resulted in black crystals formation after two or three days. Isolation of the tetra-n-butyl ammonium salt was obtained by precipitation after addition to the reaction solution of 1.07 g (3.32 mmol) of $[N(C_4H_9)_4]Br$; the yellow product was twice purified by re-precipitation from acetonitrile with water; yield 2.0 g (84 %).

$V_3Te_2W_{18}$: the procedure resembles that one for the preparation of $V_3Se_2W_{18}$, except that 227.8 mg of $K_2TeO_3\cdot3H_2O$ were used in place of H_2SeO_3 (the initial pH was 12.5).

Acronyms and abbreviations.

AcO: CH_3COO^-, acetate ion.

ADF: Amsterdam Density Functional code.

AFM: Atomic Force Microscopy.

AOPs: Advanced Oxidation Processes.

BPA: Bisphenol A.

bpy: 2,2'-bipyridine.

BSE: Back Scattered Electros

C$_{10}$: *n*-decane.

C$_{12}$: *n*-dodecane.

CHP: Cumyl-hydroperoxide.

CMRs: Catalytic Membrane Reactor.

COD: Chemical Oxygen Demand.

DLS: Dynamic Light Scattering.

DMF: Dimethylformamide.

DMSO: Dimethylsulfoxide.

DODA: Dimethyldioctadecylammonium cation.

DSC: Differential Scanning Calorimetry.

EDM: Ethylene glycol dimethacrilate.

EDX: Energy Dispersive X-ray analysis.

ESI-MS: Electrospray Ionsation Mass Spectroscopy.

ESR: Electron Spin Resonance

ET: Electron Transfer.

FID: Flame Ionisation Detector

FT-IR: Fourier Transform - Infrared spectroscopy

GC-MS: Gas Cromatography coupled with Mass Spectroscopy.

GLC: Gas-liquid Cromatography.

HA: Hydrogen Abstraction

HFIP: 1,1,1,3,3,3-*hexafluoro*-isopropanol.

HPAs: Heteropolyacids.

ILs: Ionic Liquids.

ITM-CNR: Membrane Technology Institute c/o Italian National Research Council.

LMCT: Ligand To Metal Charge Transfer.

LUMO: Lowest Unoccupied Molecular Orbital.

MB: Methylene Blue.

***m*-CPBA:** *meta* - chloroperbenzoic acid.

MMA: Methyl methacrylate.

MW: Microwave radiation.

nBu$_4$N$^+$: Tetrabutylammonium cation.

NMR: Nuclear Magnetic Resonance.

PDMS: Polydimethylsiloxane

PEEK-WC: Polyether-etherketon

PF: Phenol-Formaldehyde resins.

Pic: Picolinate.

PMMA: Coploymer of methyl methacrylate, ethylene glycol dimethacrilate.

POM: Polyoxometalate.

PS: Polysulfone

PTFE: Polytetrafluoroethylene (Teflon$^®$).

PVDF: Polyvinylidene difluoride

RfN: $[CF_3(CF_2)_7(CH_2)_3]_3CH_3N^+$ fluorinated cation.

SAXS: Small Angle X-ray Spectroscopy.

SECs: Surfactant-Encapsulated Complexes.

SEM: Scansion Electron Microscopy.

TDCPP: *meso*-tetrakis(2,6-dichlorophenyl)-porphyrin.

TEM: Transmission Electron Microscopy.

TFE: 2,2,2-trifluoroethanol

TGA: Thermogravimetry Analysis.

THF: Tetrahydrofuran.

TLC: Thin Layer Cromatography.

TMSP: Transition Metals Substituted Polyoxometalates.

TOF: Turnover Frequency.

TON: Turnover Number.

TS-1B: Modified Titanium silicalite.

UV-Vis: Ultraviolet-Visible spectroscopy.

VOCs: Volatile Organic Compounds (or solvents).

Padova, 30-01-09

Giunto al termine di questo Dottorato di Ricerca, desidero fare un sincero ringraziamento a tutte le persone che hanno collaborato e che mi hanno affiancato durante questi tre anni alla riuscita di questo lavoro.

La prima persona che desidero ringraziare è il Dr. Mauro Carraro, per la dedizione, la grande pazienza e l'entusiasmo con cui mi ha quotidianamente affiancato durante ogni fase dello svolgimento del lavoro di Tesi, per la semplicità con cui riesce a darmi la soluzione ad ogni problema che mi si presenta, per avermi insegnato come si fa Ricerca in ambito scientifico, per essere diventato prima di tutto un vero Amico, oltre che un semplice collega.

Grazie alla Dr.ssa Marcella Bonchio, per tutto il suo entusiasmo, la sua grande pazienza ed i suoi preziosissimi consigli necessari per l'avanzamento di questo lavoro di Tesi. Grazie per aver insistito a farmi iniziare il Dottorato di Ricerca: dopo tre anni riconosco l'importanza ed il valore di questa Esperienza: non solo per tutto ciò che ho fatto ed appreso, ma anche per come mi ha fatto maturare come persona.

Grazie al mio Supervisore, il Prof. Gianfranco Scorrano per credere costantemente nelle mie capacità e per seguire con constante interesse lo sviluppo del mio lavoro sperimentale.

Grazie ai miei compagni di gruppo e laboratorio: al Dr. Andrea Sartorel per tutti i suoi consigli sempre puntuali e mai fuori luogo e per il suo preziosissimo apporto per la parte di calcolo computazionale, alle Dottoresse Serena Berardi, Francesca Fabbianesi, Lucia Biasutto e al Dr. Andrea Mattarei, oltre che ai vari laureandi che si sono susseguiti in tutti questi mesi, per condividere con me gioie e fatiche durante le giornate di laboratorio.

Grazie al Dr. Raffaele Riccò per la collaborazione nell'acquisizione delle immagini AFM e al Dr. Luca Baù per l'aiuto nell'acquisizione delle analisi DLS.

Grazie alla Dr.ssa Chiara Maccato per la collaborazione nell'acquisizione delle analisi SEM e alla Dr.ssa Francesca Toma per le analisi TGA e DSC.

Grazie al gruppo del Prof. Enrico Drioli dell'ITM-CNR di Rende (CS) ed in particolare alla Dr.ssa Annarosa Gugliuzza, alla Dr.ssa Enrica Fontananova e al Dr. Giuseppe Barbieri per l'indispensabile collaborazione nella parte di studio e realizzazione delle membrane foto catalitiche.

Grazie al Prof. Markus Antonietti e a tutto il suo gruppo di ricerca , per avermi dato la possibilità di lavorare nei loro laboratori presso il Max-Planck Institute of Colloids and Interfaces di Potsdam (Germania).

Un doveroso ringraziamento va rivolto ai tecnici Gianni, Giulio, Stefano, Roberto e Mauro per la disponibilità, l'aiuto, spesso indispensabile, nell'utilizzo e nella riparazione degli strumenti di laboratorio ma anche e soprattutto per il tempo dedicato alla realizzazione materiale del foto reattore a flusso continuo.

Grazie a Cristiano, Marta, Silvia, Gianni, Francesco, Massimo che con me hanno condiviso in questi tre anni l'esperienza del Dottorato di Ricerca confrontandoci giorno dopo giorno.

Un ultimo grazie infine lo voglio dedicare a Bea e alla mia Famiglia, per il continuo supporto, l'affetto e l'amore che mi trasmettono ogni giorno.

A tutti Voi, GRAZIE! Con affetto, Martino.